Analysis of and Techniques for Adaptive Equalization for Underwater Acoustic Communication

by

Ballard J. S. Blair

B.S., Cornell University (2002)
M.S.E., Johns Hopkins University (2005)

Submitted to the
Department of Electrical Engineering and Computer Science
in partial fulfillment of the requirements for the degree of

Doctor of Philosophy

at the
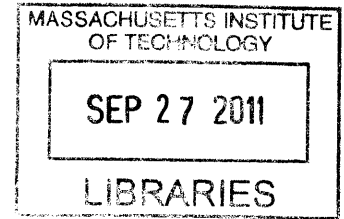
MASSACHUSETTS INSTITUTE OF TECHNOLOGY

and the

WOODS HOLE OCEANOGRAPHIC INSTITUTE

September 2011

© Ballard J. S. Blair, MMXI. All rights reserved.

The author hereby grants to MIT and WHOI permission to reproduce and distribute
publicly paper and electronic copies of this thesis document in whole or in part.

Author . . . .
Joint Program in Oceanography / Applied Ocean Science and Engineering
Massachusetts Institute of Technology
and Woods Hole Oceanographic Institute
September 2, 2011

Certified by . . . .
James C. Preisig
Associate Scientist, Woods Hole Oceanographic Institution
Thesis Supervisor

Accepted by . . . .
James C. Preisig
Chair, Joint Committee for Applied Ocean Science and Engineering
Massachusetts Institute of Technology/
Woods Hole Oceanographic Institution

Accepted by . . . .
Leslie Kolodziejski
Professor of Electrical Engineering
Chairman, Department Committee on Graduate Theses
Massachusetts Institute of Technology

Analysis of and Techniques for Adaptive Equalization for Underwater Acoustic Communication

by

Ballard J. S. Blair

Submitted to the Department of Electrical Engineering and Computer Science
on September 2, 2011 in partial fulfillment of the requirements for the degree of
Doctor of Philosophy in Electrical and Oceanographic Engineering

Abstract

Underwater wireless communication is quickly becoming a necessity for applications
in ocean science, defense, and homeland security. Acoustics remains the only prac-
tical means of accomplishing long-range communication in the ocean. The acoustic
communication channel is fraught with difficulties including limited available band-
width, long delay-spread, time-variability, and Doppler spreading. These difficulties
reduce the reliability of the communication system and make high data-rate commu-
nication challenging. Adaptive decision feedback equalization is a common method to
compensate for distortions introduced by the underwater acoustic channel. Limited
work has been done thus far to introduce the physics of the underwater channel into
improving and better understanding the operation of a decision feedback equalizer.
This thesis examines how to use physical models to improve the reliability and reduce
the computational complexity of the decision feedback equalizer. The specific topics
covered by this work are: how to handle channel estimation errors for the time varying
channel, how to use angular constraints imposed by the environment into an array
receiver, what happens when there is a mismatch between the true channel order and
the estimated channel order, and why there is a performance difference between the
direct adaptation and channel estimation based methods for computing the equalizer
coefficients. For each of these topics, algorithms are provided that help create a more
robust equalizer with lower computational complexity for the underwater channel.

Thesis Supervisor: James C. Preisig
Title: Associate Scientist, Woods Hole Oceanographic Institution

Acknowledgments

A PhD thesis is a singulalry authored document, but not one that is written in isolation. Thank you to my advisor, Dr. James Preisig, for spending countless hours guiding this research and supporting this writing. He is truly dedicated to enabling his students to produce high quality, meaningful research.

Thank you also to my thesis committee for their generous assistance: Prof. Milica Stojanovic spent many afternoons pointing me back in the right direction; I am grateful for her time, tricks, and intuition. Prof. Arthur Baggeroer was generous with his expansive knowledge and diligent to make this an accessible document. Prof. Greg Wornell always had a unique perspective from which research problems had apparent solutions.

The members of my labs both at MIT and WHOI were great in working through research ideas and clarifying research presentations. I am grateful to the members of Dr. Preisig's research group, especially Joe Papp, Milutin Pajovic, Dr. Ananya Sen Gupta, Atulya Yellepeddi, Jared Severson, and Dr. Andrey Morozov for their keen insights. Thank you also to the members of the DSPG group, especially Zahi Karim, Tom Baran, Shay Maymon, Sefa Demirtas, and Dennis Wei for time, energy, and support. I would be remiss to not mention Jon Paul Kitchens for our weekly lunch discussions where many of these ideas were born.

Like a lost puppy, I wandered through many research homes at both MIT and WHOI. I am a better, more rounded researcher for having been exposed to all these different viewpoints. I am grateful to many people for support during my wanderings: Prof. Louis Whitcomb and James Kinsey who pointed me to the Joint Program; Dr. Hanu Singh and Prof. Daniela Rus who gave me my first homes at WHOI and MIT respectively; Prof. Arthur Baggeroer for welcoming me into the MIT Acoustics group; Prof. Milica Stojanovic, Prof. John Leonard, and Prof. Alan Oppenheim, all of whom provided research groups, desks, and support over the years. A special thanks to Prof. Seth Teller for his advice and support.

One person whom I was most fortunate to meet was Prof. Alan Oppenheim; he has been an excellent mentor and supporter throughout my graduate school career. He brings an rare energy into his teaching and advising.

I am indebted to Prof. Andy Singer for allowing me to come visit his group at UIUC for a number of weeks to share ideas and expand my research horizons. Members of Dr. Singer's research group, Jun Won Choi, Erica Daly, and Thomas Riedl, have become valuable colleagues and friends.

Throughout my graduate career I have interacted with many students and researchers both at MIT and WHOI who have been excellent colleagues and friends. Drs. Brian Bingham, Rich Camilli, and Dr. Brendan Foley have all been a great inspiration and were always there to help with the finer details of life. Others who deserve special mention are Chris Murphy, Da Wang, Patrick Schmid, Sebastian Neumayer, Clay Kunz, Alexey Shmelev, Cara LaPointe, Ryan Eustice, Chris Roman, Hordur Johansson, Rob Truax, Alex Bahr, Michael Benjamin, Costas Pelekanakis, Jim Partan, Jordan Stanway, and Matt Walter. My experience in graduate school was enriched just through knowing each of these folks.

I am most grateful for and indebted to my wife, Emily. Without her loving support and her persistent encouragement this thesis would have never been completed. She was instrumental in keeping me sane and gave me the best gift of all, our son, Kobrin.

This thesis is dedicated to my wife, Emily,

whose patience and support has been a buoy

in these stormy, uncertain waters.

This bridge will only take you halfway there

To those mysterious lands you long to see:

Through gypsy camps and swirling Arab fairs

And moonlit woods where unicorns run free.

So come and walk awhile with me and share

The twisting trails and wondrous worlds I've known.

But this bridge will only take you halfway there-

The last few steps you'll have to take alone.

- Shel Silverstein

Contents

List of Figures

13

14

15

16

Acronyms

Acronym	Definition
AoA	Angle of Arrival
BPSK	Binary Phase Shift Keyed
CEB	Channel Estimate Based
DA	Direct Adaptation
DFE	Decision Feedback Equalizer
EW-RLS	Exponential-Weighted Recursive Least-Squares
FSK	Frequency Shift Keyed
IID	Independent and Identically Distributed
ISI	Inter Symbol Interference
MAE	Minimum Achievable Energy
MCM	Multiple Constraint Method
MMSE	Minimum Mean Squared Error
MSE	Mean Squared Error
MVDR	Minimum Variance Distorionless Response
PSD	Power Spectral Density
PSK	Phase Shift Keyed
QAM	Quadrature Amplitude Modulation
QPSK	Quadrature Phase Shift Keyed

Acronym	Definition
RF	Radio Frequency
RLS	Recursive Least Squares
SDE	Soft Decision Error
SINR	Signal-to-Interference-plus-Noise Ratio
SNR	Signal-to-Noise Ratio
SOFAR	Sound Fixing And Ranging
WSSUS	Wide Sense Stationary Uncorrelated Scattering

Chapter 1

Introduction

Since the dawn of time, people have looked at the surface of the ocean and wondered what secrets might be hidden in the depths. Born out of this wonder, oceanography is a science devoted to understanding the mysteries of the seas. Oceanographers have made many important discoveries that have fundamentally changed our understanding of the world. Technology is a driving force behind many of these underwater discoveries. One important part of technology, and not coincidentally the focus of this thesis, is wireless communication. In oceanography, wireless communication is used to increase portability, simplify deployments, and decrease mission cost.

Acoustic radiation is currently the only practical way to wirelessly transmit information underwater distances more than a few hundred meters. Wideband electromagnetic radiation is common in terrestrial communications but is highly attenuated after propagating short distances through the ocean: electromagnetic radiation in the megahertz to gigahertz range (radio frequency or RF radiation) propagates only a few meters before being attenuated and electromagnetic radiation in the optical range (especially blue-green light) propagates around a hundred meters. In contrast, acoustic radiation has relatively low attenuation and can propagate long distances through the ocean. Acoustics have been used to signal through thousands of kilometers of water [129] and have been used in virtually every ocean environment [77].

The goal of wireless, acoustic communication is to transmit digital data reliably with minimum data rate and maximum power constraints. There are several

challenges when communicating acoustically through the underwater channel: inter-symbol interference (ISI) caused by reverberation [76], limited signal bandwidth due to frequency dependent absorption [103], and time-variability of the channel [75]. Every ocean environment (*i.e.* every communication setup) has unique operating parameters (depth, system geometry, water column chemistry, *etc.*) so there is no universal underwater acoustic channel model for system analysis. As a result, underwater communication systems are often adaptively tuned based on *in-situ* measurements.

To mitigate channel induced signal distortions, the received signal is filtered in a structure known as an *equalizer*. An equalizer produces an estimate of the transmitted symbol using a weighted combination of the received signal and, in some structures, past symbol estimates. The metric used to gauge equalizer performance is the average squared error between the equalizer output and the transmitted data symbol.

Adaptive equalizers were initially designed for the wired telephone channel [62, 63] using several simplifying assumptions, such as slow time-variation and white observation noise. These approximations do not generally hold for the underwater acoustic channel; new thinking is needed to design equalizers that handle the harsh conditions of the underwater channel (*e.g.* large delay-spread, quickly varying coefficients, frequency selective fading, *etc.*) and that are computationally simple enough to be implemented on real-time systems. Using physical understanding of the underwater acoustic communication channel this thesis proposes several equalizer improvements with particular attention toward limiting computational complexity.

1.1   Contributions of this thesis

The goal of this thesis is to analyze past equalizer design assumptions and propose new algorithms for limiting complexity and improving performance. Specific contributions toward this goal are:

1. *A description of how the physical considerations of the communication channel affect the structure of the effective noise correlation matrix used in the computation of the equalizer coefficients.*

The effective noise includes observation noise, sensor noise, and noise from channel estimation errors. Traditionally, the effective noise correlation matrix has been approximated using a scaled identity matrix. Chapter 3 shows that the mean squared error can be reduced by as much as 4 dB using a fully populated effective noise correlation matrix and the computational complexity is reduced by assuming a Toeplitz matrix structure (which also further reduces mean squared error).

2. *Analysis showing the best non-adaptive combination of elements from a multi-element receiver that reduces computational complexity without sacrificing performance.*

   In Chapter 4, a set of static beams is found which reduce computational complexity without sacrificing too much performance (at most a decibel or two degradation in performance). Experimental data reveals that there are some channel conditions, such as calm seas with a low signal-to-noise ratio where the non-adaptive beams outperform a fully-adaptive beamspace processor. Data-driven techniques for determining the appropriate number of beams are analyzed.

3. *An analysis of how fixing the channel model order affects the mean squared error equalizer performance.*

   A channel estimate based equalizer requires a fixed number of modeled channel coefficients. In Chapter 5 it is shown that when the model has a different number of coefficients than the true channel, equalizer performance is degraded. A method of improving performance by adjusting the noise correlation matrix is detailed.

4. *A comparison of direct adaptation and channel estimate based equalizer algorithms, showing why the channel estimate based has lower mean squared error at high SNR.*

   At high SNR data symbol estimates from channel estimate based equalizers

have lower mean squared error than estimates from direct adaptation equalizers. Chapter 6 presents new analysis which explains this effect; (MMSE) equalizer coefficients have a shorter correlation window than channel coefficients, so tracking the equalizer coefficients (*i.e.* DA equalization) has higher mean squared error than tracking the channel coefficients (channel estimate based equalization).

1.2 Related work

This thesis focuses on analysis of the decision feedback equalizer (DFE) for underwater communication. There are many references which discuss the operation of the DFE in a variety of contexts, such as [79, 86]. Monsen [64] wrote a seminal paper examining the effect of DFE equalization on a fading channel where theoretical lower performance bounds were derived. Qureshi [81] wrote a nice tutorial paper summarizing the work on adaptive equalization prior to 1985.

The goal of most equalizers is to reduce the squared error between the data symbol estimate and the true data symbol. There have been several studies examining the nature of this error. Eletheriou and Falconer [31] examined how recursive least squares (RLS) tracking error affected DFE performance. They proposed separating the error into the sum of two parts: one term caused by channel estimation errors due to time variability and another term caused by noise.

Stojanovic [106] proposed an alternate decomposition of the error term: first into causal and a-causal parts and then into a channel estimation error part and a noise part. She postulated if the channel estimation error could be estimated, it could be combined with the observation noise estimate to create a total (effective) noise estimate. She and Zvonar extended this research into multi-user equalization in [111].

One form of the MMSE equation for equalizer coefficients is an inverse matrix multiplied by a column vector. Dzung [27] simplified equalizer error analysis of adaptive algorithms by replacing the inverse of the random matrix with the inverse of the expectation of the random matrix.

24

Preisig [75] examined how imperfect channel estimation affected the equalizer taps. He proposed an estimated error DFE, where the error covariance matrix is estimated using the received signal, past data symbols, and a channel estimate. His work showed definitively that the effective error can be modelled as the noise plus a term which accounts for channel estimation errors.

Building on the work of Eleftheriou and Falconer [31], Nadakuditi and Preisig [65, 66] presented a more sophisticated separation of the channel estimation error when using a recursive least squares algorithm. Employing an extended state space model they provided derivations which related the observed noise correlation matrix to both the channel and noise correlation matrices. In the same work [65, 66], Nadakuditi and Preisig presented results the effect of fixing channel model order on channel estimation errors when using a recursive least squares algorithm.

Stojanovic et al. pioneered the analysis and application of advanced equalization techniques for the underwater communication [80, 105, 107, 108, 110]. Using experimental data, she verified that equalization was possible underwater. She also examined some environmental factors that affect communication, such as noise and absorption, and derived useful approximations [101, 103].

Preisig et al. also how ocean physics affects underwater communication systems in [74, 75, 76, 78]. They focused on the effect of time-varying environments (surface waves) on communication systems and how to compensate for environmental distortions using equalization. One interesting observation was that waves act as a concave mirrors which focuses the acoustic energy and causes large, fast amplitude changes at the receiver. Li et al. [60, 59] proposed using the delay-Doppler characterization of the channel along with sparse techniques to mitigate this effect of these mirrors.

In a seminal work on multichannel, adaptive equalization for underwater communication, Stojanovic et al. [105] found that the optimal multichannel combiner is a matched filter followed by a maximum likelihood sequence estimator (MLSE). Since the MLSE is impractical due to the large channel delay spread in underwater environments (which can span hundreds of symbols), she used an adaptive DFE as the channel combiner. Using experimental data, she showed that for the underwater

channel, the mean squared error of the multichannel DFE output is not significantly greater than the mean squared error of the MLSE output.

The same set of authors showed that when the direction of arrival for all multipath components is known a multichannel DFE with a beamformer is equivalent to a multichannel DFE without a beamformer [109]. They further showed that any set of beam-weights that spans the signal space produces equivalent mean squared error performance when the observation noise is spatially and temporally white. Using the multichannel DFE with a beamformer reduced the computational complexity of the receiver when the number of multipath arrivals was less than the number of sensors.

Using physics-based constraints, the communication receiver can better estimate the channel and reduce computational complexity by reducing the number of parameters to be estimated. Kraay and Baggeroer [50] proposed using physical constraints for array processing by constraining the signal covariance matrix to be realizable when the received signal was a sum of narrowband plane waves. Their goal was to reduce the number of snapshots needed to properly estimate a covariance matrix.

Papp *et al.* [71, 72] used a different form of physical constraint: mode-filtering. They showed that mode-filtering improves array signal-processing. They also showed using experimental data that mode-filtering a signal before equalization had higher mean squared error than an equalizer with no mode-filter.

LeBlanc and Beaujean [55, 56] proposed applying principle component analysis (PCA) to acoustic communication systems with receive arrays. To improve equalizer performance the beams were decorrelating by using the eigenvectors of the received signal correlation matrix were used as the beamformer weights. They focused mainly on the decorrelating effects of this technique and not on dimensionality reduction.

Two common methods for computing adaptive equalizer coefficients are direct adaptation (DA) where the equalizer coefficients are estimated directly from the received data and channel estimate based (CEB) where a channel estimate is used to compute the coefficients. There have been several studies comparing the DA equalization with CEB equalization, but the performance comparisons contained only empirical evidence without analysis. Many authors had hypotheses about the cause of

the performance difference, but there was no consistency between them.

An often cited work comparing DA and CEB equalizers on a Rayleigh fading channel is by Shukla *et al.* [91]. The authors showed that when the channel order is known and the signal to noise ratio (SNR) is large, the DA approach had higher mean squared error than the CEB approach.

Fechtel and Meyr [32] also demonstrated a difference in mean squared error (at high SNR) between DA and CEB equalizers, assuming the CEB equalizer had perfect channel knowledge. They hypothesized that the difference was due to the lag in the DA equalizer which implicitly has to estimate the channel state information.

Lee and Cox [58] examined the performance difference between the DA and CEB methods when the the true channel order was not known. They experimentally validated that for an unknown channel length the DA method outperformed the CEB method. They also found that a matrix regularization term was effective to combat the difference in performance between the two methods. In later work [57] examined the effect of channel mismatch on the bit error rate (BER) of a maximum likelihood sequence estimator (MLSE).

An alternative to equalization is time-reversal [33, 85]. In time-reversal techniques, a channel estimate is convolved with the data signal. The channel is estimated by sending a pulse through the channel and recording the received signal. This form of channel estimation is not robust to channel variations. An array is used to either transmitted or receive (or both) which provides an array gain proportional to the number of sensors in the array. Time-reversal methods both temporally and spatially match filter the received signal to increase the effective SNR.

Time-reversal has been shown to be an effective, low-complexity method for handling the difficulties of the underwater channel [46, 47, 85] and has been extended into multi-user scenarios [95, 96, 97]. Results have been confirmed using experimental data [28, 40]. After comparing the mean squared error of time-reversal with equalization, the equalizer always had lower mean squared error [128]. An equalizer is thus generally preferred to time-reversal. Attempts have been made to include both time-reversal and equalization into one communication system [17, 18, 98].

There has been increasing interest in combining equalization with error correcting coding, a technique known as *turbo-equalization* [26, 49, 117, 118]. The data is first encoded using an error correcting code and the resulting signal is transmitted through a channel. The equalizer filters the received signal and, rather than making a symbol decision, transmits the filtered output directly to the decoder. The raw output of the equalizer without a symbol decision is known as *soft information*. A decoder uses this soft information to refine the transmitted symbol probabilities. The updated soft information is sent back to the equalizer and the process iterates.

Turbo-equalization has been shown to work well for underwater channel [19, 20, 25, 92]. One issue with turbo-equalization is its computational complexity. There has been work done to reduce the computational complexity [93, 117], but still more needed. The techniques presented in this thesis could be applied to the equalizer portion of a turbo-equalizer to improve performance and reduce computational complexity in underwater environments.

1.3   Organization

The remainder of this thesis is organized as follows: Chapter 2 provides the mathematical and conceptual background to understand the remainder of the thesis. Chapter 3 describes how channel estimation errors can be accounted for when calculating equalizer filter weights. Chapter 4 explains how knowledge of the physically constrained arrival angles can be incorporated into an array receiver to reduce computational complexity. Chapter 5 presents analysis of how assumptions of the channel order affect the equalizer error. Chapter 6 discusses the difference between the CEB and the DA equalizers. Concluding remarks and areas for future research are identified in Chapter 7.

1.4 Notation

Throughout this thesis, the following notation is used:

Symbol	Definition
a	Non-bold lowercase letters represent scalar constants
$\mathbf{a}$	Bold lowercase letters represent column vectors
$\mathbf{A}$	Bold uppercase letters represent matrices
$*$	Complex conjugate of the variable (*i.e.* a^*)
T	Transpose of a vector or matrix (*i.e.* $\mathbf{A}^T$)
H	Hermitian (conjugate transpose) of a vector or matrix (*i.e.* $\mathbf{A}^H$)
$\| \cdot \|$	2-norm of the enclosed quantity (*i.e.* $\|\mathbf{a}\|$)
$\hat{}$	Estimate of a quantity (*i.e.* $\hat{\mathbf{a}}$)
$\mathbf{I}$	Square Identity matrix (context sized)
$\mathbf{I}_M$	MxM Square Identity Matrix
$\mathbf{0}$	Zero matrix or vector (context sized)
$E\{\cdot\}$	Expectation of enclosed quantity

Chapter 2

Background

2.1 Underwater communication

The underwater channel remains one of the most challenging communication environments. Designing a reliable communication system remains an active area of research. Knowing where a system is going to be deployed is important when designing underwater acoustic (UWA) communication system. Communicating vertically through the ocean tends to be the simplest regime since often there is little multipath. The name of this environment is the Reliable Acoustic Path (RAP) [24] due to the fidelity of the channel. Baffles or directional hydrophones are used reduce effects of surface bounces.

In deep water systems there is less interaction with the surface so the communication channel is time-invariant, possibly sparse, and widely spread in delay. Modeling techniques are often employed in deep water channels to determine the locations where communication is possible due to the channel physics. The direct path is often the last to arrive in deep water since a natural waveguide exists around the sound-speed minimum in deep water [42].

In shallow water environments interactions with the time-varying ocean surface are unavoidable. There are also interactions with the bottom and nearby obstacles plus noise from waves, shipping traffic, and marine life. When operating in such a dynamic environment adaptive channel tracking and adaptive equalization techniques

are essential, such as the exponentially weighted recursive least squares (EW-RLS) algorithm.

Underwater communication began with the uncoded, analog underwater telephone or "the Gertrude" which was used to commzunicate with a manned submersible. As higher data-rates became necessary and the intended receiver was a machine instead of a person more complex systems were needed. The development of these systems began in the analog domain, but quickly switched to the digital domain where frequency shift keying (FSK) and more recently phase shift keying (PSK) (for increased bandwidth efficiency) are used for data modulation. Many detailed papers have been written concerning the history of underwater communications such as [5, 14, 15, 16, 45, 110].

The focus of this thesis is on the well-mixed, shallow-water channel where the isovelocity assumption is appropriate. Data is modulated using phase shift keying (PSK) techniques since this is the current state of the art. The following subsections outline some of the difficulties in communicating through the underwater environment to familiarize the reader and to emphasize that this is a harsh environment that requires extra effort.

2.1.1   Distance and SNR

The majority of ocean noise can be separated into one of four components: turbulence, shipping, wind, and thermal noise. Turbulence dominates in the low frequency region under 10 Hz, shipping noise is dominant in the 10-100 Hz region, wind-driven wave noise prevails in the 100 Hz -100 kHz, and thermal noise dominates above 100 kHz [102]. The total noise is the unweighted sum of these four noise components. A useful approximation of the noise power spectral density (PSD) as a function of the frequency f in kHz is

$$10 \log_{10} N(f) \approx N_1 - \eta \log_{10} f. \tag{2.1.1}$$

The above expression has units dB re μPa per Hz and the constants are $N_1 = 50$ and $\eta = 18$ [102].

Common acoustic communication frequencies are from 100 Hz to 100 kHz, so wind

driven noise is dominant. With some notable exceptions (*e.g.* snapping shrimp and breaking ice), noise in the acoustic communication frequencies is well modeled by a Gaussian random process [102, 126]. In general, the power spectral density of this process is not flat, so the noise process is not white.

Attenuation is a function of the acoustic path length l and the frequency of the signal f [10, 103]

$$A(l, f) = (l/l_r)^k a(f)^{l-l_r},$$ (2.1.2)

where k is the spreading factor (cylindrical, spherical, *etc.*), $a(f)$ is the absorption coefficient, and l_r is a reference distance. Thorp [115, 116] provided an approximate expression for the absorption coefficient as a function of frequency which is valid for frequencies in the range 500 Hz to 50 kHz. Most acoustic communication frequencies are in this range. The expression for the absorption coefficient is

$$10 \log a(f) = 0.11 \frac{f^2}{1 + f^2} + 44 \frac{f^2}{4100 + f^2} + 2.75 \cdot 10^{-4} f^2 + 0.003,$$ (2.1.3)

where the quantity $10 \log a(f)$ has units of dB/km and f has units of kHz. For frequencies lower than 500 Hz, the alternative expression

$$10 \log_{10} a(f) = 0.11 \frac{f^2}{1 + f^2} + 0.011 f^2 + 0.002$$ (2.1.4)

is a better approximation [10, 102]. Fisher and Simmons [34] tied these expressions to physical and chemical properties of sea water.

Using a narrowband approximation and ignoring any multi-path effects, the SNR can be approximated as a function of frequency and distance,

$$SNR(l, f) = \frac{P/A(l, f)}{N(f)\Delta f} = \frac{P}{A(l, f)N(f)\Delta(f)},$$ (2.1.5)

where Δf is the bandwidth of the receiver and hence the received noise (narrowband approximation) [102]. The frequency dependent portion of this expression is
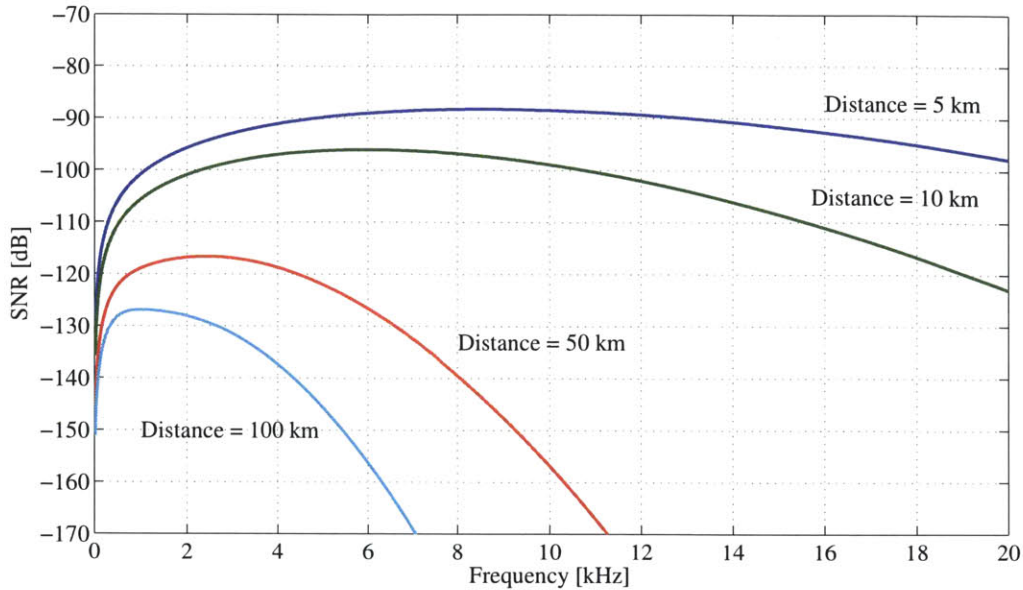
Figure 2.1.1: Signal to Noise ratio (narrowband), $1/A(l,f)N(f)$, as a function of frequency for various ranges.

encompassed in the expression $A(l, f)N(f)$ since P is the total source power across the available bandwidth. Using a practical spreading coefficient of $k = 1.5$, Figure 2.1.1 shows the relationship between frequency and SNR, recreated from [102]; both the optimal center frequency and 3 dB bandwidth are dependent on transmission range.

Jensen and Kuperman [41] performed a related analysis to find the *optimum frequency* that balanced the propagation and attenuation mechanisms of the shallow water channel, but did not account for noise power. The optimum frequency is a general feature of waveguide or ducting propagation and for shallow water channels is strongly dependent on depth [42]. Typical optimum frequencies when the water depth is 100 m are 200-800 Hz, lower than the frequencies found in [102] which included the noise characterization.

2.1.2 Delay spread of the channel

As sound travels from the transmitter to the receiver, it follows not only a direct path, but also additional paths due to reflections from the surface, reflections from the sea floor, and inhomogeneities in the sound speed profile which cause the refraction of the sound paths.

The time difference between the first received path and the last is referred to as the *delay-spread* of the channel. The delay-spread determines the fastest rate at which data can be transmitted without inter-symbol interference (ISI). Often the length of the delay-spread is in units of transmitted symbol durations, the inverse of the transmitted symbol rate. Delay spreads of tens and hundreds of symbols are not uncommon in the underwater channel. This is a stark contrast to the radio-frequency (RF) channel which often has on the order of three symbols of ISI.

The delay-spread of the underwater communications channel is due to the different paths from the transmitter to receiver. In water shallow enough for an approximately isovelocity sound speed profile the delay spread induced by the channel is due to reflections from the sea surface, reflections from the bottom, and reflections from anything in the water column. These reflections are referred to as *macro-multipath* since they are due to macro features in the environment. These features are usually assumed to be roughly time-invariant over a time-scale that is much larger than the data signaling rate [100].

The acoustic rays are better modeled as three-dimensional tubes rather than two-dimensional lines. When the tube encounters an object, the reflections are usually not point reflections, but are reflections from an area such as a rough patch of sand or rough sea surface. This causes each ray path to spread in time, sometimes by as much as a few milliseconds. The multipath due to small scale features such as surface roughness and random ocean fluctuations is referred to as *micro-multipath*. Micro-multipath is non-specular and some components of the small scale random fluctuations can be modeled statistically [100]. In the acoustics literature, the micro-multipath concept is also known as ray-tubes [42].

35
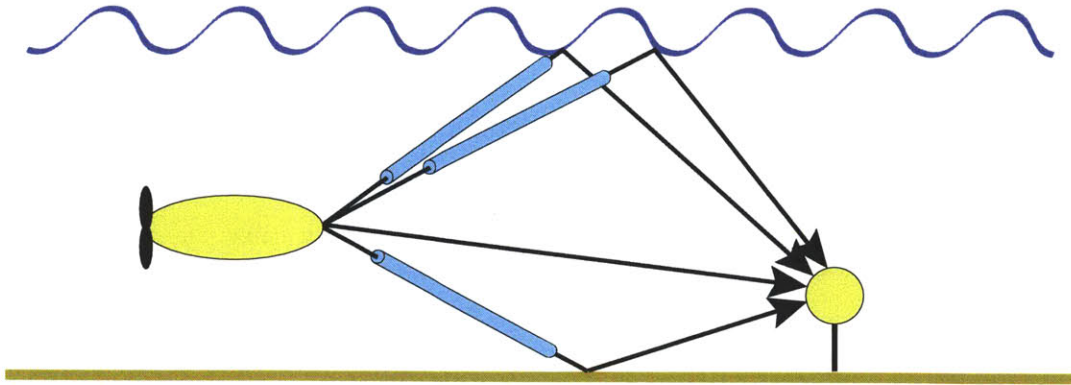
Figure 2.1.2: Diagram depicting some of the acoustic paths from the transmitter to the receiver. The black solid lines show the path and the blue cylinder are an example of the spreading in space that would cause a spread in time at the receiver.

Figure 2.1.2 shows an example of what multipath might look like in a shallow water environment. The macro-multipath is represented by the different paths (solid black lines) and the micro-multipath is a cylinder around this line, indicating the spreading radius.

In a deep water environment, in addition to surface and (less commonly) bottom bounces, fully refracted paths occur due to a local minimum in the sound speed profile. Sound tends to "favor" regions with slower sound speed and will bend towards those regions. There is a region of the ocean known as the Sound Fixing and Ranging (SOFAR) channel or the deep sound channel where the sound speed is at a minimum. The ray bending is due to Snell's law applied to a medium with a continuously changing sound speed. The deep water channel can have a large time-spread but may be sparse and is often slowly-varying compared to the time scales of equalizer adaptation relevant for acoustic communication.

Regions of little acoustic penetration due to system geometry and the sound speed profile are known as *shadow zones*. These regions can occur because of obstructions (*e.g.* sea mounts) or more importantly because of the waveguide propagation physics. Shadow zones can form in either the deep or shallow water channels [42, 119]. There is little signal processing that can be done to correct for shadow zones so compensation for shadow zones is accomplished through system placement and mission design.

2.1.3 Doppler, waves, and motion

Each of the transmitter-to-receiver paths experience varying degrees of time-variability effects due to surface waves, internal waves, platform motion, reflections from moving objects, and currents and tides. Each source of variability can induce either a Doppler shift, where all of the frequencies are shifted up or down, or a Doppler spread, where neighboring frequencies are smeared together. A typical Doppler spread is on the order of 0 to 30 Hz, but depends heavily on the transmit frequency and communication system parameters (sea surface motion, weather, platform motion, *etc.*).

Because the speed of sound is much slower than the speed of light, the Doppler effects observed in the underwater channel tend to be much more severe than in RF channels. To illustrate the Doppler effect more clearly, consider a pulse, $p(t)$, modulated with a carrier frequency of f_c and transmitted through a sound channel with constant speed of sound c_s to a receiver moving at a constant velocity v with respect to the transmitter. The propagation delay of the received signal is $\tau(t) = \tau_0 - \frac{vt}{c_s}$, where τ_0 is a reference delay. The Doppler effect is proportional to $a = v/c_s$. The transmitted signal, $s(t)$, is [104]

$$s(t) = \text{Re}\{p(t)e^{j2\pi f_c t}\}. \tag{2.1.6}$$

The signal observed by the receiver is [104]

$$r(t) = s(t + \frac{vt}{c_s} - \tau_0) = s(t + at - \tau_0) = \text{Re}\{p(t + at - \tau_0)e^{j2\pi f_c(t+at-\tau)}\}. \tag{2.1.7}$$

With respect to the center frequency the baseband receive signal (*i.e.* the received signal after demodulation and low pass filtering) is [104]

$$f(t) = e^{-j2\pi f_c \tau}p(t + at - \tau)e^{j2\pi a f_c t} \tag{2.1.8}$$

Ignoring the phase shift $2\pi f_c \tau$, there are two signal distortions observed:

1. The signal is dilated in time by a factor of $1 + a$, *i.e.* the dilated signal is $p'(t) =$

$p(t(1 + a))$. A dilation the time domain causes a corresponding contraction of the frequency response.

2. The signal has a frequency offset of af_c, which is known as a *Doppler shift*.

The dilation effect can be ignored when the time-bandwidth of the signal is appropriately small. If the bandwidth of $p(t)$ is denoted as B_p, the signal is approximately time invariant for a time B_p^{-1}. If the data packet has total duration T, then the total dilation of the packet is vT/c_S which must be much less than B_p^{-1} for dilation to be ignored. Therefore, when the time bandwidth product, TB_p, satisfies the relation

$$TB_p \ll \frac{c_s}{v}$$

dilation can be ignored; otherwise, the received signal needs to be re-sampled [120].

Another way to characterize the Doppler is through the scattering function. Assume that the channel coefficient at a particular time t and delay τ is $g(t, \tau)$. If the channel is known to be *wide sense stationary* (*i.e.* the correlation is a function of the time difference), then the temporal correlation function of the channel is

$$\mathbf{R}_g(\Delta t; \tau_1, \tau_2) = \mathrm{E}\{g(t, \tau_1)g^*(t + \Delta t, \tau_2)\}, \tag{2.1.9}$$

which is a function of three variables: the two delays, τ_1 and τ_2, and the difference in time Δt. The scattering function of the channel is defined as the Fourier transform of the temporal correlation function,

$$S_g(\lambda_d; \tau_1, \tau_2) = \int_{-\infty}^{\infty} \mathbf{R}_g(\Delta t; \tau_1, \tau_2)e^{-j2\pi\lambda_d\Delta t}\mathrm{d}\Delta t, \tag{2.1.10}$$

where λ_d is the Doppler spreading variable. At a particular delay, $\tau_1 = \tau_2$, this is an expression of the *Doppler spread* of the channel. This leads to the relationship between the coherence time of the channel, $(\Delta t)_c$, and the Doppler spread, B_d, [79]

$$(\Delta t)_c \approx \frac{1}{B_d}. \tag{2.1.11}$$

38

The coherence time, $(\Delta t)_c$, *i.e.* the time over which the channel at a particular delay is correlated, is approximately the inverse of the Doppler spread of the channel, B_d. For time-invariant channel $(\Delta t)_c = \infty$, so there is no Doppler spread.

In addition to Doppler effects, there are other channel effects caused by the waves. For certain geometries, the waves will act as a concave mirror and the focus the acoustic energy to cause severe but brief changes in the channel magnitude and phase characteristics [78, 74]. These focusing events cause the path that interacts with the surface to have a larger magnitude than the direct path and can cause instantaneous $\pi/4$ shifts in phase.

Wave motion can also inject bubbles into the water volume [77]. These create a highly variable medium for the sound to propagate through and can increase the absorption coefficient or reduce the effective height of the water column.

2.2 Channel model

An underwater communication systems consists of at least one transmitter and one receiver. Figure 2.2.1 shows an example setup for an underwater acoustic experiment.
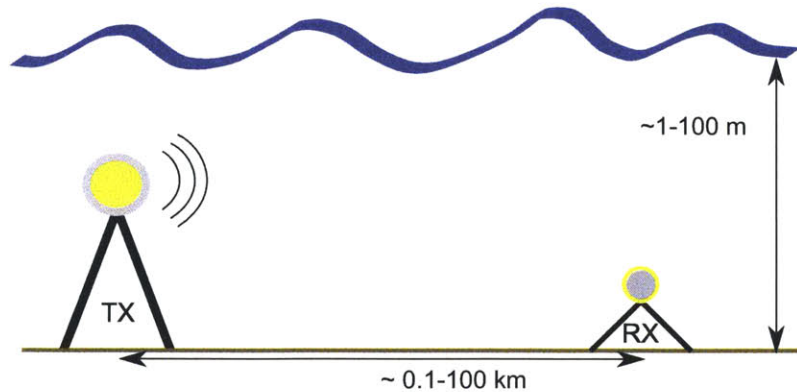
Figure 2.2.1: Possible setup for acoustic model being studied in this thesis.

Received signals are assumed to be sampled at baseband, so the analysis and processing are done in discrete time with complex valued signals. The acoustic channel is modeled with a finite extent, linear, time-varying impulse response plus additive

39

noise [79, 120]. The received signal sample at time n, $u[n]$, can be written as [75]

$$u[n] = \sum_{k=-N_a}^{N_c-1} g^*[n,k]d[n-k] + \nu[n], \tag{2.2.1}$$

where $d[n]$ is the transmitted data, $\nu[n]$ is complex, baseband noise, and $g[n,k]$ is the complex, baseband channel impulse response equating the input data at time $n-k$ to the output data at time n. The channel includes the transmit and receive filtering effects in addition to the physical propagation effects. The channel is assumed to have N_c causal coefficients and N_a acausal coefficients, where the center (zero offset) coefficient is assumed to correspond to the center of the direct arrival. This definition is particular to the isovelocity channel; in other environments the direct arrival may not be the first causal arrival (*e.g.* the direct arrival is the last arrival for the SOFAR channel). Eq. (2.2.1) can be written more compactly as

$$u[n] = \mathbf{g}^H[n]\mathbf{d}'[n] + \nu[n], \tag{2.2.2}$$

with

$$\mathbf{g}[n] = [g[n, N_c - 1] \ \ldots \ g[n, 0] \ \ldots \ g[n, -N_a]]^T \tag{2.2.3}$$

and

$$\mathbf{d}'[n] = [d[n - N_c + 1] \ \ldots \ d[n] \ \ldots \ d[n + N_a]]^T. \tag{2.2.4}$$

Stacking successive received signal samples, eq. (2.2.2) becomes a matrix-vector equation,

$$\mathbf{u}[n] = \mathbf{G}^H[n]\mathbf{d}[n] + \boldsymbol{\nu}[n], \tag{2.2.5}$$

where $\mathbf{u}[n]$ is a vector of sampled received data, $\mathbf{d}[n]$ is the transmitted data, $\boldsymbol{\nu}[n]$ is

the sampled noise vector, and $\mathbf{G}[n]$ is the channel convolution matrix. Specifically,

$$\mathbf{u}[n] \;=\; [u[n - L_c + 1] \;\ldots\; u[n] \;\ldots\; u[n + L_a]]^T \qquad (2.2.6)$$

$$\mathbf{d}[n] \;=\; [d[n - L_c - N_c + 2] \;\ldots\; d[n + L_a + N_a]]^T \qquad (2.2.7)$$

$$\boldsymbol{\nu}[n] \;=\; [\nu[n - L_c + 1] \;\ldots\; \nu[n] \;\ldots\; \nu[n + L_a]]^T \qquad (2.2.8)$$

$$\mathbf{G}[n] \;=\; \begin{bmatrix} g[n - L_c + 1, -N_c + 1] & 0 & \cdots & 0 \\ g[n - L_c + 1, -N_c + 2] & g[n - L_c + 2, -N_c + 1] & \cdots & 0 \\ \vdots & & \ddots & \vdots \\ 0 & 0 & \cdots & g[n + L_a N_a] \end{bmatrix}$$

$$\;=\; \begin{bmatrix} \mathbf{g}'_{-L_c+1}[n - L_c + 1] & \cdots & \mathbf{g}'_{L_a}[n + L_a] \end{bmatrix}, \qquad (2.2.9)$$

where L_a and L_c are the number of acausal and causal feedforward equalizer taps in each feedforward section of a decision feedback equalizer. The transmitted data symbols are assumed to be drawn from a zero-mean random-process with variance σ_d^2. The noise and transmitted data correlation matrices are defined as

$$\mathbf{R}_\nu \;\triangleq\; \mathrm{E}\{\boldsymbol{\nu}[n]\boldsymbol{\nu}^H[n]\} \qquad (2.2.10)$$

$$\mathbf{R_d} \;\triangleq\; \mathrm{E}\{\mathbf{d}[n]\mathbf{d}^H[n]\} = \sigma_d^2 \mathbf{I} = \mathbf{I}. \qquad (2.2.11)$$

The last equality for $\mathbf{R_d}$ highlights an assumption used for the remainder of this thesis (unless otherwise noted) that the transmitted data symbols are white with unit energy, *i.e.* $\sigma_d^2 = 1$.

Each of the columns of the matrix $\mathbf{G}[n]$, denoted above as $\mathbf{g}'_i[m]$, is the channel impulse response vector at time m, $\mathbf{g}[m]$, padded with zeros so the matrix multiplication $\mathbf{G}^H[n]\mathbf{d}[n]$ is equivalent to the convolution of the channel impulse response with the transmitted data from eq. (2.2.1).

To handle fractionally spaced sampling (more than one sample per symbol), the number of rows of $\mathbf{G}[n]$ is increased proportional to the fractional sampling rate (number of samples per symbol). The length of the noise and received data vectors is increased accordingly. The length of the transmitted symbol vector remains

41

unchanged. Except when noted, symbol rate sampling is assumed for notational simplicity; it is straightforward to extend the results to handle fractional-rate sample spacing.

2.3 Least-squares estimation

2.3.1 Setup

Many problems from signal processing, communications, and control have a similar form: estimate the vector $\mathbf{w}$ when the statistics of the random vector $\mathbf{x}$ and random variable y are known, ν is random noise, and

$$y = \mathbf{w}^H \mathbf{x} + \nu,$$

Since the noise is random it is not possible to estimate $\mathbf{w}$ exactly so a metric is needed to determine the quality of the estimate. An extremely common metric is the mean squared error metric which is the expected absolute difference squared between y and $y_{\text{est}} = \mathbf{w}_{\text{est}}^H \mathbf{x}$ where $\mathbf{w}_{\text{est}}$ is the estimate of $\mathbf{w}$. The minimization problem using this metric is

$$\mathbf{w}_{\text{MMSE}} = \arg\min_{\mathbf{w}_{\text{est}}} \mathrm{E}\{|y - \mathbf{w}_{\text{est}}^H \mathbf{x}|^2\}. \tag{2.3.1}$$

The solution to this minimization problem is the minimum mean squared error (MMSE) solution

$$\mathbf{w}_{\text{MMSE}} = \mathrm{E}\{\mathbf{x}\mathbf{x}^H\}^{-1}\mathrm{E}\{\mathbf{x}y^*\} = \mathbf{R}_{\mathbf{x}}^{-1}\mathbf{r}_{\mathbf{x}y} = \mathbf{P}\mathbf{r}_{\mathbf{x}y}, \tag{2.3.2}$$

where $\mathbf{R}_{\mathbf{x}} = \mathrm{E}\{\mathbf{x}\mathbf{x}^H\}$, $\mathbf{r}_{\mathbf{x}y} = \mathrm{E}\{\mathbf{x}y^*\}$, and $\mathbf{P} = \mathbf{R}_{\mathbf{x}}^{-1}$. Assuming both $\mathbf{x}$ and y are zero-mean, this solution provides the unbiased estimate of the parameter vector $\mathbf{w}$ with the minimum mean squared error. The solution can be modified to handle the non-zero mean case as well. In the communication context, the MMSE problem setup is used for channel estimation and for equalizer coefficient estimation.

When the statistics of $\mathbf{x}$ and y are not known, but there are observations available

42

(*i.e.* $\mathbf{x_1}$, y_1, $\mathbf{x_2}$, y_2, $\cdots$, $\mathbf{x_N}$, y_N), the observed data can be arranged as

$$
\mathbf{X} = \begin{bmatrix} \mathbf{x}_1^H \\ \mathbf{x}_2^H \\ \vdots \\ \mathbf{x}_N^H \end{bmatrix} \qquad \mathbf{y} = \begin{bmatrix} y_1 \\ y_2 \\ \vdots \\ y_N \end{bmatrix},
$$

and least squares methods can then be used. The least squares problem is related to the MMSE and has a very similar form. In the least squares problem, a vector $\mathbf{w}$ is sought which solves

$$
\mathbf{Xw} = \mathbf{y}.
$$

When the known matrix $\mathbf{X}$ is *tall*, *i.e.* has more rows than columns, usually there is no exact solution. A tall matrix also indicates there are more observations $\mathbf{y}$ than parameters $\mathbf{w}$. The least squares estimate minimizes the squared error between $\mathbf{Ax}$ and $\mathbf{y}$,

$$
\widehat{\mathbf{w}}_{\mathrm{LS}} = \arg\min_{\mathbf{w}} |\mathbf{y} - \mathbf{Xw}|^2 . \tag{2.3.3}
$$

The solution to this minimization problem is

$$
\widehat{\mathbf{w}}_{\mathrm{LS}} = \left(\mathbf{X}^H \mathbf{X}\right)^{-1} \mathbf{X}^H \mathbf{y} = \mathbf{X}^\dagger \mathbf{y}. \tag{2.3.4}
$$

The quantity $\mathbf{X}^\dagger = \left(\mathbf{X}^H \mathbf{X}\right)^{-1} \mathbf{X}^H$ is the Moore-Penrose pseudo-inverse of the matrix $\mathbf{X}$. If the random variables $\mathbf{x}$ and y are Gaussian distributed, the least squares solution is the maximum likelihood solution.

The MMSE framework can also be used to estimate $\mathbf{w}$ for a random vector $\mathbf{y}$ and random matrix $\mathbf{X}$ which are related by

$$
\mathbf{y} = \mathbf{w}^H \mathbf{X} + \boldsymbol{\nu},
$$

where $\boldsymbol{\nu}$ is a vector of random noise. Using the mean squared error cost function, the

43

minimization problem in this case is

$$\mathbf{w}_{\text{MMSE}} = \arg\min_{\mathbf{w}_{\text{est}}} \text{E}\{|\mathbf{y} - \mathbf{w}_{\text{est}}^H \mathbf{X}|^2\}. \tag{2.3.5}$$

and the solution is

$$\mathbf{w}_{\text{MMSE}} = \text{E}\{\mathbf{X}\mathbf{X}^H\}^{-1}\text{E}\{\mathbf{X}\mathbf{y}^*\}. \tag{2.3.6}$$

Notice that eq. (2.3.6) has the same form as eq. (2.3.2) with the matrix $\mathbf{X}$ and vector $\mathbf{y}$ from eq. (2.3.6) replacing the vector $\mathbf{x}$ and scalar y in eq. (2.3.2).

In many situations, one will have a least-squares solution and new data will arrive (*e.g.* $\mathbf{x}_{N+1}$). Given a new observation, the new least squares solution which incorporates the new data can be computed efficiently without recomputing the whole solution. One particularly effective method for computing a data-recursive least-squares solution is the recursive-least-squares (RLS) algorithm.

2.3.2 Recursive least squares (RLS) filtering algorithm

The statistics of the underwater channel are often not available and there is not yet an agreed upon model of the time variation of the underwater acoustic communication channel. The underwater channel is often assumed to be varying "reasonably" slowly so that the time-varying channel impulse response coefficients can be tracked. This assumption enables the use of the exponentially weighted recursive least-squares (EW-RLS) algorithm for estimating the channel or equalizer coefficients. This algorithm is a balance between computational complexity and effectiveness since it can track a time-varying channel effectively with reasonable complexity, $\text{O}(N^2)$, where the quantity of interest has N parameters (either the channel impulse response or the equalizer coefficients). The notation $\text{O}(\cdot)$ refers to the highest order of the computation complexity.

The EW-RLS algorithm provides an effective way to estimate the ensemble expectations in the solution to the LSE equalizer equations. This section briefly covers the algorithm with a quick derivation and a focus on the practical details for the

44

underwater channel. For more of the algorithmic details, Haykin [36] and Sayed [86] are excellent resources.

The EW-RLS algorithm approximates the expectations in the MMSE solution with time-averaged functions of the data,

$$\widehat{\mathbf{R}}_{\mathbf{x}}[n] \;\; = \;\; \widehat{\mathbf{P}}^{-1} = \sum_{i=0}^{n} \lambda^{n-i} \mathbf{x}[i] \mathbf{x}[i]^H + \delta \lambda^{n+1} \mathbf{I} \qquad (2.3.7)$$

$$\widehat{\mathbf{r}}_{\mathbf{x}y}[n] \;\; = \;\; \sum_{i=0}^{n} \lambda^{n-i} \mathbf{x}[i] y[i]^*. \qquad (2.3.8)$$

In these equations, λ is the exponential weighting factor, $0 < \lambda < 1$. The term $\delta \lambda^N \mathbf{I}$ is added to the denominator term for regularization so the algorithm is initially well behaved (δ is a system design parameter). This algorithm provides a computationally efficient data-recursive method for updating the parameter estimates [36]. When a new values $\mathbf{x}[n]$ and $y[n]$ are received, the RLS algorithm for updating the estimates $\widehat{\mathbf{w}}[n-1]$ and $\widehat{\mathbf{P}}[n-1]$ is

$$\widehat{\mathbf{w}}[0] \;\; = \;\; \mathbf{0} \qquad (2.3.9)$$

$$\widehat{\mathbf{P}}[0] \;\; = \;\; \delta^{-1} \mathbf{I} \qquad (2.3.10)$$

$$\boldsymbol{\pi}[n] \;\; = \;\; \widehat{\mathbf{P}}[n-1] \mathbf{x}[n] \qquad (2.3.11)$$

$$\mathbf{k}[n] \;\; = \;\; \frac{\boldsymbol{\pi}[n]}{\lambda + \mathbf{x}^H[n] \boldsymbol{\pi}[n]} \qquad (2.3.12)$$

$$\zeta[n] \;\; = \;\; y[n] - \widehat{\mathbf{w}}^H[n-1] \mathbf{x}[n] \qquad (2.3.13)$$

$$\widehat{\mathbf{w}}[n] \;\; = \;\; \widehat{\mathbf{w}}[n-1] + \mathbf{k}[n] \zeta^*[n] \qquad (2.3.14)$$

$$\widehat{\mathbf{P}}[n] \;\; = \;\; (\mathbf{I} - \mathbf{k}[n] \mathbf{x}^H[n]) \lambda^{-1} \widehat{\mathbf{P}}[n-1]. \qquad (2.3.15)$$

The value of exponential weighting factor determines the size of the data averaging window or *memory* of the algorithm. The memory of the algorithm is approximately $\frac{1}{1-\lambda}$ [29]. A common rule of thumb for the underwater channel is that the algorithm memory should be approximately two to three times the number of coefficients being estimated. For example, when estimating a channel that spans 100 symbols, $\lambda \approx 0.995$ for a window of twice the channel length.

45

The EW-RLS has been shown to converge to the Weiner solution asymptotically when the coefficients, $\mathbf{w}[n]$, are time-invariant and $\lambda \rightarrow 1$ [21]. The cost function that is actually being solved using the EW-RLS algorithm,

$$\widehat{\mathbf{w}}[n] = \arg\min_{\mathbf{w}} \left[\lambda^{n+1} \, \delta \, \mathbf{w}^H \mathbf{w} + \sum_{i=0}^{n} \lambda^{n-i} \left| y[i] - \mathbf{w}^H \mathbf{x}[i] \right|^2 \right], \qquad (2.3.16)$$

is slightly different from the cost function for the MMSE estimation problem [86]. The EW-RLS algorithm can also be written as a constrained form of the Kalman filter [87, 88].

2.4   Equalization

An equalizer is a structure used to mitigate ISI and channel distortions in the received signal. This thesis focuses on two particular types of equalizers: the linear equalizer (LE) and the decision feedback equalizer (DFE). The coefficients for both of these equalizer structures can be found using a least-squares type of optimization criterion. The output of the equalizer filter is an estimate of the transmitted symbol,

$$\tilde{d}[n] = \mathbf{h}^H[n]\mathbf{z}[n]. \qquad (2.4.1)$$

The vector $\mathbf{z}[n]$ either contains only received signal samples (for the LE) or received signal samples and estimates of past data symbols (for the DFE). An example of both the LE and the DFE are shown in Figure 2.4.1.

The cost function which is minimized to find the equalizer coefficients is

$$J(\mathbf{h}) = \mathrm{E}\{|\mathbf{h}^H \mathbf{z} - d|^2\}, \qquad (2.4.2)$$

and the optimization problem to find the MMSE equalizer coefficients, $\widehat{\mathbf{h}}_{\mathrm{opt}}[n]$, is represented as

$$\mathbf{h}_{\mathrm{opt}} = \arg\min_{\tilde{\mathbf{h}}} \mathrm{E}\{|\tilde{\mathbf{h}}^H \mathbf{z} - d|^2\}. \qquad (2.4.3)$$

46
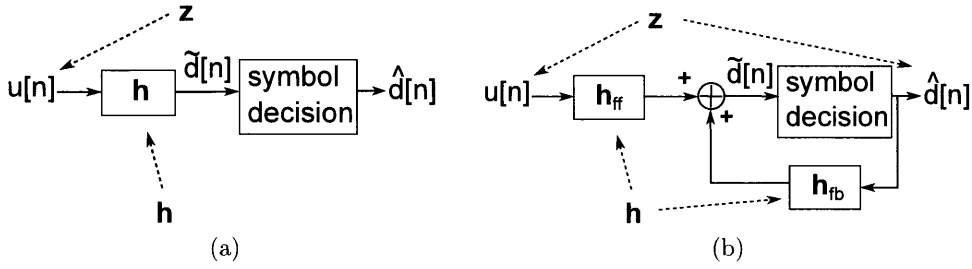
Figure 2.4.1: Illustration of the (a) linear equalizer and (b) decision feedback equalizer with the quantities **h** and **z** labeled.

The solution to this minimization is

$$\mathbf{h}_{\text{opt}}[n] = \mathbf{R_z}^{-1}[n]\mathbf{r}_{\mathbf{z}d}[n], \qquad (2.4.4)$$

where $\mathbf{R_z}[n] = \mathrm{E}\{\mathbf{zz}^H\}$ and $\mathbf{r}_{\mathbf{z}d} = \mathrm{E}\{\mathbf{z}d^*\}$. Solving for the equalizer by directly estimating $\mathbf{R_z}$ and $\mathbf{r}_{\mathbf{z}d}$ from the received signal and possible past data estimates is referred to as *Direct Adaptation* equalization (DA). Assuming the expectations are conditioned on a known channel, eq. (2.2.5) can be substituted into eq. (2.4.4) to reduce the solution to a function of the channel impulse response values and the noise statistics. This method is referred to as the channel estimate based (CEB) method of equalization. In the following subsections, the coefficients for the DA and CEB methods of both the LE and DFE are derived.

2.4.1 Linear equalizer (LE)

The linear equalizer uses a linear combination of the received signal samples to create an estimate of the transmitted symbol. This structure tends to have low computational complexity, so is often used in computation limited environments such as embedded systems. The LE algorithm is a natural place to start theoretical derivations due to its simple form.

The performance of the LE algorithm suffers when there are nulls in the channel frequency response [36]. The LE algorithm attempts to invert the nulls, and in doing so greatly amplifies the noise power at the nulls which degrades equalizer performance.

47

This behavior makes the LE algorithm less than ideal for frequency selective channels.

The coefficients of the LE can be found using eq. (2.4.1) by setting $\mathbf{z}[n]$ equal to the vector of received signal samples, $\mathbf{u}[n]$,

$$\mathbf{z}[n] = [u[n - L_c + 1] \ \ldots \ u[n] \ \ldots \ u[n + L_a]]^T = \mathbf{u}[n]. \tag{2.4.5}$$

The number of equalizer coefficients is $(L_a + L_c)r_{\text{fs}}$ where L_a and L_c are the number of acausal and causal equalizer taps respectively and r_{fs} is the number of samples per symbol (the fractional sampling rate). Substituting the expression for $\mathbf{z}[n]$ from eq. (2.4.5) into eq. (2.4.4) produces the expression for the LE coefficients,

$$\mathbf{h}_{\text{opt}} = \mathbf{h}_{\text{lin}} = \mathrm{E}\{\mathbf{u}[n]\mathbf{u}^H[n]\}^{-1}\mathrm{E}\{\mathbf{u}[n]d^*[n]\}. \tag{2.4.6}$$

In this equation, $\mathbf{R_u} = \mathrm{E}\{\mathbf{u}[n]\mathbf{u}^H[n]\}$ is the received signal autocorrelation matrix and $\mathbf{r}_{\mathbf{u}d} = \mathrm{E}\{\mathbf{u}[n]d^*[n]\}$ is the cross correlation vector between the received-signal and the transmitted-symbol. When the statistics are not known, the expectations must be estimated form the available data. Using an exponentially weighted window, the estimates of these quantities are of the form

$$\widehat{\mathbf{R}}_{\mathbf{u}}[n] = \delta^n \mathbf{I} + \sum_{i=0}^{n} \lambda^{n-i}\mathbf{u}[i]\mathbf{u}^H[i] \tag{2.4.7}$$

$$\widehat{\mathbf{r}}_{\mathbf{u}d}[n] = \sum_{i=0}^{n} \lambda^{n-i}\mathbf{u}[i]d^*[i], \tag{2.4.8}$$

where λ is the exponential weighting factor. The regularization term, $\delta^n \mathbf{I}$, is included to ensure the matrix is well conditioned. Using the estimated autocorrelation matrix and cross-correlation vector is the DA method of linear equalization. The EW-RLS algorithm provides an computationally efficient, data-recursive method for updating the equalizer coefficients.

An alternative to using these estimated quantities is to use the channel model from eq. (2.2.5). The expectation in eq. (2.4.6) can be evaluated conditioned on knowing

48

the true channel, *i.e.*

$$\mathbf{h}_{\text{opt}} = \mathbf{h}_{\text{lin}} = E\{\mathbf{u}[n]\mathbf{u}^H[n]|\mathbf{G}[n]\}^{-1}E\{\mathbf{u}[n]d^*[n]|\mathbf{G}[n]\}.$$

Conditioning on the known channel coefficients will be implicit for the remainder of the thesis and not explicitly included in the expectation terms for brevity. Using the channel model from eq. (2.2.5) in eq. (2.4.6), the expression for the LE coefficients becomes

$$\mathbf{h}_{\text{lin}}[n] = [\mathbf{G}^H[n]\mathbf{G}[n] + \mathbf{R}_\nu]^{-1}\mathbf{G}^H[n]\mathbf{s}. \tag{2.4.9}$$

In the above relation, $\mathbf{s}$ is a selection vector, the same length as $\mathbf{d}[n]$, that selects the row of the channel convolution matrix, $\mathbf{G}[n]$, corresponding to the data symbol being estimated. This row is referenced using the symbol $\mathbf{g}_0^*[n]$. The selection vector is $\mathbf{s} = [0\ 0\ \ldots\ 1\ \ldots\ 0\ 0]^T$, where the 1 is located at the symbol being estimated, $d[n]$, in the transmitted symbol vector $\mathbf{d}[n]$.

One rarely has access to the true channel impulse response coefficients, and so the channel is estimate from the received data. When a channel estimate, $\widehat{\mathbf{G}}[n]$ is used in place of the true channel to compute the equalizer coefficients, this is the CEB method of linear equalization.

The error in estimating the transmitted data after equalization, $e_{\text{LE}}[n]$, is referred to as the *soft decision error* (SDE),

$$e_{\text{LE}}[n] = \mathbf{h}_{\text{lin}}^H\mathbf{u} - d. \tag{2.4.10}$$

The *mean squared error* (MSE) is the expectation square of the absolute value of the SDE,

$$\text{MSE} = E\{|e_{\text{LE}}[n]|^2\}. \tag{2.4.11}$$

The term MSE will also be used to refer to the time averaged observed squared error

49
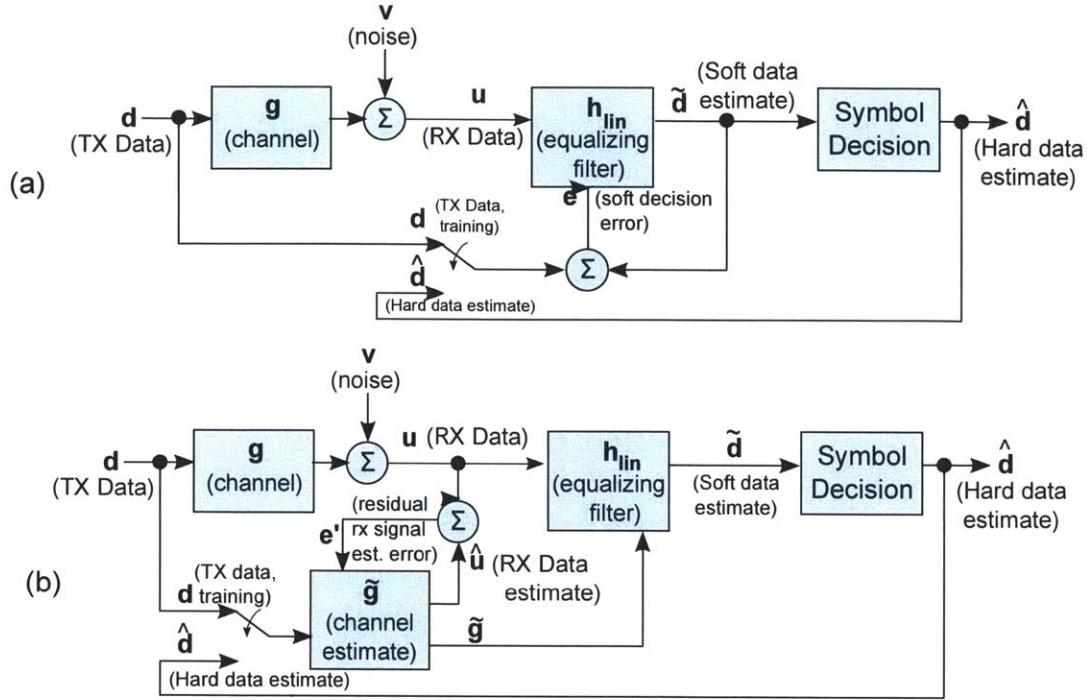
Figure 2.4.2: Schematic representation of LE methods: (a) Direct Adaptation (b) Channel Estimate Based

where the expectation is replaced with an empirical average,

$$\widehat{\mathrm{MSE}} = \frac{1}{M} \sum_{m=1}^{M} |e_{\mathrm{LE}}[m]|^2.$$

The *minimum achievable error* (MAE) is found by substituting eq. (2.2.5) and eq. (2.4.9) into eq. (2.4.11). The expression for the MAE is

$$\mathrm{MAE} = \sigma_{0,lin}^2[n] = 1 - \mathbf{g}_0^T[n][\mathbf{G}^H[n]\mathbf{G}[n] + \mathbf{R}_{\boldsymbol{\nu}}]^{-1}\mathbf{g}_0^*[n]. \tag{2.4.12}$$

2.4.2 Decision feedback equalizer (DFE)

A DFE consists of two linear filters working in concert: a feedforward section that filters the received signal and a feedback section that filters past data symbol estimates. The purpose of the feedforward filter is to collect energy and shape the response of the received signal. The feedback filter is used to cancel causal ISI by removing inter-

50

ference from past received data symbols from the received signal. By removing the causal ISI, the feedback filter increases the effective signal-to-interference-plus-noise ratio (SINR). This is one reason a DFE outperforms a LE. The sum of output of the feedforward ad feedback filters gives an estimate of the transmitted symbol. Proakis [79] and Qureshi [81] are good references for an overview of the DFE algorithm.

The feedforward and feedback equalizer coefficients are labelled respectively as $\mathbf{h}_{ff}$ and $\mathbf{h}_{fb}$. For the DFE, $\mathbf{z}[n]$ and $\mathbf{h}[n]$ from eq. (2.4.4) are defined as

$$\mathbf{z}[n] = \left[u[n-Lc+1] \ \ldots \ u[n+L_a], \ \widehat{d}[n-1] \ \ldots \ \widehat{d}[n-L_{fb}] \right]^T \quad (2.4.13)$$

$$\mathbf{h}[n] = \begin{bmatrix} \mathbf{h}_{ff}[n] \\ \mathbf{h}_{fb}[n] \end{bmatrix}, \quad (2.4.14)$$

where $\widehat{d}[m]$ is the estimated transmitted data at time m and L_{fb} is the number of feedback equalizer coefficients. Using the above definitions for $\mathbf{z}$ and $\mathbf{h}$ in eq. (2.4.9), the optimal DFE coefficients are

$$\mathbf{h}_{\mathrm{DFE}} = \begin{bmatrix} \mathbf{h}_{ff}[n] \\ \mathbf{h}_{fb}[n] \end{bmatrix} = \mathrm{E}\{\mathbf{z}\mathbf{z}^H\}^{-1}\mathrm{E}\{\mathbf{z}d^*\}, \quad (2.4.15)$$

where $\mathbf{R_z} = \mathrm{E}\{\mathbf{z}[n]\mathbf{z}^H[n]\}$ is the autocorrelation matrix of $\mathbf{z}[n]$ and $\mathbf{r}_{\mathbf{z}d} = \mathrm{E}\{\mathbf{z}[n]d^*[n]\}$ is the cross-correlation vector between elements of $\mathbf{z}[n]$ and the transmitted data symbol. Using an exponentially weighted window, the estimates of these quantities are of the form

$$\widehat{\mathbf{R}}_{\mathbf{z}}[n] = \delta^n \mathbf{I} + \sum_{i=0}^{n} \lambda^{n-i} \mathbf{z}[i]\mathbf{z}^H[i] \quad (2.4.16)$$

$$\widehat{\mathbf{r}}_{\mathbf{z}d}[n] = \sum_{i=0}^{n} \lambda^{n-i} \mathbf{z}[i]d^*[i] \quad (2.4.17)$$

where λ is again the exponential weighting factor. When the estimated auto-correlation matrix and cross-correlation vector is used, this is known as the DA-DFE algorithm.

In a DFE, previously estimated transmitted data symbols are used to estimate

51

the current symbol. The rows of the channel convolution matrix, $\mathbf{G}[n]$, corresponding to the symbols that are used in the feedback stage of the DFE are assembled into a new matrix, labeled $\mathbf{G}_{\mathrm{fb}}[n]$. Rows corresponding to symbols not used in the feedback portion are placed in a matrix $\mathbf{G}_0[n]$, referred to as the reduced channel convolution matrix. If all of the previously estimated symbols are used in the feedback stage, the channel convolution matrix can be separated as

$$\mathbf{G}[n] = \begin{bmatrix} \mathbf{G}_{\mathrm{fb}}[n] \\ \mathbf{G}_0[n] \end{bmatrix}. \qquad (2.4.18)$$

Other matrices are introduced which have the same dimensions as the channel convolution matrix. These matrices will typically be added to the channel convolution matrix during different derivations. To simplify notation, the subscript '$_{\mathrm{fb}}$' will refer to columns of these matrices in the same positions as the columns of the channel convolution matrix which correspond to symbols which are used in for feedback. The subscript '$_0$' will refer to the reduced matrix comprised of the remaining columns.

The channel model from eq. (2.2.5) can be used to create an alternative to the estimate from eq. (2.4.15). Using the separation of the channel convolution matrix in eq. (2.4.18), the channel model becomes

$$\mathbf{u}[n] = \mathbf{G}^H[n]\mathbf{d}[n] + \boldsymbol{\nu}[n] = \mathbf{G}_0^H[n]\mathbf{d}_0[n] + \mathbf{G}_{\mathrm{fb}}^H[n]\mathbf{d}_{\mathrm{fb}}[n] + \boldsymbol{\nu}[n], \qquad (2.4.19)$$

where $\mathbf{d}_{\mathrm{fb}}[n]$ correspond to the transmitted symbol positions used in the feedback section. The remainder of the symbols from $\mathbf{d}[n]$ are assembled in $\mathbf{d}_0[n]$. The DFE coefficients can be expressed as a function of the channel coefficients by substituting eq. (2.4.19) into eq. (2.4.15). The expressions for the feed forward and feedback coefficients are [75]

$$\mathbf{h}_{\mathrm{ff}}[n] = [\mathbf{G}_0^H[n]\mathbf{G}_0[n] + \mathbf{R}_{\boldsymbol{\nu}}]^{-1}\mathbf{G}^H[n]\mathbf{s} \qquad (2.4.20)$$

$$\mathbf{h}_{\mathrm{fb}}[n] = -\mathbf{G}_{\mathrm{fb}}^H[n]\mathbf{h}_{\mathrm{ff}}[n]. \qquad (2.4.21)$$
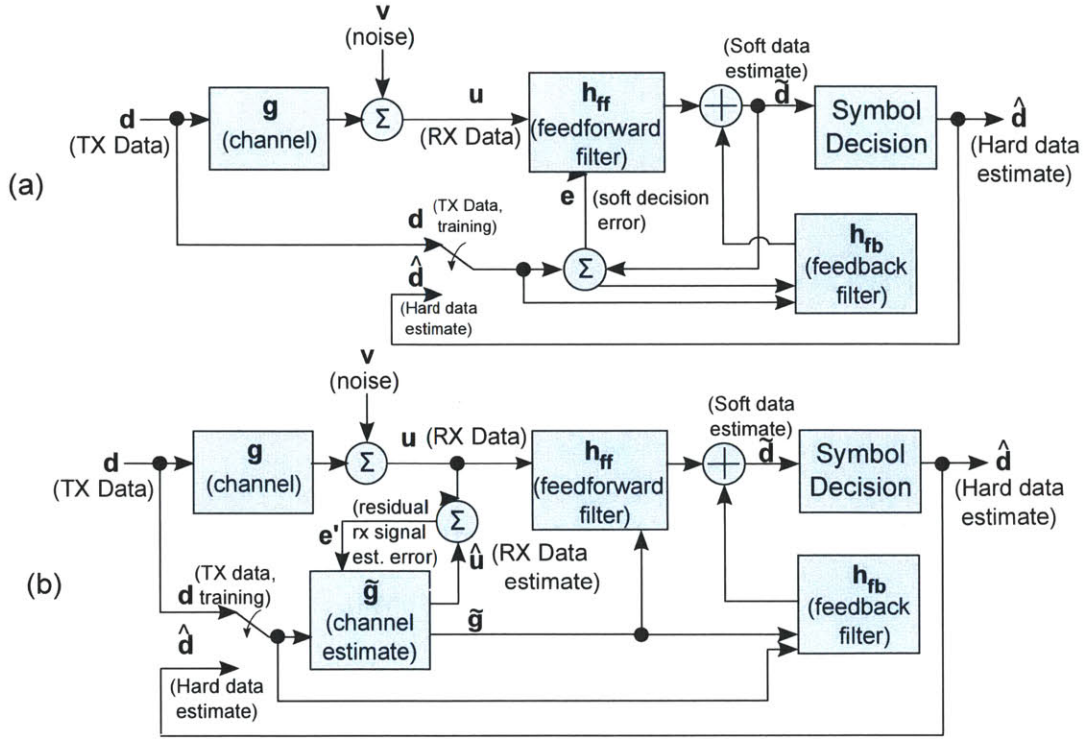
Figure 2.4.3: Schematic representation of DFE methods: (a) Direct Adaptation (b) Channel Estimate Based

The CEB method for estimating the DFE coefficients involves using channel estimates to build the channel convolution matrices in eq. (2.4.20). Figure 2.4.3 shows both the DA and the CEB forms of the DFE. For the DFE the soft decision error is

$$e_{\text{DFE}}[n] = \mathbf{h}_{\text{DFE}}^{H}[n]\mathbf{z}[n] - d[n] = \mathbf{h_{ff}}^{H}[n]\mathbf{u}[n] + \mathbf{h_{fb}}^{H}[n]\widehat{\mathbf{d}}_{\text{fb}}[n] - d[n]. \qquad (2.4.22)$$

Given $\mathbf{g}_0[n] = \mathbf{G}^{H}[n]\mathbf{s}$, the MAE is

$$\sigma_{0,dfe}^{2}[n] = \mathrm{E}\{|e_{\text{DFE}}[n]|^{2}\} = 1 - \mathbf{g}_0^{T}[n][\mathbf{G}_0^{H}[n]\mathbf{G}_0[n] + \mathbf{R}_{\boldsymbol{\nu}}]^{-1}\mathbf{g}_0^{*}[n], \qquad (2.4.23)$$

The MAE is usually not achieved when the channel is unknown and must be estimated. In this case, the MSE is

$$\mathrm{MSE} = \mathrm{E}\{|e_{\text{DFE}}[n]|^{2}\}.$$

53

Since the statistics of the error are generally not known, they must be estimated from the data. The averaged observed error,

$$\widehat{\text{MSE}} = \frac{1}{M} \sum_{m=1}^{M} |e_{\text{DFE}}[n]|^2,$$

is also referred to as the MSE.

The MAE of the LE with the MAE of the DFE can be compared by substituting the channel convolution matrix from eq. (2.4.19) into eq. (2.4.12), which gives the expression (time indexes dropped for clarity)

$$\sigma_{0,lin}^2 = 1 - \mathbf{s}^H \mathbf{G} [\mathbf{G}_0^H \mathbf{G}_0 + \mathbf{G}_{\text{fb}}^H \mathbf{G}_{\text{fb}} + \mathbf{R}_\nu]^{-1} \mathbf{G}^H \mathbf{s} \qquad (2.4.24)$$

$$= \sigma_{0,dfe}^2 + \mathbf{h}_{\text{ff}}^H [\mathbf{I} + \mathbf{W}\mathbf{Q}^{-1}]^{-1} \mathbf{W} \mathbf{h}_{\text{ff}}. \qquad (2.4.25)$$

In this relation, $\mathbf{W} = \mathbf{G}_{\text{fb}}^H \mathbf{G}_{\text{fb}}$, $\mathbf{Q} = \mathbf{G}_0^H \mathbf{G}_0 + \mathbf{R}_\nu$, and $\mathbf{h}_{\text{ff}}$ is eq. (2.4.20). Both $\mathbf{R}_\nu$ and $\mathbf{G}_0^H \mathbf{G}_0$ are Hermitian and positive-definite (assuming $\mathbf{G}_0 \neq \mathbf{0}$), so $\mathbf{Q}$ is positive definite. $\mathbf{W}$ is a positive semi-definite matrix equal to zero when $\mathbf{G}_{\text{fb}} = 0$.

$$\mathbf{h}_{\text{ff}}^H [\mathbf{I} + \mathbf{W}\mathbf{Q}^{-1}]^{-1} \mathbf{W} \mathbf{h}_{\text{ff}} \geq 0.$$

Thus, the MAE of the DFE is always less than the MAE of the LE, except when either $\mathbf{G}_{\text{fb}} = 0$ or the feedforward equalizer coefficients are in the null space of $\mathbf{G}_{\text{fb}}$, which is not common.

2.5   Channel estimation

The underwater channel is well modeled by a finite number of linear coefficients. When all of the statistics of the transmitted and received data are known, these coefficients can be estimated using (linear) MMSE methods. Assuming the channel coefficients are time invariant, the MMSE channel coefficients are a solution to the optimization problem

$$\mathbf{g}_{\text{opt}} = \arg \min_{\mathbf{g}} \text{E}\{|\mathbf{g}^H \mathbf{d}[n] - u[n]|^2\}, \qquad (2.5.1)$$

where $\mathbf{d}[n]$ is a vector of transmitted data, $u[n]$ is the received data, and $\mathbf{g}$ are the channel coefficients. The solution to this optimization has the form

$$\mathbf{g}_{\text{MMSE}} = \mathbf{R_d}^{-1} \mathbf{r_{d}u}, \qquad (2.5.2)$$

where

$$\mathbf{R_d} = \text{E}\{\mathbf{d}[n]\mathbf{d}^H[n]\} \qquad (2.5.3)$$

$$\mathbf{r_{d}u} = \text{E}\{\mathbf{d}[n]u^*[n]\}. \qquad (2.5.4)$$

In practice, the statistics of the transmitted and received data are not known fully and must be estimated. A method known as least squared error (LSE) channel estimation is often used. In this method the true expectations are replaced with the observed time-averages. As the number of samples increases, the time-averages will converge to the true solution. Therefore, when the channel is time-invariant and a sufficient number of channel observations are available, MMSE and LSE channel estimation are practically equivalent.

After N symbols have been received, the LSE channel estimate has the form

$$\widehat{\mathbf{g}}_{\text{LSE}} = \widehat{\mathbf{R}}_{\mathbf{d}}^{-1} \widehat{\mathbf{r}}_{\mathbf{d}u}, \qquad (2.5.5)$$

where

$$\widehat{\mathbf{R}}_{\mathbf{d}} = \frac{1}{N} \sum_{i=1}^{N} \mathbf{d}[i]\mathbf{d}^{H}[i] \tag{2.5.6}$$

$$\widehat{\mathbf{r}}_{\mathbf{d}u} = \frac{1}{N} \sum_{i=1}^{N} \mathbf{d}[i]u^{*}[i]. \tag{2.5.7}$$

Using an EW-RLS algorithm, the estimates are

$$\widehat{\mathbf{R}}_{\mathbf{d}} = \delta^{N}\mathbf{I} \sum_{i=1}^{N} \lambda^{N-i}\mathbf{d}[i]\mathbf{d}^{H}[i] \tag{2.5.8}$$

$$\widehat{\mathbf{r}}_{\mathbf{d}u} = \sum_{i=1}^{N} \lambda^{N-i}\mathbf{d}[i]u^{*}[i]. \tag{2.5.9}$$

Scaling factors common to both estimates are not included here since they will eventually cancel out.

Both the MMSE and LSE channel estimators are unbiased. Under the assumption that the noise is zero-mean, the estimate of the channel is also unbiased, even if the number of coefficients in the model differs from the number of channel coefficients in the true channel.

For example, consider the following scenario: the true channel has N coefficients in length and the modeled channel estimator only contains $N-1$ coefficients. The true channel is unknown and time-invariant. If the true channel is written as

$$\mathbf{g}[n] = [g[n,0] \ \ldots \ g[n,N-1]]^{T},$$

the truncated channel is

$$\mathbf{g}'[n] = [g[n,0] \ \ldots \ g[n,N-2]]^{T},$$

and the truncated transmitted data vector is

$$\mathbf{d}'[n] = [d[n-N+2] \ \ldots \ d[n]].$$

56

Using the linear model from eq. (2.2.2) the channel estimate is

$$
\begin{aligned}
\mathbf{g}_{\text{reduced}}[n] &= \mathbf{R}_{\mathbf{d}'}^{-1}\mathbf{r}_{\mathbf{d}'u} \\
&= \mathrm{E}\{\mathbf{d}'[n]\mathbf{d}'^{H}[n]\}^{-1}\mathrm{E}\{\mathbf{d}'[n]u^{*}[n]\} \\
&= \mathbf{I}_{N-1}^{-1}\mathrm{E}\{\mathbf{d}'[n](\mathbf{g}^{H}[n]\mathbf{d}[n] + \nu[n])^{*}\} \\
&= \mathrm{E}\{\mathbf{d}'[n]\mathbf{d}^{H}[n]\mathbf{g}[n]\} + \mathrm{E}\{\mathbf{d}'[n]\nu^{*}[n]\} \\
&= \begin{bmatrix} \mathbf{I}_{N-1} & \mathbf{0}_{N-1\times 1} \\ \mathbf{0}_{1\times N-1} & 0 \end{bmatrix}\mathbf{g}[n] + 0 \\
&= \mathbf{g}'[n] \tag{2.5.10}
\end{aligned}
$$

Therefore, the channel estimate is unbiased (for the modeled parameters) even when the number of channel coefficients in the model differs from the number of channel coefficients in the true channel.

2.6 Summary

In this chapter, topics included difficulties of the underwater channel, linear estimation, equalization, and channel modeling. The remainder of this thesis focuses on the DFE where the coefficients are calculated from the data using an EW-RLS algorithm. Effects that are specific to the underwater channel are used to examine and improve the performance of the DFE for underwater channels.

Chapter 3

Effective noise correlation matrix: Equalizer improvements through a structured matrix

3.1 Introduction

Often overlooked in the CEB-DFE formulation is there are two quantities needed to calculate the equalizer coefficients: an estimate of the channel impulse response and an estimate of the effective noise correlation matrix [81]. The effective noise includes both the observation noise and terms due to channel modeling errors. This effective noise correlation matrix is usually approximated as a scaled identity matrix with a scaling equal to the inverse signal to noise ratio (SNR). [79, 91]. For the underwater channel, this turns out to be a poor estimate. Preisig [75] demonstrated theoretically and experimentally that using a full estimate of the effective noise correlation matrix for computing the equalizer coefficients reduces the mean squared error after equalization.

In a shallow water communication channel, neighboring channel impulse response coefficients often exhibit correlated fluctuation [103]. Figure 3.1.1 shows an example of a measured time-varying impulse response from the surface processes and acoustic communication experiment (SPACE08) in 2008. Notice that the amplitudes of
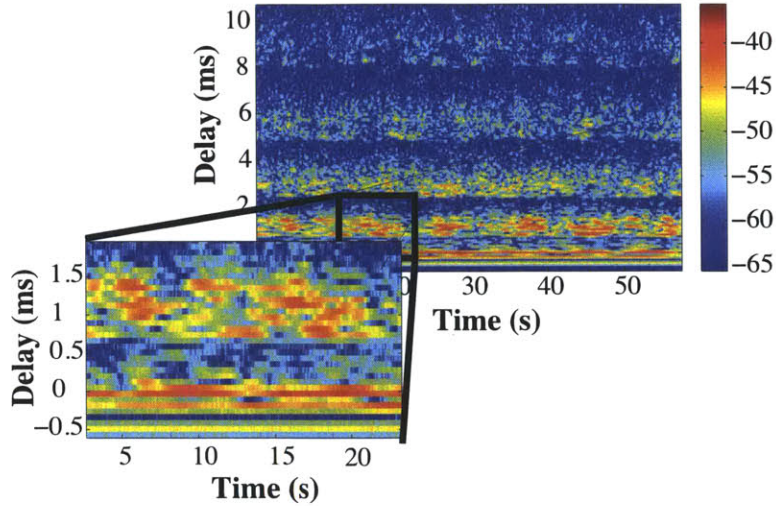
Figure 3.1.1: The magnitude of an estimated channel impulse response at 1 km from the transmitter (SPACE08 experiment).

neighboring channel coefficients rise and fall together in time.

The work presented in this chapter shows that correlated fluctuations are responsible for the effective noise correlation matrix having a non-diagonal structure. The correlation matrix is shown to be well approximated by a Toeplitz matrix, which leads to a computationally efficient algorithm for computing the DFE filter coefficients.

3.2 Channel estimate based DFE

The DFE is widely used in the underwater environment because it is a computationally tractable way to mitigate channel effects [110]. Recall from Section 2.4 that the coefficients of the decision feedback equalizer have the form

$$\mathbf{h}_{\text{ff}}[n] = (\mathbf{G}_0^H[n]\mathbf{G}_0[n] + \sigma_d^{-2}\mathbf{R}_v)^{-1}\mathbf{g}_0 \tag{3.2.1}$$

$$\mathbf{h}_{\text{fb}}[n] = -\mathbf{G}_{\text{fb}}^H[n]\mathbf{h}_{\text{ff}}[n]. \tag{3.2.2}$$

Figure 3.2.1 shows a block diagram of the structure of the CEB-DFE, where estimates of the channel are used in place of the true (unknown) channel.

For terrestrial RF communication systems, the observation noise, $\boldsymbol{\nu}[n]$, is assumed

60
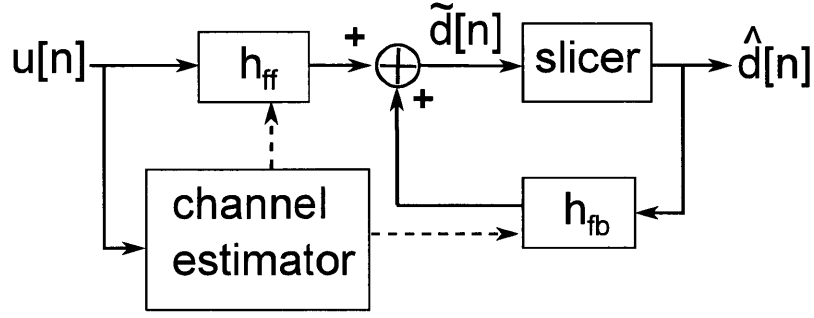
Figure 3.2.1: Illustration of the structure of a CEB-DFE.

to be a stationary, zero-mean, white noise process with variance σ_ν^2 [79]. This implies that the observation noise correlation matrix, $\sigma_d^{-2}\mathbf{R}_\nu$ is a scaled identity matrix [91], such that $\mathbf{R}_v = \rho\mathbf{I}$, where ρ is defined as the inverse SNR,

$$\rho = \frac{\sigma_\nu^2}{\sigma_\mathrm{d}^2}. \tag{3.2.3}$$

3.3 Structure of the effective noise correlation matrix

In underwater communication systems the channel coefficients are rarely known a-priori and must be estimated from the received data. Due to observation noise and the time-variability of the channel, the estimate of the channel usually contains some error. This estimation error can be represented as

$$\mathbf{G}[n] = \widehat{\mathbf{G}}[n-1] + \mathbf{\Gamma}[n], \tag{3.3.1}$$

where $\widehat{\mathbf{G}}[n-1]$ is the estimate of the channel convolution matrix using data up until time $n-1$ and $\mathbf{\Gamma}[n]$ is the error in the estimate. Using this model, the received data

61

vector can be rewritten as

$$\begin{aligned}
\mathbf{u}[n] &= \mathbf{G}^H[n]\mathbf{d}[n] + \boldsymbol{\nu}[n] \\
&= \widehat{\mathbf{G}}^H[n-1]\mathbf{d}[n] + \boldsymbol{\Gamma}^H[n]\mathbf{d}[n] + \boldsymbol{\nu}[n] \\
&= \widehat{\mathbf{G}}^H[n-1]\mathbf{d}[n] + \boldsymbol{\mu}[n],
\end{aligned} \tag{3.3.2}$$

where $\boldsymbol{\mu}[n]$ is the effective noise,

$$\boldsymbol{\mu}[n] = \boldsymbol{\Gamma}^H[n]\mathbf{d}[n] + \boldsymbol{\nu}[n]. \tag{3.3.3}$$

The first term in the effective noise includes noise due to channel estimation errors and the second term is the observation noise.

In much of the literature on equalization the effective noise is modeled as a scaled identity matrix. Preisig [75] demonstrated that the performance of a DFE can be greatly improved by calculating the equalizer coefficients using an estimate of the correlation matrix of the effective noise computed from the signal estimation residual error. Assuming that the transmitted data symbols are IID with variance σ_d^2, the effective noise correlation matrix, $\mathbf{R}_{\boldsymbol{\mu}}$, is

$$\begin{aligned}
\mathbf{R}_{\boldsymbol{\mu}}[n] &= \mathrm{E}\{\boldsymbol{\mu}[n]\boldsymbol{\mu}^H[n]\} \\
&= \mathrm{E}\{(\boldsymbol{\Gamma}^H[n]\mathbf{d}[n] + \boldsymbol{\nu}[n])(\boldsymbol{\Gamma}^H[n]\mathbf{d}[n] + \boldsymbol{\nu}[n])^H\} \\
&= \sigma_{\mathrm{d}}^2\mathbf{R}_{\boldsymbol{\Gamma}}[n] + \mathbf{R}_{\boldsymbol{\nu}}[n],
\end{aligned} \tag{3.3.4}$$

where

$$\mathbf{R}_{\boldsymbol{\Gamma}}[n] = \mathrm{E}\{\boldsymbol{\Gamma}^H[n]\boldsymbol{\Gamma}[n]\} \tag{3.3.5}$$

is the channel estimation error correlation matrix.

When the MMSE channel estimate is used, the error is zero-mean and uncorrelated with the estimator. The feedforward and feedback DFE equalizer coefficients can be

written as

$$\widehat{\mathbf{h}}_{ff}[n] = (\widehat{\mathbf{G}}_0^H[n-1]\widehat{\mathbf{G}}_0[n-1] + \mathbf{R}_\Gamma[n] + \sigma_d^{-2}\mathbf{R}_v[n])^{-1}\mathbf{g}_0$$

$$\widehat{\mathbf{h}}_{fb}[n] = -\widehat{\mathbf{G}}_{fb}^H[n-1]\widehat{\mathbf{h}}_{ff}[n]. \qquad (3.3.6)$$

The errors for the entire channel convolution matrix are contained in $\mathbf{R}_\Gamma$, so the effect of channel estimation errors in the feedback equalizer coefficients are contained in the term $\mathbf{h}_{ff}$.

The feedback equalizer coefficients have the same form as before with the estimate used in place of the true channel coefficients. An additional term has appeared in the feedforward equalizer coefficients that is a product of the channel convolution matrix error terms. The next section analyzes the structure of the channel convolution error matrix and explains why there are off-diagonal terms in the underwater channel.

3.4 Why there are off-diagonal terms in the effective noise correlation matrix

In much of the equalization literature the effective noise correlation matrix is modeled as a scaled identity matrix, where the scaling is (approximately) the inverse SNR. In underwater communication systems, the mean squared error of the estimated data symbols after DFE equalization is increased by using this approximation [75]. The physical cause of the off-diagonal terms has not previously been shown. In this section, statistical analysis is provided which indicates that the off-diagonal terms are caused by correlated fluctuations of neighboring channel impulse response coefficients.

3.4.1 Using the Markov channel model for noise analysis

To obtain analytical results, the dynamics of the channel impulse response coefficients are assumed to follow a first-order Markov model,

$$\mathbf{g}[n+1] = \alpha\mathbf{g}[n] + \boldsymbol{v}[n+1], \qquad (3.4.1)$$

63

where α is a scalar model parameter with $|\alpha| < 1$ and all vectors are $N \times 1$, where $N = N_a + N_c$ is the channel length (as defined in Section 2.2). The process noise vector, $\boldsymbol{v}[n]$, has a correlation matrix defined as

$$\mathbf{R}_v = \mathrm{E}\{\boldsymbol{v}[n]\boldsymbol{v}^H[n]\}.$$

When analyzing the structure of the effective noise correlation matrix, two types of error can be defined: the effective noise, $\mu[n]$, and the channel estimation error, $\boldsymbol{\gamma}$.

Recall that the effective noise, $\mu[n]$, is the difference between the actual received signal and estimate of the received signal using a channel estimate based upon data up to and including time $n - 1$,

$$\mu[n] = u[n] - \widehat{u}[n]$$
$$= u[n] - \widehat{\mathbf{g}}^H[n-1]\mathbf{d}'[n]. \tag{3.4.2}$$

In the literature, the effective noise is also known as the received data prediction error [66] since the channel model can be thought of as a prediction filter. The channel estimate, $\widehat{\mathbf{g}}^H[n-1]$, is found using an EW-RLS estimation algorithm. The time index of the channel estimate is $[n-1]$ since only transmitted symbols up until time $n-1$ is used in the channel estimate.

Using the channel model from eq. (2.2.2),

$$u[n] = \mathbf{g}^H[n]\mathbf{d}'[n] + \nu[n],$$

the effective noise eq. (3.4.2) can be rewritten as

$$\mu[n] = \mathbf{g}^H[n]\mathbf{d}'[n] + v[n] - \widehat{\mathbf{g}}^H[n-1]\mathbf{d}'[n]$$
$$= (\mathbf{g}[n] - \widehat{\mathbf{g}}[n-1])^H\mathbf{d}'[n] + \nu[n]$$
$$= \boldsymbol{\gamma}^H[n]\mathbf{d}'[n] + \nu[n]. \tag{3.4.3}$$

64

The term, $\boldsymbol{\gamma}[n]$ is the *a priori* channel estimation error,

$$\boldsymbol{\gamma}[n] = \mathbf{g}[n] - \widehat{\mathbf{g}}[n - 1]. \tag{3.4.4}$$

Nadakuditi and Preisig [65, 66, 75] noted that the channel coefficients and channel estimation error could be modeled using an extended state space model,

$$\begin{bmatrix} \mathbf{g}[n] \\ \boldsymbol{\gamma}[n] \end{bmatrix} = \begin{pmatrix} \alpha\mathbf{I} & \mathbf{0} \\ (\alpha - 1)\mathbf{I} & \mathbf{I} - \widehat{\mathbf{k}}[n - 1]\mathbf{d}^H[n - 1] \end{pmatrix} \begin{bmatrix} \mathbf{g}[n - 1] \\ \boldsymbol{\gamma}[n - 1] \end{bmatrix}$$
$$+ \begin{pmatrix} \boldsymbol{\nu}[n] \\ \boldsymbol{\nu}[n] - \widehat{\mathbf{k}}[n - 1]v[n] \end{pmatrix}. \tag{3.4.5}$$

The adaptation gain vector, $\widehat{\mathbf{k}}[n]$, is defined as

$$\widehat{\mathbf{k}}[n] = \left(\sum_{i=1}^{n} \lambda^{n-i} \mathbf{d}[i]\mathbf{d}^H[i] \right)^{-1} \mathbf{d}[n] \qquad 0 \le \lambda \le 1. \tag{3.4.6}$$

Using direct averaging methods [51], the channel estimation error correlation matrix, $\mathbf{R}_\gamma$, can be approximated as [65, 66]

$$\mathbf{R}_\gamma \approx \mathrm{E}\{\widehat{\mathbf{R}}_\gamma\} = \mathrm{E}\{\boldsymbol{\gamma}[n]\boldsymbol{\gamma}^H[n]\}$$
$$= \chi(\alpha, \lambda)\mathbf{R}_{\boldsymbol{v}} + \beta(\lambda)\rho\mathbf{I}. \tag{3.4.7}$$

In these calculations, the observation noise and transmitted data symbols are both assumed to be white with variance σ_ν^2 and σ_d^2 respectively. The symbol ρ is the inverse SNR, $\rho = \sigma_\nu^2/\sigma_d^2$, as in the previous section. The scaling parameters $\chi(\alpha, \lambda)$ and $\beta(\lambda)$ are [66]

$$\chi(\alpha, \lambda) = \frac{(1 - \alpha\lambda)(1 - \alpha^*) + (1 - \alpha^*\lambda)(1 - \alpha)}{(1 - |\alpha|^2)(1 + \lambda)(1 - \alpha\lambda)(1 - \alpha^*\lambda)} \tag{3.4.8}$$

$$\beta(\lambda) = \frac{(1 - \lambda)}{(1 + \lambda)}. \tag{3.4.9}$$

The channel estimation error correlation matrix from eq. (3.4.7) is the sum of two

quantities: $\chi(\alpha, \lambda)\mathbf{R}_v$ and $\beta(\lambda)\rho\mathbf{I}$. The first quantity, $\chi(\alpha, \lambda)\mathbf{R}_v$, is the part of the channel estimation error caused by the time-variability of the channel. This error is sometimes called *lag-error* [31]. The second quantity, $\beta(\lambda)\rho\mathbf{I}$, is the part of the channel estimation error due to the observation noise. For a time-invariant channel, only the second component is present.

Assuming white observation noise, the second quantity in the sum from eq. (3.4.7) is diagonal so the off-diagonal elements must come from the first quantity of the sum, $\chi(\alpha, \lambda)\mathbf{R}_v$. Experimentally, the channel estimation errors tend to dominate the observation noise for the observed range of SNR, so the first quantity in the sum from eq. (3.4.7) is dominant even when the noise is not white. Since, $\chi(\alpha, \lambda)$ is a scaling, the channel process noise correlation matrix, $\mathbf{R}_v$ must contain diagonal elements caused by correlation between channel process noise coefficients. The off-diagonal elements in $\mathbf{R}_\gamma$ are caused by correlations in the channel coefficient process noise. In the next section, this observation is used to show that the off-diagonal elements in the effective noise correlation matrix are caused by correlated changes in the channel coefficients.

3.4.2 Structure of effective noise correlation matrix using Markov channel update model

The effective noise components, $\mu[n]$ from eq. (3.4.2) can be stacked into a vector,

$$\boldsymbol{\mu}[n] = \Big[\mu[n + N_a] \quad \cdots \quad \mu[n] \quad \cdots \quad \mu[n - N_c + 1]\Big]^T. \tag{3.4.10}$$

Recall that in eq. (3.3.3), this effective noise vector is related to the channel estimation error and the observation noise by the relation

$$\boldsymbol{\mu}[n] = \boldsymbol{\Gamma}^H[n]\mathbf{d}[n] + \boldsymbol{\nu}[n].$$

For clarity in this discussion, the columns of $\boldsymbol{\Gamma}[n]$ are labeled as

$$\boldsymbol{\Gamma}[n] = \Big[\boldsymbol{\gamma}_0'[n] \quad \boldsymbol{\gamma}_1'[n] \quad \cdots \quad \boldsymbol{\gamma}_{N-1}'[n]\Big], \tag{3.4.11}$$

where $\boldsymbol{\gamma}_i'[n]$ is the appropriate channel estimation error vector, $\boldsymbol{\gamma}_i[n]$, padded with zeros so $\boldsymbol{\Gamma}[n]$ is a convolution matrix (see Section 2.2 for details of the channel convolution matrix). The $(i,j)^{th}$ element of the $\mathbf{R_\Gamma}[n]$ matrix is

$$\left[\mathbf{R_\Gamma}[n]\right]_{(i,j)} = \mathrm{E}\{\boldsymbol{\gamma}_i'^{H}[n]\boldsymbol{\gamma}_j'[n]\}. \tag{3.4.12}$$

Assuming the process noise, $\boldsymbol{v}$ is stationary, the elements of $\mathbf{R_\Gamma}[n]$ are constant, *i.e.* $\mathbf{R_\Gamma}[n] = \mathbf{R_\Gamma}$. Furthermore, the matrix $\mathbf{R_\Gamma}$ is Toeplitz [75], with the elements of the ith diagonal equal to the sum of the elements of the ith diagonal of $\mathbf{R_\gamma}$ [75]. Assuming the observation noise is white, the off-diagonal terms in the effective noise correlation matrix are due to correlated fluctuations in neighboring channel coefficients.

The next section shows how the assumption of a Toeplitz matrix can be exploited to create an algorithm which both reduces computational complexity and improves performance over previously proposed algorithms.

3.5 Estimating the effective noise correlation matrix

Section 3.3 showed that the effective noise correlation matrix is the sum of observation noise correlation matrix and a term caused by channel estimation errors. Section 3.3 also showed that using the assumptions of a slowly varying channel and stationarity of the observation noise statistics, the effective noise correlation matrix is Toeplitz. The current section provides an algorithm for estimating the entire effective noise correlation matrix by estimating first row and using the Toeplitz-Hermitian structure.

Recall from eq. (3.3.3) that the effective observation noise is the difference between the received signal and the estimated received signal using past transmitted and the estimated channel,

$$\boldsymbol{\mu}[n] = \mathbf{u}[n] - \widehat{\mathbf{G}}^{H}[n-1]\widehat{\mathbf{d}}[n].$$

The previous section showed that the effective noise correlation matrix is approx-

imately Toeplitz, so the effective noise correlation matrix can be constructed using only an estimate of the first column. This estimate can be computed using the biased correlation of the received signal prediction error,

$$\widehat{\mu}_i[n] = \frac{1}{L_{\text{ff}}} \sum_{j=1}^{L_{\text{ff}}-i} \mu^*[n, i+j]\mu[n, j], \quad i = 0, \ldots, L-1, \tag{3.5.1}$$

where $\mu[n, j]$ is the jth element of the effective noise vector at time n, $L_{\text{ff}} = L_c + L_a$ is the number of feedforward equalizer coefficients, and $\widehat{\mu}_i$ is the ith component of the biased received signal prediction error vector correlation estimate.

Assuming the effective noise is ergodic a time-average of $\widehat{\mu}_i[n]$ is a good estimate of the effective-noise correlation at lag i. To accommodate time-variability an exponentially-windowed sample average is used to approximate the ensemble average,

$$\widehat{\mathbf{R}}_{\mu,[1,i]}[n] = \frac{(1 - \lambda_{\text{corr}})}{(1 - \lambda_{\text{corr}}^{n+1})} \sum_{k=0}^{n} \lambda_{\text{corr}}^{n-k} \, \widehat{\mu}_i[k]. \tag{3.5.2}$$

Using an exponentially-windowed sample average allows the time-varying nature of the statistics to be captured through λ_{corr} while approximating the value of $\mathbf{R}_{\mu,[1,i]}$, the ith component of the first row of the effective noise correlation matrix at time n. The complete effective noise correlation matrix is constructed using assuming a Toeplitz-Hermitian structure of the effective noise correlation matrix.

Implementing the correlation using a fast Fourier transform to compute the autocorrelation the computational complexity of the proposed algorithm is $O\left(L_{\text{ff}} \log_2(L_{\text{ff}})\right)$. Previously proposed algorithms had complexity of $O(L_{\text{ff}}^2)$ since there was a necessary vector outer product. For an underwater channel where the feedforward coefficients can number in the tens or hundreds, the proposed algorithm has a noticeably lower computational complexity.

To summarize the advantages of using the proposed algorithm for estimating the effective noise covariance matrix over previously proposed algorithms:

- The number of components that must be tracked is reduced from L_{ff}^2 to L_{ff}. This helps with the memory requirements and enables extra ensemble averaging

since the diagonals of the correlation matrix are averaged.

- The structure of the interference plus noise correlation matrix is easily modified, *i.e.* if the effective noise correlation matrix is known to be tri-diagonal, then only two coefficients have to be tracked.

- There is a performance improvement due to restricting matrix to be Toeplitz.

- The computational complexity is reduced from $O(L_{\text{ff}}^2)$ to $O\left(L_{\text{ff}} \log_2(L_{\text{ff}})\right)$.

The first point is especially interesting since underwater communication problems are often data limited due to time-variation of the channel. This method provides a way to more effectively use the available data. In the next section the proposed algorithm and others are compared using a CEB-DFE on experimental data.

3.6 Experimental results

The SPACE08 was performed off the coast of Martha's Vineyard, MA from Oct. 14th through Nov. 1st, 2008. The water depth was approximately 15 meters, the transmitter was approximately 4 meters from the sea floor and the bottom of the receive arrays were about 3.25 meters above the sea floor. For the data analyzed here the distance from the transmitter to the receiver was 200 meters. The receiver was the twelfth receive element from the bottom of a 24 element array with 5 centimeter element spacing. Figure 3.6.1 illustrates the setup of this experiment.

The data signal had a bandwidth of $B = 6.51$ kHz and was modulated onto a carrier with frequency $f_c = 12.5$ kHz. The sampling frequency was $f_s = 39062.5$ samples/second. The transmitted signal analyzed here is a 4095-length M-sequence that was repeated 89 times for a packet that is one minute in length (with some zero-padding). The data was modulated using binary phase shift keying (BPSK) onto a square-root raised cosine pulse.
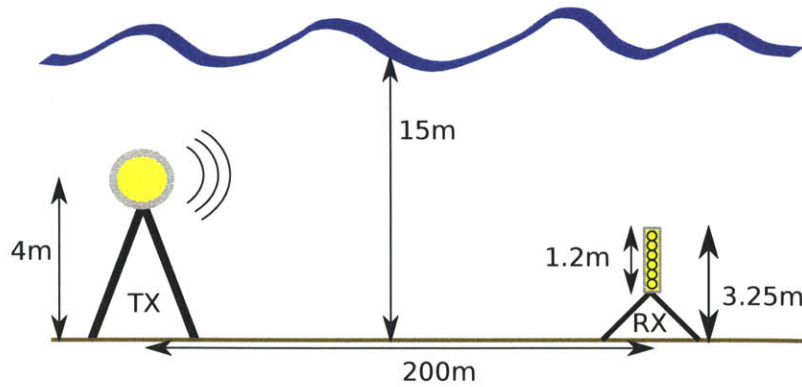
Figure 3.6.1: Setup of the SPACE08 experiment for the 1 km receiver.

3.6.1 Fluctuation of effective SNR

Using the experimental data the first quantity examined is the fluctuation of the estimated effective noise correlation matrix coefficients. Figure 3.6.2 shows the top-left estimated element of the effective noise correlation matrix as it evolves over a minute long data packet. This plot shows that the effective noise statistics are time-varying and need to be tracked. The coherence time of these coefficients is apparently around five seconds, which is very long compared with the sampling period, so an assumption of time-invariance over the averaging window is reasonable.

The curve in figure 3.6.2 highlights the variability of the observed SNR over the packet duration. A single element of the effective noise correlation matrix changes by more than 5 dB over an interval of less than ten seconds. Only using an average value would lead to increased residual mean-squared-error after equalization.

3.6.2 DFE comparison

To determine the effectiveness of the proposed algorithm several methods for approximating the effective noise correlation matrix were examined. Table 3.6.1 provides a description of each of the methods.

The mean squared error is the squared magnitude of the residual data estimation

70
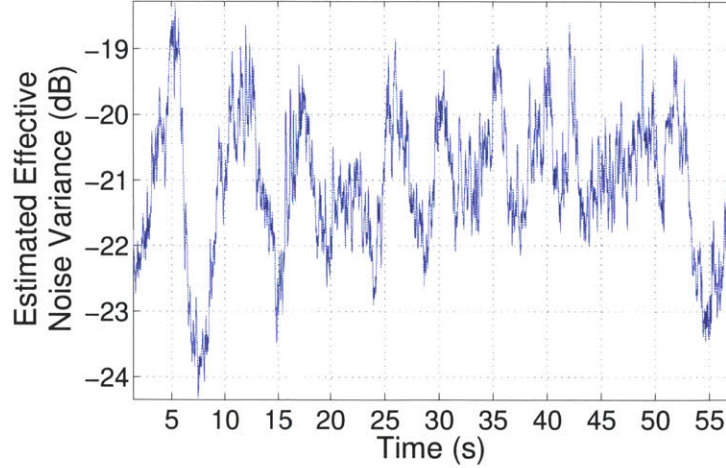
Figure 3.6.2: Top-left element of the estimated effective noise correlation matrix, $\left[\widehat{\mathbf{R}}_{\mu}\right]_{(1,1)}$, from October 26, 2008 at time 0800. The variance is tracked using an exponential window algorithm.. This value is a measure of the effective noise variance. Over the one minute packet there is a 5 dB peak to peak change with a coherence time of approximately five seconds.

Table 3.6.1: Description of methods compared using the SPACE08 data set.

Method Label	Description
AMB	CEB-DFE where the effective noise correlation matrix is approximated as a scaled identity matrix where its scaling is based on the SNR measured from the basebanded data before any equalization.
DIAG	CEB-DFE where the top-right entry of the estimated effective noise correlation matrix, $\left[\widehat{\mathbf{R}}_{\mu}\right]_{(1,1)}$, is used as an estimate of the effective noise variance. The effective noise correlation matrix is approximated as a scaled identity matrix.
SING	CEB-DFE where the effective noise correlation matrix is approximated by a diagonal matrix with entries equal to the main diagonal of $\widehat{\mathbf{R}}_{\mu}$.
FULL	CEB-DFE where the full effective noise correlation matrix is estimated from the data.
TOEP	CEB-DFE where the effective noise correlation matrix is estimated as a Topelitz-Hermitian matrix as described in this chapter.

71
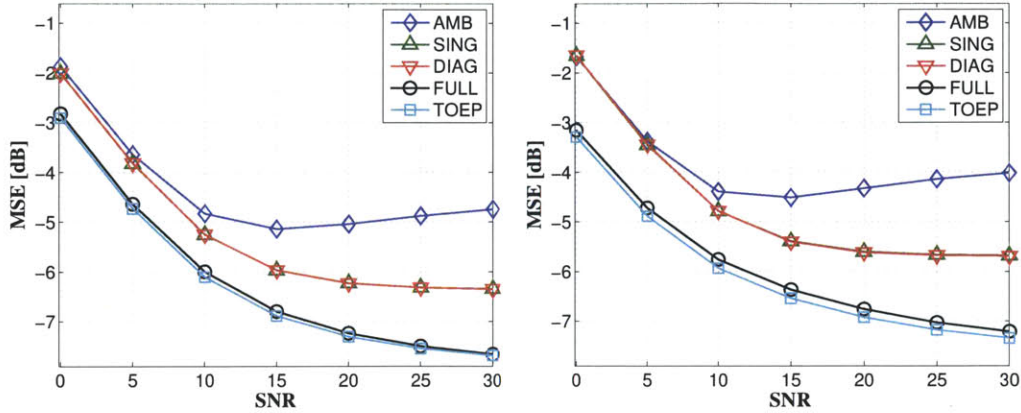
(a) Data from October 23, 2008 at time 1800. (b) Data from October 20, 2008 at time 1200.
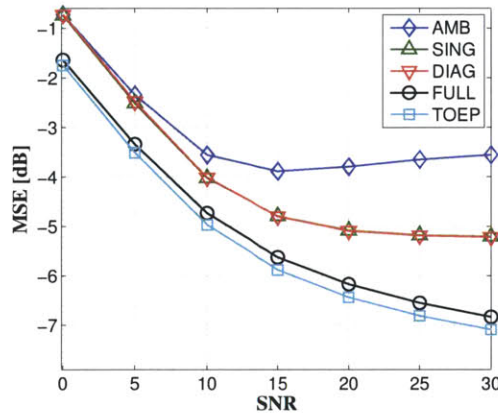
(c) Data from October 26, 2008 at time 0800.

Figure 3.6.3: Mean squared error (MSE) results after DFE for SPACE08 experiment 200m data using different estimates of the effective noise correlation matrix defined in Table 3.6.1. Data is ordered from (a) calm conditions to (c) stormy conditions.

error before any symbol decisions are made:

$$\epsilon_{\mathrm{MSE}} = \frac{\frac{1}{M} \sum_{i=1}^{M} |d[i] - \widetilde{d}[i]|^2}{\sigma_d^2} \tag{3.6.1}$$

where M is the number of transmitted symbols. In these results, $M = 100,000$. The in-band SNR is varied by adding an appropriately scaled realization of the ambient noise which was recorded using the same hydrophone shortly after the signal transmission ended.

Figure 3.6.3 shows the mean squared error from three different days of the SPACE08 experiment. These figures are ordered from the calmest ocean conditions on the top to the roughest conditions at the bottom. On October 23 (Julian day 297) the wave height was 0.5 meters, 1.2 meters on October 20 (Julian day 294), and 3 meters on October 26 ((Julian day 300).

The data shows that there is a penalty for assuming that the estimated noise matrix is diagonal (labeled *DIAG* in the plot). The data also show that there is no additional penalty for estimating this diagonal matrix using only one estimated value and a Toeplitz structure (labeled *SING* in this plot).

The plot labeled *AMB* is created using an equalizer which estimated the effective noise correlation matrix as the diagonal matrix with the diagonal equal to the inverse of an SNR measured from the received signal. This approximation does not account for channel estimation errors so as the SNR is increased there is a model mismatch between the estimated and the true effective noise correlation matrix, so above a threshold the MSE will increase with SNR (as observed).

The results show that a DFE using an effective noise correlation matrix calculated using the proposed method (*TOEP*) slightly outperforms one using an matrix calculated with no Toeplitz constraint (*FULL*). This data emphasizes the overall gain since there is a slight performance improvement and there is decrease in the amount of computation needed.

The improvement in performance is the result of the reduction in the number of free parameters that must be estimated when the Toeplitz assumption is imposed.

The results also demonstrate that assuming that the effective noise correlation matrix is diagonal and therefore not accounting for the full correlation structure of this noise results in a significant performance loss.

Therefore, the proposed method imposes appropriate structure on the estimated effective noise correlation matrix to both improve performance with respect to other proposed or commonly used approaches and to reduce computation complexity when compared to the next best performing method.

73

3.7 Conclusions

In this chapter, the existence of non-zero off-diagonal elements in the effective noise correlation matrix has been justified based upon the physical characteristics of the underwater acoustic propagation environment; the fluctuations of neighboring taps of the channel impulse response are correlated which causes off-diagonal terms appear in the effective noise correlation matrix.

An algorithm exploiting the Toeplitz and Hermitian structure of this matrix was developed that not only reduces computational complexity when compared to algorithms that do not impose the Toeplitz constraint but also results in a DFE whose performance is better than that achieved by DFEs using other estimators of the matrix. The reduction in computational complexity is important in array systems where the number of coefficients being estimated is quite large and efficient algorithms are needed for practical implementation.

Experimental data indicated that the statistics of the effective noise need to be tracked to prevent loss of system performance. The variance of the effective noise can vary by as much as 5 dB in a minute-long packet.

The literature on equalization of RF channels uses a non-adaptive, diagonal estimate of the effective noise correlation matrix. Methods described in this chapter could be applied to equalizers for RF channels to reduce the mean squared error of the equalized symbols.

Chapter 4

Physically constrained beamspace processing for a multichannel DFE

4.1 Introduction

Multichannel decision feedback equalization that has one feedforward section for each sensor and one feedback section for the whole system has been shown to be a nearly optimal method for handling the difficulties of the underwater communication channel [105]. When there are a large number of array elements, however, the implementation with one feedforward section per sensor may be prohibitive due to the rate of channel variability verses the degrees of freedom and high computational complexity. Channel time-variability limits the time-interval over which the constant channel assumption is reasonable thus limiting the averaging interval of adaptive algorithms. The computational complexity is proportional to the square of the number of channels. Both of these problems can be mitigated through beamspace processing, where the number of DFE feedforward sections is now the number of beams.

Beamforming is a spatial filtering technique; only energy from certain directions is passed through. Using a narrowband assumption, the received signal including all multipath components arrives in a restricted angular space due to channel physics, beams can be used to pass a restricted angular space, therefore reducing the problem dimensionality, without reducing the available degrees of freedom of the received

75

signal. Processing in beamspace both reduces the amount of data needed for averaging and reduces the computational complexity.

Stojanovic *et al.* [109] showed that when the angle of arrival (AoA) is known for all paths through the environment, the noise is spatially and temporally white, and the signal is narrowband the MMSE solution for the beamformer weights is a matrix with each column equal to an array manifold vector, one for each path. In the same paper, Stojanovic proposed an adaptive method to find the beamformer weights since the AoA are often unknown. This method is observed to work well [109], but does not significantly reduce the computational complexity.

In the current work a non-adaptive method is proposed which finds the optimal set of beams for a given range for the AoA on each path. This provides robustness of the beamformer to arrival direction and allows the beams to be computed off-line. Using an MMSE criterion, the optimal beamformer weights for a range of AoA on a line array are shown to be the Discrete Prolate Spheroidal Sequences (DPSS). Slepian is attributed with discovering the DPSS [94]. These sequences have a number of nice properties, such as mutual orthogonality, symmetry and real-value coefficients. Many methods have been studied for finding the DPSS [73].

In this thesis, a vertical line-array receiver is assumed. This choice is made for a number of reasons: first, the physics of the acoustic channel will naturally bound the angle of arrival. Second, when using a narrow-band assumption on a line-array the array manifold vectors are complex exponential functions which simplifies the derivations. Third, the available experimental data uses a vertical line-array receiver.

The proposed method in this chapter to bound the AoA range uses a geometric ray-path model of sound propagation. The ray-path model along with the assumption of a Pekeris waveguide [42], provides the AoA span and number of arrivals within a given delay spread. When the number of arrivals in the delay span is less than the number of sensors, there are fewer feedforward sections in the multichannel DFE for a beamspace where there is one section for each arrival than in sensor space where there is one section for each sensor. The ray-path model parameters such as water column depth, propagation distance, and transmitter and receiver geometry are often either

known *a-priori* or can be measured *in-situ* using commonly available instruments and techniques.

The proposed methods for determining the beamformer weights and the number of beams are verified using experimental data from the Surface Processes and Acoustic Communication Experiment (SPACE08) performed in at the Martha's Vineyard Coastal Observatory in 2008.

4.2 Receiver structure

The receiver structure studied throughout this chapter consists of a wideband beamformer followed by a multichannel DFE, which is an extension of the DFE introduced in Section 2.4. This structure allows for flexibility in the design of both the beamformer and the DFE. The beamformer reduces the signal-space dimensionality from the number of sensors down to the number of beams. The multichannel DFE equalizes, coherently combines, and estimates the transmitted symbol.

4.2.1 Multichannel decision feedback equalization

Recall that the decision feedback equalizer (DFE) consists of two linear filters working together: the feedforward filter collects the energy from the received signal and shapes its response and the feedback filter cancels the inter-symbol interference (ISI) from previously received symbols [61, 81]. The general DFE equation is

$$\tilde{d}[n] = \sum_{\ell=-L_a}^{L_c-1} h_{\text{ff}}^*[\ell]u[n-\ell] + \sum_{\ell=1}^{L_{\text{fb}}} h_{\text{fb}}^*[\ell]\hat{d}[n-\ell], \qquad (4.2.1)$$

where $u[n]$ is the baseband received data, $\hat{d}[n]$ is the past symbol decisions, and $\tilde{d}[n]$ is the filtered received data before a symbol decision has been made. The $L_a + L_c$ feedforward filter coefficients are represented as $h_{\text{ff}}[n]$, where L_a is the number of acausal coefficients and L_c is the number of causal coefficients. The L_{fb} feedback coefficients as $h_{\text{fb}}[n]$. The total number of DFE coefficients is $L = L_a + L_c + L_{\text{fb}}$.
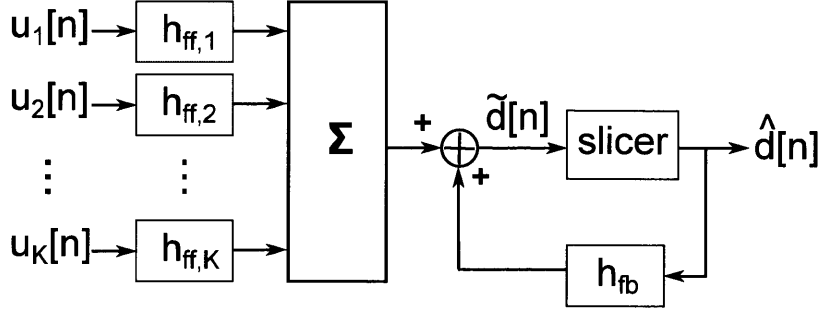
Figure 4.2.1: A multichannel decision feedback equalizer.

Using vector notation, the DFE equation can be written more compactly,

$$\tilde{d}[n] = \mathbf{h}_{\text{ff}}^{H}\mathbf{u}[n] + \mathbf{h}_{\text{fb}}^{H}\hat{\mathbf{d}}[n] = \mathbf{h}^{H}\mathbf{z}[n], \tag{4.2.2}$$

where $\mathbf{u}[n]$ is a vector of received signal samples and $\hat{\mathbf{d}}[n]$ is a vector of past data symbol estimates. Both of these vectors are defined more carefully in Section 2.4. Two vectors are reintroduced for notational simplicity: $\mathbf{h}^{T} = [\mathbf{h}_{\text{ff}}^{T}\ \mathbf{h}_{\text{fb}}^{T}]$ is a vector of filter coefficients and $\mathbf{z}^{T}[n] = [\mathbf{u}^{T}[n]\ \hat{\mathbf{d}}^{T}[n]]$ is a data vector containing both the received data and the past symbol estimates.

This framework can be modified to accommodate multiple receivers by expanding the definition of the filter and data vectors. When there are K receive elements, the vectors $\mathbf{h}$ and $\mathbf{z}[n]$ are

$$\mathbf{h} = \begin{bmatrix} \mathbf{h}_{\text{ff},1} \\ \mathbf{h}_{\text{ff},2} \\ \vdots \\ \mathbf{h}_{\text{ff},K} \\ \mathbf{h}_{\text{fb}} \end{bmatrix} \qquad \mathbf{z}[n] = \begin{bmatrix} \mathbf{u}_1[n] \\ \mathbf{u}_2[n] \\ \vdots \\ \mathbf{u}_K[n] \\ \hat{\mathbf{d}}[n] \end{bmatrix},$$

where $\mathbf{u}_i[n]$ is the vector of data received at the ith receive element and $\mathbf{h}_{\text{ff},i}$ is the vector of feedforward filter coefficients for the ith receive element. See Figure 4.2.1 for an illustration of the functionality of a multichannel DFE.

A fractionally sampled equalizer is often used to reduce synchronization errors

78

[82]. Using the supplied framework, the feedforward filters will each have $r_{\rm fs}$ samples per received symbol, while the feedback filter will remain the same length. At each iteration, the data fed into each channel of the feedforward equalizer are moved ahead by $r_{\rm fs}$ samples.

Using data until time n, the LSE solution for the DA-DFE filter coefficients is

$$\mathbf{h}[n] = \left(\sum_{i=-\infty}^{n} \mathbf{z}[i]\mathbf{z}^H[i] \right)^{-1} \left(\sum_{i=-\infty}^{n} \mathbf{z}[i]d^*[i] \right). \tag{4.2.3}$$

Notice that the filter coefficients now explicitly depend on time due to the dependence on the received data. Using an EW-RLS algorithm, the DA-DFE filter coefficients are computing using the relation

$$\mathbf{h}[n] = \left(\sum_{i=-\infty}^{n} \lambda^{n-i}\mathbf{z}[i]\mathbf{z}^H[i] \right)^{-1} \left(\sum_{i=-\infty}^{n} \lambda^{n-i}\mathbf{z}[i]d^*[i] \right). \tag{4.2.4}$$

The DA-DFE structure is used in this chapter because it has low complexity compared with the CEB-DFE (also known as the MMSE DFE). Since the CEB-DFE algorithm requires an inversion of an $L \times L$ matrix, the complexity is $O(L^3)$. The DA-DFE algorithm uses a data-recursive update to find a new solution, so the complexity is only $O(L^2)$. A second reason the DA-DFE is used is that the performance difference between the DA-DFE and CEB-DFE is negligible when the SNR is moderate to low, which is where many underwater communication systems operate. There is an in-depth comparison of the DA and CEB DFE in Chapter 6.

4.2.2 Beamforming

In Eq. (4.2.4), the number of filter coefficients being estimated is $K \times (L_a + L_c) + L_{\rm fb}$. In underwater acoustic communication systems, a common practice is to set the number of feedforward equalizer coefficients based on the delay spread of the significant received signal energy. Using this criterion the use of tens of coefficients per feedforward section is common resulting in high computational complexity. Stojanovic *et*
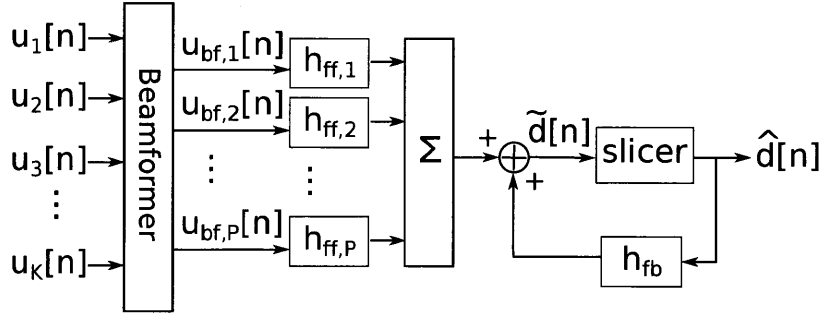
Figure 4.2.2: A multichannel decision feedback equalizer with a beamformer front-end to reduce computational complexity.

al. [109] noted that, when the signal is narrowband, the observation noise is spatially and temporally white (or whitened), and the number and direction of all arrivals is known, using beamformed data is equivalent to full sensor-space processing.

Beamforming can be viewed as a mapping of the received signal from the physical sensor space to beam space. This is accomplished by applying a spatial windowing function with desired spatial-spectral characteristics. Even though underwater acoustic communication data is not narrowband, the following wideband beamforming method can be used with a linear array: a discrete Fourier transform (DFT) is applied first to the data, beamforming is applied separately to each frequency bin, and the inverse DFT is applied to the result. The beamforming operation can be represented by the expression

$$\mathbf{u}_{\text{bf}}(\omega) = \Phi^H(\omega)\mathbf{u}(\omega), \qquad (4.2.5)$$

where $\Phi(\omega)$ is the $K \times P$ beamforming matrix at frequency ω. The notation $\mathbf{u}(\omega)$ represents the Fourier transform of the received data and $\mathbf{v}(\omega)$ represents the beamformed data, both at at frequency ω . The elements of the vectors are

$$\mathbf{u}(\omega) = \begin{bmatrix} u_1(\omega) \\ u_2(\omega) \\ \vdots \\ u_K(\omega)]^T \end{bmatrix} \qquad \mathbf{u}_{\text{bf}}(\omega) = \begin{bmatrix} u_{\text{bf},1}(\omega) \\ u_{\text{bf},2}(\omega) \\ \vdots \\ u_{\text{bf},P}(\omega)]^T \end{bmatrix},$$

where $u_k(\omega)$ is the received data from sensor k and $u_{bf,p}(\omega)$ is the received data in beam. There are many good references covering beamforming more completely such as [37, 43, 121].

The input to the DA-DFE is the output of a wideband beamformer, $\mathbf{u}_{bf}(\omega)$, transformed into the time domain. Since the number of beams, P, is often much less than the number of sensors, K, this results in a system with algorithmic complexity of $O((K/P)^2)$ which is much less than the sensor-space system, which has complexity $O(K^2)$. Figure 4.2.2 shows the DA-DFE with a beamformer.

4.3 Geometric ray-tracing propagation model

Beamforming is a useful method because it reduces computational complexity and potentially increases performance. After deciding to use a beamformer, the next questions a system designer might ask are "How many beams should one use?" and "What beam weights are best?" A common idea in the beamforming literature is to use an algorithm to track each arrival angle separately and create a set of beams which are the array manifold vectors pointed in the estimated arrival directions [7, 121, 124]. These methods tend to be computationally complex since the angles of arrival are time-varying. Stojanovic *et al.* [105] noted that when designing an acoustic communication system, the beamformer does not need to separate arrivals into separate beams since the feedforward equalizer adaptive combines the arrivals together by combining the beams.

Since channel motion induces changes in the arrival angles, the approach proposed in this chapter is to use a geometric model of the arrival structure to calculate a minimum and maximum arrival angle and use a set of beams which span that angular range.

Ray tracing is a common method used for high frequency acoustics (above 1 kHz) [42]. In the ray tracing model considered in this chapter, the channel is assumed to be a Pekaris waveguide with an pressure release surface and a soft, flat bottom. At a boundary the angle of incidence equals the angle of reflection, so a geometric

81

Table 4.3.1: Table of elevation arrival angles and delays for first five arrivals using geometric model with a flat surface and flat bottom.

Path	Arrival Angle (in radians)	Delay (in seconds)
Direct	$\frac{\pi}{2} + \arctan\left(\frac{d_R - d_T}{\ell_{\mathrm{TR}}}\right)$	$\frac{\sqrt{(d_R - d_t)^2 + \ell_{\mathrm{TR}}^2}}{c_w}$
Bottom	$\frac{\pi}{2} + \arctan\left(\frac{2d_w - d_R - d_T}{\ell_{\mathrm{TR}}}\right)$	$\frac{\sqrt{(2d_w - d_R - d_T)^2 + \ell_{\mathrm{TR}}^2}}{c_w}$
Surface	$\frac{\pi}{2} - \arctan\left(\frac{d_R + d_T}{\ell_{\mathrm{TR}}}\right)$	$\frac{\sqrt{(d_R + d_T)^2 + \ell_{\mathrm{TR}}^2}}{c_w}$
Surface-Bottom	$\frac{\pi}{2} + \arctan\left(\frac{2d_w - d_R + d_T}{\ell_{\mathrm{TR}}}\right)$	$\frac{\sqrt{(2d_w - d_R + d_T)^2 + \ell_{\mathrm{TR}}^2}}{c_w}$
Bottom-Surface	$\frac{\pi}{2} - \arctan\left(\frac{2d_w + d_R - d_T}{\ell_{\mathrm{TR}}}\right)$	$\frac{\sqrt{(2d_w + d_T - d_T)^2 + \ell_{\mathrm{TR}}^2}}{c_w}$

propagation model only depends on the water column depth, the speed of sound, the depth of the transmitter and receiver, and the distance between the transmitter; parameters that are readily available in many oceanographic applications. In the Pekeris waveguide, there is a soft bottom so paths which have propagation angles above some critical angle are lost. In this work there is no need to know what the critical angle is only that there are a limited number of paths.

Table 4.3.1 contains the delay and elevation angle of arrival for the earliest arriving paths, using the notation

d_w water column depth [m]

d_T transmitter depth [m]

d_R receiver depth [m]

ℓ_{TR} distance from transmitter to receiver [m]

c_w speed of sound in seawater [m/s]

A ray-path model with a finite number of paths is approximately accurate since there are only a small number of paths propagating below the critical angle. The arrival angles are bounded within the range of the propagating paths. Figure 4.3.1 illustrates this bounded arrival structure for the case of three propagating paths: the direct path, the bottom bounce path, and the surface bounce path.

The equations for computing the angle of arrival can be extended to an arbitrary τ_{path}. For simplification the last surface the signal interacts with before the receiver
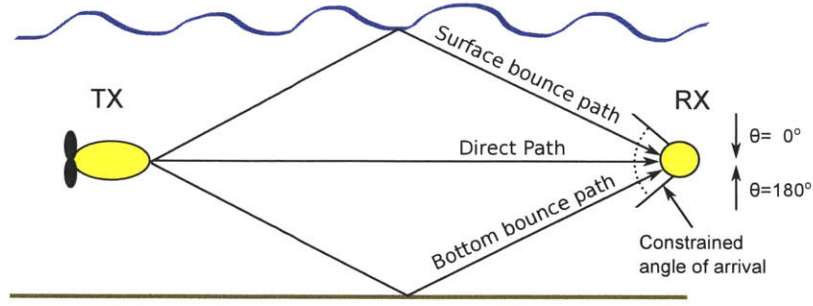
Figure 4.3.1: Illustration of multipath and the physically constrained angle of arrival for the shallow water communications channel. The angle of arrival of a path from the surface is defined to as $\theta = 0^0$, from the bottom $\theta = 180^0$, and broadside $\theta = 90^0$.

is specified. When the last bounce is a surface bounce, the angle of arrival is

$$\theta_{\text{path,surface}} = \arcsin\left(\frac{\ell_{\text{TR}}}{c_w \cdot \tau_{\text{path}}}\right). \tag{4.3.1}$$

When the last bounce is a bottom bounce, the angle of arrival is

$$\theta_{\text{path,bottom}} = \frac{\pi}{2} + \arccos\left(\frac{\ell_{\text{TR}}}{c_w \cdot \tau_{\text{path}}}\right). \tag{4.3.2}$$

Using an delay, τ_{relative}, relative to the shortest path (i.e. when the propagation path is of length ℓ_{TR}), the equations for angle of arrival can be rewritten. When the last bounce is a surface bounce, the AoA expression becomes

$$\theta_{\text{path,surface}} = \arcsin\left(\left(\frac{c_w \cdot \tau_{\text{relative}}}{\ell_{\text{TR}}} + 1\right)^{-1}\right). \tag{4.3.3}$$

When the last bounce is a bottom bounce, the AoA expression becomes

$$\theta_{\text{path,bottom}} = \frac{\pi}{2} + \arccos\left(\left(\frac{c_w \cdot \tau_{\text{relative}}}{\ell_{\text{TR}}} + 1\right)^{-1}\right). \tag{4.3.4}$$

Figure 4.3.2 shows the estimated delay and angle of arrival for signals propagating along each path using the ray model (the white crosses) as well as estimates of the actual intensity estimated from the data as a function of delay and angle using data collected during the SPACE08 experiment (described in Section 4.7).

83
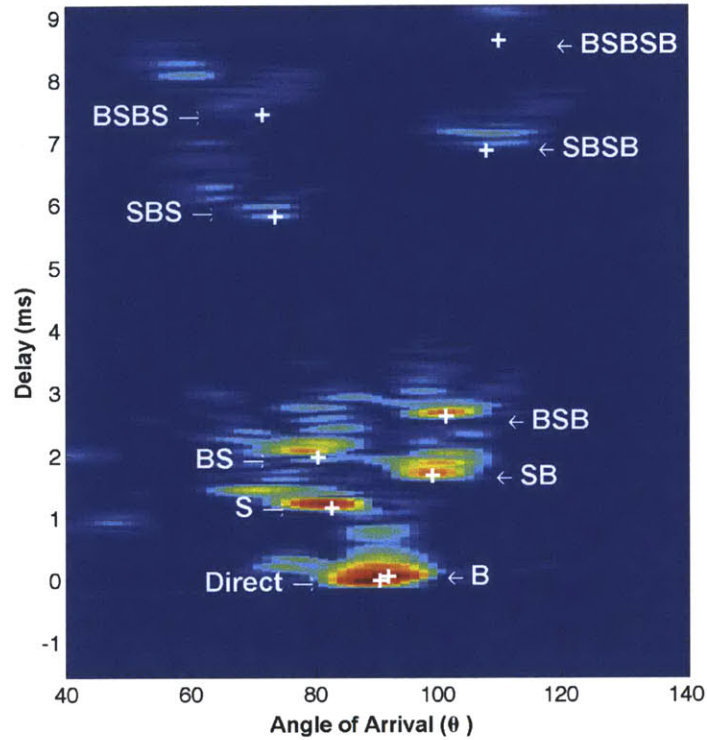
Figure 4.3.2: Estimated angle of arrival and delay of the channel impulse response arrivals from the from the SPACE08 experiment from Julian day 297 at time 1800. The white crosses indicate the arrival points calculated from the geometrical arrival model. The arrivals are labeled according to their interaction with the surface and bottom from the transmitter to the receiver: S indicates a surface bounce and B a bottom bounce.

4.4 Optimal beams for bounded angle-of-arrival subspace

4.4.1 Channel model

The previous section provided a limited method for estimating the number of beams impinging on a receiving array, but a natural question arises, "How is the number of arrivals related to the number of beams needed to capture the signal energy?" Stojanovic, *et al.* [109] showed that the number of beams should equal the number of arrivals. To show this, a framework for analyzing the problem is described. The vector of signals traveling along P paths, received by a linear array with K elements can be modeled as

$$
\mathbf{u}[n] =
\begin{bmatrix}
u_0[n] \\
\vdots \\
u_{k-1}[n]
\end{bmatrix}
=
\begin{bmatrix}
1 & \cdots & 1 \\
e^{-j\phi_1} & \cdots & e^{-j\phi_p} \\
\vdots & & \vdots \\
e^{-j(K-1)\phi_1} & \cdots & e^{-j(K-1)\phi_p}
\end{bmatrix}
\begin{bmatrix}
y_1[n] \\
\vdots \\
y_P[n]
\end{bmatrix}
+
\begin{bmatrix}
\nu_1[n] \\
\vdots \\
\nu_P[n]
\end{bmatrix}
$$

$$
= \mathbf{\Phi}\mathbf{y}[n] + \boldsymbol{\nu}[n]. \tag{4.4.1}
$$

In the expression above, $\boldsymbol{\nu}[n]$ is a vector of noise components assumed to be independent of the signal and $\mathbf{\Phi}$ is a matrix whose columns are the array manifold vectors pointed in the arrival direction characterized by $\phi_k = \frac{2\pi f}{c_w} d_s \times u_k$. The direction u_k is defined as $u_k = \cos(\theta_k)$ and θ_k is the AoA of the kth path, f is the signal frequency being examined, c_w is the speed of sound in water (assuming isovelocity channel). d_s is the sensor spacing. The array manifold vector for a uniformly spaced linear array is [121]

$$
\mathbf{v}(u_k) =
\begin{bmatrix}
1 \\
e^{-j\frac{2\pi f}{c_w} d_s u_k} \\
\vdots \\
e^{-j\frac{2\pi f}{c_w}(K-1)d_s u_k}
\end{bmatrix}. \tag{4.4.2}
$$

The vector $\mathbf{y}[n]$ is called the *path space signal* since it is the transmitted data

85

symbols convolved with the impulse response along each path (not including phase shift terms in $\mathbf{\Phi}$),

$$\mathbf{y}[n] = \mathbf{G}_p^H[n]\mathbf{d}'[n]. \tag{4.4.3}$$

The overall path channel impulse response matrix, $\mathbf{G}_p[n]$, includes transmitter and receiver filtering. Defining N_a as the maximum number of acausal channel coefficients across all paths and N_c as the maximum number of causal channel coefficients across all paths, the ith column of $\mathbf{G}_p[n]$ is the effective channel of the ith path at time n,

$$\mathbf{g}_i[n] = \begin{bmatrix} g_i[n, N_c - 1] & \dots & g_i[n, 0] & \dots & g_i[n, -N_a] \end{bmatrix}^T, \tag{4.4.4}$$

where $g_i[m, \ell]$ is the channel impulse response coefficient for the ith path at time m and delay ℓ.

The transmitted symbol vector, $\mathbf{d}'[n]$, (defined similarly to eq. (2.2.4)) is

$$\mathbf{d}'[n] = [d[n - N_c + 1] \quad \dots \quad d[n] \quad \dots \quad d[n + N_a]]^T, \tag{4.4.5}$$

where $d[m]$ is the transmitted data symbol at time m. A common simplifying assumption to use spatially and temporally white observation noise $\boldsymbol{\nu}[n]$. This assumption is most accurate when the SNR is very high and instrumentation noise dominates the environmental ambient noise. Stojanovic *et al.* [109] showed that a multichannel DFE with a beamformer which used $\mathbf{\Phi}$ as the beamforming weight matrix operated with minimum mean squared error, *i.e.*

$$\mathbf{u}_{\text{bf}}[n] = \mathbf{\Phi}^H \mathbf{u}[n], \tag{4.4.6}$$

where $\mathbf{u}_{\text{bf}}[n]$ is the beamformed data. Furthermore, when the signal is narrowband and the noise is spatially and temporally white, any beamforming matrix $\mathbf{B}$ that satisfies

$$\mathbf{\Phi}^H \mathbf{B} \left(\mathbf{B}^H \mathbf{B} \right)^{-1} \mathbf{B}^H \mathbf{\Phi} = \mathbf{\Phi}^H \mathbf{\Phi} \tag{4.4.7}$$

can be used as the beamformer weight matrix to achieve minimum mean squared

error performance. The matrix $\mathbf{B}(\mathbf{B}^H\mathbf{B})\mathbf{B}^H$ is a projection matrix, so eq. (4.4.7) implies that any matrix that describes a subspace which contains $\boldsymbol{\Phi}$ does not increase the mean squared error performance of the multichannel DFE.

One example of a matrix which satisfies the condition of eq. (4.4.7) is the identity matrix, $\mathbf{I}$, where the beamspace is the sensor-space. Reducing the number of beams, however, reduces the computational complexity and also improves system performance by reducing the number of adapting parameters. This reasoning strongly suggest that the number of beams should be minimized. The minimum number of beams implied by eq. (4.4.7) is the number of arrival paths.

4.4.2 Derivation of optimal beams

In most underwater settings the arrival angles for the different multipath components are unknown, so the matrix $\boldsymbol{\Phi}$ is also unknown. Adaptively tracking beam weights which minimize the mean squared error performance is one way to circumvent this issue [109]. Unfortunately, this adds additional computational complexity and the adaptation method described in [109] is observed to be unstable under certain conditions (shown experimentally in Section 4.7).

An alternate method proposed in the current work is to create a non-adaptive set of beams based on observed environmental parameters. In the shallow water (Pekeris) waveguide there are only a finite number of propagating paths under our model assumptions, so there are a finite number of arrivals [42]. The arrival angles for the multipath components are bounded to $u_{\min} < u < u_{\max}$, where $u = \cos(\theta)$. Without loss of generality the angle of arrival range is assume to be centered, so $-u_{\min} = u_{\max} = u_0$. Any non-centered range can be centered by introducing a phase shift in the beam weights.

The condition in eq. (4.4.7) cannot be met with equality for a continuous range of angles. The problem is equivalent to a discrete filter design problem with a unity constraint over an angular range. Neither of these problems can be solved exactly in a finite dimensional space. Each column of $\boldsymbol{\Phi}$ is an array manifold vector parametrized by an angle of arrival, θ. A new metric is proposed which minimizes average distortion

87

of the inner product of two array manifold vectors over the angular range of interest. The beamformer weight matrix, $\mathbf{B}_{\text{opt}}$, is found as a solution to the optimization problem,

$$\mathbf{B}_{\text{opt}} = \min_{\mathbf{B}} \int_{-u_0}^{u_0} \int_{-u_0}^{u_0} \left| \mathbf{v}^H(u_1')\mathbf{v}(u_2') - \mathbf{v}^H(u_1')\mathbf{B}(\mathbf{B}^H\mathbf{B})^{-1}\mathbf{B}^H\mathbf{v}'(u_2') \right|^2 \mathrm{d}u_1' \mathrm{d}u_2'. \quad (4.4.8)$$

The form of this problem is similar to one recently studied by Kitchens in chapter 5 of his PhD thesis [48]. The solution from Kitchens proposed was to build a matrix of the desired rank where the columns are the eigenvectors corresponding to the maximum eigenvalues of the matrix

$$\mathbf{R_u} \triangleq \int_{-u_0}^{u_0} \mathbf{v}(u)\mathbf{v}^H(u)\mathrm{d}u. \quad (4.4.9)$$

A key part of the proof in [48] uses the Poincare separation theorem to show that the eigenvectors corresponding to the maximum eigenvalues are the solution to this problem. The details of the proof imply that a whole family of metrics give rise to this same solution: any metric that preserves the eigenvalue ordering is equivalent. One result is that finding the subspace which minimizes the distortion of the inner product is equivalent to finding the subspace that minimizes the average squared difference between the array manifold vectors and their projection. Other cost functions also produce the same solutions, and hence different interpretations, but these are not explored further in this thesis.

Using array manifold vectors for linear array (see eq. (4.4.2)), the form of this solution is the same (within scaling) to a problem studied by Slepian in [94]. In this work he showed that the eigenvectors of the matrix in eq. (4.4.9) are the set of discrete prolate spheroidal sequences (DPSS). Thus, a solution to eq. (4.4.8) is a matrix where the columns are the first P discrete prolate spheroidal sequences, where P is the number of paths.

4.4.3 Discrete prolate spheroidal sequences

The discrete prolate spheroidal sequences were discovered by Slepian in 1970s [94] while trying to answer the question: "What is the fixed-length, real sequence with the most energy within a specified bandwidth?" The DPSS are real and have a number of surprising and useful symmetry properties [94]. Since their discovery DPSS have been used in many areas of signal processing, most notably for multi-taper spectral estimation [73, 114].

The set of DPSS specified of a given length, N_{DPSS}, and target normalized bandwidth, W, form a complete orthogonal basis. Note that only about $2N_{\mathrm{DPSS}}W$ sequences will have a majority of their energy within the specified bandwidth [94]. Figure 4.4.1 shows an example of the first 5 DPSS weights for $N_{\mathrm{DPSS}} = 24$ and $W = 0.12$. Note that the energy of the fifth beam is starting to leak outside of the specified bandwidth.

DPSS are sometimes avoided is that there is no closed form solution for finding the DPSS values. Fortunately, efficient methods for finding the sequence values are quite prevalent in the literature, $e.g.$ [8, 73, 94]. In the current work, the DPSS beam weights are found for a specified bandwidth, which corresponds to the angle of arrival range. The number of DPSS beams can range from one to the number of sensors. The DPSS beam weights are orthogonal since the set of DPSS are orthogonal by definition. If the number of beams desired is equal to the number of sensors, the beamformer weight matrix is unitary.

4.5 Alternative beamforming strategies

In the previous section the optimal beam-weights were found to be the DPSS when the angle of arrivals are unknown but bounded to a specified range. The algorithm for determining the DPSS can have high computational complexity, the beam-weights are symmetric, and they are only optimal for the specified criterion. In this section, a variety of alternative beamforming strategies are presented for comparison with the DPSS beams-weights.
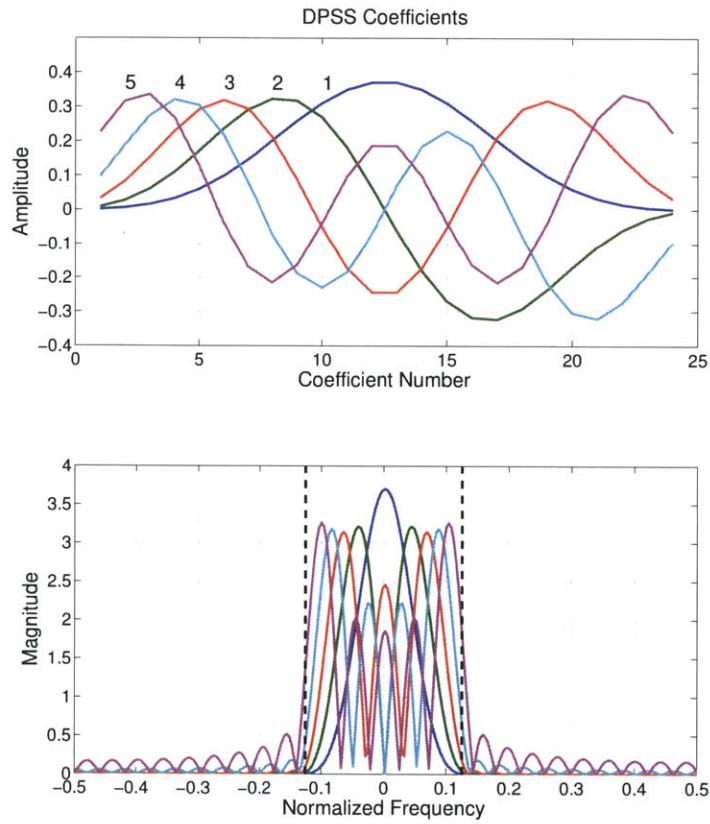
Figure 4.4.1: First 5 DPSS coefficients for the DPSS with 24 coefficients constrained within a normalized bandwidth bounded by ± 0.12.
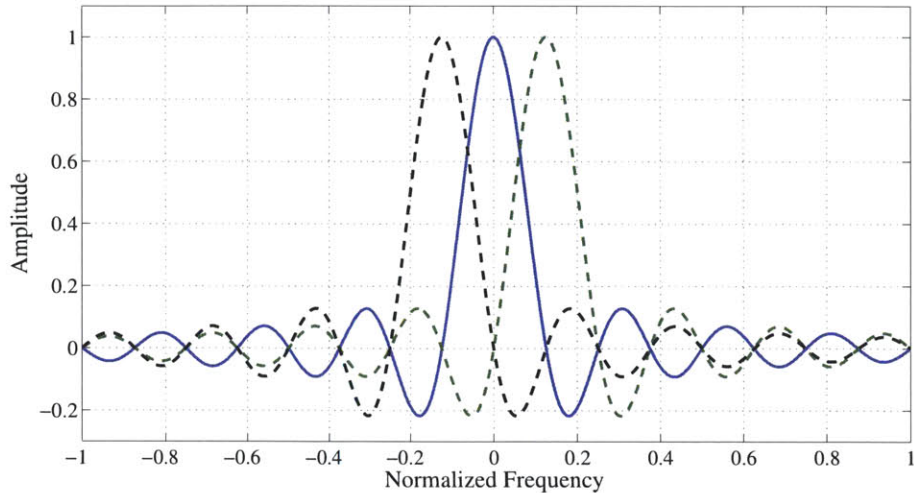
Figure 4.5.1: Uniform weighted beampattern in k space at the design frequency of the array. Note that the peak of beam is at the null of the adjacent beams.

The methods for determining the beam-weights in this section are chosen either because of their relative simplicity (steered uniform beams), they were well-established in the literature (MVDR, MCM, principle-component, and fully adaptive methods), or they exploited some property that potentially improved performance while reducing computational complexity (time-aligned beams and hybrid methods).

4.5.1 Uniform beamformer

One alternative set of beam weights is uniformly weighted beams. As the name implies, the beam weight coefficients all have the same magnitude. The beam weights are the array manifold vectors with angles specified so that neighboring beams are orthogonal at the design frequency, usually specified as $f_d = \frac{c_w}{2d_s}$ for an array with sensor spacing of d_s. The first beam placed is placed at broadside which ensures that the beams are placed symmetrically. Figure 4.5.1 shows an example of adjacent beams at the f_d.

91

(a)   (b)
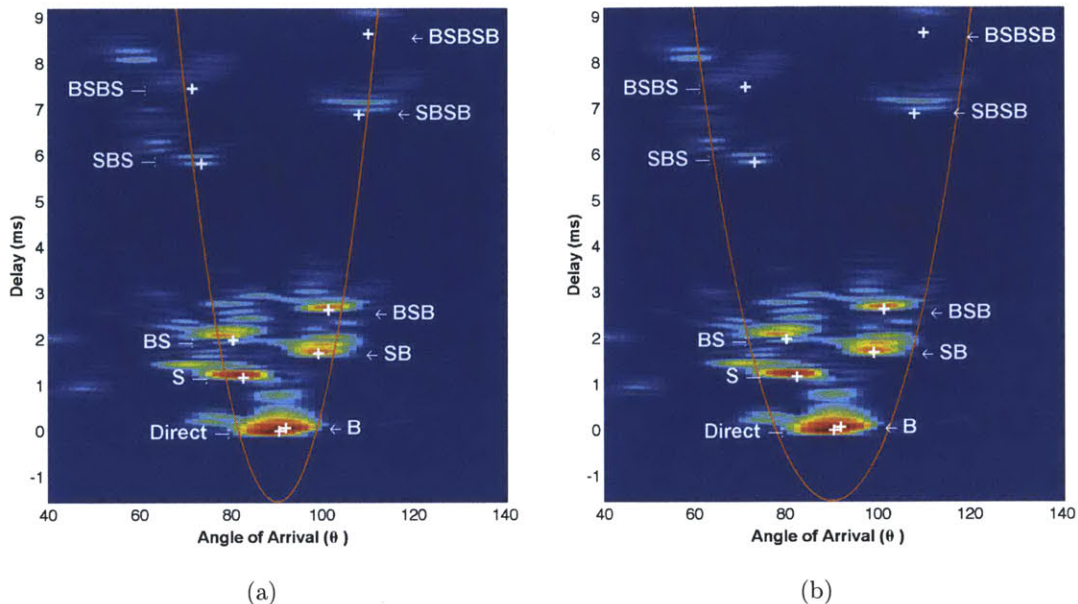
Figure 4.5.2: Arrivals from SPACE08 data during calm weather conditions. The orange line specifies the delay calculated for the time-aligned uniform beam weights. Figure (a) shows the bounds for $\alpha_b = 1$ and figure (b) with $\alpha_b = \frac{1}{2}$.

4.5.2 Uniform beamformer time-aligned

The geometric ray-path model devised in Section 4.3 indicates that the arrival delay depends on the angle of arrival. The method for finding the uniform beams described above produces a specific set of angles where the beams are steered. Using the expressions from Section 4.3, the path delays can be computed for the specified beam angles.

Recall that for white observation noise, the feedforward section of the DFE is a matched filter. Using the estimated the path delay for the beam angle, only the feedforward coefficients corresponding to delays after the arrival are included in the feedforward section; the feedforward coefficients corresponding to regions where no signal energy is expected are discarded. This reduces the dimensionality of the adaptive equalizer which reduces the computational complexity.

Using the geometric ray-path model, the estimated arrival delay, τ_m for a specified

92

arrival angle, θ, is

$$\tau_m(\theta) = \alpha_b \frac{\ell_{\mathrm{TR}}^2}{c} \csc^2(\theta) - \tau_{\mathrm{offset}}, \qquad (4.5.1)$$

The parameters α_b and τ_{offset} are design parameters introduced to account for inaccuracies of the ray-path model and decrease sensitivity of the beams to channel motion. The expression $\csc(\theta)$ is the cosecant of θ (*i.e.* the reciprocal of the sine of θ.) The parameter α_b is a scaling factor used to widen the bound and the parameter τ_{offset} is an delay offset. Here these parameters are set to $\alpha_b = 1/2$ and $\tau_{\mathrm{offset}} = 10 * N_s/f_s$, where N_s is the number of samples per symbol and f_s is the sampling frequency. Figure 4.5.2 illustrates two values of the scaling parameter $\alpha_b = 1$ and $\alpha_b = \frac{1}{2}$.

4.5.3 Principle component (eigenvector) beamforming

A desirable property of the beamformed received signal is that the beams are mutually uncorrelated. LeBlanc and Beaujean [55, 56] proposed achieving this using principle component analysis (PCA) on the estimated received signal correlation matrix, $\widehat{\mathbf{R}}_u$. To see that this is the correct method consider the objective:

$$\mathrm{E}\{u_{\mathrm{bf},i}^H[n]u_{\mathrm{bf},j}[n]\} = \alpha_{\mathrm{PCA}}\delta_{i,j}. \qquad (4.5.2)$$

In this expression $u_{\mathrm{bf},i}$ is the received signal beamformed with beam i, α_{PCA} is a scaling, and $\delta_{i,j}$ is the Kronecker delta

$$\delta_{i,j} = \begin{cases} 1 & i = j \\ 0 & i \neq j \end{cases}.$$

Using the expression, $u_{\mathrm{bf},i} = \mathbf{w}_{\mathrm{PCA},i}^H \mathbf{u}[n]$, and evaluating the expectation in eq. (4.5.2)) gives

$$\mathbf{w}_{\mathrm{PCA},i}^H \mathbf{R}_u \mathbf{w}_{\mathrm{PCA},j} = \alpha_{\mathrm{PCA}}\delta_{i,j}. \qquad (4.5.3)$$

One solution for $\mathbf{w}_{\text{PCA}_i}$ is the eigenvectors of $\mathbf{R_u}$. The received data correlation matrix is not available and so it is estimated using

$$\widehat{\mathbf{R}}_\mathbf{u}[n] = \sum_{j=n-N+1}^{N} \mathbf{u}[j]\mathbf{u}^H[j]. \qquad (4.5.4)$$

The scaling parameter α_{PCA} becomes the eigenvalue associated with the ith eigenvector.

LeBlanc and Beaujean focused mainly on decorrelating the data. This method not only decorrelates the beamformed data but by using the largest eigenvalue first captures the most signal energy for a specified number of beams.

In this thesis the eigenvectors corresponding to a specified number of the largest principle components (eigenvalues) of the estimated received signal correlation matrix are used as beamforming weights.

4.5.4 MVDR and MCM beamforming

The techniques discussed up to this point have not taken the spatial spectrum of the noise into account. For many underwater channels, the noise wavenumber spectrum is colored due to the nature of underwater noise [119, 42]. When the noise correlation matrix is known or well-estimated, the minimum variance distortionless response (MVDR), which is similar to the Capon beamformer [13], is a common structure used in the beamforming community. This beamformer provides the minimum variance response such that signals arriving from the specified angle of arrival are not distorted.

The constrained optimization problem from finding the MVDR beam weights is

$$\begin{aligned}\mathbf{w}_{\text{MVDR}} = \;&\underset{\mathbf{w}}{\arg\min} \quad \mathrm{E}\{|\mathbf{w}^H\mathbf{s}|^2\}\\&\text{subject to} \quad \mathbf{w}^H\mathbf{v}(u_1) = 1.\end{aligned} \qquad (4.5.5)$$

In this formulation, $\mathbf{s} = \mathbf{v}(u_1) + \boldsymbol{\nu}$ is the signal vector, $\mathbf{w}_{\text{MVDR}}$ is beamformer weight vector, $\mathbf{v}(u_1)$ is the array manifold vector pointing at direction $u_1 = \cos\theta_1$ (θ_1 is the AoA), $\boldsymbol{\nu}$ is a noise vector, and $\mathbf{w}^H\mathbf{v}(u_1) = 1$ is the distortionless criterion. The

solution to this optimization problem is $\mathbf{w}_{\text{MVDR}}$, [121]

$$\mathbf{w}_{\text{MVDR}} = \left[\mathbf{v}(u_1)\mathbf{R}_\nu^{-1}\mathbf{v}(u_1)\right]^{-1}\mathbf{R}_\nu^{-1}\mathbf{v}(u_1), \qquad (4.5.6)$$

where $\mathbf{R}_\nu$ is the noise correlation matrix.

One shortcoming of the MVDR framework is that it is sensitive to model mismatch. For example when the signal is treated as noise, it is rejected when the true signal is

$$\mathbf{s} = \mathbf{v}(\tilde{u}_1) + \nu,$$

and the difference between the two angles is $\Delta u_1 = |\tilde{u}_1 - u_1| > \frac{c_w}{Kd_sf}$ (assuming white noise). This difficulty can be handled when using multiple MVDR beams by ensuring the difference is not too big between two neighboring specified distortionless response angles, *i.e.* for two MVDR beams with specified angles u_1 and u_2,

$$|u_2 - u_1| < \frac{c_w}{Kd_sf}.$$

Another difficulty of using MVDR beams occurs when the noise is highly directional; regardless of SNR, signals arriving near strong noise directions are highly attenuated. The purpose of a beamformer in a communication system is to collect as much signal energy as possible to increase the observed SNR. Creating a beamformer which potentially rejects signal energy is non-ideal.

One method to partially mitigate this shortcoming is to use the multiple constraint method (MCM) proposed by Schmidt *et al.* [89]. The MCM imposes additional constraints to ensure that directions near the distortionless direction are not attenuated too heavily. In the present case, the additional constraints ensure notches don't appear in the main lobe of the beamformer.

The MVDR optimization problem from eq. (4.5.5) withadditional constraints is

the MCM constrained optimization problem

$$\mathbf{w}_{\mathrm{MCM}} = \underset{\mathbf{w}}{\arg\min} \quad \mathrm{E}\{|\mathbf{w}^H\mathbf{s}|^2\}$$

$$\text{subject to} \quad \mathbf{w}_{\mathrm{MCM}}^H \mathbf{v}(u_1) = 1$$

$$\mathbf{w}_{\mathrm{MCM}}^H \mathbf{v}(u_2) = b_2 \qquad (4.5.7)$$

$$\vdots$$

$$\mathbf{w}_{\mathrm{MCM}}^H \mathbf{v}(\mathbf{u}_{N_{\mathrm{mc}}}) = b_{N_{\mathrm{mc}}}.$$

In the above expressions, b_i is a constraint and N_{mc} is the number of constraints. The first constraint is the distortionless constraint in the desired look direction, u_1, so $b_1 = 1$. One method for setting the additional constraints, borrowed from [89], is to set $b_i = \mathbf{v}^H(u_1)\mathbf{v}(u_i)$, the inner product of the distortionless direction with the constraint direction. Setting all $b_i = 1$ uses too many degrees of freedom and limits the noise rejection capability outside of the constraint directions. The constraint directions are usually chosen to be within the main-lobe response of the distortionless direction.

Building a vector $\mathbf{b}$ of constraint values and a matrix $\mathbf{V}$, where each column is an array manifold matrix pointed in a constraint direction, *i.e.*

$$\mathbf{b} = \begin{bmatrix} b_1 \\ b_2 \\ \cdots \\ b_{n_{\mathrm{mc}}} \end{bmatrix} \qquad \mathbf{V} = \begin{bmatrix} \mathbf{v}(u_1) & \mathbf{v}(u_2) & \cdots & \mathbf{v}(u_{N_{\mathrm{mc}}}) \end{bmatrix},$$

the constraints can be written more compactly as

$$\mathbf{w}_{\mathrm{MCM}}^H \mathbf{V} = \mathbf{b}. \qquad (4.5.8)$$

The solution for the beamformer weights using MCM is [89]

$$\mathbf{w}_{\mathrm{MCM}} = \mathbf{R}_\nu^{-1}\mathbf{V}\left[\mathbf{V}^H\mathbf{R}_\nu^{-1}\mathbf{V}\right]^{-1}\mathbf{b}^*. \qquad (4.5.9)$$

To create a set of beams, a set of directions are chosen (*e.g.* evenly spaced angles over the range of interest) and MCM beam weights are calculated for each beam direction. The distortionless directions chosen for the set of MCM beams (one distortionless direction per beam) are the same as the steered directions of the uniform beams described in the previous section. The reason for this choice is that when the noise is white, the MCM beamformer weight matrix equals the uniform beamformer weight matrix.

This procedure can be extended by enforcing mutual orthogonality among the beams. The multichannel DFE with orthogonal MCM beams, however, had higher observed output mean squared error than a multichanel DFE with non-orthogonal MCM beams. This result appeared in every data set tested, so the additional effort of constraining the beams to be orthogonal appears to not be worthwhile.

Both the MVDR or MCM beamforming weight are non-ideal for communication systems because the goal of both MVDR and MCM methods is to reject energy from certain directions. The main purpose of the beamformer in a communication system is to gather as much signal energy as possible and preserve as many degrees of freedom for future adaptation by the DFE. Thus, a multichannel DFE using either MVDR or MCM beam weights won't perform as well as other proposed methods.

4.5.5 Adaptive time-domain beamforming

One method to avoid the complications of the narrowband assumption is to work entirely in the time domain. Initial work on an adaptive array with tapped delay line processing was done by Compton *et al.* [22, 23, 84, 122, 123]. Recently, Stojanovic *et al.* [109] proposed a time-domain, adaptive beamformer with a multichannel DFE. The beamformer and the DFE are adapted together using the same error to update their coefficients using an RLS algorithm.

The procedure for finding the multichannel DFE coefficients when using a beamformer is very similar to the procedure for finding the multichannel DFE coefficients without a beamformer. The beamformed and equalized data before a symbol decision

is made are

$$\tilde{d}[n] = \begin{bmatrix} \mathbf{h}_{\text{ff},1}[n-1] \\ \mathbf{h}_{\text{ff},2}[n-1] \\ \vdots \\ \mathbf{h}_{\text{ff},M}[n-1] \end{bmatrix}^{H} \begin{bmatrix} \mathbf{U}^{T}[n]\widehat{\mathbf{c}}_{1}^{*}[n-1] \\ \mathbf{U}^{T}[n]\widehat{\mathbf{c}}_{2}^{*}[n-1] \\ \vdots \\ \mathbf{U}^{T}[n]\widehat{\mathbf{c}}_{M}^{*}[n-1] \end{bmatrix} + \mathbf{h}_{\text{fb}}^{H}[n-1]\widehat{\mathbf{d}}[n-1]. \qquad (4.5.10)$$

In this expression, $\mathbf{U}$ is an $L_{\text{ff}} \times K$ matrix of the received signal where each column corresponds to one sensor ($L_{\text{ff}} = L_a + L_c$ is the number of feedforward coefficients in each feedforward section of the DFE), $\widehat{\mathbf{c}}_i$ is a vector the ith beam weights, $\mathbf{h}_{\text{ff},i}$ is a vector of the ith feedforward section coefficients, $\mathbf{h}_{\text{fb}}$ is the feedback coefficients, and $\widehat{\mathbf{d}}_{\text{fb}}$ is a vector of past data estimates. The time index on all estimated vectors indicates the time at which the estimate was made (all are a lag-1 estimates). The time index on the feedback data indicates that the most recent estimate is the last piece of data.

A more compact representation is

$$\tilde{d}[n] = \mathbf{h}_{\text{ff}}^{H}[n-1]\mathbf{q}_c[n] + \mathbf{h}_{\text{fb}}^{H}[n-1]\widehat{\mathbf{d}}[n-1], \qquad (4.5.11)$$

where, $\mathbf{h}_{\text{ff}}$, is a vector of all the feedforward DFE coefficients and

$$\mathbf{q}_c = \begin{bmatrix} \mathbf{U}^{T}[n]\widehat{\mathbf{c}}_{1}^{*}[n-1] \\ \mathbf{U}^{T}[n]\widehat{\mathbf{c}}_{2}^{*}[n-1] \\ \vdots \\ \mathbf{U}^{T}[n]\widehat{\mathbf{c}}_{M}^{*}[n-1] \end{bmatrix}.$$

An even more compact representation is given by

$$\widetilde{d}[n] = \mathbf{h}^{H}[n]\mathbf{x}[n], \qquad (4.5.12)$$

where

$$\mathbf{h}[n] = \begin{bmatrix} \mathbf{h}_{\mathrm{ff}}[n] \\ \mathbf{h}_{\mathrm{fb}}[n] \end{bmatrix}, \tag{4.5.13}$$

and

$$\mathbf{x}[n] = \begin{bmatrix} \mathbf{q}_c[n] \\ \mathbf{d}_{\mathrm{fb}}[n-1] \end{bmatrix}. \tag{4.5.14}$$

The equalizer coefficients are found as the solution to the exponentially windowed least squares optimization problem,

$$\mathbf{h}[n] = \arg\min_{\mathbf{h}'} \sum_{i=1}^{n} \lambda^{n-i} \left| \widehat{d}[i] - \mathbf{h}'\mathbf{x}[i] \right|^2. \tag{4.5.15}$$

where $\hat{d}[i]$ is the transmitted data symbol estimate at time i and λ is the exponential weighting coefficient. The solution to this optimization problem is

$$\mathbf{h}[n] = \left(\sum_{i=0}^{n} \lambda^{n-i} \mathbf{x}[i]\mathbf{x}^H[i] \right)^{-1} \left(\sum_{i=0}^{n} \lambda^{n-i} \mathbf{x}[i]\hat{d}^*[i] \right). \tag{4.5.16}$$

A key observation for finding the beamforming coefficients is that in eq. (4.5.10), the beamformer and the feedforward filter are interchangeable. Thus, the data estimate can be rewritten as

$$\tilde{d}[n] = \begin{bmatrix} \widehat{\mathbf{c}}_1[n-1] \\ \widehat{\mathbf{c}}_2[n-1] \\ \vdots \\ \widehat{\mathbf{c}}_M[n-1] \end{bmatrix}^H \begin{bmatrix} \mathbf{U}[n]\mathbf{h}_{\mathrm{ff},1}^*[n-1] \\ \mathbf{U}[n]\mathbf{h}_{\mathrm{ff},2}^*[n-1] \\ \vdots \\ \mathbf{U}[n]\mathbf{h}_{\mathrm{ff,M}}^*[n-1] \end{bmatrix} + \mathbf{h}_{\mathrm{fb}}^H[n-1]\hat{\mathbf{d}}_{\mathrm{fb}}[n-1]. \tag{4.5.17}$$

Eq. (4.5.17) can be rewritten as

$$\tilde{d}[n] = \widehat{\mathbf{c}}[n-1]\mathbf{q}_h[n] + \mathbf{h}_{\mathrm{fb}}^H[n-1]\hat{\mathbf{d}}[n-1], \tag{4.5.18}$$

99

where $\widehat{\mathbf{c}}[n]$ a vector of the adaptive beam weights stacked together and

$$
\mathbf{q}_h[n] = \begin{bmatrix} \mathbf{U}[n]\mathbf{h}_{\text{ff},1}^*[n-1] \\ \mathbf{U}[n]\mathbf{h}_{\text{ff},2}^*[n-1] \\ \vdots \\ \mathbf{U}[n]\mathbf{h}_{\text{ff},\text{M}}^*[n-1] \end{bmatrix}
$$

The beamforming coefficients found by solving the exponentially windowed least-squares problem

$$
\widehat{\mathbf{c}}[n] = \arg\min_{\mathbf{c}'} \sum_{i=1}^{n} \lambda^{n-i} \left| \widehat{d}[i] - \mathbf{h}_{\text{fb}}^H[i]\widehat{d}[i-1] - \mathbf{c}'^H \mathbf{q}_h[i] \right|^2 . \tag{4.5.19}
$$

The solution to this optimization problem is

$$
\widehat{\mathbf{c}}[n] = \left(\sum_{i=0}^{n} \lambda^{n-i} \mathbf{q}_h[i]\mathbf{q}_h^H[i] \right)^{-1} \left(\sum_{i=0}^{n} \lambda^{n-i} \mathbf{q}_h[i] \left(\widehat{d}[i] - \mathbf{h}_{\text{fb}}^H[i]\widehat{\mathbf{d}}[i-1] \right)^* \right) . \tag{4.5.20}
$$

Comparing eqs. (4.5.16) and (4.5.20) reveals that the error term being minimized is the same, which allows for a parallel implementation.

The adaptive beamforming algorithm tends to work well in practice, but the algorithmic stability is hard to analyze due to nonlinearities. Instabilities have been observed in implementation, even when used in training mode where actual transmitted symbols are used instead of symbol decisions.

This use of the same error metric for adaptation of both the beams and the equalizer coefficients could lead to a variety of failure modes. If one of the beams has a very low weight or two of the beams are highly correlated, the inverse matrix is ill-conditioned . The reverse situation also occurs when one feedforward section of the DFE is all low weights. These situations occur when the problem is over-parametrized, *i.e.* more beams are used than paths and there are a limited number of snapshots. Figure 4.5.3 shows the interconnectedness of the adaptive algorithm. Since there is so much interconnection and the use of shared quantities is non-linear, instabilities could easily occur when using the algorithm.
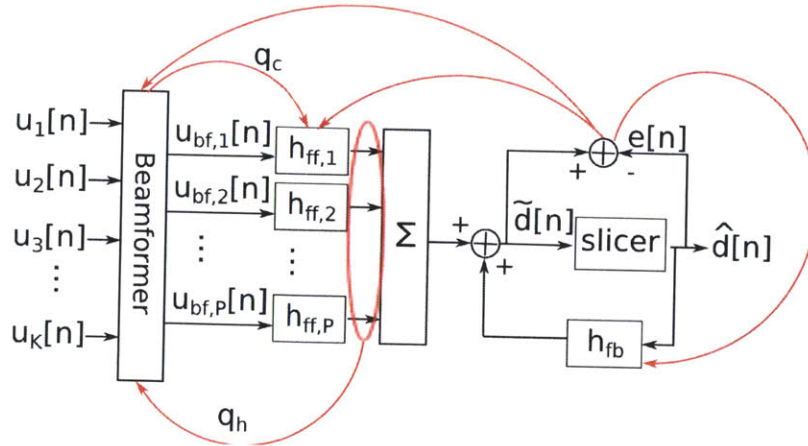
Figure 4.5.3: Interconnections in adaptive beamformer-DFE algorithm, which could lead to possible instabilities.

4.5.6 Hybrid methods

To harness both the computation reduction of the non-adaptive beams with the performance of the adaptive methods a hybrid method is proposed. In this method the received signal is sent through an initial beamformer which reduces the dimensionality of the data from sensor space to a beamspace. This beamformed data is fed into an adaptive beamformer algorithm and then into the multichannel DFE.

The main idea behind this method is that using a non-adaptive beamforming method, such as DPSS, preserves more of the signal energy and has similar computational advantages to reducing dimensionality by ignoring some of the receive sensors. Additionally, there are fewer parameters for the adaptive beamformer to adjust (due to the dimension reduction), which could improve performance in highly time-varying environments. A block diagram of this method is shown in figure 4.5.4. The beamformed data is represented as $\mathbf{u}'[n]$ after the initial beamformer, which has $B > P$ beams.

4.6 Estimating the number of beams

In the previous sections, many methods for finding beampatterns for a given number of beams were presented. In this thesis there has been no strong guidance yet into

101
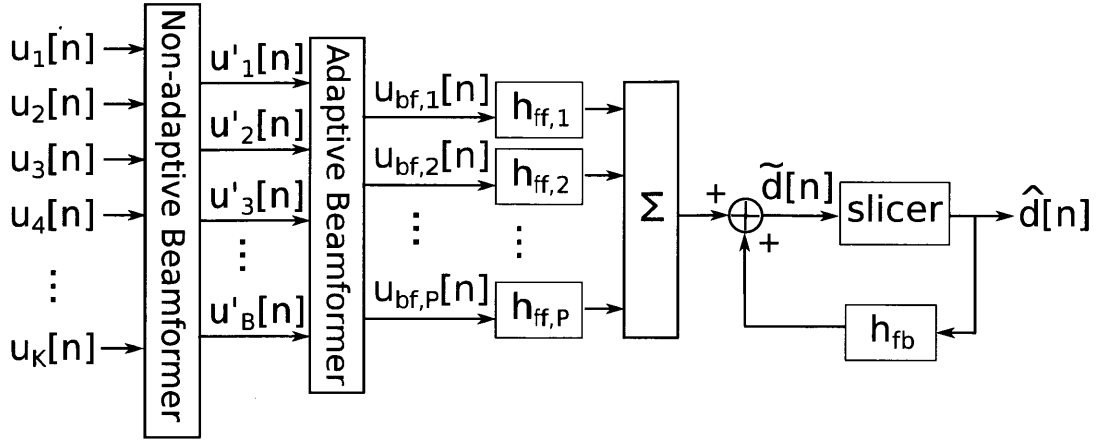
Figure 4.5.4: Hybrid-method for combining non-adaptive beamformer with adaptive beamformer. First the data is beamformed using a non-adaptive beamformer, such as a set of DPSS beams or uniformly weighted beams, and then the signal is sent through an equalizer and beamformer which are allowed to adapt to the signal.

how to choose the number of beams to use, except that the number of beams should be equal to the number of paths.

In this section, several methods are presented for estimating the number of arrivals impinging on the array. These methods fall into three broad classes: (i) physics-based methods, (ii) information theoretic methods, and (iii) generalized χ^2 methods. Physics-based methods use the ray-path model presented in Section 4.3 and environmental parameters to estimate the number of arrivals. Information theoretic methods use eigenvalue analysis to create an estimate of the rank of the signal subspace. Generalized χ^2 methods assume the channel is Rayleigh fading and match the estimated received signal statistics to a generalized χ^2 distribution to determine the number of degrees of freedom and hence the number of arrival paths.

The aim of this section is to evaluate these methods and describe their relative strengths and weaknesses. The results show that generalized χ^2 methods produce an estimate of the number of beams which nearly matches the knee in the observed multichannel DFE performance curves. Physics-based methods produce a slightly higher estimate, but one that is still reasonable. Information theoretic methods produce a estimate much higher than the observed data seems to support.

4.6.1 Physics-based method

Section 4.3 described a geometric ray-path model of the acoustic propagation environment. Along with the assumption of a constant, known sound speed this model provides not only the angle bounds discussed earlier but also the number of propagation paths. Figure 4.3.1 shows an illustration of the propagation paths.

The number of equalizer taps in each feedforward section is assumed to either be specified or determined from the channel impulse response estimate. Generally, the number of taps is chosen such that there are enough to span most of the energetic portion of the channel impulse response. If the specific channel impulse response is not available, the number of taps is usually specified for a range of expected channels and the available computing resources.

At first glance this may appear to be a chicken and egg problem because one might expect that while examining the channel impulse response the number of paths should be clear. The energetic region of a channel, however, is much easier to estimate than to determine the number of arrival paths. Figure 4.6.1 shows the evolution in time of a channel impulse response estimate when the communication distance was 1 km. The delay spread with significant energy is approximately 10 ms. The number of significant multipath components is not obvious from the channel impulse response estimate.

The delay spread of the channel with significant energy could be found by inserting a sequence with good correlation properties (*e.g.* an M-sequence) into the communications packet and correlating the received signal with the same sequence. This algorithm could be efficiently implemented and the delay spread can be determined automatically. The author knows of no similarly simple techniques to determine the number of significant arrivals.

Once the number of coefficients per feedforward section is known, the ray-path model is used to compute the number of arrival paths which fall within a specified delay extent (*i.e.* the number of feedforward equalizer coefficients). Recall that Table 4.3.1 shows the expressions for the first five arrivals.

103
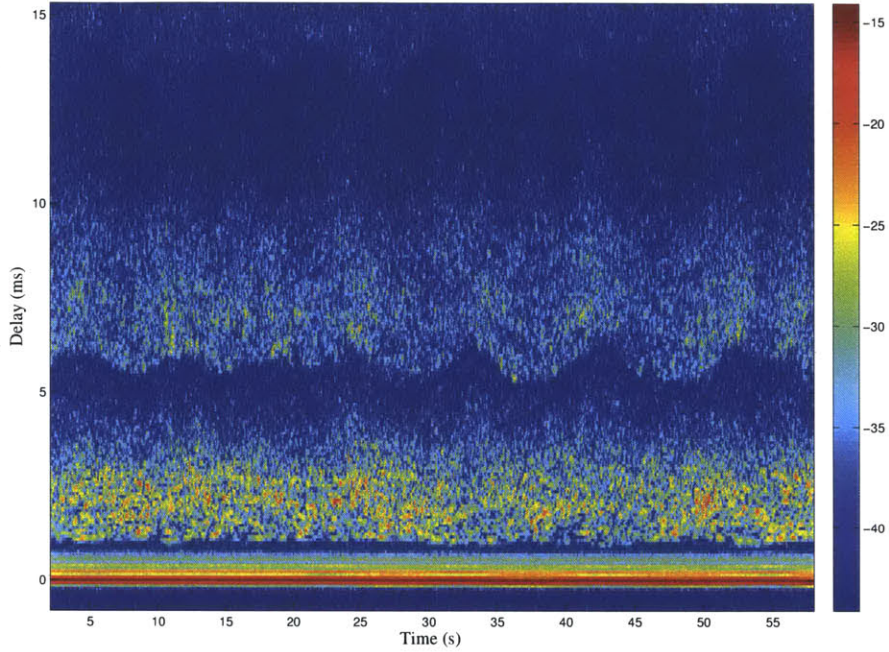
Figure 4.6.1: Estimate of a time-varying channel impulse response. The data is from the SPACE08 experiment, with a 1000 m propagation distance from transmitter to receiver and a RLS channel estimator is used. The color scale indicates the magnitude of the channel estimate in time and delay. This figure illustrates that the channel delay spread is simple to approximate, but the number of multipath arrivals is not apparent.

4.6.2 Information theoretic methods

Description of estimator

Using information theory a method can be derived for determining the number of arrivals directly from the data. The methods explored here assume that the plane-wave propagation model is valid (narrowband assumption). The key observation of these methods is that when the received signal correlation matrix, $\mathbf{R_u} = \mathrm{E}\{\mathbf{u}[n]\mathbf{u}^H[n]\}$, and the observation noise correlation matrix, $\mathbf{R_\nu} = \mathrm{E}\{\boldsymbol{\nu}[n]\boldsymbol{\nu}^H[n]\}$, are both known the whitened correlation matrix, $\mathbf{R_\nu}^{-1}\mathbf{R_u}$ has P eigenvalues greater than one and $K - P$ eigenvalues equal to one, where P is the number of paths and K is the number of receive sensors. An eigenvalue decomposition of the whitened correlation matrix ex-

actly estimates the number of paths which is equal to the appropriate number of beams [109].

Unfortunately, neither the observation noise correlation matrix nor the received signal correlation matrix is known and both must be estimated from the data. The estimated received signal correlation matrix and the estimated whitened received signal correlation matrix both have K unique eigenvalues in general [121]. Therefore, an eigenvalue decomposition of the estimated whitened received signal correlation matrix does not reveal the number of components directly. Using hypothesis testing, however, the number of multipath components can be estimated from the eigenvalues of the estimated whitened received signal correlation matrix [121].

The received signal correlation matrix can be decomposed as

$$\mathbf{R_u} = \mathbf{\Psi} + \mathbf{R}_\nu \tag{4.6.1}$$

where

$$\mathbf{\Psi} = \mathbf{\Phi} \mathbf{R_y} \mathbf{\Phi}^H. \tag{4.6.2}$$

$\mathbf{\Phi}$ is the full column rank array manifold matrix and $\mathbf{R_y}[n] = \mathrm{E}\{\mathbf{y}[n]\mathbf{y}^H[n]\}$ is the path space signal correlation matrix, as defined in eq. (4.4.3). If the transmitted data symbols are unit energy and white, then

$$\mathbf{R_y}[n] = \mathbf{G}_p^H[n]\mathbf{G}_p[n].$$

Assuming that $\mathbf{R_y}$ is non-singular, the rank of $\mathbf{\Psi}$ is equivalently equal to the number of paths P, the rank of $\mathbf{R_y}$, and the number of columns in $\mathbf{\Psi}$. If $\mathbf{\Psi}$ is $K \times K$, then the $K - P$ eigenvectors of $\mathbf{\Psi}$ are zero.

If the observation noise is white, then $\mathbf{R}_\nu$ has the form

$$\mathbf{R}_\nu = \sigma_\nu^2 \mathbf{I}, \tag{4.6.3}$$

If the noise is not white, but the noise correlation matrix, $\mathbf{R}_\nu$ is either known

a-priori or can be estimated, then the received data can be whitened to produce an equivalent whitened problem

$$\tilde{\mathbf{u}} = \mathbf{R}_\nu^{-1/2}\mathbf{u}, \tag{4.6.4}$$

and

$$\mathbf{R}_{\tilde{\mathbf{u}}} = \mathbf{R}_\nu^{-1/2}\mathbf{\Psi}\mathbf{R}_\nu^{-1/2} + \mathbf{I}. \tag{4.6.5}$$

In acoustic underwater communication problems neither the noise correlation matrix, $\mathbf{R}_\nu$ nor the signal plus noise correlation matrix $\mathbf{R}_\mathbf{u}$ is known *a-priori* and both must be estimated from the data,

$$\widehat{\mathbf{R}}_\mathbf{u}[n] = \frac{1}{N}\sum_{m=n-N+1}^{n} \mathbf{u}[m]\mathbf{u}^H[m] \tag{4.6.6}$$

$$\widehat{\mathbf{R}}_\nu[n] = \frac{1}{N}\sum_{m=n-N+1}^{n} \mathbf{u}_\nu[m]\mathbf{u}_\nu^H[m]. \tag{4.6.7}$$

In eq. (4.6.7), $\mathbf{u}_\nu$ are noise only samples, which can be taken during quiet periods between packets. Eqs. (4.6.6) and (4.6.7) are the maximum likelihood estimates of the received signal correlation matrix and the observation noise correlation matrix, respectively, when both the observation noise and the data are described by zero-mean Gaussian distributions.

In this section, the problem of interest is to estimate the number of significant multipath components P from the estimated received signal correlation matrix, $\widehat{\mathbf{R}}_u$. Assuming the noise is white with unit variance (the noise can be whitened as above) this problem is equivalent to determining how many of the eigenvalues of $\mathbf{R}_u$ are statistically greater than one, given only the noisy estimate $\widehat{\mathbf{R}}_u$.

A collection of techniques which solve this problem have their roots in information theory [121]. The two techniques explicitly discussed are the Akaike Information Criterion (AIC) [2, 3] and the Bayesian Information Criterion (BIC) [83, 90]. There has also been a flurry of activity lately by Nadakuditi and others solving this same subspace rank estimation problem using random matrix theory [67, 69, 68], but these results are not discussed explicitly here.

Both the AIC and the BIC are problems that seek to solve a cost function parametrized by a positive integer r,

$$J(r) = -2\log p_{\mathbf{u}}(\mathbf{u}|\hat{\boldsymbol{\xi}}^{(r)}) + \pi(r), \qquad (4.6.8)$$

where $\log p_{\mathbf{u}}(\mathbf{u}|\hat{\boldsymbol{\xi}}^{(r)})$ is the log-likelihood of $\mathbf{u}$ for estimated parameters $\hat{\boldsymbol{\xi}}^{(r)}$ and $\pi(r)$ is a penalty term related to the number of degrees of freedom in the model.

The parameter vector, $\boldsymbol{\xi}^{(r)}$, contains: the maximum likelihood estimate of the observation noise variance, $(\hat{\sigma}_w^2)_{ml}$, the maximum likelihood estimate of the r largest eigenvalues, $(\widehat{\lambda}_i)_{ml}$ $i = 1, \ldots, r$, and the corresponding eigenvectors, $(\widehat{\boldsymbol{\beta}}_i)_{ml}$ $i = 1, \ldots, r$ of the received signal correlation matrix, $\mathbf{R_u}$. If the received data are drawn from a Gaussian distribution (i.e. the observation noise and the signal are Gaussian), the eigenvalues and eigenvectors of the sample received signal correlation matrix are the maximum likelihood estimates, i.e. [4]

$$\widehat{\mathbf{R}}_{\mathbf{u}} = \sum_{m=1}^{K} \widehat{\boldsymbol{\beta}}_m \widehat{\boldsymbol{\beta}}_m^H \widehat{\lambda}_m \qquad (4.6.9)$$

$$(\widehat{\lambda}_i)_{ml} = \widehat{\lambda}_i \quad i = 1, \ldots, r \qquad (4.6.10)$$

$$(\widehat{\boldsymbol{\beta}}_i)_{ml} = \widehat{\boldsymbol{\beta}}_i \quad i = 1, \ldots, r \qquad (4.6.11)$$

$$(\widehat{\sigma}_w^2)_{ml} = \frac{1}{K-r} \sum_{i=r+1}^{K} \widehat{\lambda}_i \qquad (4.6.12)$$

where the subscript $_{ml}$ indicates the maximum likelihood estimate of the true parameter. The maximum likelihood estimates of the elements of $\widehat{\boldsymbol{\xi}}^{(r)}$ are

$$\widehat{\boldsymbol{\xi}}^{(r)} = \left[\widehat{\sigma}_\nu^2, \widehat{\lambda}_1, \ldots, \widehat{\lambda}_r, \widehat{\boldsymbol{\beta}}_1^T, \ldots, \widehat{\boldsymbol{\beta}}_r^T \right]^T \qquad (4.6.13)$$

The total number of degrees of freedom in the parameter vector $\widehat{\boldsymbol{\xi}}^{(r)}$ is the number of parameters that can be freely changed where real parameters have one degree of freedom and complex parameters have two. Without constraints, the number of degrees of freedom in the parameter vector is 1 from the observed noise variance, r

from the real valued eigenvalues, and $2rK$ from the complex eigenvectors, for a total of $1 + r + 2rK$. The eigenvectors are constrained to be unit norm, which reduces the available degrees of freedom by $2r$, and mutually orthogonal which removes another $2\frac{1}{2}r(r-1)$. Therefore, the total number of available degrees of freedom in the parameter vector $\widehat{\boldsymbol{\xi}}^{(r)}$ is

$$\text{DoF}(\widehat{\xi}^{(r)}) = r + 1 + 2rK - 2r - r(r-1) = r(2K - r) + 1$$

The difference between the AIC and the BIC is the form of the penalty function. The penalty function for the AIC is the available number of degrees of freedom in the parameter vector $\widehat{\boldsymbol{\xi}}^{(r)}$. The penalty function for the BIC is the available number of degrees of freedom in $\widehat{\boldsymbol{\xi}}^{(r)}$ scaled by half the log of the number of snapshots. The additional scaling term on the BIC penalty function leads to lower estimates of the number of observed paths than the AIC (on average) [90].

The parametrized log-likelihood function can be written as [125, 121]

$$L_r(r) = -\log p_{\mathbf{u}}(\mathbf{u}|\widehat{\xi}^{(r)}) = N(K - r)\log\left\{\frac{\frac{1}{K-r}\sum_{i=r+1}^{K}\widehat{\lambda}_i}{(\prod_{i=r+1}^{K}\widehat{\lambda}_i)^{\frac{1}{K-r}}}\right\} \tag{4.6.14}$$

where N is the number of snapshots available. The log of the ratio of the arithmetic to the geometric means of a noisy data set is a measure of the additional information gained by the knowledge that true data are all equal to the arithmetic mean of the observed data [127], *i.e.* how "surprising" a discovery would be that the true data are all equal to the arithmetic mean. This interpretation of the parametrized log-likelihood fits intuitively well for the AIC and BIC measures which attempt to determine the number of equal eigenvalues of the received signal correlation matrix.

Using the expressions for both the log-likelihood ratio and the penalty function, the BIC and AIC can be written as

$$\text{AIC}(r) \triangleq 2L_r(r) + 2(r(2K - r)) \tag{4.6.15}$$

$$\text{BIC}(r) \triangleq 2L_r(r) + (r(2K - r) + 1)\log N \tag{4.6.16}$$

The estimate of the number of observed paths (the rank of the signal subspace) is

$$\widehat{P}_{\mathrm{AIC}} = \arg\min_{r} \mathrm{AIC}(r) \qquad (4.6.17)$$

$$\widehat{P}_{\mathrm{BIC}} = \arg\min_{r} \mathrm{BIC}(r) \qquad (4.6.18)$$

The estimate produced using the BIC is consistent, *i.e.* as the number of snapshots approaches ∞, the estimate converges to the true value. The estimate produced using the AIC is not consistent [125], but with finite amounts of data, the AIC tends to give a better estimate of the signal subspace rank than the BIC [121].

Effectiveness of information theoretic methods for determining number of observed paths

One pitfall of these information theoretic methods is that the signal-subspace dimension estimate tends to be higher than the number of paths when the channel is time-varying. These information theoretic methods use an assumption that the matrix $\mathbf{\Phi}$ is constant over the averaging window. For a rapidly varying underwater channel, this may not be the case.

When the channel is varying in time, the estimated dimension can be greater than the number of paths. To illustrate this point, consider a unit energy signal that changes direction halfway through an averaging window, *i.e.*

$$\mathbf{u}[n] = \begin{cases} \mathbf{v}(\theta_0) & n < \frac{N_{\mathrm{win}}}{2} \\ \mathbf{v}(\theta_1) & n \geq \frac{N_{\mathrm{win}}}{2}, \end{cases} \qquad (4.6.19)$$

In the above expressions, $\mathbf{v}(\theta_i)$ is the array manifold vector parametrized by the angle of arrival θ_i and N_{win} is the window length. The time-averaged signal will have an estimated signal subspace dimension of 2, even though at any time instant there is only one path present.

This hazard is intrinsic to the framework of these estimators and the only work around is to shorten the data averaging time. Random-matrix methods attempt to

109

accomplish this by minimizing the amount of data needed to estimate the statistics (see *e.g.* [69]). For a constantly varying channel, however, there is no window short enough so the channel appears entirely stationary.

Another issue with reducing the averaging window is the validity of the narrowband assumption. One way to enforce the narrowband assumption when using wideband data is to first take the discrete Fourier transform (DFT) of the received signal and then process each resultant frequency bin individually, but the available data is reduced proportionally to the DFT length. Note that the AIC and BIC are correctly estimating the observed subspace signal dimension. Unfortunately, in the case of a time-varying channel, this dimension is not necessarily equal to the number of observed paths ($\widehat{P}_{\text{AIC,BIC}} \geq P$). Using these methods may lead one to use more beams than are strictly necessary, reducing the benefits of beamspace processing.

4.6.3   Generalized χ^2 testing

Generalized χ^2 random variables

An alternative statistical method for determining the number of beams is from the atmospheric science community [11] and is based on statistical analysis of χ^2 random variables. A χ^2 random variable is the sum of the squares of independent and identically distributed Gaussian random variables with zero mean and unit variance [70]. Changing the random variables in the sum to circularly-symmetric complex Gaussian random variables with variance σ^2 is a generalization of the χ^2 random variable and is what is referred to in this chapter as a generalized χ^2 random variable (also describes a gamma-distributed random variable).

As an example of a generalized χ^2 random variable, consider

$$\kappa = \sum_{i=1}^{D} |q_i|^2,$$

where $q_i \sim \mathcal{CN}(0, \sigma^2)$, *i.e.* q_i is circularly symmetric complex Gaussian distributed with mean zero and variance σ^2. This implies that κ is a generalized χ^2 random

variable with

$$
\begin{aligned}
\mathrm{E}\{\kappa\} &= \mu_\kappa = D\sigma^2 \\
\mathrm{var}(\kappa) &= \sigma_\kappa^2 = 2D\sigma^4
\end{aligned}
\tag{4.6.20}
$$

The number of *degrees of freedom* (DoF) of a χ^2 random variable is equal to the number of independent random variables in the sum. The number of independent random variables in a circularly complex Gaussian random variable is two: one for the real part and one for the imaginary. The estimate of the number of paths will soon be shown to be the number of complex circularly symmetric Gaussian random variables in the sum, or half the number of degrees of freedom in the generalized χ^2 random variable. A way to calculate the number of complex random variables in the generalized χ^2 random variable, κ, is [11]

$$
P_\kappa = \frac{1}{2}D = \frac{\mu_\kappa^2}{\sigma_\kappa^2}.
\tag{4.6.21}
$$

Using the Rayleigh fading model to create a generalized χ^2 random variable

A pertinent example of a generalized χ^2 random variable is the sum of the squared absolute value of the coefficients of a Rayleigh fading channel, *i.e.* $\sum_i |g_i|^2$. When a channel is Rayleigh fading, generalized χ^2 analysis can be used to determine the number of channel coefficients which equals the number of paths.

Over narrow frequency ranges, the underwater communication channel appears approximately Rayleigh fading [53]. The narrowband Rayleigh fading channel model considered in this section characterizes the fluctuations in each path using one random variable,

$$
\mathbf{g}_i(t) = \widetilde{g}_i(t)\mathbf{v}(\theta_i)\delta(t - \tau_i).
\tag{4.6.22}
$$

In the above expression, $\widetilde{g}_i(t)$ is a circularly-symmetric complex-Gaussian random process, $\mathbf{v}(\theta_i)$ is an array manifold vector with angle of arrival θ_i, and $\delta(t - \tau_i)$ is the path delay. When using a discrete time system, the channel is sampled at times $t = mT$, where T is the sampling period and m is an integer.

Recall from eq. (4.4.3) that the received signal has the form

$$\mathbf{u}[n] = \mathbf{\Phi}\mathbf{G}_p^H[n]\mathbf{d}'[n] + \boldsymbol{\nu}[n] \qquad (4.6.23)$$

Several simplifying assumptions are made throughout this section to clarify the analysis:

1. The path delays, τ_i, are multiples of the sampling period and no two paths have the same delay. These conditions imply that there is exactly one nonzero coefficient per column of $\mathbf{G}_p$ and at most one nonzero coefficient per row.

2. The channel path coefficients, $\widetilde{g}_i$, are IID and distributed as $\widetilde{g}_i \sim \mathcal{CN}(0, \sigma_g^2)$.

3. Each sensor observes the same channel, $\mathbf{G}_p[n]$. This implies a the array is short enough so there is not significant path length difference from top to bottom for any observed paths.

4. The observation noise is spatially and temporally white with zero mean and variance σ_ν^2.

5. The transmitted data symbols are IID with zero mean and unit variance (*i.e.* $\sigma_d^2 = 1$).

The first assumption is very approximate, but allows for some interesting results that are supported by the data. The next two assumptions simplify the analysis significantly and the effect of relaxing these assumptions is discussed later in the section. The fourth assumption is accurate in the high SNR regime, but the observed results do not appear to be sensitive to this assumption. The last assumption is standard in communications research.

To determine the number of multipath components, a functional of the received data vector is created,

$$F[n] = \mathbf{u}^H[n]\mathbf{u}[n]. \qquad (4.6.24)$$

112

Substituting the channel model from eq. (4.6.23) into this functional gives

$$F[n] = (\boldsymbol{\Phi}\mathbf{G}_p^H[n]\mathbf{d}'[n] + \boldsymbol{\nu}[n])^H(\boldsymbol{\Phi}\mathbf{G}_p^H[n]\mathbf{d}'[n] + \boldsymbol{\nu}[n]). \qquad (4.6.25)$$

After performing the multiplications the expanded version of the function is

$$F[n] = \mathbf{d}'^H[n]\mathbf{G}_p[n]\boldsymbol{\Phi}^H\boldsymbol{\Phi}\mathbf{G}_p^H[n]\mathbf{d}'[n] \qquad (4.6.26)$$
$$+ \boldsymbol{\nu}^H[n]\boldsymbol{\Phi}\mathbf{G}_p^H[n]\mathbf{d}'[n] + \mathbf{d}'^H[n]\mathbf{G}_p[n]\boldsymbol{\Phi}^H\boldsymbol{\nu} + \boldsymbol{\nu}^H[n]\boldsymbol{\nu}[n].$$

In the above expression, the vector of transmitted symbols, $\mathbf{d}'[n]$, has time-invariant statistics and the symbols are IID. Since the data is independent of both the channel and the noise, terms including $\mathbf{d}'[n]$ are replaced by their expected value with respect to the transmitted data symbols. Over the averaging windows of the time averaging used to estimate the statistics of the received data, this assumption does not introduce noticeable errors. Using this substitution, eq. (4.6.26) becomes

$$F[n] = \mathrm{Tr}(\boldsymbol{\Phi}\mathbf{G}_p^H[n]\mathbf{G}_p[n]\boldsymbol{\Phi}^H) + \boldsymbol{\nu}[n]^H\boldsymbol{\nu}[n]. \qquad (4.6.27)$$

The first term is found using the identity of the trace operator, $\mathrm{Tr}(\mathbf{AB}) = \mathrm{Tr}(\mathbf{BA})$. The second and third terms from eq. (4.6.26) vanish since the transmitted data symbols are zero mean and uncorrelated with the observation noise.

Using the assumption that $\mathbf{G}_p[n]$ contains exactly one non-zero entry per column and at most one non-zero entry per row, $\mathbf{G}_p^H[n]\mathbf{G}_p[n]$ is the diagonal matrix

$$\mathbf{G}_p^H[n]\mathbf{G}_p[n] = \begin{bmatrix} |g_1[n]|^2 & 0 & 0 & \cdots & 0 \\ 0 & |g_2[n]|^2 & 0 & \cdots & 0 \\ 0 & 0 & |g_3[n]|^2 & \cdots & 0 \\ \vdots & \vdots & \vdots & \ddots & \vdots \\ 0 & 0 & 0 & \cdots & |g_P[n]|^2 \end{bmatrix}.$$

The delay index on the channel coefficients is not shown since there is only one non-

zero coefficient per path.

Recall that the ith column of the array manifold matrix, $\boldsymbol{\Phi}$, is the array manifold vectors for a linear array, $\mathbf{v}(\theta_i)$. Using the relation, $\mathbf{v}^H(\theta_i)\mathbf{v}(\theta_i) = K$, eq. (4.6.27) becomes

$$\text{Tr}(\boldsymbol{\Phi}\mathbf{G}_p^H[n]\mathbf{G}_p[n]\boldsymbol{\Phi}^H) = K\sum_{i=1}^{P}|g_i[n]|^2.$$

All of these assumptions and matrix manipulations lead to a usable form of the functional

$$F[n] = K\sum_{i=1}^{P}|g_i[n]|^2 + \sum_{j=1}^{K}|\nu_i[n]|, \qquad (4.6.28)$$

where $\boldsymbol{\nu}^H[n]\boldsymbol{\nu}[n]$ is written using sum notation. Both the channel coefficients, g_i, and the observation noise terms, ν_i, are circularly-symmetric, complex Gaussian random variables. Therefore, the functional $F[n]$ is the sum of two generalized χ^2 random variables: one for the channel coefficients and one for the noise.

Determining the number of beams from the Rayleigh fading model

Given the number of sensors is K and the number of non-zero channel coefficients (*i.e.* the number of paths) is P, the mean, μ_F, and variance, σ_F^2, of the functional, $F[n]$, are

$$\mu_F = KP\sigma_g^2 + K\sigma_\nu^2 \qquad (4.6.29)$$

$$\sigma_F^2 = 2K^2P\sigma_g^4 + 2K\sigma_\nu^4. \qquad (4.6.30)$$

The inverse signal to noise ratio is defined as

$$\rho = \frac{\sigma_\nu^2}{\sigma_d^2\sigma_g^2}. \qquad (4.6.31)$$

Applying the same ratio test to determine the number of complex components of a generalized χ^2 random variable from eq. (4.6.21) to the functional, $F[n]$ produces the relation

$$P_F = \frac{\mu_F^2}{\sigma_F} = \frac{K(P+\rho)^2}{KP+\rho^2}. \qquad (4.6.32)$$

114

There are three interesting regions of ρ_{SNR} for the estimated path count, P_F: high SNR ($\rho \approx \infty$), low SNR ($\rho \approx 0$), and the maximum path count estimate which occurs when $\rho = K$. In the high SNR region, the parameter $\rho \to 0$, so $P_F \approx P$, $i.e.$ the path count estimate equals the number of paths. In the low SNR region, the parameter $\rho \to \infty$, so $P_F \approx K$, the number of sensors since the noise space is full rank.

For the same channel statistics as the SNR is decreased the estimated number of paths increases. This could be desirable feature of this estimator since as the SNR is decreased, the estimator allows for more beams which implies better noise immunity (if the noise on each beam is assumed to be independent). More beams also implies more parameters to estimate so components with more variability are not able to be tracked. Thus, this behavior of the estimator should be taken into account when designing systems which use χ^2 methods for estimating the number of paths.

The DoF count estimate is not a monotonic function of ρ_{SNR}, but the relation

$$P_F \leq P + K \qquad (4.6.33)$$

can be verified by substitution. Equality is achieved when $\rho = K$. Thus, P_F can be greater than the number of sensors, but only for a very low SNR ($i.e.$ $\rho \approx K$).

Another way to estimate the degrees of freedom in a χ^2 random variable is proposed in [6, 11, 113, 12] based on the received signal correlation matrix $\mathbf{R_u}$. In this approach, the estimated number of degrees of freedom is

$$P_{\text{ef}} = \frac{(\text{Tr}(\mathbf{R_u}))^2}{\text{Tr}(\mathbf{R_u^2})} = \frac{\left(\sum_{i=1}^{K} \lambda_i\right)^2}{\sum_{i=1}^{K} \lambda_i^2} \qquad (4.6.34)$$

where λ_i is the ith eigenvalue of the received signal correlation matrix. In the literature this method assumes that the received data vector $\mathbf{u}[n]$ is a Gaussian random vector, where each element is zero-mean and unit variance, which is not the case for the underwater communication problem. This function of the eigenvalues, however, turns out to be a reasonable estimator of the number of paths in the underwater channel; The numerator and the denominator are evaluated independently to justify

that eq. (4.6.34) is a good estimator of the number of paths.

The trace of the received signal correlation matrix is equivalent to the mean of $F[n]$, through the relation

$$\mathrm{E}\{F[n]\} = \mathrm{E}\{\mathbf{u}^H[n]\mathbf{u}[n]\} = \mathrm{E}\{\mathrm{Tr}(\mathbf{u}[n]\mathbf{u}^H[n])\} = \mathrm{Tr}(\mathbf{R}_u). \qquad (4.6.35)$$

Thus, the numerator of P_{ef} is the square of the expected value of $F[n]$, which is also the numerator of P_F.

The denominator of eq. (4.6.34) is more complicated to justify. A first step is to substitute the received signal model from eq. (4.6.23) into the expression for the received signal correlation matrix,

$$\mathbf{R_u} = \mathrm{E}\{\mathbf{u}[n]\mathbf{u}^H[n]\} = \mathrm{E}\{(\mathbf{\Phi}\mathbf{G}_p[n]\mathbf{d}'[n] + \boldsymbol{\nu}[n])(\mathbf{\Phi}\mathbf{G}_p[n]\mathbf{d}'[n] + \boldsymbol{\nu}[n])^H\}. \qquad (4.6.36)$$

Evaluating the expectation with respect to the transmitted symbols, the noise, and the channel coefficients, the received signal correlation matrix is

$$\mathbf{R_u} = \sigma_g^2\mathbf{\Phi}\mathbf{\Phi}^H + \sigma_\nu^2\mathbf{I}, \qquad (4.6.37)$$

where the noise is still assumed to be spatially and temporally white. Since $\mathrm{E}\{F[n]\} = \mathrm{Tr}(\mathbf{R}_u)$, the terms in eq. (4.6.37) correspond exactly to the terms in eq. (4.6.29). Comparing terms, the trace of the matrix product, $\mathbf{\Phi}\mathbf{\Phi}^H$ is

$$\mathrm{Tr}(\mathbf{\Phi}\mathbf{\Phi}^H) = KP. \qquad (4.6.38)$$

Using eq. (4.6.37) and eq. (4.6.38) the expression for $\mathrm{Tr}(\mathbf{R}_u^2)$ becomes

$$\mathrm{Tr}(\mathbf{R}_u^2) = \mathrm{Tr}\big((\sigma_g^2\mathbf{\Phi}\mathbf{\Phi}^H + \sigma_\nu^2\mathbf{I})^2\big)$$
$$= \sigma_g^4\alpha_{\mathrm{ef}} + 2KP\sigma_g^2\sigma_\nu^2 + K\sigma_\nu^4. \qquad (4.6.39)$$

116

In this expression, the quantity α_{ef} is defined as

$$\alpha_{\text{ef}} = \text{Tr}\left((\boldsymbol{\Phi}\boldsymbol{\Phi}^H)^2\right). \tag{4.6.40}$$

Recall that the columns of the matrix $\boldsymbol{\Phi}$ are array manifold vectors, which can be parametrized by an AoA θ. The ith column of $\boldsymbol{\Phi}$ is denoted as $\mathbf{v}(\theta_i)$. The expression for α_{ef} is

$$\alpha_{\text{ef}} = \sum_{k=1}^{P}\sum_{\ell=1}^{P}\left|\mathbf{v}^H(\theta_k)\mathbf{v}(\theta_\ell)\right|^2 = K^2P + 2\sum_{k=1}^{P-1}\sum_{\ell=k+1}^{P}\left|\mathbf{v}^H(\theta_k)\mathbf{v}(\theta_\ell)\right|^2 = K^2P + 2\gamma_{\text{ef}}. \tag{4.6.41}$$

The expression for γ_{ef} depends on the angles $\theta_1, \ldots, \theta_P$ which depend on the particulars of the communication channel. Thus there is no way to further simplify the expression for γ_{ef}. The parameter γ_{ef}, however, can be bounded by

$$0 \leq \gamma_{\text{ef}} < \frac{1}{2}K^2P(P-1),$$

which implies bounds for α_{ef},

$$K^2P \leq \alpha_{\text{ef}} \leq K^2P^2.$$

The lower bound is achieved when all of the array manifold vectors are orthogonal, *i.e.* $\mathbf{v}^H(\theta_k)\mathbf{v}(\theta_\ell) = 0$ when $k \neq \ell$. The upper bound is achieved when all of the array manifold vectors are the same, *i.e.* $\mathbf{v}(\theta_1) = \mathbf{v}(\theta_2) = \cdots = \mathbf{v}(\theta_P)$.

Using the derived expressions for the numerator and denominator, the estimate of the arrivals, P_{ef} is

$$P_{\text{ef}} = \frac{(\text{Tr}(\mathbf{R_u}))^2}{\text{Tr}(\mathbf{R_u^2})} = \frac{K^2(P+\rho)^2}{\alpha_{\text{ef}} + 2KP\rho + K\rho^2} \tag{4.6.42}$$

In the low-SNR region ($\rho \to \infty$), regardless of the path AoA, the number of arrivals estimate $P_{\text{ef}} \approx K$. In the high SNR region ($\rho \to 0$), the result depends on the alignment of the array manifold vectors. When the array manifold vectors are

orthogonal $P_{ef} \approx P$. When the array manifold vectors are not orthogonal in the high SNR region, then $P_{ef} < P$. In the degenerate case when all of the array manifold vectors are equal, $P_{ef} = 1$.

The dependence of P_{ef} on the AoA in the high SNR regime has some nice interpretations and nice results. When two AoA are nearly equal, the DoF count estimate is reduced since fewer beams are needed to capture energetic paths. This is generally a positive results since highly time-varying paths will likely be ignored. Reducing the number of beams does place additional constraints on DFE since there are fewer adaptive parameters, so the end effect on residual error is unclear.

P_{ef} is a monotonically decreasing function of the SNR, so there is no local maximum like there was for P_F. As the SNR decreases, there is a smooth transition of the number of paths estimated from the high SNR estimate to K.

An additional result is that the term $2\text{Tr}(\mathbf{R_u^2})$ is an upper-bound of σ_F^2,

$$
\begin{aligned}
\sigma_F^2 &= K^2 P \sigma_g^4 + K \sigma_\nu^4 \\
&\leq K^2 P \sigma_g^4 + 2 K P \sigma_g^2 \sigma_\nu^2 + K \sigma_\nu^4 \\
&\leq \alpha_{ef} \sigma_g^4 + 2 K P \sigma_g^2 \sigma_\nu^2 + K \sigma_\nu^4 \\
&= \text{Tr}(\mathbf{R_u^2}).
\end{aligned}
\tag{4.6.43}
$$

The expression in the second line is the lower bound of $\text{Tr}(\mathbf{R_u^2})$. Equality of all terms is achieved when $\rho = \infty$, $i.e.$ at very low SNR. In other SNR regions, $\sigma_F^2 < \text{Tr}(\mathbf{R_u^2})$. Using the equality relation from eq. (4.6.35) and the inequality relation from eq. (4.6.43), the number of arrival estimators are related by

$$
P_{ef} \leq P_F.
\tag{4.6.44}
$$

Estimating the number of paths from the received signal

The true statistics of the received signal and noise are not known and must be estimated from the received signal. In this subsection, estimators based on estimated statistics are presented.

One method for estimating the number of paths from the data is to directly estimate the statistics of $F[n]$, a modified version of the *method of moments* from [6, 11]. Replacing the mean and variance of $F[n]$ in eq. (4.6.32) with estimates based on a length M sliding window gives the estimate of the number of arrivals,

$$\widehat{P}_F = \frac{\left(\frac{1}{M}\sum_{i=1}^M F[n-i]\right)^2}{\left(\frac{1}{M}\sum_{i=1}^M F^2[n-i]\right) - \left(\frac{1}{M}\sum_{i=1}^M F[n-i]\right)^2}. \tag{4.6.45}$$

This method circumvents the need for explicit calculation of the PDF of F but there is no guaranteed upper bound on the estimated number of paths.

A second method for estimating the number of paths from the received signal is to create an estimate of the received signal correlation matrix, $\widehat{\mathbf{R}}_{\mathbf{u}}$. This estimator uses the function of the eigenvalues from eq. (4.6.34), with the estimated correlation matrix eigenvalues, $\widehat{\lambda}_i$, in place of the true correlation matrix eigenvalues, λ_i. This estimator is

$$\widehat{P}_{\text{ef}} = \frac{\left(\text{Tr}(\widehat{\mathbf{R}}_{\mathbf{u}})\right)^2}{\text{Tr}(\widehat{\mathbf{R}}_{\mathbf{u}}^2)} = \frac{\left(\sum_{i=1}^K \widehat{\lambda}_i\right)^2}{\sum_{i=1}^K \widehat{\lambda}_i^2}. \tag{4.6.46}$$

The last section stated that $\widehat{\lambda}_i$ is the maximum likelihood estimate of λ_i. Therefore, the path count estimate $\widehat{P}_{\text{ef}}$ is a maximum likelihood estimate of P_{ef}. Due to the way they are computed the number of arrival estimates using both both the true eigen-structure P_{ef} and the estimated $\widehat{P}_{\text{ef}}$ are guaranteed to be within $1 \leq P_{\text{ef}}, \widehat{P}_{\text{ef}} \leq K$.

Effectiveness of χ^2 methods for determining number of observed paths

The use of generalized χ^2 techniques for creating number of path estimators has distinct advantages over the information theoretic methods. There is not the same requirement that AoA for the different paths are time-invariant when using generalized χ^2 techniques: the method of moments estimator, $\widehat{P}_F \approx P_F$, has no explicit dependence on the AoA and the eigenvalue ratio estimate, $\widehat{P}_{\text{ef}} \approx P_{\text{ef}}$, is upper bounded by the number of paths in the high SNR region.

The generalized χ^2 methods have less dependence on the variation of the AoA

than the information theoretic methods since both rely on eigenvalues of the received signal correlation matrix. The information theoretic methods, however, are based on a successive ratio test [121], so the change in the individual eigenvalues (caused by a change of an AoA) can drastically change the estimate. By contrast, the generalized χ^2 rely only on aggregate eigenvalues, so individual eigenvalues (and thus the changes in AoA) play a decreased role in determining the number of paths.

There are some things to keep in mind when using generalized χ^2 analysis for underwater channels. First, the underwater channel is only approximately Rayleigh fading [52, 130], so the proposed channel model can be inaccurate. This causes some degradation in the performance [11], but the effect can be mitigated by using narrower DFT bins so that the Rayleigh fading assumption is more accurate [53]. Also, each of the multipath arrivals does not have the same energy, which reduces the accuracy of the estimator. Fortunately, eighty to ninety percent of the degrees of freedom are captured using χ^2 types of estimation methods [39].

4.7 Experimental evidence

In this section, experimental evidence is presented for methods of computing the beam weights and the number of beams to use.

4.7.1 SPACE08 experiment setup

The SPACE08 was performed off the coast of Martha's Vineyard, MA from Oct. 14th through Nov. 1st, 2008. The water depth was approximately 15 meters, the transmitter was approximately 4 meters from the sea floor, and the top of the receive arrays were about 3.25 meters above the sea floor. Figure 4.7.1 illustrates the experimental setup.

The carrier frequency was $f_c = 12.5$ kHz, the bandwidth was $B = 6.51$ kHz, and the sampling frequency was $f_s = 39.06$ kHz. The transmitted signal was the first 20,000 symbols of a repeated binary phase shift keyed (BPSK) encoded, 4095-length M-sequence.
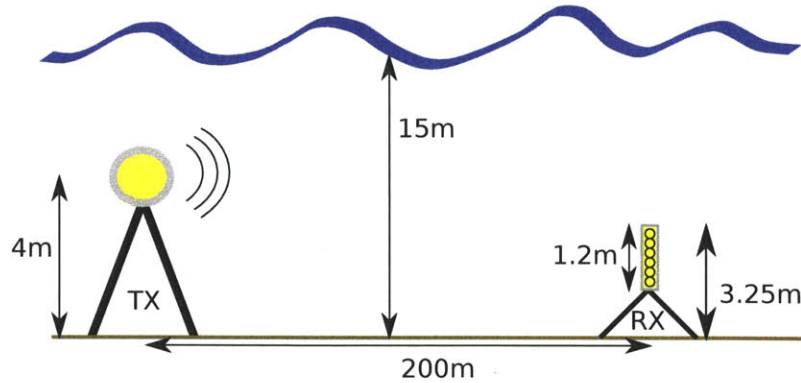
Figure 4.7.1: Setup of SPACE08 experiment

Before processing, the carrier was removed, the data was low-pass filtered, and the data was down-sampled to two samples per symbol. Time alignment of the signal was achieved through the use of an M-sequence timing signal at the beginning of the packet.

The receiver was a 24-element vertical array with 5 cm element spacing placed. The array was 200 meters from the transmitter to the southwest.

Every two hours, all of the acoustic signals being tested for the experiment were sent sequentially. This entire collection of signals made up one time *epoch*, which are referred to by the time and Julian day they were transmitted. Each epoch is labelled by the Julian date and time of the start of transmission of its first packet.

4.7.2   Comparing methods for computing beam weights

Three epochs were chosen from different days with a variety of sea surface conditions: day 297 at time 1800, day 294 at time 1200, and day 300 at time 0800. These three epochs range from calm on day 297 to high stormy seas on day 300. Each of the methods described in Section 4.5 was tested for each one of these epochs, as was the full sensor-space processing and sensor-space processing using a number of sensors equal to the number of beams.

The DFE parameters were chosen as follows: the number of acausal coefficients in each feedforward section is $L_a = 10$. The number of causal coefficients in each feedforward section is $L_c = 40$. The number of feedback filter coefficients is $L_{fb} = 23$.

This allowed the feedforward filter to capture most of the signal energy and the feedback filter to cancel most of the ISI. The received signal was sampled twice per symbol (*i.e.* the fractional sampling rate was 2).

An EW-RLS algorithm was used to estimate the DA-DFE equalizer taps. In order to ensure that the observed results were not an artifact of the choice of the exponential weighting factor, λ, seven different values were tested from $\lambda = 0.996$ to $\lambda = 0.9995$. The minimum mean squared error results across all λ are shown in the figures below.

Using the ray-path modeled described in Section 4.3 with the experiment geometry, the number of significant arrivals was estimated to be seven. Thus, 7 beams were created using each of the proposed methods for determining the beam weights (except for the time-aligned uniform beams which only used 5). The broadside angle is defined to be at 90° with the surface at 0° and the seafloor at 180°. The elevation angles examined for the beamspace methods were from 75.5^o to 104.5^o. For the DPSS method, the angular spread used was 70.3^o to 109.7^o.

For the hybrid methods, the number of beams for the initial beamformer was chosen to be 12. This number was chosen because it was higher than the estimated number of arrivals but was much less than the number of sensors.

The mean squared error (MSE) at the output of the equalizer, is , ϵ_{MSE}, was the metric used to compare the different methods. This MSE is

$$\epsilon_{\mathrm{SDE}} = \frac{1}{N} \sum_{n=1}^{N} \frac{|d[n] - \tilde{d}[n]|^2}{|d[n]|^2}, \qquad (4.7.1)$$

where $d[n]$ is the transmitted symbol and $\tilde{d}[n]$ is the filtered data before the symbol decision.

Due to the large array gain, the bit error rate (BER) was nearly zero, even as the SNR was degraded in all examined cases. The SNR was degraded by adding a scaled version of an ambient noise signal recorded during a silent period in the epoch.

Figure 4.7.3 shows the results from the day 297, time 1800 epoch, day 294, time 1200 epoch, and day 300, time 0800 epoch. The input SNR is the ratio of the measured incoherent signal energy to noise energy before equalization. The observed input SNR

Table 4.7.1: Input signal to noise ratio for each of the data epochs examined from the SPACE08 experiment.

Epoch	Input SNR
Day 297, time 1800	41.2 dB
Day 294, time 1200	37.2 dB
Day 300, time 0800	35.2 dB

for each epoch is given in Table 4.7.1.

The results show that the adaptive methods and the hybrid adaptive generally outperform the non-adaptive methods and generally the DPSS methods outperform the other non-adaptive methods. As the sea surface conditions become rougher, adaptive methods tend to have the lowest MSE. The non-adaptive methods have an assumed angular spread that is violated when the sea-surface becomes too rough.

The performance of the reduced sensor adaptive method (which uses 12 sensors to create the 7 adaptive beams) reduces relative to the non-adaptive hybrid methods as sea surface condition become rougher. This result implies that using hybrid methods provides less sensitivity to surface conditions than simply ignoring sensor data.

The MCM and MVDR methods are the only methods studied which takes the observed noise correlation structure into account, so one would expect them to outperform the other methods. The reason they do not is that methods such as MVDR and MCM were designed with the goal of *rejecting* unwanted signals. The goal of a communication system is to *accept* as many desirable signals as possible. That the MCM method is slightly worse than that of the uniform beams is not surprising since the uniform beams gather more energy from the angular range of interest than the MCM method.

For comparison of computationally similar methods, seven of the twenty-four sensors were used as the input to a multichannel equalizer. Several configurations of the seven sensors were tested and the best configuration for each epoch is shown on the figures. In all cases, the best seven sensors perform at least 2 dB worse than either the proposed methods or the full sensor space. Thus, for the same computational complexity, the proposed methods improve the performance dramatically and compete
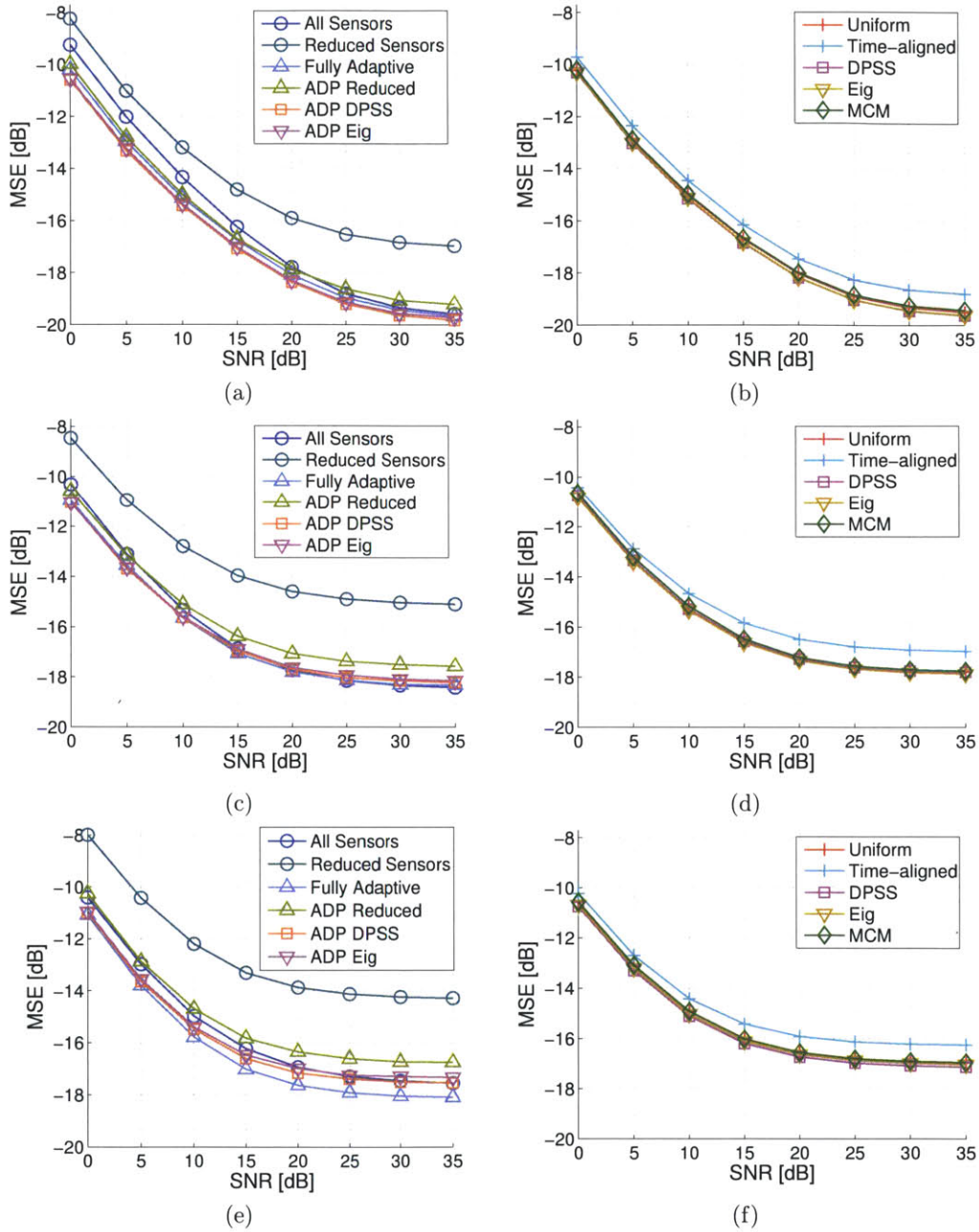
Figure 4.7.2: Comparison of beamforming methods using SPACE08 experimental data. The left column ((a), (c), and (e)) contains the beamspace and adaptive methods. The right column ((b), (d), and (f)) contains the non-adaptive methods. (a) and (b) are results using data taken on day 297, time 1800, calm conditions. (c) and (d) are results using data taken on day 294, time 1200, smooth, rolling waves. (e) and (f) are results using data taken on day 300, time 0800, very stormy conditions.
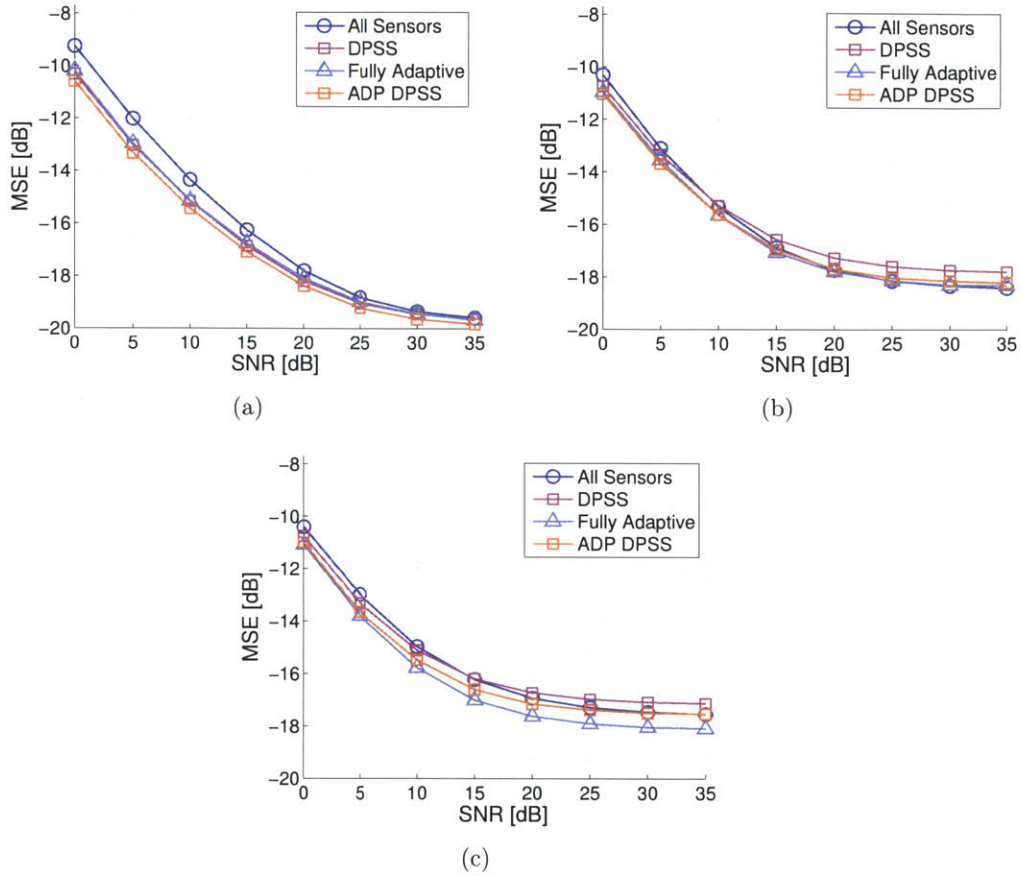
Figure 4.7.3: Results from SPACE08 comparing the beamspace, adaptive, non-adaptive, and hybrid methods for three sea surface conditions: (a) calm [day 297, time 1800] (b) rolling waves [day 294, time 1200] and (c) [day 300, time 0800]. In all three cases, the relative performance of the beamspace processing is reduced as the SNR is reduced. For the other methods the performance is approximately equivalent with the adaptive methods having the best performance as the sea surface conditions become rougher.

Table 4.7.2: Description of beamforming methods labels.

Legend Entry	Description
All Sensors	Complete sensor space using all available sensors.
Reduced Sensors	Sensor space using 7 best sensors.
Uniform	7 uniformly weighted steered beams steered to null of neighbor.
Time-aligned	Uniformly weighted beams only equalized in region of expected channel energy.
DPSS	7 Discrete prolate spheroidal beams with angle span calculated using ray-path model.
Eig	Beams composed of eigenvectors corresponding to largest 7 principle components of received signal correlation matrix.
MCM	7 Multiple constraint beams steered in same directions as uniform weighted beamformer.
Fully Adaptive	Adaptive beamformer with 7 beams.
ADP Reduced	Adaptive beamformer with 7 beams using only 12 sensors
ADP DPSS	12 beam DPSS beamformer followed by 7 beam adaptive beamformer.
ADP Eig	12 beams corresponding to largest 12 principle components of the received signal correlation matrix followed by 7 beam adaptive beamformer.
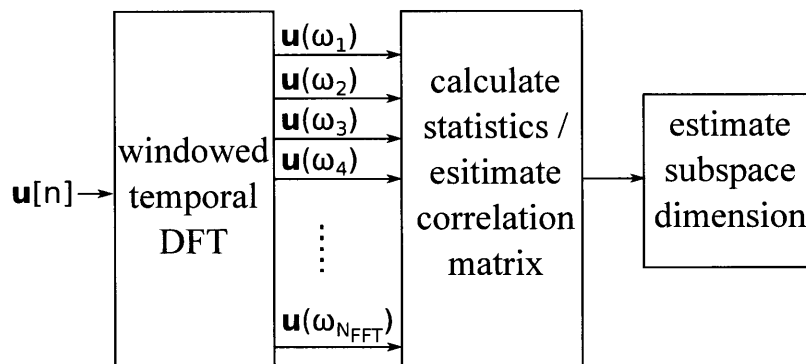
Figure 4.7.4: Procedure for estimating the subspace dimension from data.

quite favorable with the full sensor space results.

All results presented in this section are sensitive to the choice of the exponential weighting factor, λ. Finding the optimal λ for a given channel is beyond the scope of this work. Further work on adaptively tracking the optimal exponential weighting factors is merited.

4.7.3 Comparing methods for estimating number of beams

In this subsection, the methods for computing the number of beams are compared using experimental data. This data used is taken from the SPACE08 experiment, from the day 297, time 1800 epoch.

To determine the number of beams, the data is windowed using a Hann window (to reduce side-lobe levels) and then passed through a discrete Fourier transform. The statistics and correlation matrix are then calculated for each temporal frequency bin which are then used to estimate the number of arrivals. This process is illustrated in Figure 4.7.4.

One way to increase the effective averaging times is to average several estimates together. In figure 4.7.5 estimates are shown for temporal frequencies from 0 to $f_s/2$ for four different averaging windows: 50, 100, 500, and 1000 sample windows. The carrier frequency is shown in a thick dashed lines and the signal bandwidth is shown in black dash-dot lines. A 512 point DFT was used with an overlap of 256 samples and a total data block length of 500,000 samples. The carrier frequency is $f_c = 12.5$ kHz

Table 4.7.3: Estimated number of arrival estimates across bandwidth of transmitted signal (SPACE08 data). The averaging window indicates the amount of data used to make an individual estimate. The estimates are averaged across the entire 500,000 sample data-set. The window overlap amount is half of the averaging window length.

| Data Set | Ave. Win | Estimation Method | | | |
		AIC	*BIC*	*DoF - MM*	*DoF - Eig*
	50	22.18	20.06	2.33	2.14
Day 297, Time 1800	100	22.39	20.84	2.83	1.96
	500	22.85	22.42	4.34	1.80
	1000	22.90	22.71	4.82	1.77

and the sampling frequency is $f_s = 39.06$ kHz.

The subspace estimation results show a big difference between the information theoretic methods and the other methods. The reason for the gap between the methods is due to channel motion, which causes the AIC and BIC methods to produce a high estimate of the signal subspace due to averaging of the moving signal.

To determine which, if any, of the studied methods effectively estimates the useful number of beams, the MSE at the output of the multichannel DFE is compared when different numbers of beams are used. This experiment is performed for two of proposed beam-weight methods: the DPSS beams and the fully adaptive beams. The results are shown in Figure 4.7.6.

The results shown in figure 4.7.5 for show a leveling off around the number of beams corresponding to the number of arrivals predicted by the ray-path model. The knee of the curves occurs before this value and appears to be well estimated by the χ^2 methods. The estimates produced using the AIC and BIC methods appear to be much higher than the data indicates are useful.

At high SNR, the DPSS method continues to improve slightly as the number of beams is continually increased, but at low SNR both methods show a distinct leveling off at around seven beams. The χ^2 methods provide a reliable, data driven method for computing the number of beams needed to achieve good performance in this experiment.

An interesting feature of these plots is that the number of beams used could also
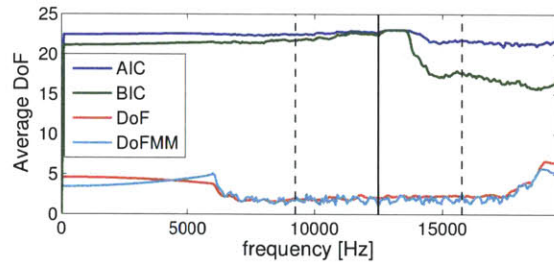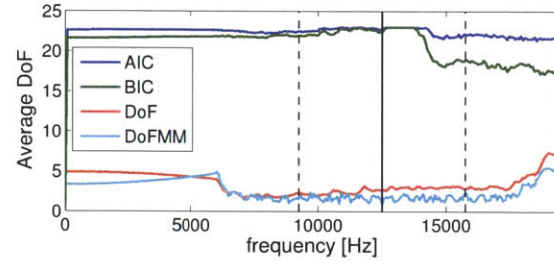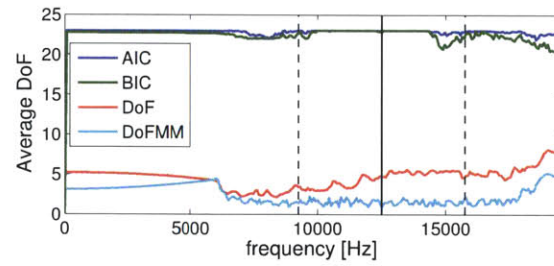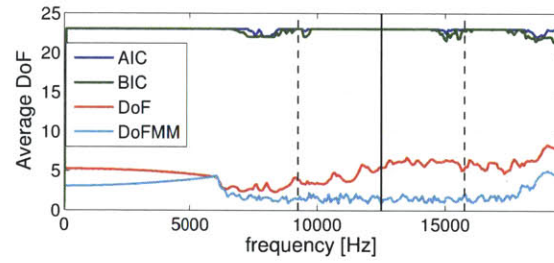
Figure 4.7.5: Number of arrival estimation for data gathered on day 297, time 1800 at the SPACE08 experiment. All results presented use $500,000$ signal sample, with 6 samples per transmitted symbol. Four different methods are presented: AIC is the Akaike information criterion, BIC is the Bayesian Information Criterion, DoF is the generalized χ^2 method using the correlation matrix, and DoFMM is generalized χ^2 the method of moments. Different averaging windows are used: (a) length 50 averaging window, (b) length 100 averaging window, (c) length 500 averaging window, and (d) length 1000 averaging window. samples is used and in (b) an averaging window of 1000 samples is used. There was an overlap length of half the averaging window. The solid black line shows the carrier frequency and the dash-dot lines show the transmitted signal bandwidth.
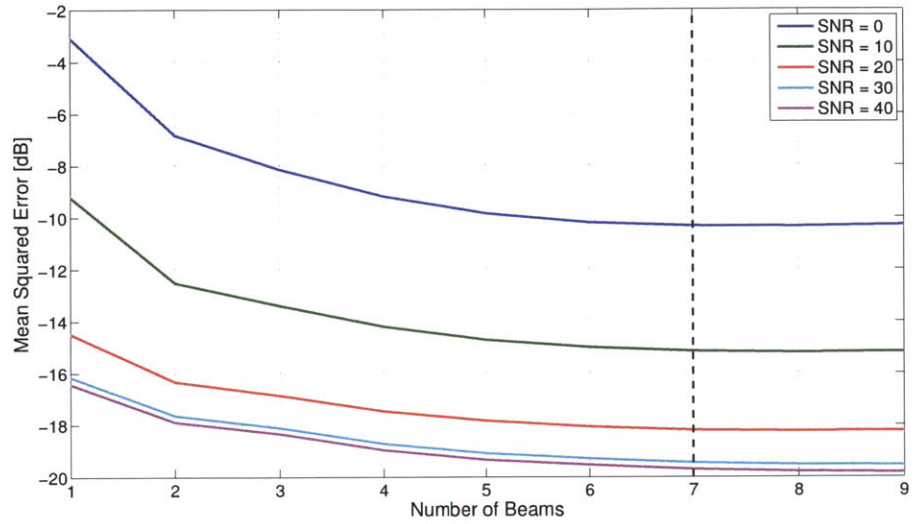
(a)
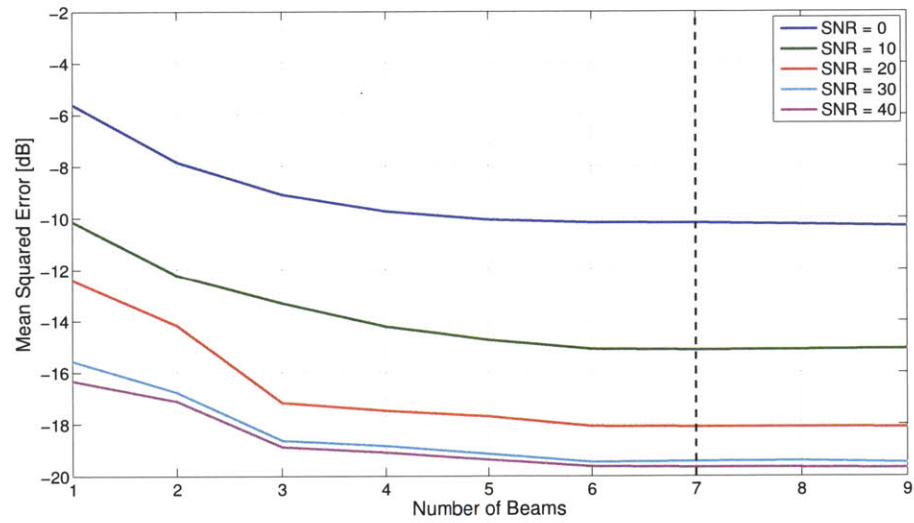
(b)

Figure 4.7.6: Comparison of mean squared error verses the number of beams for (a) DPSS beamformer and (b) Fully Adaptive beamformer. The black dashed line is the number of arrivals estimated by the ray-path model.

be reduced without too much loss in performance. Thus, if computational complexity is of chief concern, and often it is, the number of beams could be reduced, especially at high SNR, to as low as three beams with only about 1dB loss of performance.

4.7.4 MACE10 experiment setup

The SPACE08 was performed off the coast of Martha's Vineyard, MA on July 23, 2010. The signals were transmitted at a depth of around 80m to an 12 element vertical array receiver with 5 cm element spacing, which was attached to a buoy. The transmit hydrophone was an ITC-1007, which was towed from a distance of 500 m from the receive array to a distance of 4500m and back. There were two tows in this experiment. The data presented is from the second tow.

The carrier frequency of the transmitted signal was $f_c = 13$ kHz, the bandwidth was $B = 4.88$ kHz, and the sampling frequency was $f_s = 39.06$ kHz. The transmitted signal was the first 50,000 symbols of a repeated binary phase shift keyed (BPSK) encoded, 2047-length M-sequence.

4.7.5 MACE10 experimental results

The MACE10 experiment is very similar to the SPACE08 experiment in terms of the type of data transmitted and the hardware used. The key difference between the two experiments is that the MACE10 experiment had a moving transmitted (and stationary receiver). Thus, there is more channel variability in the MACE10 data compared with the SPACE08 data.

Figure 4.7.7 shows the results of the various beamforming methods on the MACE10 data set. Two beamforming methods were not tested on the MACE10 data set, the reduced adaptive beamformer (using fewer sensors to do adaptive processing) and the MCM beamformer. All of the data shown here used 5 beams for beamforming.

In figure 4.7.7, the adaptive methods all have a rapid decrease in performance as the SNR is lowered. When compared with the non-adaptive beamforming methods, shown in Figure 4.7.8. This reduction in performance is due to a sudden instability
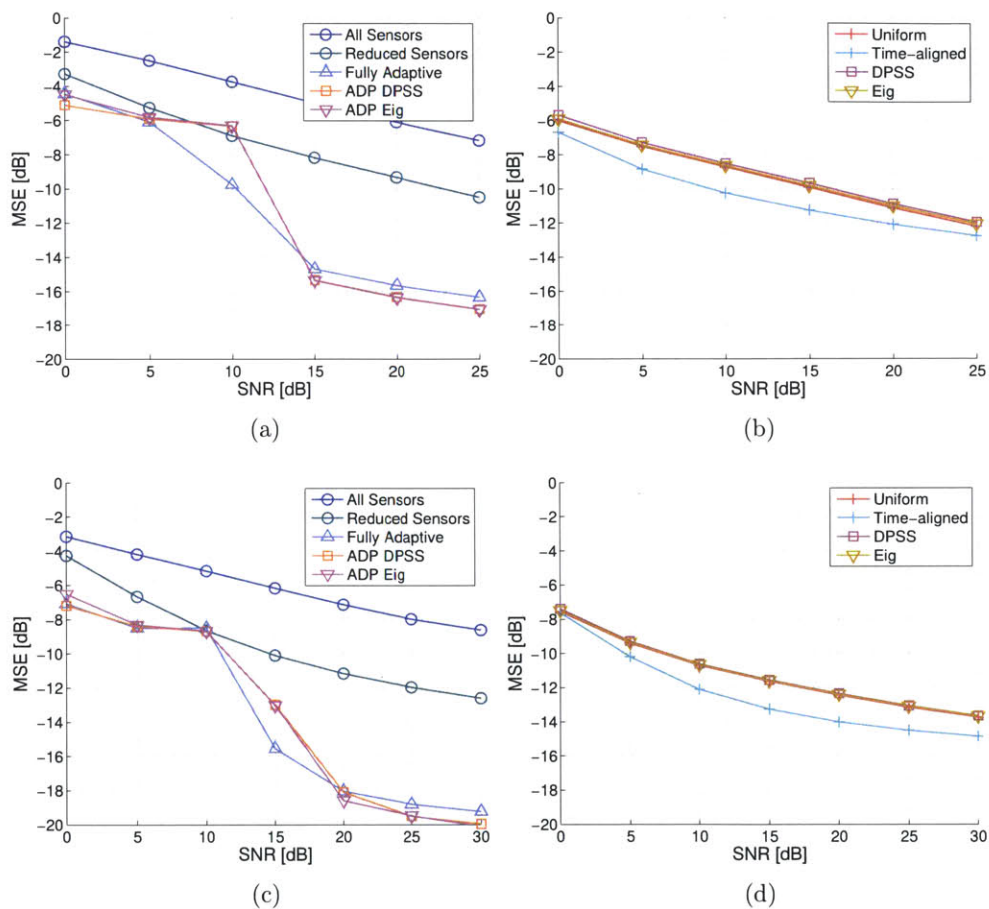
Figure 4.7.7: Comparison of beamforming methods using MACE10 experimental data. The left column ((a), and (c)) contains the beamspace and adaptive methods. The right column ((b) and (d)) contains the non-adaptive methods. The two rows represent different data sets, taken two minutes. The first column was taken at time 1810, and the second at time 1812. Note that the adaptive methods have a significant, relative loss of performance at low SNR.
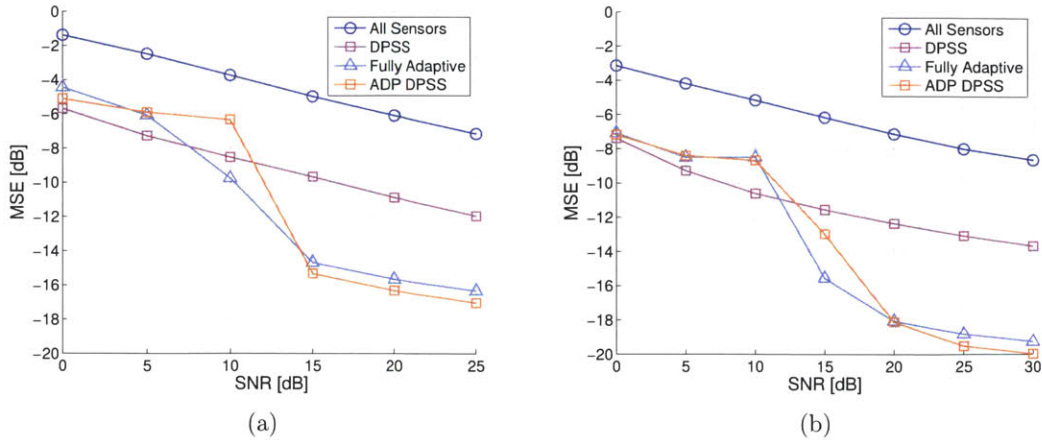
Figure 4.7.8: Results from MACE10 comparing the beamspace, adaptive, non-adaptive, and hybrid methods for two different data packets: (a) at time 1810 (b) at time 1812. Both of these results show the relative performance degradation of the adaptive results compared with the non-adaptive results. This is due to the instabilities in the adaptive algorithm forcing the use of longer averaging windows.

within the adaptive algorithm. This results in a jump in the mean square error observed without any immediate correction. This effect can be seen in Figure 4.7.9.

From the results, there is an apparent problem with the adaptive beamforming methods for certain values of the parameters. Further investigation is needed to fully characterize this phenomenon and to determine mitigating techniques.

4.8 Conclusions

This chapter investigated beamspace processing for a multichannel DFE. Assuming white spatial and temporal observation noise, the optimal beams for unknown but bounded arrival angles were found to be the discrete prolate spheroidal sequences. This set of beamforming weights was observed to be very tolerant to environmental mismatch since multiple beams covered the same angular range.

A variety of other beamforming methods were proposed for comparison with the DPSS beams. These include uniform beams, time-aligned uniform beams, MVDR (MCM) beams, adaptive beams, and hybrid methods. Using the SPACE08 experi-

133
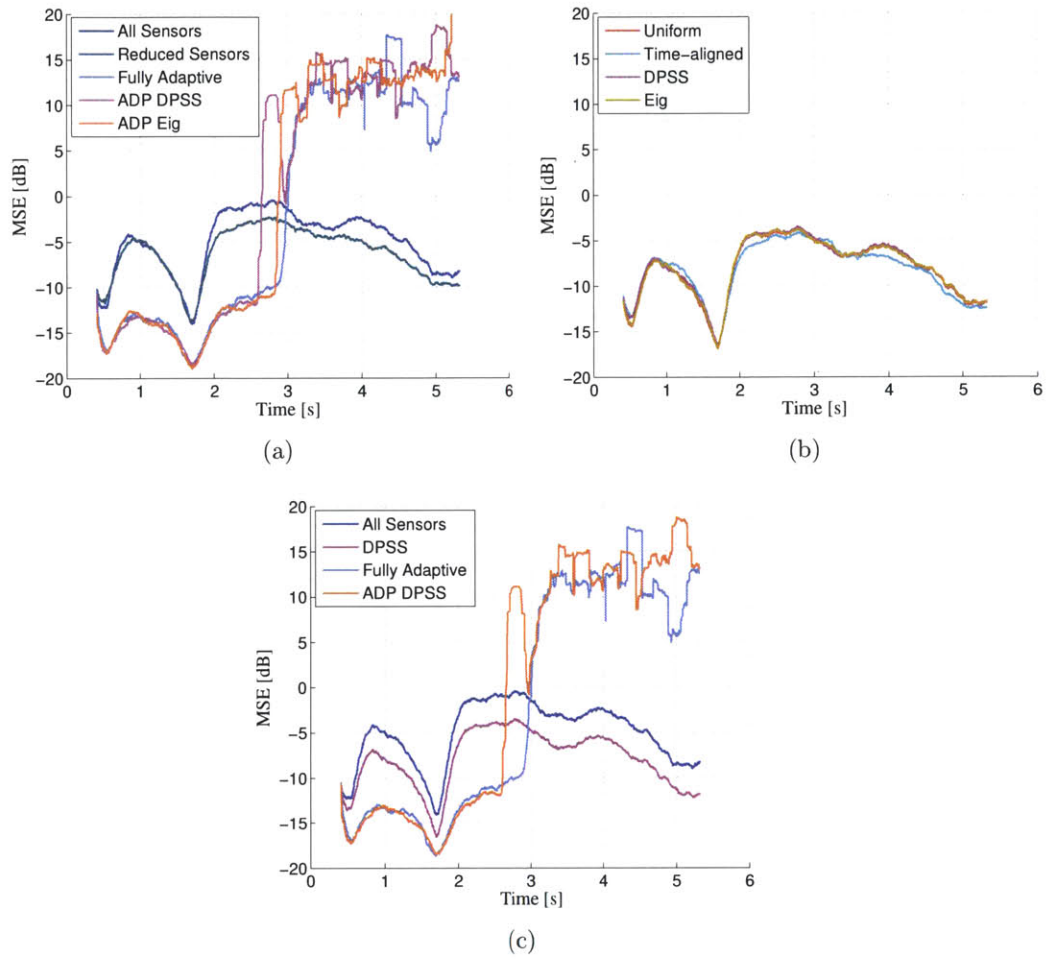
Figure 4.7.9: Results from MACE10 comparing MSE for the data set from time 1812 at an SNR of 10dB with $\lambda = 0.996$. (a) shows the adaptive and beamspace results, (b) shows the non-adaptive methods, and (c) compares the two. Notice that all of the adaptive methods have a point where the algorithm becomes unstable and the estimates are no longer valid.

mental data, all of the proposed methods were shown to have similar mean squared error performance on calm days and the adaptive methods, previously proposed by Stojanovic et al, outperform all other methods when the channel was quickly varying. The adaptive methods outperformed the non-adaptive methods in this case because the adaptive beamformer could adaptively change the effective number of beams and stormy conditions caused the observed angle bound to be larger than the bound used to compute the non-adaptive beams.

The proposed method of using DPSS beam weights had lower computational complexity than the fully adaptive approach proposed by Stojanovic because the beam weights can be computed offline. Furthermore, the proposed non-adaptive methods did not exhibit the same non-linear instabilities observed when using the fully adaptive approach.

Several methods were investigated for estimating the number of arrivals from the data including information theoretic methods (AIC and BIC), generalized χ^2 methods for finding the numbers of degrees of freedom, and ray-path modeling of the multipath arrivals to calculate the number of arrivals. Derivations were shown detailing the effectiveness of generalized χ^2 methods for determining the number of beams to use.

The methods for determining the number of beams were compared using the SPACE08 experimental data. The generalized χ^2 methods were found to have the best estimate of the appropriate number of beams to use based on the mean squared error. The ray-path modeling methods also provided a reasonable estimate, but one that is slightly higher than is necessary for the data studied.

Chapter 5

The effect of fixing channel model order on equalizer performance

5.1 Introduction

Underwater wireless communication hardware is designed to be used in a variety of environments. Without knowledge of the particular underwater operating environment, some parameters, such as number of equalizer coefficients or channel delay spread, may need to be hardwired for system usability. This chapter examines the errors introduced when the number of coefficients in a channel model used to create equalizer coefficients differs from the number of channel coefficients in the true channel. The analysis presented in this chapter is a special case of the effective noise analysis from Chapter 3. The structure of this special case facilitates a special compensation algorithm that improves performance but which could not be used in the more general case. In this chapter, the channel estimation errors are due to model order mismatch and the observation noise is ignored.

The reverberation time of the channel can range from less than ten to over hundreds of milliseconds and can change over time. This variation can make estimating the channel length very challenging. Underestimating the length of a channel can wreak havoc on equalizer performance [58]. Fortunately, the noise caused by using a different number of channel coefficients in the modeled channel than there are in the

true channel can be estimated and used to improve equalizer performance.

This chapter focuses on analyzing changes in equalizer performance due to channel length estimation errors. Studies to date on this topic have been highly empirical and the solutions have been somewhat ad-hoc. The goal of this chapter is to provide an intuitive analysis that explains shortcomings of previously proposed solutions and points to new solutions for the LE and the DFE. The analysis in this chapter explains the increase in mean squared error of the equalized signal due to the use of a different number of coefficients in the modeled channel than in the true channel. The results do not include channel estimation error which will further increase the MSE. An algorithm is presented to include unmodeled channel coefficients in the equalizer coefficient calculations which reduces the output MSE. Experimental data is used to validate the proposed algorithm.

5.2 Assumptions

To streamline the analysis and emphasize the desired effects, three common assumptions about the transmitted data and observation noise are made in this chapter:

1. The transmitted data is modeled as samples of a discrete white random process with unit variance. For a length M transmitted data vector $\mathbf{d}[n]$, this implies $E\{\mathbf{d}[n]\mathbf{d}^H[n]\} = \mathbf{I}_M$.

2. The observation noise and the transmitted data are uncorrelated. This implies that for a complex, baseband noise vector $\boldsymbol{\nu}'[n]$ and a transmitted data vector $\mathbf{d}'[m]$, $E\{\boldsymbol{\nu}[n]\mathbf{d}^H[m]\} = \mathbf{0}$.

3. The estimates of past data are assumed to be perfect, *i.e.* $\hat{\mathbf{d}} = \mathbf{d}$, removing the error dependence from data estimation and isolating the channel length estimation errors.

4. The channel estimate is assumed to be perfect for the specified number of channel coefficients. Only errors from having a different number of coefficients in the

model than in the true channel are considered; other types of channel estimation error are not considered.

5. The channel impulse response is assumed to be of finite extent (FIR).

The first three assumptions are quite common and do not lessen the generality or usefulness of the derived results. The fourth assumption is made to focus the methods on compensating for channel length mismatch. The last assumption is reasonable given observed experimental data. For the remainder of this chapter, time index is dropped for notational simplicity.

The channel convolution matrix, $\mathbf{G}$ described in Section 2.2 is important to the derivations in this chapter. To simplify discussion, the rows of the channel convolution matrix are labeled as

$$\mathbf{G}^T = \begin{bmatrix} \tilde{\mathbf{g}}_{-L_c-N_c+2} & \cdots & \tilde{\mathbf{g}}_0 & \cdots & \tilde{\mathbf{g}}_{L_a+N_a} \end{bmatrix}, \tag{5.2.1}$$

where the index is a relative offset from the zero column, corresponding to the data symbol currently being estimated (*i.e.* d_0).

5.3 Approach

The central question of this chapter is "How does an incorrect assumption about the number of channel coefficients affect equalization?" To answer this question, the equalizer coefficients computed using an incorrect channel length assumption are compared with the equalizer coefficients calculated using the true channel length.

As discussed in Section 2.2, convolution can be written as a matrix multiplication. The true channel convolution matrix can be split into the sum of an estimated channel convolution matrix and a delta offset,

$$\mathbf{G} = \widehat{\mathbf{G}} + \mathbf{\Delta G}. \tag{5.3.1}$$

139

Recall from Section 2.4 that the linear equalizer coefficients can be found using

$$\mathbf{h}_{\text{lin}}[n] = [\mathbf{G}^H[n]\mathbf{G}[n] + \mathbf{R}_\nu]^{-1}\mathbf{g}_0^*, \tag{5.3.2}$$

and the DFE equalizer coefficients can be found using

$$\mathbf{h}_{\text{ff}}[n] = [\mathbf{G}_0^H[n]\mathbf{G}_0[n] + \mathbf{R}_\nu]^{-1}\mathbf{g}_0^* \tag{5.3.3}$$

$$\mathbf{h}_{\text{fb}}[n] = -\mathbf{G}_{\text{fb}}^H[n]\mathbf{h}_{\text{ff}}[n]. \tag{5.3.4}$$

Using the expression from eq. (5.3.1) with (2.4.9) and (2.4.20), the effect of channel estimation errors is observable in both the equalizer coefficients and the mean squared error (MSE). This formulation is not specific to channel length error estimation and can be generalized to other types of errors, such as wrongly guessing a sparsity constraint. The focus in this chapter is on channel length errors since the analysis points to a tractable solution.

Notation is used to highlight the difference between quantities computed using the true channel parameters from quantities computed using a estimated or assumed channel parameters. If the true channel has N coefficients, the channel impulse response is $\mathbf{g}[n] = [g[n,0], \ g[n,1], \ \ldots \ g[n,N-1]]^T$. Similarly, if the estimated channel has length M the estimated channel impulse-response is

$$\widehat{g}[n,i] = \begin{cases} g[n,i] & i < N \\ 0 & i \geq N, \ \text{when M > N} \end{cases}. \tag{5.3.5}$$

The vector $\widehat{\mathbf{g}}$ is defined as

$$\widehat{\mathbf{g}}[n] = [\widehat{g}[n,0] \ \widehat{g}[n,1] \ \ldots \ \widehat{g}[n,M-1]]^T, \tag{5.3.6}$$

and the estimated channel convolution matrix, $\widehat{\mathbf{G}}$ is the estimated channel vectors padded with zeros so that the result is the same when multiplying the $\widehat{\mathbf{G}}^H\mathbf{d}$ as when convolving the estimated channel with the transmitted data. Now, from eq. (5.3.1),

$\Delta \mathbf{G}$ is computed as $\mathbf{G} - \widehat{\mathbf{G}}$, where $\widehat{\mathbf{G}}$ will have rows with all zero elements appended appropriately so the two matrices are the same dimension.

Note that in both eq. (2.4.9) and eq. (2.4.20), the channel convolution matrix appears as a product with itself and with multiplication by a selection matrix. Padding this matrix with zero columns and appropriately modifying the selection vector so it acts on the same column of $\mathbf{G}$ does not change the result.

In the case of overestimation of the channel length $\Delta \mathbf{G} = \mathbf{0}$ so $\mathbf{G} = \widehat{\mathbf{G}}$. Thus, under the described conditions, overestimating the channel length does not increase the MSE of the equalizer. This assumes that channel impulse response coefficients are perfectly known for the assumed channel length. In practice the expectation is estimated through time averaging which increases the MSE [66], but these effects are not taken into account in this chapter. Underestimating the channel increases the MSE (even with perfect channel knowledge) due to the unmodelled ISI. The next sections explore the effects of assuming too short of a channel length.

5.3.1   LE analysis

Change in equalizer coefficients

The analysis of a LE is started by first rewriting the optimal equalizer coefficients as an estimate plus an offset

$$\mathbf{h}_{\text{lin}} = \widehat{\mathbf{h}}_{\text{lin}} + \delta \mathbf{h}_{\text{lin}}, \tag{5.3.7}$$

where $\widehat{\mathbf{h}}_{\text{lin}}$ are the coefficients derived from using the estimated channel, $\widehat{\mathbf{G}}$. The expression for $\widehat{\mathbf{h}}_{\text{lin}}$ is

$$\widehat{\mathbf{h}}_{\text{lin}} = [\widehat{\mathbf{G}}^{H} \widehat{\mathbf{G}} + \mathbf{R}_{\nu}]^{-1} \widehat{\mathbf{g}}_{0}^{*}. \tag{5.3.8}$$

Using eq. (5.3.1), this equation can be rewritten as

$$
\begin{aligned}
\widehat{\mathbf{h}}_{\text{lin}} &= [(\mathbf{G} - \Delta \mathbf{G})^{H}(\mathbf{G} - \Delta \mathbf{G}) + \mathbf{R}_{\nu}]^{-1} \widehat{\mathbf{g}}_{0}^{*} \\
&= [\mathbf{G}^{H}\mathbf{G} - \mathbf{G}^{H}\Delta \mathbf{G} - \Delta \mathbf{G}^{H}\mathbf{G} + \Delta \mathbf{G}^{H}\Delta \mathbf{G} + \mathbf{R}_{\nu}]^{-1} \widehat{\mathbf{g}}_{0}^{*}.
\end{aligned} \tag{5.3.9}
$$

141

To simplify the derivations, the following quantities are defined

$$\mathbf{Q} = \mathbf{G}^H\mathbf{G} + \mathbf{R}_\nu \qquad (5.3.10)$$

$$\mathbf{W} = \mathbf{G}^H\Delta\mathbf{G} + \Delta\mathbf{G}^H\mathbf{G} - \Delta\mathbf{G}^H\Delta\mathbf{G} \qquad (5.3.11)$$

$$\widehat{\mathbf{g}}_0 = \mathbf{g}_0 - \delta\mathbf{g}_0. \qquad (5.3.12)$$

Note that both $\mathbf{Q}$ and $\mathbf{W}$ are Hermitian. Using these substitutions, the equation for the coefficients becomes a function of the difference between the terms from the true channel, $\mathbf{Q}$, and the error terms, $\mathbf{W}$. The definition of $\mathbf{W}$ includes cross terms between the true channel and the channel estimation error that have been missing from previous analysis in the literature.

Eq. (5.3.9) can be rewritten as

$$
\begin{aligned}
\widehat{\mathbf{h}}_{\mathrm{lin}} &= [\mathbf{Q} - \mathbf{W}]^{-1}(\mathbf{g}_0 - \delta\mathbf{g}_0)^* \\
&= \mathbf{Q}^{-1}\mathbf{g}_0^* - \mathbf{Q}^{-1}\delta\mathbf{g}_0^* + \mathbf{Q}^{-1}[\mathbf{I} - \mathbf{W}\mathbf{Q}^{-1}]^{-1}\mathbf{W}\mathbf{Q}^{-1}(\mathbf{g}_0 - \delta\mathbf{g}_0)^* \\
&= \mathbf{h}_{\mathrm{lin}} - \mathbf{Q}^{-1}\delta\mathbf{g}_0^* + \mathbf{Q}^{-1}[\mathbf{I} - \mathbf{W}\mathbf{Q}^{-1}]^{-1}\mathbf{W}\mathbf{Q}^{-1}(\mathbf{g}_0 - \delta\mathbf{g}_0)^*. \quad (5.3.13)
\end{aligned}
$$

The second equality comes from applying the Woodbury identity. The third equality comes the expression for the LE coefficient matrix in eq. (2.4.9). Rearranging terms, the form of the perturbation of the equalizer coefficients is found to be

$$\delta\mathbf{h}_{\mathrm{lin}} = \mathbf{Q}^{-1}[\mathbf{I} - \mathbf{W}\mathbf{Q}^{-1}]^{-1}\mathbf{W}\mathbf{Q}^{-1}\widehat{\mathbf{g}}^* - \mathbf{Q}^{-1}\delta\mathbf{g}_0^*. \qquad (5.3.14)$$

The term $\delta\mathbf{g}_0$ is a result of using a longer equalizer than channel estimate. If the equalizer is the same length or less than the estimated channel, and the only channel estimation errors are due to length underestimation, this term is zero. A common engineering practice is to use equalizers that are shorter than the channel estimate delay spread. Following this practice, $\delta\mathbf{g}_0 = 0$ for the remainder of this chapter. The

final form of the change in the equalizer coefficients is

$$\delta \mathbf{h}_{\text{lin}} = \mathbf{Q}^{-1}[\mathbf{I} - \mathbf{W}\mathbf{Q}^{-1}]^{-1}\mathbf{W}\mathbf{Q}^{-1}\mathbf{g}_0$$
$$= [\mathbf{Q} - \mathbf{W}]^{-1}\mathbf{W}\mathbf{h}_{\text{lin}}, \tag{5.3.15}$$

i.e. the offset of the equalizer coefficients from the MMSE solution is a linear combination of the MMSE solution (equalizer coefficients) where the weighting is a function of the channel estimation error.

Change in MAE

This section describes how the channel length estimation errors change the minimum achievable error (MAE) assuming knowledge of the channel impulse-response coefficient values, if not their number. The first step is to calculate the mean squared error using the estimated filter coefficients. The MAE term is then isolated using eq. (2.4.12). The terms which are not included in the MAE are referred to as the excess error.

The estimated error can be written as

$$\widehat{e}_{\text{lin}} = \widehat{\mathbf{h}}^H \mathbf{u} - d. \tag{5.3.16}$$

and then the expected mean squared error can be written as

$$\mathrm{E}\{|\widehat{e}_{\text{lin}}|^2\} = \mathrm{E}\{|\widehat{\mathbf{h}}^H \mathbf{u} - d|^2\} \tag{5.3.17}$$
$$= \mathrm{E}\{\widehat{\mathbf{h}}^H \mathbf{u}\mathbf{u}^H \widehat{\mathbf{h}} - \widehat{\mathbf{h}}^H \mathbf{u}d^* - d\mathbf{u}^H \widehat{\mathbf{h}} + dd^*\}. \tag{5.3.18}$$

Using the assumption that $\sigma_d^2 = \mathrm{E}\{dd^*\} = 1$ and the relations from eq. (2.2.5) and $\widehat{\mathbf{h}} = \mathbf{h}_{\text{lin}} - \delta\mathbf{h}$, eq. (5.3.18) simplifies to

$$\mathrm{E}\{|\widehat{e}_{\text{lin}}|^2\} = 1 - \mathbf{g}_0^T[\mathbf{G}^H\mathbf{G} + \mathbf{R}_\nu]^{-1}\mathbf{g}_0^* + \delta\mathbf{h}^H[\mathbf{G}^H\mathbf{G} + \mathbf{R}_\nu]\delta\mathbf{h}. \tag{5.3.19}$$

Notice that the first two terms are the MAE, $\sigma_{0,lin}^2$. Substituting the relation from

eq. (5.3.15) into eq. (5.3.19) produces an alternate form of the expected MSE,

$$
\begin{aligned}
E\{|\widehat{e}_{\text{lin}}|^2\} &= \sigma_{0,lin}^2 + (\mathbf{Q}^{-1}[\mathbf{I} - \mathbf{W}\mathbf{Q}^{-1}]^{-1}\mathbf{W}\mathbf{Q}^{-1}\mathbf{g}_0)^H \mathbf{Q}\mathbf{Q}^{-1}[\mathbf{I} - \mathbf{W}\mathbf{Q}^{-1}]^{-1}\mathbf{W}\mathbf{Q}^{-1}\mathbf{g}_0^* \\
&= \sigma_{0,lin}^2 + \mathbf{h}_{\text{lin}}\mathbf{W}^H[\mathbf{I} - \mathbf{W}\mathbf{Q}^{-1}]^{-H}\mathbf{Q}^{-1}[\mathbf{I} - \mathbf{W}\mathbf{Q}^{-1}]^{-1}\mathbf{W}\mathbf{h}_{\text{lin}}. \quad (5.3.20)
\end{aligned}
$$

Note that the matrix $\mathbf{Q}$ is Hermitian and positive definite.

The matrix

$$
\mathbf{A} = \mathbf{W}^H[\mathbf{I} - \mathbf{W}\mathbf{Q}^{-1}]^{-H}\mathbf{Q}^{-1}[\mathbf{I} - \mathbf{W}\mathbf{Q}^{-1}]^{-1}\mathbf{W} \quad (5.3.21)
$$

is Hermitian and positive semidefinite, so the quantity $\mathbf{h}_{\text{lin}}{}^H\mathbf{A}\mathbf{h}_{\text{lin}} \geq 0$. This last term is the excess error introduced by underestimating the channel length. This result is similar to the result presented in [75], except here there is an apparent structure of the excess error.

Interpretation of results

So far, the effect of underestimating the channel length on the linear equalizer coefficients and the MAE has been described. This analysis has assumed the use of the CEB equalization algorithm since there is no concept of channel length included in the DA equalization algorithm.

In the matrix $\mathbf{W}$ from eq. (5.3.11), the term $\mathbf{\Delta G}^H\mathbf{\Delta G}$ always has a strong diagonal component equal to the energy (2-norm) in the unmodelled coefficients. The regularization term proposed by Lee and Cox [58] can be viewed as a very crude approximation to this cross term. Preisig [75] explicitly estimates this term but does not capture the cross terms.

The cross terms $\widehat{\mathbf{G}}^H\mathbf{\Delta G}$ and $\mathbf{\Delta G}^H\widehat{\mathbf{G}}$ that appear in the $\mathbf{W}$ matrix provide a measure of the interaction between the missing coefficients and the estimated channel. Specifically, if the channel is sparse and most of the coefficients are clustered together with one outlier, the cross terms indicate how much the outlier will interact with the channel. When there are at least $L_a + L_c$ zeros (*i.e.* number of zeros equal to the

144

equalizer length), the cross terms are zero. In this case, the only remaining term in $\mathbf{W}$ is $\mathbf{\Delta G}^H \mathbf{\Delta G}$, which can be folded into the noise correlation matrix, as in [75].

Compensating for estimation error

Using the assumption that the transmitted data is white, $\mathbf{\Delta G}$ can be estimated using the estimated channel convolution matrix

$$\epsilon_{\text{lin}} = \widehat{\mathbf{G}}^H \widehat{\mathbf{d}} - \mathbf{u}. \tag{5.3.22}$$

Right multiplying both sides by $\widehat{\mathbf{d}}'^H$, where $\widehat{\mathbf{d}}'$ is an estimated transmitted data vector that is twice the length of the equalizer (assuming all estimates are correct) and substituting for $\mathbf{u}$ using eq. (2.2.5) produces

$$\begin{aligned}
\mathrm{E}\{\epsilon_{\text{lin}}\mathbf{d}'^H\} &= \mathrm{E}\{\widehat{\mathbf{G}}^H \mathbf{d}\mathbf{d}'^H - (\mathbf{G}^H\mathbf{d} + \boldsymbol{\nu})\mathbf{d}'^H\} \\
&= (\mathbf{G}' - (\mathbf{\Delta G}'))^H \mathbf{I} - \mathbf{G}'^H \mathbf{I} \\
&= \mathbf{\Delta G}'^H. \tag{5.3.23}
\end{aligned}$$

In these equations, $\mathbf{G}'$ is the true channel convolution matrix with a length of twice the length of the equalizer (length of $\mathbf{d}'$) and $\mathbf{\Delta G}'$ is the offset matrix with this same length parameter. The second equality follows from eq. (5.3.1).

The expression for the MSE from Preisig's work [75] has a form which is missing the cross terms,

$$\begin{aligned}
\mathrm{E}\{|\epsilon_{\text{lin}}|^2\} &= \mathrm{E}\{|\widehat{\mathbf{G}}^H\mathbf{d} - \mathbf{G}^H\mathbf{d} - \boldsymbol{\nu}|^2\} \\
&= \mathrm{E}\{|(\mathbf{G} - \mathbf{\Delta G})^H\mathbf{d} - \mathbf{G}^H\mathbf{d} - \boldsymbol{\nu}|^2\} \\
&= \mathbf{\Delta G}^H \mathbf{\Delta G} + \mathbf{R}_\nu. \tag{5.3.24}
\end{aligned}$$

In this formulation, there is no way to differentiate the channel offset term, $\mathbf{\Delta G}$ from the noise correlation matrix.

Using the estimated offset, $\mathbf{\Delta G}'$, the linear equalizer coefficients are

$$\widehat{\mathbf{h}}_{\text{lin}} = [\mathrm{E}\{\epsilon_{\text{lin}}'\epsilon_{\text{lin}}'^{H}\} + \mathbf{\Delta G}'^{H}\mathbf{\Delta G}' + \widehat{\mathbf{G}}^{H}\widehat{\mathbf{G}} + \mathbf{\Delta G}'^{H}\widehat{\mathbf{G}} + \widehat{\mathbf{G}}^{H}\mathbf{\Delta G}']^{-1}\widehat{\mathbf{g}}_0^{*} \qquad (5.3.25)$$

where $\epsilon_{\text{lin}}' = \epsilon_{\text{lin}} - \mathbf{\Delta G}'^{H}\mathbf{d}' = \mathbf{\Delta G}''^{H}\mathbf{d}' + \boldsymbol{\nu}$ is the modified observed error with $\mathbf{\Delta G}''$ defined as the part of the offset not estimated using the proposed method, $\mathbf{\Delta G} = \mathbf{\Delta G}' + \mathbf{\Delta G}''$. The term $\mathrm{E}\{\epsilon_{\text{lin}}'\epsilon_{\text{lin}}'^{H}\}$ represents an estimate of the effective noise correlation matrix, introduced in Chapter 3. Evaluating this expectation (across the data symbols and noise) and combining terms, eq. (5.3.25) becomes

$$\widehat{\mathbf{h}}_{\text{lin}} = [\mathbf{R}_{\nu} + \mathbf{\Delta G}''^{H}\mathbf{\Delta G}'' + \widehat{\mathbf{G}}'^{H}\widehat{\mathbf{G}}']^{-1}\mathbf{g}_0, \qquad (5.3.26)$$

where $\widehat{\mathbf{G}}' = \widehat{\mathbf{G}} + \mathbf{\Delta G}'$ is the original estimated channel plus an estimate of the next $L_A + L_c$ coefficients, i.e. a longer channel estimate. The effective noise due to channel length estimation errors is reduced since previously un-modeled channel coefficients are included in the channel model of the above expression. If the system designer believes there is still significant energy in the true channel not included in channel model, the above procedure can be repeated, extending the channel model further. The estimates of $\mathbf{\Delta G}$ used in this formulation are noisy, so the reduction in the effective noise will not be as much as shown.

The effective noise correlation matrix is calculated using the difference between the received data and the received data estimate. Using the proposed method for increasing the effective length of the channel model does not change this calculation, so the cross-terms, $\mathbf{\Delta G}'^{H}\mathbf{\Delta G}''$ and $\mathbf{\Delta G}''^{H}\mathbf{\Delta G}'$, are still missing in eq. (5.3.26). The expected MSE of the equalizer, however, is reduced by extending the channel model since the excess MSE is proportional to the modeling error.

5.3.2   DFE analysis

The analysis for the DFE closely mirrors that of the LE and will follow a similar line of reasoning. The change in equalizer coefficients due to channel length estimation errors

is presented first, followed by MAE analysis, discussion, and methods for channel compensation.

Changes in equalizer coefficients

A useful method for analyzing the excess error when computing the equalizer coefficients is to write the optimal equalizer coefficients as the sum of the estimated coefficients and an offset,

$$\mathbf{h_{ff}} = \widehat{\mathbf{h}}_{ff} + \delta\mathbf{h_{ff}} \tag{5.3.27}$$

$$\mathbf{h_{fb}} = \widehat{\mathbf{h}}_{fb} + \delta\mathbf{h_{fb}}. \tag{5.3.28}$$

The DFE feedforward filter derivation is almost identical to the LE derivation, where $\mathbf{G}$ and $\mathbf{h}_{\text{lin}}$ from the LE derivation are replaced by $\mathbf{G}_0$ and $\mathbf{h}_{ff}$ in the DFE derivation. The feed-forward estimated filter coefficients have the same form as the LE coefficients eq. (5.3.9)

$$\widehat{\mathbf{h}}_{ff} = [\mathbf{G}_0^H\mathbf{G}_0 - \mathbf{G}_0^H\mathbf{\Delta G}_0 - \mathbf{\Delta G}_0^H\mathbf{G}_0 - \mathbf{\Delta G}_0^H\mathbf{\Delta G}_0 + \mathbf{R}_\nu]^{-1}\widehat{\mathbf{g}}_0^*. \tag{5.3.29}$$

Following this logic, the change in the DFE feedforward coefficients is similar to the change in the LE coefficients from eq. (5.3.15). In the case of the DFE, the change is written as

$$\delta\mathbf{h_{ff}} = \mathbf{Q}'^{-1}[\mathbf{I} - \mathbf{W}'\mathbf{Q}'^{-1}]^{-1}\mathbf{W}'\mathbf{Q}'^{-1}\mathbf{g}_0^*, \tag{5.3.30}$$

where $\mathbf{Q}' = [\mathbf{G}_0^H\mathbf{G}_0 + \mathbf{R}_\nu]$ and $\mathbf{W}' = \mathbf{G}_0^H\mathbf{\Delta G}_0 + \mathbf{\Delta G}_0^H\mathbf{G}_0 + \mathbf{\Delta G}_0^H\mathbf{\Delta G}_0$ where we have split $\mathbf{\Delta G}$ into the same sections as we split $\mathbf{G}$ previously. Including the perturbation into the feedback section is written as

$$
\begin{aligned}
\widehat{\mathbf{h}}_{fb} &= -\widehat{\mathbf{G}}_{fb}\widehat{\mathbf{h}}_{ff} \\
&= -(\mathbf{G}_{fb} - \mathbf{\Delta G}_{fb})(\mathbf{h}_{ff} - \delta\mathbf{h}_{ff}) \\
&= -\mathbf{G}_{fb}\mathbf{h}_{ff} + \mathbf{G}_{fb}\delta\mathbf{h}_{ff} - \mathbf{\Delta G}_{fb}(\mathbf{h}_{ff} - \delta\mathbf{h}_{ff}).
\end{aligned} \tag{5.3.31}
$$

Subtracting off $\mathbf{h}_{\text{fb}}$ from both sides, we get the change is

$$\delta\mathbf{h}_{\text{fb}} = \mathbf{\Delta G}_{\text{fb}}(\widehat{\mathbf{h}}_{\text{ff}}) - \mathbf{G}_{\text{fb}}\delta\mathbf{h}_{\text{ff}}. \tag{5.3.32}$$

Change in MAE

Starting with the estimated error,

$$\widehat{e}_{\text{dfe}} = \widehat{\mathbf{h}}_{\text{ff}}^{H}\mathbf{u} + \widehat{\mathbf{h}}_{\text{fb}}^{H}\widehat{\mathbf{d}}_{\text{fb}}, \tag{5.3.33}$$

the squared error becomes

$$\mathrm{E}\{|\widehat{e}_{\text{dfe}}|^2\} = \mathrm{E}\{|\widehat{\mathbf{h}}_{\text{ff}}^{H}\mathbf{u} + \widehat{\mathbf{h}}_{\text{fb}}^{H}\widehat{\mathbf{d}}_{\text{fb}} - d|^2\}. \tag{5.3.34}$$

Expanding and substituting into this equation similar to LE analysis, one arrives at the solution for the MSE,

$$\mathrm{E}\{|\widehat{e}_{\text{dfe}}|^2\} = \sigma_{0,dfe}^2 + \widehat{\mathbf{h}}_{\text{ff}}^{H}(\mathbf{\Delta G}_{\text{fb}}^{H}\mathbf{\Delta G}_{\text{fb}})\widehat{\mathbf{h}}_{\text{ff}} + \delta\mathbf{h}_{\text{ff}}^{H}[\mathbf{G}_0^{H}\mathbf{G}_0 + \mathbf{R}_\nu]^{-1}\delta\mathbf{h}_{\text{ff}}$$

$$\mathrm{E}\{|\widehat{e}_{\text{dfe}}|^2\} = \sigma_{0,dfe}^2 + \widehat{\mathbf{h}}_{\text{ff}}^{H}(\mathbf{\Delta G}_{\text{fb}}^{H}\mathbf{\Delta G}_{\text{fb}})\widehat{\mathbf{h}}_{\text{ff}} +$$

$$\mathbf{h}_{\text{ff}}^{H}\mathbf{W}'^{H}[\mathbf{I} - \mathbf{W}'\mathbf{Q}'^{-1}]^{-H}\mathbf{Q}'^{-1}[\mathbf{I} - \mathbf{W}'\mathbf{Q}'^{-1}]^{-1}\mathbf{W}'\mathbf{h}_{\text{ff}}. \tag{5.3.35}$$

This expression has an additional term which accounts for the error in estimating the feedback portion of the channel. Both excess error terms are non-negative again. The extra error term is the energy from the error in estimating the feedback filter coefficients.

Discussion

Much of the discussion for the LE still holds true for the DFE. One key difference is the additional error term in the DFE excess error, $\widehat{\mathbf{h}}_{\text{ff}}^{H}(\mathbf{\Delta G}_{\text{fb}}^{H}\mathbf{\Delta G}_{\text{fb}})\widehat{\mathbf{h}}_{\text{ff}}$. This term shows that estimation errors in the feedback portion of the channel show up as squared terms in the excess error. The excess error from the feedforward section is uncorrelated with the excess error in the feedback section. So even with perfect feedforward coefficient

148

estimation there will still be excess error in the DFE

Another difference between the DFE and the LE is how the structure of $\mathbf{\Delta G}$ enters into the error equation. There is no longer a strong diagonal term, so one would expect regularization methods [75, 58] will not reduce the MSE in the case of the DFE.

Compensating for estimation error

Estimating the DFE offset term $\mathbf{\Delta G}'$ follows a similar derivation to the LE case. This is because estimating the error introduced by the channel estimate has nothing to do with the equalizer structure. Therefore the procedure for the DFE is exactly the same as for the LE, with only the labels changed,

$$\epsilon_{\text{dfe}} = \widehat{\mathbf{G}}^H \widehat{\mathbf{d}} - \mathbf{u} \tag{5.3.36}$$

$$\text{E}\{\epsilon_{\text{dfe}} \mathbf{d}'^H\} = \mathbf{\Delta G}'^H \tag{5.3.37}$$

$$\epsilon_{\text{dfe}}' = \epsilon_{\text{dfe}} - \mathbf{\Delta G}'^H \mathbf{d}'. \tag{5.3.38}$$

Once the channel estimate is computed, the channel convolution matrix is split into the feedforward and feedback sections, $\mathbf{\Delta G}_0'$ and $\mathbf{\Delta G}_{\text{fb}}'$ respectively. Substituting the channel offset into the equalizer coefficient equations, the feedforward and feedback portions of the equalizer equations become

$$\widehat{\mathbf{h}}_{\text{ff}}' = [\epsilon_{\text{dfe}}' \epsilon_{\text{dfe}}'^H + \widehat{\mathbf{G}}_0'^H \widehat{\mathbf{G}}_0']^{-1} \mathbf{g}_0^*$$

$$\widehat{\mathbf{h}}_{\text{ff}}' = \mathbf{R}_w + \widehat{\mathbf{G}}_0'^H \widehat{\mathbf{G}}_0']^{-1} \mathbf{g}_0^*$$

$$\widehat{\mathbf{h}}_{\text{fb}}' = -[\widehat{\mathbf{G}}_{\text{fb}} + \mathbf{\Delta G}_{\text{fb}}'] \widehat{\mathbf{h}}_{\text{ff}}'. \tag{5.3.39}$$

The feed-forward section is the feedforward coefficients as if a longer channel model (by $L_a + L_c$ coefficients) was used originally, with a new effective noise matrix which includes the channel coefficients which are still not modeled. The estimate of the effective noise correlation matrix, $\mathbf{R}_w = \mathbf{R}_\nu + \mathbf{\Delta G}''^H \mathbf{\Delta G}'''$, is the same effective correlation matrix as for the LE. This estimate will be exact if the term $\mathbf{\Delta G}''^H \mathbf{\Delta G}' + \mathbf{\Delta G}'^H \mathbf{\Delta G}'$

149

is zero (*i.e.* there is no correlation between channel coefficients not modeled and the extended model). The estimated feedback coefficients include the channel length extension. There is additional noise introduced into the estimate (not explicitly modeled here) due to the errors in estimating $\mathbf{\Delta G'}$.

5.4 Performance analysis using simulations

This section provides some simple examples to validate these results. These simulations were executed in MATLAB and the results are presented in the following sections. All of the simulations use an EW-RLS algorithm. This method is practical and approximately equals the MMSE solution for time-invariant channels [36, 86].

Often the noise statistics are often not known, so the implementation of the correction algorithms involves using an exponential weighting algorithm to estimate the ensemble correlation matrices. This method is preferred to a running average since the channel may not be time-invariant, but is assumed to be slowly varying. To illustrate this method, assume quantity to be estimated is $E\{b\}$. The observations are denoted as $\tilde{b}[n]$.

$$E\{b[n]\} \approx \frac{1-\lambda}{1-\lambda^{n+1}} \sum_{i=0}^{n} \lambda^{n-i} \tilde{b}[i] \tag{5.4.1}$$

Only the DFE is shown in simulation since the LE is a special case of the DFE when the feedback filter has zero coefficients.

5.4.1 Time-invariant channel

For the time-invariant channel the channel coefficients are constant for all time. The channel time index is dropped in this subsection for brevity, so the ith time-invariant channel coefficient is represented as $g[i] \triangleq g[n, i]$ for all n.

One example to illustrate the induced error term caused by using a lower channel model order than the true channel order is a true channel with length 3 and a modeled

channel with length 2. The estimated channel convolution matrix has the form

$$\widehat{\mathbf{G}} = \begin{bmatrix} g[1] & g[0] & 0 \\ 0 & g[1] & g[0] \end{bmatrix}, \tag{5.4.2}$$

and the offset matrix has the form

$$\mathbf{\Delta G} = \begin{bmatrix} g[2] & 0 & 0 & 0 \\ 0 & g[2] & 0 & 0 \end{bmatrix} \tag{5.4.3}$$

Since there is only one channel coefficient not included in the model, the term $\mathbf{\Delta G}^H \mathbf{\Delta G}$ is equal to

$$\mathbf{\Delta G}^H \mathbf{\Delta G} = |g[2]|^2 \mathbf{I}$$

The results for a length 7, randomly chosen stationary channel are shown in Figures 5.4.1 and 5.4.2 (DFE). Figure 5.4.1 is for a 7-coefficient linear equalizer and figure 5.4.2 is from a DFE with 7 feed-forward coefficients and 6 feedback coefficients. The transmitted data packets were 60,000 4-QAM symbols long and all results assume perfect symbol estimation (no data estimation errors). The data estimates are assumed to be perfect to confine the observed error to the channel length estimation errors.

The results illustrate that the proposed method for correcting the CEB equalizer works and is approximately equal to the DA approach. Also, while the LE does worse than the DFE in for all SNR in terms of MSE and BER, the difference between the regularization approaches and the bias estimated approach is less for the LE than the DFE as expected by analysis because the previously proposed methods include only $\mathbf{\Delta G}^H \mathbf{\Delta G}$ and not the cross terms.

5.4.2 Rayleigh-fading channel

The second case of interest is a non-stationary channel. Again the channel impulse-response length is assumed to be underestimated by one coefficient. The analysis is very similar to the time-invariant channel, except this example illustrates that the
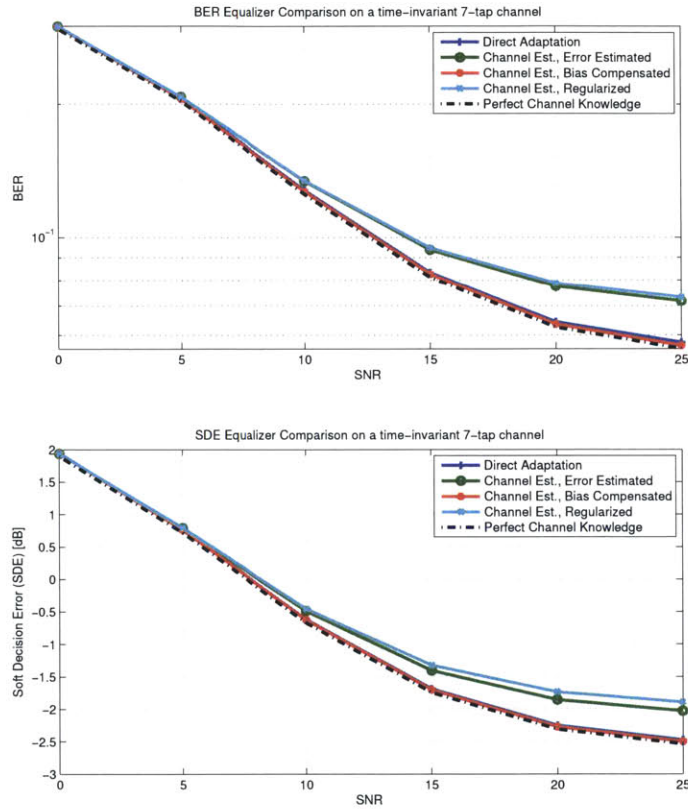
Figure 5.4.1: (a) BER and (b) MSE comparison of different LE approaches for a simulated 7-coefficient stationary channel. The approaches include DA, CE error-estimated (Preisig [75]), CEB bias compensated, CEB regularized (Lee and Cox [58]), and optimal where perfect channel knowledge is assumed (no channel length estimation error).
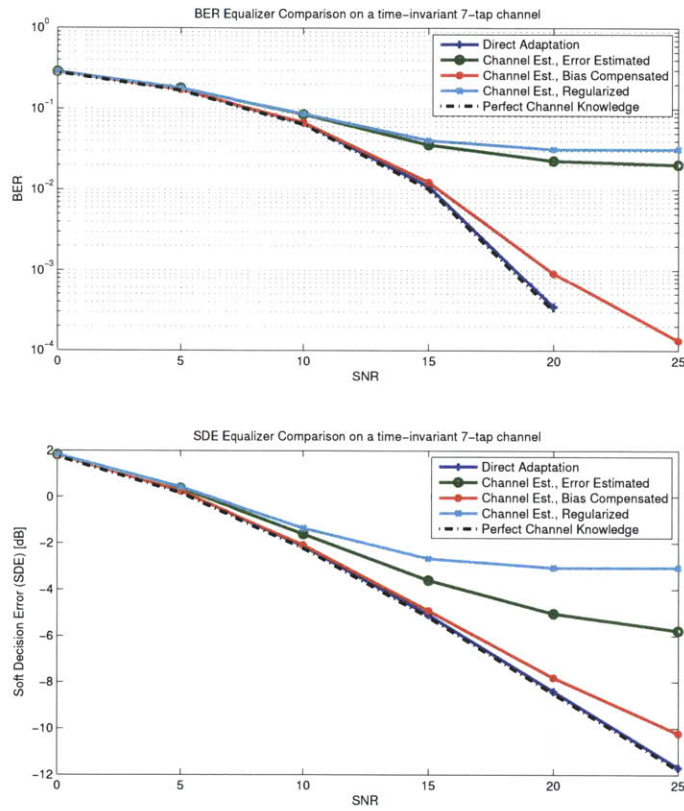
Figure 5.4.2: (a) BER and (b) MSE comparison of different DFE approaches for a simulated 7-coefficient stationary channel. The approaches include DA, CE error-estimated (Preisig [75]), CEB bias compensated, CEB regularized (Lee and Cox [58]), and optimal where perfect channel knowledge is assumed (no channel length estimation error).
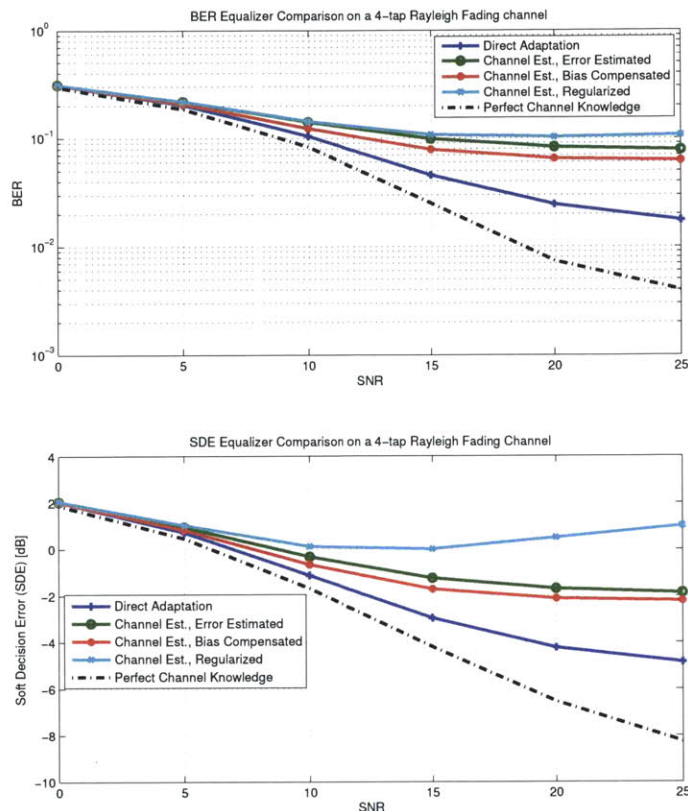
Figure 5.4.3: (a) BER and (b) MSE comparison of different DFE approaches for a simulated 7-coefficient Rayleigh channel. The approaches include DA, CE error-estimated (Preisig), CEB bias compensated, CEB regularized (Lee and Cox), and optimal where perfect channel knowledge is assumed (no channel length estimation error).

proposed methods are robust when there is channel motion.

The simulation was for a length 4, Rayleigh fading channel, where each coefficient fades independently. The coherence time (inverse of the Doppler spread) of the channel was one second, and each coefficient had equal energy (variance). The sampling rate was 2400 samples per second and the data packet was 60000 4-QAM modulated symbols.

The results again confirm that the proposed method outperforms other CEB equalization methods, but the DA method outperforms them all. One unexpected result was that the regularization method proposed by Lee *et al.* [58] had an increasing MSE as the SNR increased. This model includes time-variation which leads so there are

errors both due channel estimation errors and errors due to the channel model having fewer coefficients than the true channel. The regularization parameter proposed by Lee *et al.* does not depend on SNR and so the regularization parameter introduces an additional modeling error between the MMSE regularization parameter (the inverse SNR for white noise) and the modeled regularization parameter, which is exacerbated as the SNR is increased.

.

The DA approach now clearly outperforms all the CEB approaches, but the proposed bias corrected CEB approach performs better than any previously proposed method. Also, there is now a large gap between the optimal equalizer which has perfect channel knowledge and the estimated equalizers which estimate the channel coefficients. This gap did not appear in the time-invariant channel examples and is likely due to channel estimation errors not related to underestimating the number of channel coefficients.

5.5   Experimental evidence

5.5.1   RACE08 - experimental setup

The data presented is from the Reschedule Acoustic Communication Experiment (RACE08) which took place in Narragansett Bay at the University of Rhode Island's Narragansett Bay Campus from March 1-March 17, 2008. The data presented was transmitted using an ITC-1007 spherical transducer with a resonant frequency of approximately 11 kHz and a bandwidth of approximately 10 KHz. The receiver was a 12 element vertical array with 12 cm spacing located approximately 1000 m in a direction of 120^0 from the transducer.

The transmitter and receivers used a sampling frequency of $f_s = 39062.5$ samples per second. There was an anti-aliasing filter at the receivers with a cut-off of about 18.5 KHz.

The water was approximately a constant 10 m depth from transmitter to receiver.

The data presented were recorded on the last day of the experiment in the 11AM data cycle. The conditions were fairly calm with some small waves and light wind.

The signals were BPSK modulated, LDPC encoded data packets with 25,000 symbols per packet transmitted at a rate of 6 samples per symbol or approximately 6510 symbols per second. A Hamming window was employed to reduce side-lobe effects. The carrier frequency was 12 kHz to be near the resonance of the transducer.

Before equalization, the data was low-pass filtered, transfered to baseband, and down-sampled to two samples per symbol. Time alignment of the signal was achieved through the use of an M-sequence timing signal at the beginning of the packet.

5.5.2 Experimental results

The channel was modeled as having 8 coefficients (6 causal and 2 a causal coefficients) clustered around the direct-path arrival. The equalizer was an 8 feed-forward coefficient (3 causal and 5 acausal), 5 feedback coefficient DFE. This structure was chosen to capture the width of the main arrival and to cancel out nearby interference.

The three structures studied were the DA, the proposed bias compensating CEB, and the bias estimating CEB. The regularized model was not examined since the error-estimating equalizer was always shown to perform better.

Figure 5.5.1 shows the estimated channel using an RLS channel estimator. This estimated channel is much wider than the CEB equalizers estimate so we can see the structure of the channel. It appears as if most of the energy arrives with the direct arrival, although there is an anomalous acausal arrival. There is also some structure and motion in the causal part of the channel that is probably due to wave motion, but these arrivals are very weak.

Figure 5.5.2 shows that DA equalizer outperforms both the CEB approaches, but that the bias compensated CEB equalizer does better than the error-estimating. This is nice empirical validation that the bias compensating method may be worth deploying on a real world system if there are other reason to use a CEB equalizer.

Channel Estimate for RACE08 Data Packet
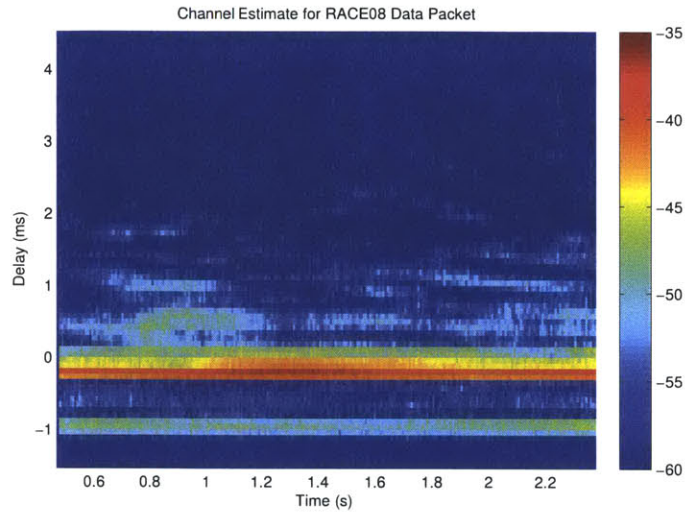
Figure 5.5.1: Channel estimate for the observed data packet. Fairly calm conditions with little channel spread.

5.6   Discussion

This chapter presented a clear look at the effect of using incorrect estimates of the channel length on equalization. Inaccurate channel length information will only affect CEB equalization since the DA equalizer algorithm has no notion of channel state information. Analysis was presented to illustrate that only under-estimating the channel length effects the MSE of the output of the equalizer.

Simulation and experimental data confirmed that an under-estimation of the channel length does negatively effect performance and in this case, the DA algorithm outperforms the CEB. A method for recovering the missing channel information through post-processing of the information was proposed and analyzed. Even when including this additional information, the DA has the lowest MSE due to channel estimation error.
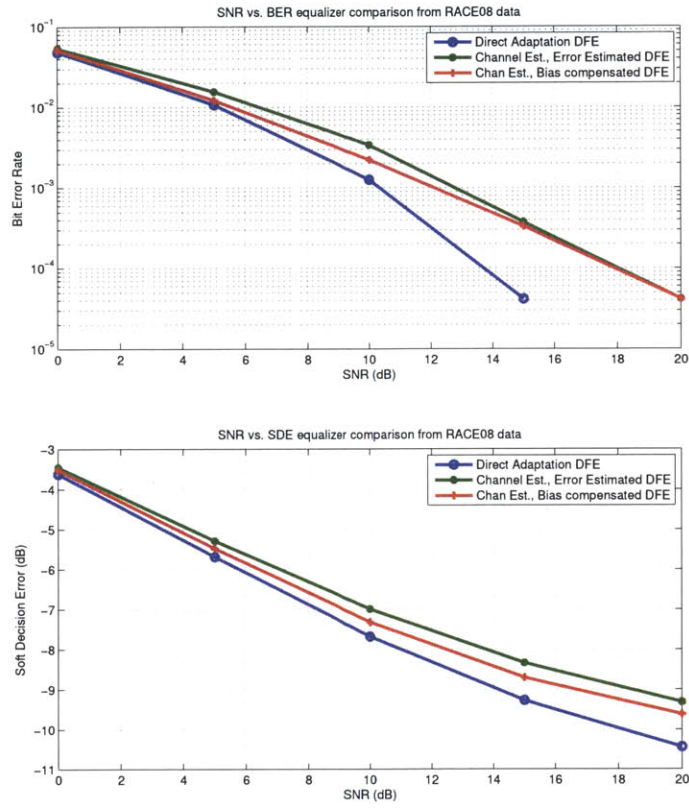
Figure 5.5.2: (a) BER and (b) MSE comparison of different DFE equalizer approaches. The three approaches included are DA, CEB bias compensated, and the CEB error estimated proposed by Preisig [75]. The approach proposed by Lee *et al.* [58] is not included because the previous results showed that it was not an optimal approach, *i.e.* the average error increased with SNR.

Chapter 6

Comparing techniques for computing equalizer coefficients

6.1 Introduction

Decision feedback equalization has been used for many years to improve bit-rate and reliability of underwater communication [105]. Coefficients for an equalizer can be estimated either directly from the received data (Direct Adaptation) or from a channel estimate (Channel Estimate Based). The CEB-DFE has better performance (*i.e.* lower residual estimation error) while the DA-DFE has lower computational complexity.

The CEB equalizer outperforms the DA equalizer when comparing MSE after equalization [91, 131]. The question remains, "Why there is a performance difference between equalizers build using the DA method and those build using the CEB method?" This chapter examines the reasons for the performance difference between these two equalizer coefficient methods and compares the methods when used in an underwater acoustic communication system.

A key conceptual difference between the DA-DFE and CEB-DFE is the coefficients being *tracked*, *i.e.* the coefficients that are adaptively estimated. For the CEB-DFE, the *channel* coefficients are estimated from the received data; for the DA-DFE, the *equalizer* coefficients are being estimated from the received data.

The CEB-DFE tracks the physical channel, a parameter that is much easier to conceptualize. A particular shape of the channel impulse response implies something about the physical world that can be observed through other means. For instance, if there is a strong channel path at a certain delay, then there must be some reflector, such as a boat or a fish, that one could go find. The dynamics of the channel are thus related to a physical model of the world.

The DA-DFE tracks the equalizer coefficients, a more abstract quantity. The coefficients satisfy an optimality criterion, but are not parameters that necessarily relate directly to the physical world. The dynamics of the equalizer coefficients and thus of the DA-DFE are much more convoluted and are only related to the channel coefficients through a non-linear function.

Two theories for the performance difference between the DA-DFE and the CEB-DFE have evolved in the literature:

1. The received data correlation matrix is ill-conditioned and thus the DA algorithm is limited by numerical error. [131]

2. The channel estimate based equalizer requires fewer samples to fully characterize the channel. [91]

This chapter shows that neither of these two hypothesis are entirely correct. Instead, the evidence indicates that the performance difference is related to the coherence time of the equalizer coefficients and the channel impulse response coefficients: the channel coefficients have a longer coherence time than the equalizer coefficients, so the CEB method which relies on the channel estimate can be estimated over more samples than can DA equalizer coefficients. Thus the estimation noise is higher in the DA method than the CEB method. This result is verified using simulations of time-varying channels.

In the next section of this chapter, two models of channel coefficient correlation are described: the Markov model and the Gaussian model. In Section 6.3 the structure of the channel convolution matrix is briefly described including a description of what each column and row position signifies. Section 6.4 describes the explicit dependence

the equalizer coefficients have on the channel coefficients and how changes in channel coefficients propagate through the equalizer coefficient formulation. Section 6.5 presents a linear perturbation model to simplify the nonlinear relationship between the equalizer and channel coefficients. Sections 6.6 and 6.7 describe the correlation of the equalizer coefficients and show the correlation empirically through simulation results. Section 6.8 is a discussion of the chapter results.

6.2 Channel coefficient correlation models

An assumption that the channel impulse response is slowly varying (compared with the averaging window) is common when estimating the channel impulse response coefficients (or the equalizer coefficients). A reasonable question to ask at this point is what does the term *slowly varying* actually mean. This section presents two channel coefficient correlation models: Markov correlation (also known as auto-recursive correlation) where the correlation falls off exponentially and Gaussian correlation which has a bell-curve shaped correlation function.

6.2.1 Markov correlation model

In a Markov channel model, also known as an auto-recursive channel model, all statistical information from past channel coefficients is contained in the current coefficient. This model has been previously shown to be a useful description of the underwater channel [30]. Under the Markov model, the ith channel coefficient is modeled using the relation

$$g[n+1, i] = \alpha g[n, i] + \nu_g[n, i],\tag{6.2.1}$$

where α is a complex scaling parameter (also known as the auto-recursive parameter), $v[n, i]$ is zero-mean, Gaussian white noise with variance $\sigma_{v,i}^2$, and $g[n, i]$ is the ith channel coefficient at time n. The scaling parameter is bounded such that $|\alpha| < 1$ so the channel coefficient is bounded, *i.e.* has finite energy. For simplicity, the remainder of this section assumes α is real and positive, but the expressions can be modified
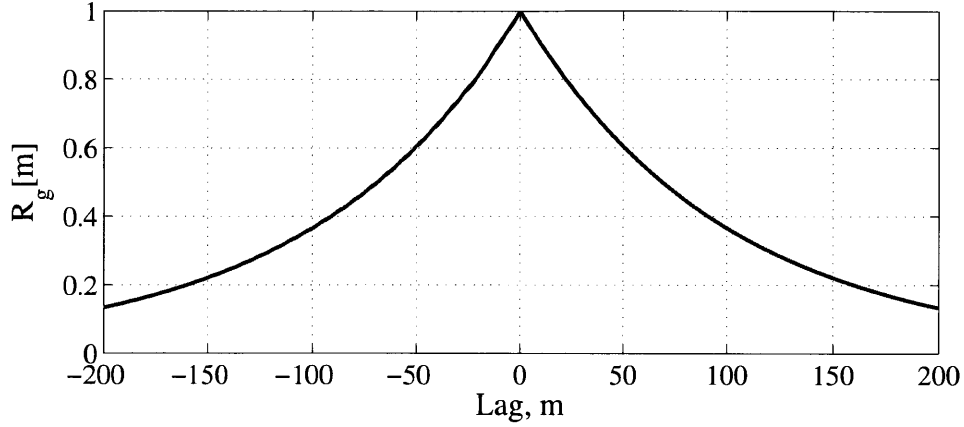
Figure 6.2.1: Correlation function for Markov channel model with $\alpha = 0.99$ and $\sigma_{v,i} = 0.0199$.

to handle a complex α in a straightforward manor. Often the channel is modeled as slowly varying in time, which implies $\alpha \approx 1$.

The correlation function, $R_{g,i}[m]$, of the ith channel coefficient when using a Markov model is

$$R_{g,i}[m] = \mathrm{E}\{g[n,i]g^*[n+m,i]\} = \sigma_{v,i}^2 \left(\frac{\alpha^{|m|}}{1-\alpha^2} \right). \qquad (6.2.2)$$

Figure 6.2.1 shows the correlation function with $\alpha = 0.99$ and $\sigma_{v,i} = 0.0199$.

The quantity N_{win} is defined as twice the number of time-steps before the correlation function is scaled by e^{-1}, i.e. twice the number of time steps m until $|R_{g,i}[m]| = e^{-1}R_{g,i}[0]$. The scaling parameter, α can be expressed in terms of N_{win} through the relation

$$\alpha = e^{-2/N_{\text{win}}}. \qquad (6.2.3)$$

The ith channel coefficient energy or variance equals the correlation function at zero lag, i.e. $\sigma_{g,i}^2 = R_{g,i}[0]$, so the process noise variance of the ith channel coefficient is

$$\sigma_{v,i}^2 = \sigma_{g,i}^2(1 - \alpha^2). \qquad (6.2.4)$$

With a specified correlation window length and channel coefficient energy, all

162

parameters of the channel correlation model are determined. Sometimes the fade-rate, f_r, and sampling frequency, f_s, are given rather than the correlation window length. In this case, the parameters can be determined using the relation

$$N_{\text{win}} = f_s/(2f_r).$$
(6.2.5)

The fade-rate is defined as the width of the power spectral density (PSD) of fading process. The fade-rate is also referred to as the *Doppler spread* of the channel. The reciprocal of the fade-rate is the *coherence-time* of the channel. In this thesis, the coherence-time is defined as the lag at which the correlation function is scaled by e^{-1}, *i.e.* the lag m at which $|R_{g,i}[m]| = e^{-1}R_{g,i}[0]$ (same as [91]).

6.2.2 Gaussian correlation model

The shape of the Gaussian model correlation function is more rounded and less peaked than the Markov model. The Gaussian correlation model has a correlation function that is a Gaussian function,

$$\mathbf{R}_{g,i}[m] = \mathrm{E}\{g[n,i]g^*[n+m,i]\} = \sigma_{g,i}^2 e^{-\frac{m^2}{2\beta^2}},$$
(6.2.6)

where

$$\beta = \frac{f_s}{2\pi f_r}.$$
(6.2.7)

The correlation function with $\sigma_{g,i}^2 = 1$ and $\beta = \frac{100}{\sqrt{2}}$ is shown in Figure 6.2.2. Note that this function has lower tails than the Markov model.

When simulating a channel with a Gaussian correlation function, zero-mean, unit-variance, Gaussian white noise is convolved with a Gaussian function, $h_{\text{GF}}[n]$. The function coefficients are defined as

$$h_{\text{GF}}[n] = \sqrt{\frac{\sigma_{g,i}^2}{\sqrt{2\pi\beta^2}}e^{-\frac{n^2}{2\beta^2}}} \qquad \forall n.$$
(6.2.8)

There are several notable features about the Gaussian correlation function. The

163
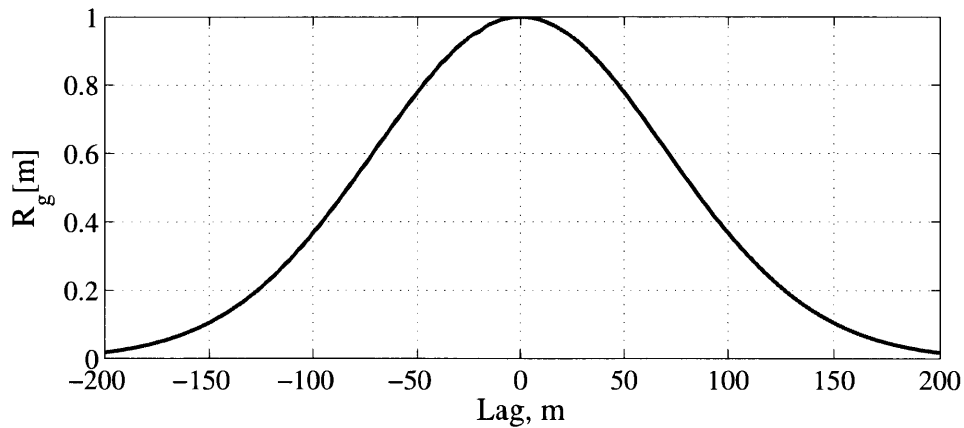
Figure 6.2.2: Correlation function for Gaussian channel model with $\sigma_g^2 = 1$ and $\beta = \frac{100}{\sqrt{2}}$.

first is that the Fourier transform of a Gaussian function is also a Gaussian function, so the PSD of the channel impulse response coefficients will also have a Gaussian shape. The lag m at which the correlation function is reduced by a scale factor of e^{-1}, i.e. $|R_{g,i}[m]| = e^{-1}R_{g,i}[0]$, is $m = \sqrt{2} \cdot \beta$ (see eq. (6.2.6)).

6.3 Structure of the channel convolution matrix

Recall that the received signal is modeled as

$$\mathbf{u}[n] = \mathbf{G}^H[n]\mathbf{d}'[n] + \boldsymbol{\nu}[n], \tag{6.3.1}$$

where $\mathbf{u}[n]$ is a vector of received data, $\mathbf{d}'[n]$ is a vector of transmitted data, $\boldsymbol{\nu}[n]$ is a noise vector, and $\mathbf{G}[n]$ is the channel convolution matrix (described in Section 2.2). If the channel is time invariant and the received data is sampled once per symbol, the channel convolution matrix is a constant Toeplitz matrix. If the signal is sampled more than once per symbol (known as fractionally-spaced sampling), the matrix is no longer strictly Toeplitz, but still has a Toeplitz-like structure. Symbol-spaced sampling is assumed for the remainder of the chapter due to notationally simplicity, but the derived results apply when fractionally-spaced sampling is used.

164

Each position of the channel convolution matrix corresponds to a different time and delay of the time-varying channel. Recall from Section 2.2 that the (complete) channel convolution matrix can be separated into a feedback portion, $\mathbf{G}_{\text{fb}}$, and a remainder portion, $\mathbf{G}_0$, referred to as the reduced channel convolution matrix. The received signal sample vector in eq. (2.2.5) can be rewritten as

$$\mathbf{u}[n] = \begin{bmatrix} \mathbf{G}_{\text{fb}}^H[n] & \mathbf{G}_0^H[n] \end{bmatrix} \begin{bmatrix} \mathbf{d}_{\text{fb}}[n] \\ \mathbf{d}_0[n] \end{bmatrix} + \boldsymbol{\nu}[n]. \tag{6.3.2}$$

This equation implies that column position corresponds to the (zero-padded) channel realization and the row position indicates which input data symbol the channel coefficient is multiplied.

6.4 Models of time-varying equalizer coefficients

Equalizer coefficients are functions of the channel coefficients. Therefore, when the channel coefficients vary with time, the equalizer coefficients are also time-varying. The relation between channel coefficients and equalizer is highly non-linear, so how the equalizer coefficients are affected by a channel coefficient perturbation is not clear. In this section, three equalizer coefficient models are proposed which explicitly include channel perturbations.

6.4.1 General channel variation model

To determine the response of the equalizer coefficients to a perturbation in the channel, a reasonable first step is to apply a perturbation, $\boldsymbol{\Delta}\mathbf{G}$ to the channel convolution matrix and analyze the results. The perturbation is the change in the channel convolution matrix from one time step to the next,

$$\mathbf{G}[n+1] = \mathbf{G}[n] + \boldsymbol{\Delta}\mathbf{G}[n]. \tag{6.4.1}$$

Substituting this relation into eq. (2.4.20), the expression for the DFE coefficients becomes

$$
\begin{aligned}
\mathbf{h}_{\mathrm{ff}}[n+1] &= (\mathbf{G}_0^H[n+1]\mathbf{G}_0[n+1] + \mathbf{R}_\nu)^{-1}\mathbf{g}_0^*[n+1] \\
&= (\mathbf{G}_0^H[n]\mathbf{G}_0[n] + \mathbf{R}_\nu + \Delta\mathbf{G}^H[n]\mathbf{G}[n] + \mathbf{G}^H[n]\Delta\mathbf{G}[n] + \Delta\mathbf{G}^H[n]\Delta\mathbf{G}[n])^{-1} \\
&\quad \times (\mathbf{g}_0^*[n] + \delta\mathbf{g}^*[n]) \qquad\qquad\qquad\qquad\qquad\qquad\qquad\qquad\qquad (6.4.2)
\end{aligned}
$$

$$
\begin{aligned}
\mathbf{h}_{\mathrm{fb}}[n+1] &= -\mathbf{G}_{\mathrm{fb}}[n+1]\mathbf{h}_{\mathrm{ff}}[n+1] \\
&= -(\mathbf{G}_{\mathrm{fb}}[n] + \Delta\mathbf{G}_{\mathrm{fb}}[n])\mathbf{h}_{\mathrm{ff}}[n+1], \qquad\qquad\qquad\qquad\qquad (6.4.3)
\end{aligned}
$$

where $\delta\mathbf{g}[n]$ is the row of $\Delta\mathbf{G}[n]$ in the same row position as $\mathbf{g}_0$ is in $\mathbf{G}$ and $\Delta\mathbf{G}$ is a matrix made up of the same row positions as $\mathbf{G}_{\mathrm{fb}}$. Using the substitutions

$$
\begin{aligned}
\mathbf{Q}[n] &= \mathbf{G}_0^H[n]\mathbf{G}_0[n] + \mathbf{R}_\nu \\
\mathbf{W}[n] &= \Delta\mathbf{G}^H[n]\mathbf{G}[n] + \mathbf{G}^H[n]\Delta\mathbf{G}[n] + \Delta\mathbf{G}^H[n]\Delta\mathbf{G}[n],
\end{aligned}
$$

equation (6.4.2) can be rewritten using the matrix inversion lemma [44] as

$$
\mathbf{h}_{\mathrm{ff}}[n+1] = (\mathbf{I} + \mathbf{Q}^{-1}[n]\mathbf{W}[n])^{-1}(\mathbf{h}_{\mathrm{ff}}[n] + \mathbf{Q}^{-1}[n]\delta\mathbf{g}^*[n]). \qquad (6.4.4)
$$

This type of analysis was used in Chapter 5 to examine the effect of channel model order mismatch where the $\Delta\mathbf{G}$ included un-modeled channel coefficients. In the present case $\Delta\mathbf{G}$ is due to channel motion induced estimation errors.

The form of the feedforward coefficients implies that there is a nonlinear relationship between the channel perturbation and the equalizer perturbation. In the low SNR regime when the observation noise is white, the term $(\mathbf{I} + \mathbf{Q}^{-1}[n]\mathbf{W}[n])$ is nearly diagonal (diagonally dominant) since the variance of the noise is much larger than the channel coefficients and the channel coefficient perturbation, so the equalizer perturbation is approximately linear [35].

This model of perturbation is not properly constrained because any position of the channel convolution matrix can be perturbed where in normal operation only the first

column of the channel convolution matrix is perturbed. The next section presents a model without this inaccuracy.

6.4.2 Channel convolution matrix update model

In the model from the previous section, all elements of the channel convolution matrix could change from one time step to the next (the entire channel convolution matrix was perturbed). When updating the equalizer coefficients every symbol, the majority of matrix elements are just shifted to new positions; only the first column contains values not previously in the matrix. The update model presented in this section examines the dynamics of the equalizer coefficients using the this constrained update of the channel convolution matrix.

The channel is assumed to be varying according to a Markov model,

$$\mathbf{g}[n+1] = \alpha\mathbf{g}[n] + \boldsymbol{v}[n], \tag{6.4.5}$$

where α is the Markov coefficient (same for all elements of channel vector) and $\boldsymbol{v}[n]$ is the process noise vector. Statistical correlations Channel coefficients have statistically correlated variation when the corresponding elements of the process noise vector, of $\boldsymbol{v}[n]$, are statistically correlated.

To simplify notation, two new matrices are defined: the "shift" matrix, $\mathbf{S}_M$, and the "choice" matrix, $\mathbf{C}_M$, the subscript M is the matrix dimension. The shift matrix, $\mathbf{S}_M$, is an $M \times M$ square matrix which has ones along the diagonal directly above the main diagonal and zeros everywhere else.

$$\mathbf{S}_M = \begin{bmatrix} 0 & 1 & 0 & \cdots & 0 \\ 0 & 0 & 1 & \cdots & 0 \\ \vdots & & & \ddots & \vdots \\ 0 & 0 & 0 & \cdots & 1 \\ 0 & 0 & 0 & \cdots & 0 \end{bmatrix}_{M \times M} \tag{6.4.6}$$

Multiplying by this matrix shifts the existing data to new positions from one time

167

step to the next.

The choice matrix serves two functions: first, it selects the leftmost column from the channel convolution matrix and, second, it scales that column by the Markov coefficient, α. $\mathbf{C}_M$ is a square $M \times M$ matrix that has α as the bottom left element. All remaining elements are all zero.

$$\mathbf{C}_M = \begin{bmatrix} \alpha_g & 0 & 0 & \cdots & 0 \\ 0 & 0 & 0 & \cdots & 0 \\ \vdots & & & \ddots & \vdots \\ 0 & 0 & 0 & \cdots & 0 \\ 0 & 0 & 0 & \cdots & 0 \end{bmatrix}_{M \times M} \tag{6.4.7}$$

If N is the total number of channel coefficients and L_{ff} is the number of feedforward equalizer coefficients per feedforward section, then the channel convolution matrix has dimension $(L_{ff} + N - 1) \times L_{ff}$. The update equation for the channel convolution matrix is

$$\mathbf{G}[n+1] = \mathbf{S}_{L_{ff}+N-1}^H \mathbf{G}[n]\mathbf{S}_{L_{ff}} + \mathbf{G}[n]\mathbf{C}_{L_{ff}} + \mathbf{\Upsilon}[n] \tag{6.4.8}$$

The matrix $\mathbf{\Upsilon}[n]$ has dimensions $(L_{ff} + N - 1) \times L_{ff}$ and contains the zero-padded realization of the process noise at time n in the first column and all other elements are zero. The noise realizations from previous time-steps are already included in the convolution matrix, $\mathbf{G}[n]$, so past noise realizations are not included in $\mathbf{\Upsilon}[n]$.

Including the variation model into the DFE formulation from eq. (2.4.20) gives

$$\mathbf{h}_{ff}[n+1] = (\mathbf{G}_0^H[n+1]\mathbf{G}_0[n+1] + \mathbf{R}_\nu)^{-1}\mathbf{g}_0^*[n+1]$$

$$= ((\mathbf{S}_L^H\mathbf{G}_0[n]\mathbf{S}_L + \mathbf{G}_0[n]\mathbf{C}_{L_{ff}} + \mathbf{\Upsilon}_0[n])^H(\mathbf{S}_L^H\mathbf{G}_0[n]\mathbf{S}_L + \mathbf{G}_0[n]\mathbf{C}_{L_{ff}} + \mathbf{\Upsilon}_0[n]))^{-1}$$

$$\times ((\mathbf{S}_L^H\mathbf{G}_0[n]\mathbf{S}_L + \mathbf{G}_0[n]\mathbf{C}_{L_{ff}} + \mathbf{\Upsilon}_0[n])\mathbf{s})$$

$$= \left(\begin{bmatrix} (\alpha\mathbf{g}[n] + \boldsymbol{v}[n])^H(\alpha\mathbf{g}[n] + \boldsymbol{v}[n]) & (\alpha\mathbf{g}[n] + \boldsymbol{v}[n])^H\mathbf{G}_0'[n+1] \\ \mathbf{G}_0'^H[n+1](\alpha\mathbf{g}[n] + \boldsymbol{v}[n]) & \mathbf{G}_0''^H[n]\mathbf{G}_0''[n] \end{bmatrix} + \mathbf{R}_\nu \right)^{-1}$$

$$\times ((\mathbf{S}_L^H\mathbf{G}_0[n]\mathbf{S}_L + \mathbf{G}_0[n]\mathbf{C}_{L_{ff}} + \mathbf{\Upsilon}_0[n])\mathbf{s}) \tag{6.4.9}$$

168

$$\mathbf{h_{fb}}[n+1] = -\mathbf{G_{fb}}[n+1]\mathbf{h_{ff}}[n+1]$$

$$= -(\mathbf{S}_{L_{fb}}^{H}\mathbf{G_{fb}}[n]\mathbf{S}_{L_{ff}} + \mathbf{G_{fb}}[n]\mathbf{C}_{L_{ff}} + \mathbf{\Upsilon_{fb}}[n])\mathbf{h_{ff}}[n+1]. \qquad (6.4.10)$$

In the above expressions, $\mathbf{s}$ is the selection vector described in Section 2.4, $\boldsymbol{v}[n]$ is the first column of the $\mathbf{\Upsilon}[n]$ matrix corresponding to the process noise vector. The subscripts $_0$ and $_{fb}$ indicate the matrix partition described in eq. (2.4.18).

The prime notation is used to indicate channel convolution matrices that have been shifted in a particular way: a single prime (*i.e.* $\mathbf{G}'$) indicates that all entries in the channel convolution matrix have been shifted to the right (the last column was removed and a column of zeros was appended to the left). A double prime (*i.e.* $\mathbf{G}''$) indicates that all of the entries have been shifted right and down, shifting in zeros from the left and top.

This model describes how changes in the channel impulse response propagate through the channel convolution matrix product. The change first manifests itself in the top and left of the channel convolution matrix product. During the next $L-1$ time steps (for a total of L steps) the change would move up the channel convolution matrix one row at a time and move through the channel convolution product matrix ($\mathbf{G}[n]\mathbf{G}^{H}[n]$) from the right and bottom and work toward the top and left.

The trace of the matrix is equal to the sum of the eigenvalues of the matrix. The matrix $\mathbf{Q}[n]$ is defined as $\mathbf{Q}[n] = \mathbf{G}_{0}^{H}[n]\mathbf{G}_{0}[n] + \mathbf{R}_{\nu}$. The $\mathbf{L_{ff}} - 1 \times \mathbf{L_{ff}} - 1$ principle submatrix of $\mathbf{Q}[n]$ is denoted as $\mathbf{Q}_{P}[n]$. The bottom right element of $\mathbf{Q}[n]$ is represented by the symbol $q_{L_{ff}L_{ff}}[n]$ and the term $\delta\mathbf{g}[n]$ is defined as $\delta\mathbf{g}[n] = (\alpha - 1)\mathbf{g}[n] + \boldsymbol{v}[n]$.

The Poincare separation theorem states that if the eigenvalues of $\mathbf{Q}[n]$ (denoted $\lambda_{Q,i}$, $i = 1, \cdots, L_{ff}$) and $\mathbf{Q}_{P}[n]$ (denoted $\widetilde{\lambda}_{Q,i}$, $i = 1, \cdots, L_{ff}$) are ordered from greatest to least, then the following relationship between the eigenvalues is satisfied, [38]

$$\lambda_{Q,1} \geq \widetilde{\lambda}_{Q,1} \geq \lambda_{Q,2} \geq \cdots \geq \widetilde{\lambda}_{Q,L_{ff}-1} \geq \lambda_{Q,L_{ff}}. \qquad (6.4.11)$$

This relationship bounds the changes in each of the eigenvalues from one step to the

169

next (with the least eigenvalue lower bounded by zero). In addition, at each time step the trace of $\mathbf{Q}[n]$ changes by $\Delta_Q = |\delta\mathbf{g}[n]|^2 - \left[\mathbf{Q}[n]\right]_{(L_{ff}L_{ff})}$, so the change in the greatest eigenvalue is also bounded and so the change in energy of the channel convolution matrix product is bounded. Although this argument shows that the changes in the spectrum of the matrix $\mathbf{Q}[n]$ is bounded, empirically, the changes are not only bounded but smooth. Therefore, the change in equalizer coefficients should also be smooth.

When the observation noise is white with variance σ_ν^2, the diagonal matrix $\mathbf{R}_\nu = \sigma_\nu^2\mathbf{I}$ acts as a regularization term. This limits the maximum eigenvalues of $\mathbf{Q}^{-1}[n]$ to σ_ν^{-1}, which limits the maximum change in the energy of the equalizer coefficients. In this case, when the SNR is low, the diagonal noise correlation matrix dominates in $\mathbf{Q}[n]$, so $\mathbf{Q}[n]$ becomes nearly diagonal (diagonally dominant). This implies that the perturbation of the equalizer coefficients is approximately linear with similar dynamics to the channel coefficients. This result will also be seen when analyzing the equalizer coefficients using a linear perturbation model.

The structure of the updates to $\mathbf{Q}[n]$, where the matrix indicates that at each step, the matrix update is rank two. Thus a low-complexity method for updating the CEB-DFE could be constructed where the inverse matrix is updated using a rank two update. This idea is not explored further in this thesis, but merits future study.

The model presented in this section shows the exact dependence of the equalizer coefficients on the change in the channel coefficients; few parts of the equalizer matrix equation are changing from one time-step to the next. In the next subsection, the variation of this complete model is simplified into a block variation model.

6.4.3 Block variation model

The channel convolution matrix update model introduced in the last section is accurate but cumbersome. To ease use of an equalizer coefficient variation model, a block variation model is introduced where the channel convolution matrix is only updated every L_{ff} time steps, where L_{ff} is the number of DFE feedforward coefficients. The update will change the whole matrix instantaneously so the changes do not propa-

170

gate through as in the previous model, which simplifies the analysis of the equalizer coefficient dynamics.

To model block changes, eq. (6.2.1) is applied to the whole channel convolution matrix rather than only a channel vector.

$$\mathbf{G}[n+1] = \alpha \mathbf{G}[n] + \mathbf{\Upsilon}[n] \qquad (6.4.12)$$

where $\mathbf{\Upsilon}[n]$ is now a fully populated channel noise matrix appropriately zero-padded to account for shifting effects. Substituting this model into eq. (2.4.20), the channel equalizer coefficients can be written as

$$
\begin{aligned}
\mathbf{h}_{\mathrm{ff}}[n+1] &= (\mathbf{G}_0^H[n+1]\mathbf{G}_0[n+1] + \mathbf{R}_\nu)^{-1}\mathbf{g}_0^*[n+1] \\
&= ((\alpha\mathbf{G}_0[n] + \mathbf{\Upsilon}_0[n])^H(\alpha\mathbf{G}_0[n] + \mathbf{\Upsilon}_0[n]))^{-1}(\alpha\mathbf{g}_0 + \boldsymbol{v}_0[n])^* \\
&= (|\alpha|^2\mathbf{G}_0^H[n]\mathbf{G}_0[n] + \alpha\mathbf{\Upsilon}_0^H[n]\mathbf{G}_0[n] + \alpha^*\mathbf{G}_0^H[n]\mathbf{\Upsilon}_0[n] + \mathbf{\Upsilon}_0^H[n]\mathbf{\Upsilon}_0[n])^{-1}\times \\
&\quad\ (\alpha\mathbf{g}_0 + \boldsymbol{v}_0[n])^* \qquad\qquad (6.4.13) \\
\mathbf{h}_{\mathrm{fb}}[n+1] &= -\mathbf{G}_{\mathrm{fb}}[n+1]\mathbf{h}_{\mathrm{ff}}[n+1] \\
&= -(\alpha\mathbf{G}_{\mathrm{fb}}[n] + \mathbf{\Upsilon}_{\mathrm{fb}}[n])\mathbf{h}_{\mathrm{ff}}[n+1]. \qquad (6.4.14)
\end{aligned}
$$

This model highlights the effect a channel perturbation has on the equalizer coefficients. This model behaves as if the channel perturbed at some time, followed by L time steps where the channel maintains the perturbed value. The equalizer coefficients all change simultaneously from one steady state value to the next. In this case, the matrix $\mathbf{\Upsilon}[n]$ is full column rank so there are not the same eigenvalue bounds shown for the previous model.

This model also highlights the nonlinear relation between the equalizer coefficients and the channel coefficients. Even when the channel coefficients have simple dynamics, such as the Markov model, the change in equalizer coefficients to a channel perturbation is unclear. This idea of a block changing channel is used again when studying the correlation structure of the equalizer coefficients.

With the exception of the block variational model, which is used as a tool for

describing the channel when evaluating equalizer coefficient correlation, the three models presented in this section will not be used again in this thesis. They are included in this chapter to complete the discussion and allow one to visualize the precise relationship between the channel and equalizer coefficients. The channel convolution matrix update model is especially illustrative of the one-step update of the equalizer coefficients and highlights the nonlinear relationship between the channel and equalizer coefficients.

6.5 First-order Taylor expansion of equalizer coefficients

Another method for determining the change in equalizer coefficients due to a change in the channel coefficients is the Taylor expansion of the equalizer coefficients. This provides a linearized model of the equalizer coefficient dynamics and a way to compare the channel coefficient dynamics and the equalizer coefficient dynamics.

The derivation of the first-order Taylor expansion is presented in two steps: first, the derivation is given for a scalar channel (*i.e.* a channel with one coefficient). Second, the derivation is presented for a Taylor expansion of and equalizer with more than one ceofficient (a vector equalizer). The channel length and equalizer length are assumed to be equal throughout these derivations. The time index is dropped for clarity.

6.5.1 Scalar equalizer coefficient based on scalar channel perturbation

To gain intuition into the dependence of the feedforward equalizer coefficients on the dynamics of the channel coefficients, the scalar channel and scalar equalizer are analyzed. For the scalar channel, the first order Taylor expansion answers the question of "What is the (approximate) magnitude of the equalizer coefficient perturbation, $\delta h = h(g + \delta g, g^* + \delta g^*) - h(g, g^*)$, caused by a channel impulse response perturbation δg?" The scalar channel provides a clear view of the interplay between the dynamics

172

of the channel and the dynamics of the equalizer.

For a scalar channel, the equalizer coefficient that minimize the MMSE cost function is

$$h(g, g^*) = \frac{g^*}{g^* g + \sigma_\nu^2}. \tag{6.5.1}$$

The Taylor expansion of the equalizer coefficient about the channel coefficient is

$$h(g + \delta g, g^* + \delta g^*) \approx h(g, g^*) + \frac{\partial h}{\partial g} \delta g + \frac{\partial h}{\partial g^*} \delta g^*. \tag{6.5.2}$$

After evaluating the partial derivatives and rearranging terms, the Taylor expansion becomes

$$h(g + \delta g, g^* + \delta g^*) = \frac{(g + \delta g)^*}{gg^* + \sigma_\nu^2} - \left(\frac{g^* \delta g + g \delta g^*}{gg^* + \sigma_\nu^2} \right) h(g, g^*). \tag{6.5.3}$$

The expression for the linear perturbation model of the equalizer coefficient is

$$h(g + \delta g, g^* + \delta g^*) = h(g, g^*) + \delta h. \tag{6.5.4}$$

From eq. (6.5.3), the equalizer coefficient perturbation term is

$$\delta h = \frac{\delta g^*}{gg^* + \sigma_\nu^2} - \left(\frac{g^* \delta g + g \delta g^*}{gg^* + \sigma_\nu^2} \right) h(g, g^*). \tag{6.5.5}$$

Derivation of first-order Taylor expansion for scalar equalizer

Throughout this chapter, a variable and its conjugate are treated as two separate complex variables, as done in [9]; the partial derivative with respect to a variable treats the conjugate of the variable as a constant.

The partial derivatives of h with respect to g and with respect to g^* is

$$\begin{aligned} \frac{\partial h}{\partial g} &= -\frac{(g^*)^2}{(gg^* + \sigma_\nu^2)^2} \\ \frac{\partial h}{\partial g^*} &= -\frac{gg^*}{(gg^* + \sigma_\nu^2)^2} + \frac{1}{gg^* + \sigma_\nu^2}. \end{aligned}$$

173

The linear perturbation model of the equalizer coefficient around the point g is

$$
\begin{aligned}
h(g + \delta g, g^* + \delta g^*) &\approx h(g, g^*) + \frac{\partial h}{\partial g}\delta g + \frac{\partial h}{\partial g^*}\delta g^* \\
&= h(g, g^*) - \frac{(g^*)^2}{(gg^* + \sigma_\nu^2)^2}\delta g - \frac{gg^*}{(gg^* + \sigma_\nu^2)^2}\delta g^* + \frac{1}{gg^* + \sigma_\nu^2}\delta g^* \\
&= \frac{(g + \delta g)^*}{gg^* + \sigma_\nu^2} - \left(\frac{g^*\delta g + g\delta g^*}{gg^* + \sigma_\nu^2}\right)h(g, g^*).
\end{aligned}
$$

The last equality comes from substituting eq. (6.5.1) for both expansion and simplification of terms. Using the first-order Taylor expansion, the equalizer coefficients can be written as

$$
\begin{aligned}
h(g + \delta g, g^* + \delta g^*) &= h(g, g^*) + \delta h \\
&\approx h(g, g^*) + \frac{\delta g^*}{gg^* + \sigma_\nu^2} - \left(\frac{g^*\delta g + g\delta g^*}{gg^* + \sigma_\nu^2}\right)h(g, g^*),
\end{aligned}
$$

which implies

$$
\delta h = \frac{\delta g^*}{gg^* + \sigma_\nu^2} - \left(\frac{g^*\delta g + g\delta g^*}{gg^* + \sigma_\nu^2}\right)h(g, g^*).
$$

Interpretation of results for scalar equalizer

There are two interesting quantities that can be extracted from the first order Taylor expansion of the equalizer coefficients. The first is the normalized change in the equalizer coefficients verses the channel coefficients. The second quantity is the behavior of the linear model in the extreme SNR regions.

Using eqns. (6.5.1) and (6.5.5), the normalized change in the equalizer coefficient, $\frac{\delta h}{h}$, can be written in terms of the normalized change of the channel coefficient, $\frac{\delta g}{g}$ as

$$
\begin{aligned}
\frac{\delta h}{h} &= \frac{\frac{\delta g^*}{gg^* + \sigma_\nu^2} - \left(\frac{g^*\delta g + g\delta g^*}{gg^* + \sigma_\nu^2}\right)h(g, g^*)}{\frac{g^*}{gg^* + \sigma_\nu^2}} \\
&= \frac{\delta g^*}{g^*} - \frac{\frac{\delta g}{g} + \frac{\delta g^*}{g^*}}{1 + \frac{\sigma_\nu^2}{gg^*}} \\
&= \frac{\delta g^*}{g^*}\left(\frac{\sigma_\nu^2}{|g|^2 + \sigma_\nu^2}\right) - \frac{\delta g}{g}\left(\frac{|g|^2}{|g|^2 + \sigma_\nu^2}\right).
\end{aligned}
\tag{6.5.6}
$$

Thus, the normalized change in the equalizer coefficient is a combination of the normalized change of the channel coefficient and its conjugate. This implies that $\left|\frac{\delta h}{h}\right| \leq \left|\frac{\delta g}{g}\right|$, *i.e.* the absolute normalized change of the equalizer coefficient is less than or equal to the absolute normalized change in the channel coefficient, and so the equalizer coefficient should change slower than the channel coefficient in this model. Empirically, this turns out not to be the case, which implies that the linearized perturbation model does not accurately capture the dynamics of the equalizer coefficients. Analysis of δh is still illuminating in the at extreme ranges of SNR.

At low SNR where $|g|^2 \ll \sigma_\nu^2$, eq. (6.5.5) is approximated as

$$\delta h \approx \frac{\delta g^*}{\sigma_\nu^2}. \tag{6.5.7}$$

The term

$$\left(\frac{g^*\delta g + g\delta g^*}{gg^* + \sigma_\nu^2}\right) h(g, g^*) = \left(\frac{(g^*\delta g + g\delta g^*)g^*}{(gg^* + \sigma_\nu^2)^2}\right) \approx 0$$

because the term σ_ν^4 appears in the denominator and is much greater than the channel coefficients at low SNR.

At high SNR where $|g|^2 \ll \sigma_\nu^2$, eq. (6.5.5) is approximated instead as

$$\delta h \approx \frac{\delta g}{g} h(g, g^*). \tag{6.5.8}$$

The change in the equalizer coefficient in the high SNR region still depends on the current equalizer coefficient value.

One result of these derivations is that at low SNR, the dynamics of equalizer coefficient and the channel coefficient are very similar. At high SNR the dynamics of the equalizer and channel coefficients are very different. In later section it is shown that the coherence time of the equalizer coefficients in the high SNR region decreases as with the channel coefficient correlation.

175

6.5.2 Vector equalizer coefficients based on vector channel

A more realistic scenario than the scalar case is the multi-coefficient channel and a multi-coefficient equalizer. When the channel has more than one coefficient, however, the mathematics is more involved. This section presents the first-order Taylor expansion of the multi-coefficient equalizer which provides a method for comparing the dynamics of the equalizer and channel coefficient dynamics.

Only the DFE feedforward coefficient dynamics are analyzed. This is done because the feedback coefficient dynamics are similar to the channel coefficient dynamics. The subscript $_{ff}$ is dropped from all of the equalizer coefficient labels because only one part of the equalizer is being analyzed. For simplification, the channel is assumed to change in block increments so the channel convolution matrix is Toeplitz.

The first order Taylor expansion of the DFE feedforward (or LE) coefficients is

$$\mathbf{h}(\mathbf{g} + \delta\mathbf{g}, \mathbf{g}^* + \delta\mathbf{g}^*) \approx \mathbf{h}(\mathbf{g}, \mathbf{g}^*) + \frac{\partial\mathbf{h}}{\partial\mathbf{g}}\delta\mathbf{g} + \frac{\partial\mathbf{h}}{\partial\mathbf{g}^*}\delta\mathbf{g}^*, \tag{6.5.9}$$

where $\frac{\partial\mathbf{h}}{\partial\mathbf{g}}$ is the Jacobian of $\mathbf{h}$ with respect to $\mathbf{g}$. The column vector $\delta\mathbf{g}[n]$ is a channel coefficient perturbation. The elements of $\delta\mathbf{g}[n]$ (at time n) are

$$\delta\mathbf{g}[n] = \begin{bmatrix} \delta g[n,0] & \delta g[n,1] & \cdots & \delta g[n, N-1] \end{bmatrix}^T. \tag{6.5.10}$$

Substituting for the Jacobian matrices in eq. (6.5.9), the first-order perturbation model of the equalizer coefficients is

$$\mathbf{h}(\mathbf{g} + \delta\mathbf{g}, \mathbf{g}^* + \delta\mathbf{g}^*) \approx \mathbf{h}(\mathbf{g}_0, \mathbf{g}_0^*) + \mathbf{Q}^{-1}\delta\mathbf{g}^* - \mathbf{Q}^{-1}\left[\delta\mathbf{G}_0^H\mathbf{G}_0 + \mathbf{G}_0^H\delta\mathbf{G}_0\right]\mathbf{h}(\mathbf{g}_0, \mathbf{g}_0^*). \tag{6.5.11}$$

The matrix $\delta\mathbf{G}_0$ is an upper triangular matrix,

$$\delta\mathbf{G}_0[n] = \begin{bmatrix} \delta g[n,0] & \delta g[n,1] & \delta g[n,2] & \cdots & \delta g[n,N-1] \\ 0 & \delta g[n,0] & \delta g[n,1] & \cdots & \delta g[n,N-2] \\ 0 & 0 & \delta g[n,0] & \cdots & \delta g[n,N-3] \\ \vdots & & & \ddots & \vdots \\ 0 & 0 & 0 & \cdots & \delta g[n,0] \end{bmatrix}, \qquad (6.5.12)$$

where $\delta g[n,i]$ is the ith element for the $\delta\mathbf{g}[n]$ vector at time n. The channel is modeled as block changing, so all elements have the same time-index n. The matrix $\delta\mathbf{G}_0$ has a similar structure to the reduced channel convolution matrix

$$\mathbf{G}_0[n] = \begin{bmatrix} g[n,0] & g[n,1] & g[n,2] & \cdots & g[n,N-1] \\ 0 & g[n,0] & g[n,1] & \cdots & g[n,N-2] \\ 0 & 0 & g[n,0] & \cdots & g[n,N-3] \\ \vdots & & & \ddots & \vdots \\ 0 & 0 & 0 & \cdots & g[n,0] \end{bmatrix}. \qquad (6.5.13)$$

In this matrix, $g[n,i]$ is the ith coefficient of the channel impulse response vector $\mathbf{g}[n]$. The channel is assumed to be block changing so all channel coefficients again have the same time index. For the remainder of this section, the time-index n is suppressed for brevity so $g[i] \triangleq g[n,i]$.

Derivation of first-order Taylor expansion of vector equalizer

Recall from above that the first-order Taylor expansion of the equalizer coefficients with respect to the channel coefficients is

$$\mathbf{h}(\mathbf{g}+\delta\mathbf{g}, \mathbf{g}^*+\delta\mathbf{g}^*) \approx \mathbf{h}(\mathbf{g}, \mathbf{g}^*) + \frac{\partial\mathbf{h}}{\partial\mathbf{g}}\delta\mathbf{g} + \frac{\partial\mathbf{h}}{\partial\mathbf{g}^*}\delta\mathbf{g}^*$$

When there are N channel coefficients, the Jacobian of the equalizer coefficients

with respect to the channel coefficients are defined as

$$J(\mathbf{h}, \mathbf{g}) = \frac{\partial \mathbf{h}}{\partial \mathbf{g}} = \begin{bmatrix} \frac{\partial \mathbf{h}}{\partial g[0]} & \frac{\partial \mathbf{h}}{\partial g[1]} & \cdots & \frac{\partial \mathbf{h}}{\partial g[N-1]} \end{bmatrix}. \tag{6.5.14}$$

Similarly, the Jacobian of the channel coefficients with respect to the conjugate of the channel coefficients is

$$J(\mathbf{h}, \mathbf{g}^*) = \frac{\partial \mathbf{h}}{\partial \mathbf{g}^*} = \begin{bmatrix} \frac{\partial \mathbf{h}}{\partial g^*[0]} & \frac{\partial \mathbf{h}}{\partial g^*[1]} & \cdots & \frac{\partial \mathbf{h}}{\partial g^*[N-1]} \end{bmatrix}. \tag{6.5.15}$$

In this derivation, a complex variables and their conjugates are assumed to be two different variables as proposed in [9]. Also, the following matrix identity is used throughout the derivation (see *e.g.* [54]),

$$\frac{d\mathbf{A}^{-1}(t)}{dt} = -\mathbf{A}^{-1}(t) \frac{d\mathbf{A}^{-1}(t)}{dt} \mathbf{A}^{-1}(t) \tag{6.5.16}$$

In this identity, $\mathbf{A}(t)$ is an invertible matrix whose elements are functions of a parameter t.

Recall from eq. (2.4.20) that the DFE feedforward coefficients are

$$\mathbf{h} = [\mathbf{G}_0^H \mathbf{G}_0 + \mathbf{R}_\nu]^{-1} \mathbf{G}_0^H \mathbf{e}_0 = \mathbf{Q}^{-1} \mathbf{g}_0^* \tag{6.5.17}$$

where $\mathbf{e}_i$ is a column vector with a '1' in the $(i+1)^{\text{th}}$ position and all other elements zero, *e.g.*

$$\mathbf{e}_2 = \begin{bmatrix} 0 & 0 & 1 & 0 & \cdots & 0 \end{bmatrix}^T \tag{6.5.18}$$

The column vector $\mathbf{g}_0^*$ is the complete channel impulse response vector and the conjugate transpose of the first row of the reduced channel convolution matrix, $\mathbf{G}_0$.

$$\mathbf{g}_0^* = \begin{bmatrix} g^*[0] & g^*[1] & \cdots & g^*[N-1] \end{bmatrix}^T \tag{6.5.19}$$

Defining the matrix $\mathbf{Q}$ as

$$\mathbf{Q} = \mathbf{G}_0^H \mathbf{G}_0 + \mathbf{R}_\nu, \tag{6.5.20}$$

178

the partial derivative of the equalizer coefficients is

$$\frac{\partial \mathbf{h}}{\partial g[i]} = \frac{\partial}{\partial g[i]} \mathbf{Q}^{-1} \mathbf{g}_0^*$$

$$= -\mathbf{Q}^{-1} \frac{\partial \mathbf{Q}}{\partial g[i]} \mathbf{Q}^{-1} \mathbf{g}_0^*$$

$$= -\mathbf{Q}^{-1} \mathbf{G}_0^H \mathbf{S}_N^i \mathbf{h}(\mathbf{g}, \mathbf{g}^*). \tag{6.5.21}$$

The second equality comes from substituting eq. (6.5.16) into the first equality. The matrix S_N is the shift matrix defined in eq. (6.4.6) and the matrix $\mathbf{S}_N^0$ is assumed to be the identity matrix. The last equality comes from evaluating the partial derivative with respect to the channel coefficient $g[i]$. The noise correlation matrix $\mathbf{R}_\nu$ has no dependence on $g[i]$ so its derivative evaluates to zero. The reduced channel convolution matrix is Toeplitz so the Jacobian is also Toeplitz. To obtain the last equality, the relation $\mathbf{h}(\mathbf{g}, \mathbf{g}^*) = \mathbf{Q}^{-1} \mathbf{g}_0^*$ from eq. (6.5.17) is substituted into the second equality.

The partial derivative of the equalizer coefficients is

$$\frac{\partial \mathbf{h}}{\partial g^*[i]} = \frac{\partial}{\partial g^*[i]} \mathbf{Q}^{-1} \mathbf{g}_0^*$$

$$= -\mathbf{Q}^{-1} \frac{\partial \mathbf{Q}}{\partial g^*[i]} \mathbf{Q}^{-1} \mathbf{g}_0^* + \mathbf{Q}^{-1} \frac{\partial \mathbf{g}_0^*}{\partial g^*[i]}$$

$$= -\mathbf{Q}^{-1} \left(\mathbf{S}_N^i \right)^H \mathbf{G}_0 \mathbf{h}(\mathbf{g}, \mathbf{g}^*) + \mathbf{Q}^{-1} \mathbf{e}_i. \tag{6.5.22}$$

The additional term $\mathbf{Q}^{-1} \mathbf{e}_i$ is the ith column of the inverse of the matrix $\mathbf{Q}$. The complete Jacobian matrices can be constructed from the component results

$$J(\mathbf{h}, \mathbf{g}) = \left[-\mathbf{Q}^{-1} \mathbf{G}_0^H \mathbf{S}_N^0 \mathbf{h}(\mathbf{g}, \mathbf{g}^*) \quad \cdots \quad -\mathbf{Q}^{-1} \mathbf{G}_0^H \mathbf{S}_N^{N-1} \mathbf{h}(\mathbf{g}, \mathbf{g}^*) \right] \tag{6.5.23}$$

$$J(\mathbf{h}, \mathbf{g}^*) = \left[-\mathbf{Q}^{-1} (\mathbf{S}_N^0)^H \mathbf{G}_0 \mathbf{h}(\mathbf{g}, \mathbf{g}^*) \quad \cdots \quad -\mathbf{Q}^{-1} (\mathbf{S}_N^{N-1})^H \mathbf{G}_0 \mathbf{h}(\mathbf{g}, \mathbf{g}^*) \right] + \mathbf{Q}^{-1}$$

$$\tag{6.5.24}$$

The quantities of interest in eq. (6.5.9) are the Jacobian matrices times the channel coefficient perturbation vectors, i.e. $J(\mathbf{h}, \mathbf{g})\delta\mathbf{g}$ and $J(\mathbf{h}, \mathbf{g}^*)\delta\mathbf{g}^*$. The product

$J(\mathbf{h}, \mathbf{g})\delta\mathbf{g}$ is

$$J(\mathbf{h}, \mathbf{g})\delta\mathbf{g} = -\sum_{i=1}^{N-1} \delta g[i]\mathbf{Q}^{-1}\mathbf{G}_0^H\mathbf{S}_N^i\mathbf{h}(\mathbf{g}, \mathbf{g}^*)$$

$$= -\mathbf{Q}^{-1}\mathbf{G}_0^H\left(\sum_{i=1}^{N-1} \delta g[i]\mathbf{S}_N^i\right)\mathbf{h}(\mathbf{g}, \mathbf{g}^*)$$

$$= -\mathbf{Q}^{-1}\mathbf{G}_0^H\delta\mathbf{G}_0\mathbf{h}(\mathbf{g}, \mathbf{g}^*), \qquad (6.5.25)$$

where the matrix $\delta\mathbf{G}_0$ is defined in eq. (6.5.12). Similarly, the product $J(\mathbf{h}, \mathbf{g})\delta\mathbf{g}$ is

$$J(\mathbf{h}, \mathbf{g})\delta\mathbf{g} = -\mathbf{Q}^{-1}\delta\mathbf{G}_0^H\mathbf{G}_0\mathbf{h}(\mathbf{g}, \mathbf{g}^*) + \mathbf{Q}^{-1}\delta\mathbf{g}_0^* \qquad (6.5.26)$$

Substituting the relations from eqns. (6.5.25) and (6.5.26) into eq. (6.5.9), the first-order Taylor expansion of the equalizer coefficients is

$$\mathbf{h}(\mathbf{g} + \delta\mathbf{g}, \mathbf{g}^* + \delta\mathbf{g}^*) \approx \mathbf{h}(\mathbf{g}_0, \mathbf{g}_0^*) + \mathbf{Q}^{-1}\delta\mathbf{g}^* - \mathbf{Q}^{-1}\left[\delta\mathbf{G}_0^H\mathbf{G}_0 + \mathbf{G}_0^H\delta\mathbf{G}_0\right]\mathbf{h}(\mathbf{g}, \mathbf{g}^*)$$

The equalizer coefficients from a channel perturbation can be written as

$$\mathbf{h}(\mathbf{g} + \delta\mathbf{g}, \mathbf{g}^* + \delta\mathbf{g}^*) = \mathbf{h}(\mathbf{g}, \mathbf{g}^*) + \delta\mathbf{h}$$

From the first order Taylor expansion, the perturbation term is

$$\delta\mathbf{h} \approx \mathbf{Q}^{-1}\delta\mathbf{g}^* - \mathbf{Q}^{-1}\left[\delta\mathbf{G}_0^H\mathbf{G}_0 + \mathbf{G}_0^H\delta\mathbf{G}_0\right]\mathbf{h}(\mathbf{g}, \mathbf{g}^*) \qquad (6.5.27)$$

Notice that the relation for the vector equalizer reduces to the relation for the scalar equalizer from eq. (6.5.5) when the number of equalizer and channel coefficients is reduced to one.

Interpretation of results for vector equalizer

The form of the equalizer perturbation, $\delta\mathbf{h}$, at high and low SNR reveals the equalizer dynamics in these regions. The eigenvalues of the matrix $\mathbf{G}_0^H\mathbf{G}_0$ are denoted $\lambda_{g,i}$ and

180

the eigenvalues of the matrix $\mathbf{R}_\nu$ are denoted $\lambda_{r,i}$ for $i = 1, \cdots, N$. The eigenvalues are ordered from greatest to least, $i.e.$ $\lambda_{g,1}$ is the greatest eigenvalue of the matrix $\mathbf{G}_0^H \mathbf{G}_0$.

At low SNR, $\lambda_{r,N-1} \gg \lambda_{g,1}$ so $\mathbf{G}_0^H \mathbf{G}_0 + \mathbf{R}_\nu \approx \mathbf{R}_\nu$. Treating $\mathbf{G}_0^H \mathbf{G}_0$ as a Hermitian perturbation matrix, the maximum perturbation of the eigenvalues of $\mathbf{R}_\nu$ is $\lambda_{g,1}$. Since this perturbation is small, the eigen-structure of $\mathbf{R}_\nu$ will not change noticeably when perturbed by $\mathbf{G}_0^H \mathbf{G}_0$ [99].

Using this assumption, eq. (6.5.27) becomes

$$\begin{aligned} \delta\mathbf{h} &= \mathbf{R}_\nu^{-1} \delta\mathbf{g}_0^* + \mathbf{R}_\nu^{-1} \left[\delta\mathbf{G}_0^H \mathbf{G}_0 + \mathbf{G}_0^H \delta\mathbf{G}_0 \right] \mathbf{R}_\nu^{-1} \mathbf{g}_0^* \\ &\approx \mathbf{R}_\nu^{-1} \delta\mathbf{g}_0^* \end{aligned} \tag{6.5.28}$$

The term

$$\mathbf{R}_\nu^{-1} \left[\delta\mathbf{G}_0^H \mathbf{G}_0 + \mathbf{G}_0^H \delta\mathbf{G}_0 \right] \mathbf{R}_\nu^{-1} \mathbf{g}_0^*$$

is approximately zero since the inverse noise correlation term dominates. The equalizer coefficients have the form of a whitened match filter.

When the SNR is low eq. (6.5.28) can be used to approximate the perturbed equalizer coefficients as

$$\mathbf{h}(\mathbf{g} + \delta\mathbf{g}, \mathbf{g}^* + \delta\mathbf{g}^*) \approx \mathbf{R}_\nu^{-1} (\mathbf{g} + \delta\mathbf{g})^*. \tag{6.5.29}$$

At low SNR the dynamics of the equalizer coefficients and the channel coefficients are equivalent. A perturbation of the channel coefficients causes a proportional change in the equalizer coefficients.

Rearranging the relation for the equalizer coefficient perturbation, $\delta\mathbf{h}$ so the terms based on $\delta\mathbf{g}$ are separated from those based on $\delta\mathbf{g}^*$ simplifies the analysis at high SNR. A relationship between the channel coefficients and the channel convolution function that simplifies the derivation is

$$\delta\mathbf{g}^* = \delta\mathbf{G}_0^H \mathbf{e}_0 \tag{6.5.30}$$

Substituting this relation into the equalizer coefficient perturbation from eq. (6.5.27) gives an expression for the equalizer perturbation,

$$\delta\mathbf{h} = \mathbf{Q}^{-1}\delta\mathbf{G}^{H}\left(\mathbf{e}_0 - \mathbf{G}_0\mathbf{h}(\mathbf{g},\mathbf{g}^*)\right) - \mathbf{Q}^{-1}\mathbf{G}_0^{H}\delta\mathbf{G}_0\mathbf{h}(\mathbf{g},\mathbf{g}^*). \tag{6.5.31}$$

At high SNR, the reduced channel convolution matrix product dominates the noise correlation matrix, $i.e.$ $\lambda_{g,N-1} \gg \lambda_{r,1}$, so $\mathbf{Q} \approx \mathbf{G}_0^{H}\mathbf{G}_0$. Substituting this approximation and definition of the equalizer coefficients from eq. (2.4.20) into eq. (6.5.31) gives

$$\delta\mathbf{h} \approx (\mathbf{G}_0^{H}\mathbf{G}_0)^{-1}\delta\mathbf{G}_0^{H}\left(\mathbf{I} - \mathbf{G}_0(\mathbf{G}_0^{H}\mathbf{G}_0)^{-1}\mathbf{G}_0^{H}\right)\mathbf{e}_0 - (\mathbf{G}_0^{H}\mathbf{G}_0)^{-1}\mathbf{G}_0^{H}\delta\mathbf{G}_0\mathbf{h}(\mathbf{g},\mathbf{g}^*)$$

The term $\left(\mathbf{I} - \mathbf{G}_0(\mathbf{G}_0^{H}\mathbf{G}_0)^{-1}\mathbf{G}_0^{H}\right)$ is a projection matrix onto the null space of $\mathbf{G}_0$ [112]. Assuming $g_0 \neq 0$ the matrix $\mathbf{G}_0$ is full rank, so the null space is empty. The perturbation term becomes

$$\delta\mathbf{h} \approx -(\mathbf{G}_0^{H}\mathbf{G}_0)^{-1}\mathbf{G}_0^{H}\delta\mathbf{G}_0\mathbf{h}(\mathbf{g},\mathbf{g}^*) \tag{6.5.32}$$

Therefore, at high SNR the equalizer coefficient perturbation depends on the unperturbed values of the equalizer coefficients.

6.6   Correlation structure of equalizer coefficients

A final way to evaluate the equalizer dynamics is by determining the equalizer coefficient correlation structure based on the correlation structure of the channel coefficients. In this section, the extreme SNR regions are analyzed.

At low SNR, the equalizer coefficient correlation is equivalent to the channel coefficient correlation, a result previewed in the last section. When the channel and equalizer coefficients have the same dynamics, the CEB and DA methods have similar error performance, which is supported by experimental data [91].

At high SNR, equalizers with more than one coefficient are well approximated

by a scalar equalizers; the analysis of a single coefficient equalizer produces results applicable to the multiple channel equalizer.

The estimated equalizer coefficient correlation functions are presented in the next section. These functions indicate that the coherence time of the equalizer coefficients is less than the channel coefficients. There is therefore a shorter data averaging window for the equalizer coefficients than the channel coefficients. The equalizer coefficients calculated using the DA method will have higher error than CEB equalizer coefficients. Simulation data supports this hypothesis of the relative performance between the two algorithms [91].

Recall from eq. (2.2.5) that DFE feedforward coefficients are

$$\mathbf{h}_{\mathrm{ff}}[n] = \mathbf{Q}[n]^{-1}\mathbf{g}_0^*[n] = (\mathbf{G}_0^H[n]\mathbf{G}_0[n] + \sigma_d^{-2}\mathbf{R}_\nu)^{-1}\mathbf{g}_0^*[n], \qquad (6.6.1)$$

where the transmitted symbol energy, σ_d^2, is explicitly reintroduced.

In this section, the channel is assumed to be *Rayleigh Fading* with the variance of each channel coefficients equal to σ_g^2. If the channel coefficients are independently varying and the noise is white with variance σ_ν^2, the average SNR of the communications channel is $\frac{N\sigma_d^2\sigma_g^2}{\sigma_\nu^2}$, where N is the number of channel coefficients.

Recall that the ith eigenvalue of $\mathbf{G}_0^H\mathbf{G}_0$ is denoted by $\lambda_{g,i}$ for $i = 1, \cdots, N$, and that the eigenvalues are ordered from greatest to least, *i.e.*

$$\lambda_{g,1} \geq \lambda_{g,2} \geq \cdots \geq \lambda_{g,N}$$

Similarly, the eigenvalues of the noise correlation matrix are

$$\lambda_{r,1} \geq \lambda_{r,2} \geq \cdots \geq \lambda_{r,N}$$

6.6.1 Correlation of equalizer coefficients at low SNR

At low SNR, the noise energy (scaled by the transmit symbol energy) dominates over the channel energy and so $\lambda_{r,N} \gg \lambda_{g,1}$. The matrix $\mathbf{Q}[n]$ can be approximated as

$$\mathbf{Q}[n] = \mathbf{G}_0^H[n]\mathbf{G}_0[n]\sigma_d^{-2}\mathbf{R}_\nu \approx \sigma_d^{-2}\mathbf{R}_\nu.$$

The time dependence of $\mathbf{Q}[n]$ is removed because the noise statistics are stationary.

The DFE feedforward equalizer coefficients at low SNR are

$$\mathbf{h}_{\text{ff}}[n] \approx \mathbf{R}_\nu^{-1}\sigma_d^2\mathbf{g}_0^*[n] \tag{6.6.2}$$

Note that the equalizer coefficients in eq. (6.6.2) are the whitened match filter of the channel coefficients.

The correlation matrix of the channel coefficients at lag m is defined as

$$\mathbf{R}_g[m] = \mathrm{E}\{\mathbf{g}[n]\mathbf{g}^H[n+m]\}. \tag{6.6.3}$$

Similarly, the equalizer coefficient correlation matrix is

$$\mathbf{R}_h[m] = \mathrm{E}\{\mathbf{h}[n]\mathbf{h}^H[n+m]\} \tag{6.6.4}$$

Substituting the expression from eq. (6.6.2) into eq. (6.6.4), the equalizer correlation becomes

$$\mathbf{R}_h[m] \approx \mathbf{R}_\nu^{-1}\mathbf{R}_g^*[m]\mathbf{R}_\nu^{-1} \tag{6.6.5}$$

When the noise is white, $\mathbf{R}_\nu = \sigma_\nu^2\mathbf{I}$, the equalizer coefficient correlation matrix at lag m is

$$\mathbf{R}_h[m] \approx \sigma_\nu^{-4}\mathbf{R}_g^*[m] \tag{6.6.6}$$

This relation shows that the equalizer coefficient correlation is a scaled version of the channel coefficient correlation. By normalizing the correlation matrices so that the maximum value is one the channel and equalizer coefficient correlation matrices are

equal.

Since the channel and equalizer coefficients have the same correlation, the averaging window lengths used for both sets of coefficients are equal. The DA and CEB methods of calculating the equalizer coefficients therefore have the same error performance at low SNR. This has been confirmed in the literature [91] and is shown with simulation data later in this chapter.

6.6.2 Correlation of equalizer coefficients at high SNR

At high SNR $(\lambda_{g,N} \gg \lambda_{r,1})$, the received data correlation matrix, $\mathbf{Q}[n]$, has the approximation

$$\mathbf{Q}[n] \approx \mathbf{G}_0[n]\mathbf{G}_0^H[n]. \tag{6.6.7}$$

because the reduced channel convolution matrix product, $\mathbf{G}_0\mathbf{G}_0^H$, dominates the noise correlation matrix. The dominant term of $\mathbf{Q}[n]$ is the reduced channel convolution matrix product, so $\mathbf{Q}[n]$ is time-dependent.

When the SNR is high, the equalizer coefficient correlation matrix is

$$\mathbf{R}_h[m] = E[\mathbf{h}[n]\mathbf{h}^H[n+m]] \approx E\left[\left(\mathbf{G}_0^H[n]\mathbf{G}_0[n]\right)^{-1}\mathbf{g}_0^*[n]\mathbf{g}_0^T[m]\left(\mathbf{G}_0^H[m]\mathbf{G}_0[m]\right)^{-1}\right].$$
$$\tag{6.6.8}$$

The expectation is over the channel impulse response coefficients. Since the channel impulse response coefficients appear in both the numerator and denominator the expectation is hard to evaluate. The equalizer correlation matrix is also no longer a linear function of the channel correlation matrix, so one would not expect the normalized correlation of the equalizer and channel coefficients to be equivalent.

Scalar approximation of vector equalizer

At high SNR, the terms in eq. (6.6.1) can be written as

$$(\mathbf{G}_0^H[n]\mathbf{G}_0[n])\mathbf{h}_{\mathrm{ff}}[n] = \mathbf{g}_0^*[n]. \tag{6.6.9}$$

The conjugate of the channel coefficients are the vector product of the reduced convolution matrix product and the feedforward equalizer coefficients. When the channel is block changing, the reduced channel convolution matrix when the feedback equalizer spans the complete delay-spread is given in eq. (6.5.13).

Using the column vector $\mathbf{e}_0$, where the first element is a one and the rest are zero, the first column of the reduced channel convolution matrix is

$$\mathbf{G}_0^H[n]\mathbf{G}_0[n]\mathbf{e}_0 = \begin{bmatrix} g[n,0]g^*[n,0] \\ g[n,0]g^*[n,1] \\ g[n,0]g^*[n,2] \\ \vdots \\ g[n,0]g^*[n,N-1] \end{bmatrix}. \tag{6.6.10}$$

This relation implies a surprising result,

$$\mathbf{G}_0^H[n]\mathbf{G}_0[n]\mathbf{e}_0 = g[n,0]\mathbf{g}^*[n].$$

The MMSE equalizer coefficients at high SNR are

$$\mathbf{h}[n] = \begin{bmatrix} 1/g[n,0] & 0 & 0 & \ldots & 0 \end{bmatrix}^T. \tag{6.6.11}$$

Upon reflection, this result is not too surprising because the MMSE feedback section removes all ISI, so inverting the first channel coefficient is the optimal equalizer with no noise. Regardless of channel length, only one feedforward coefficient is needed at very high SNR. This is not meant to be a way to reduce order (although it does merit further study), but is meant to provide a tractable way to analyze the vector equalizer using a scalar approximation. The next part provides an analysis of the scalar equalizer correlation.

In practical equalizer implementations, a single equalizer coefficient would probably not be desirable since the ISI cancellation is not perfect due to estimation error. In this case, the feedforward section is used to reduce and reshape the residual error.

Expectation of single coefficient equalizer

The last section argued that at high SNR regime with a block-changing channel the DFE feedforward section has only one energetic coefficient. As a result, the analysis of the single coefficient equalizer is sufficient to characterize the full feedforward section. In this section, a statistical analysis is given for the single coefficient equalizer showing that the equalizer coefficient has finite variance and thus a correlation function exists. In the next section, empirical results are presented which verify the proposition that the equalizer coefficients have a shorter correlation time than do channel coefficients.

Recall from eq. (6.5.1) that the single coefficient equalizer is

$$h = \frac{g^*}{g^* g + \sigma_\nu^2}. \tag{6.6.12}$$

The channel coefficients are assumed to be Rayleigh fading, *i.e.* modeled as circularly-symmetric, complex Gaussian random variables. One property of circularly-symmetric random variables is that the magnitude and phase are independent. The magnitude is Rayleigh distributed and the phase uniformly is distributed from 0 to 2π [70].

The zero mean property of the equalizer coefficient is derived first. In eq. (6.6.12), the complex channel coefficient can be rewritten in magnitude-phase form, *i.e.*

$$g = |g| e^{j\theta_g},$$

to give an alternative relation for the equalizer coefficient

$$h = \frac{|g| e^{-j\theta_g}}{|g|^2 + \sigma_\nu^2}. \tag{6.6.13}$$

Since θ and $|g|$ are independent, the expectation of the channel coefficient is

$$\begin{aligned} \mathrm{E}\{h\} &= \mathrm{E}\{\frac{|g| e^{-j\theta_g}}{|g|^2 + \sigma_\nu^2}\} \\ &= \mathrm{E}\{e^{-j\theta_g}\} \mathrm{E}\{\frac{|g|}{|g|^2 + \sigma_\nu^2}\} \\ &= 0, \end{aligned} \tag{6.6.14}$$

since

$$E\{e^{-j\theta_g}\} = \frac{1}{2\pi} \int_0^{2\pi} e^{-j\theta} d\theta = 0.$$

The finite variance property of the channel coefficient is calculated next. Since the equalizer coefficient is zero-mean, the variance is $E\{|h|^2\}$. Substituting the expression for the equalizer coefficient from eq. (6.6.12) and evaluating the expectation (a complete proof is below), the equalizer coefficient variance is

$$E\{|h|^2\} = \frac{1}{2\sigma_g^2} \left[-1 + (1+\rho)e^\rho \int_\rho^\infty \frac{e^{-z}}{z} dz \right]. \tag{6.6.15}$$

In this expression, $\rho = \sigma_\nu^2/\sigma_g^2$ is a modified version of the inverse signal to noise ratio, σ_g^2 is the variance of the channel coefficient, and σ_ν^2 is the observation noise variance. The integral term,

$$E_1(\rho) = \int_\rho^\infty \frac{e^{-z}}{z} dz$$

is a special integral known as the *exponential integral function*, with well known bounds [1],

$$\frac{1}{2} \ln \left(1 + \frac{2}{\rho} \right) < e^\rho E_1(\rho) < \ln \left(1 + \frac{1}{\rho} \right). \tag{6.6.16}$$

The lower bound of the variance is interesting for small values of ρ. As $\rho \to 0$ (*i.e.* $\sigma_\nu^2 \to 0$), the variance of the equalizer coefficients monotonically increases and is bounded away from zero. This implies that as the SNR is increased, the variance of the equalizer coefficients also increases.

The upper bound implies that

$$(1+\rho)\ln \left(1 + \frac{1}{\rho} \right) < \infty, \qquad \rho > 0, \tag{6.6.17}$$

and so the variance of the equalizer coefficient is finite,

$$E\{|h|^2\} = \frac{1}{2\sigma_g^2} \left[-1 + (1+\rho)e^\rho E_1(\rho) \right] < \infty, \qquad \rho, \sigma_g^2 > 0. \tag{6.6.18}$$

Since the variance is bounded, the correlation function of the equalizer exists. The

correlation function of the channel coefficients are examined empirically in the next section.

Derivation of equalizer coefficient variance The variance of the equalizer coefficient is $\mathrm{E}\{|h|^2\}$. The term $|h|^2$ is

$$|h|^2 = \frac{|g|^2}{(|g|^2 + \sigma_\nu^2)^2}. \tag{6.6.19}$$

The channel coefficient g is complex Gaussian with variance σ_g^2. This implies that $\zeta = |g|^2$ is exponentially distributed with a PDF

$$p_\zeta(\zeta) = \frac{1}{\sigma_g^2} e^{\frac{-\zeta}{\sigma_g^2}}. \tag{6.6.20}$$

Using this PDF, the expectation $\mathrm{E}\{|h|^2\}$ can be directly evaluated using the expression

$$\mathrm{E}\{|h|^2\} = \frac{1}{\sigma_g^2} \int_0^\infty \frac{\zeta}{(\zeta + \sigma_\nu^2)^2} e^{\frac{-\zeta}{\sigma_g^2}} \mathrm{d}\zeta. \tag{6.6.21}$$

Making a change of variable, $x = \zeta/\sigma_\nu^2$, the integral becomes slightly cleaner,

$$\mathrm{E}\{|h|^2\} = \frac{1}{\sigma_g^2} \int_0^\infty \frac{x}{(x + 1)^2} e^{-\rho x} \mathrm{d}x, \tag{6.6.22}$$

with $\rho = \sigma_\nu^2/\sigma_g^2$.

To evaluate this integral, integration by parts is used repeatedly. The first few

solution steps are

$$
\begin{aligned}
\mathrm{E}\{|h|^2\} &= \frac{1}{\sigma_g^2} \int_0^\infty \frac{x}{(x+1)^2} e^{-\rho x} \mathrm{d}x \\
&= \frac{1}{\sigma_g^2} \left[-\rho \int_0^\infty e^{-\rho x} \mathrm{d}x + \rho \int_0^\infty \frac{e^{-\rho x}}{1+x} \mathrm{d}x + \rho \int_0^\infty e^{-\rho x} \ln(1+x) \mathrm{d}x \right] \\
&= \frac{1}{\sigma_g^2} \left[-1 + \rho \int_0^\infty \frac{e^{-\rho x}}{1+x} \mathrm{d}x + \rho \int_0^\infty e^{-\rho x} \ln(1+x) \mathrm{d}x \right] \\
&= \frac{1}{\sigma_g^2} \left[-1 + \rho^2 \int_0^\infty e^{-\rho x} \ln(1+x) \mathrm{d}x + \rho \int_0^\infty e^{-\rho x} \ln(1+x) \mathrm{d}x \right] \\
&= \frac{1}{\sigma_g^2} \left[-1 + \rho(1+\rho) \int_0^\infty e^{-\rho x} \ln(1+x) \mathrm{d}x \right]
\end{aligned}
$$

Another change of variable $y = (1 + x)$ simplifies the remaining integral,

$$
\begin{aligned}
\mathrm{E}\{|h|^2\} &= \frac{1}{\sigma_g^2} \left[-1 + \rho(1+\rho) \int_1^\infty e^{-\rho(y-1)} \ln(y) \mathrm{d}y \right] \\
&= \frac{1}{\sigma_g^2} \left[-1 + \rho(1+\rho)e^\rho \int_1^\infty e^{-\rho y} \ln(y) \mathrm{d}y \right]
\end{aligned}
$$

One final change of variable, $z = \rho y$ and some further simplification get the expectation into the same form given earlier,

$$
\begin{aligned}
\mathrm{E}\{|h|^2\} &= \frac{1}{\sigma_g^2} \left[-1 + \rho(1+\rho)e^\rho \int_\rho^\infty e^{-z} \ln\left(\frac{z}{\rho}\right) \frac{\mathrm{d}z}{\rho} \right] \\
&= \frac{1}{\sigma_g^2} \left[-1 + (1+\rho)e^\rho \int_\rho^\infty \left(e^{-z} \ln(z) - e^{-z} \ln(\rho) \right) \mathrm{d}z \right] \\
&= \frac{1}{\sigma_g^2} \left[-1 + (1+\rho)e^\rho \int_\rho^\infty \frac{e^{-z}}{z} \mathrm{d}z \right] .
\end{aligned}
$$

6.7 Simulation results: equalizer correlation

In this section simulations results are presented that show the coherence time of equalizer coefficients is less than the coherence time of the channel impulse-response coefficients.
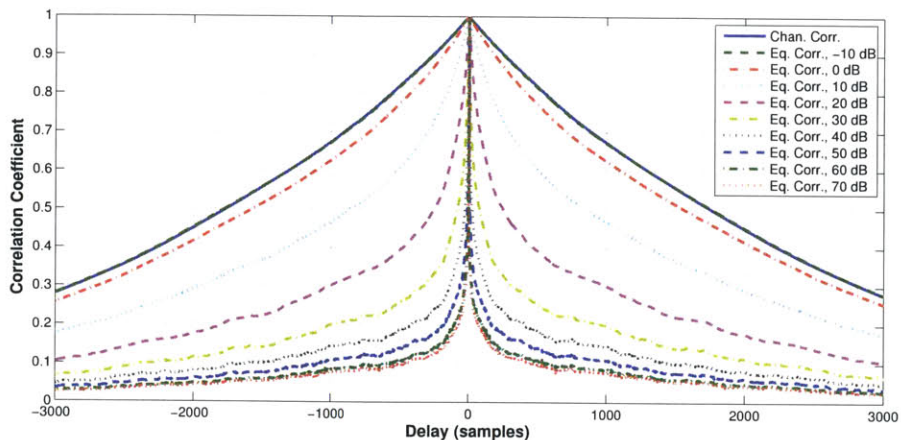
Figure 6.7.1: The correlation of a single-coefficient Markov channel with a correlation window of $N_{\mathrm{win}} = 2400$ symbols. There is a smooth transition from the channel correlation down to a minimum correlation as the SNR increases.

6.7.1 Single-coefficient channel with Markov correlation

The first simulation presented is a one-coefficient Markov channel. In this simulation, the sampling frequency is $f_s = 2400$ samples per second, and the fading rate is $1/2$ second (so the correlation width at $1/e$ is 2400 samples). The channel coefficients are unit variance so $\sigma_g^2 = 1$.

Figure 6.7.1 shows the correlation function for a single coefficient channel with the parameters as described above. The channel coefficients are shown to have a longer correlation window than the equalizer coefficients. Perfect channel knowledge is assumed when calculating the equalizer coefficients, so there is no channel estimation error.

The results show that the coherence time of the equalizer coefficients in the noise free case is much lower than the channel impulse response coefficient correlation.

Figure 6.7.1 also shows the effect of reducing the SNR. There is a transition from the low-noise (high SNR) regime at SNR of 60 and greater to the high-noise (low SNR) regime where the channel coefficients and the equalizer coefficients have approximately the same correlation function.

No attempt has been made to analytically capture the transition from low SNR
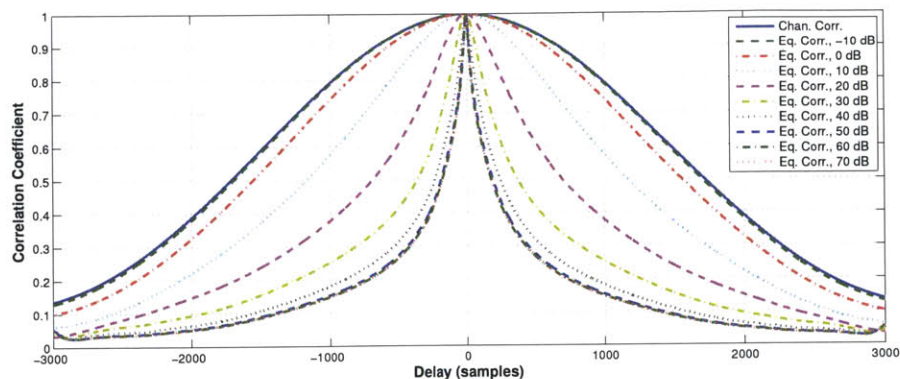
191

Figure 6.7.2: The correlation of a single-coefficient Gaussian channel with a correlation window of $N_{\text{win}} = 2400$ symbols. There is still a smooth transition from the channel correlation down to a minimum correlation as the SNR increases, with a slightly different shape than the AR(1) channel.

operating regime to the high SNR operating regime. The simulation results imply that the coherence time of the equalizer coefficients is monotonically non-increasing with SNR.

6.7.2 Single-coefficient channel with Gaussian correlation

Figure 6.7.2 plots the correlation function of the channel and equalizer coefficients when the channel has a Gaussian shaped correlation function. Similar results are observed are observed with this correlation function shape as were observed for a Markov correlation model. At high SNR, the equalizer coefficients have a shorter correlation time than the channel coefficients regardless of the shape of the correlation function.

6.7.3 10-coefficient Markov Correlated channel

This sections provides simulation results which verify the claims that the multi-coefficient equalizer is well approximated by inverting the first channel impulse response coefficient in the noise-free regime. A 10-coefficient WSSUS channel model is used, where each coefficient is generated independently using a Markov correlation model. The energy in each coefficient is assumed to be equal and the direct-path is
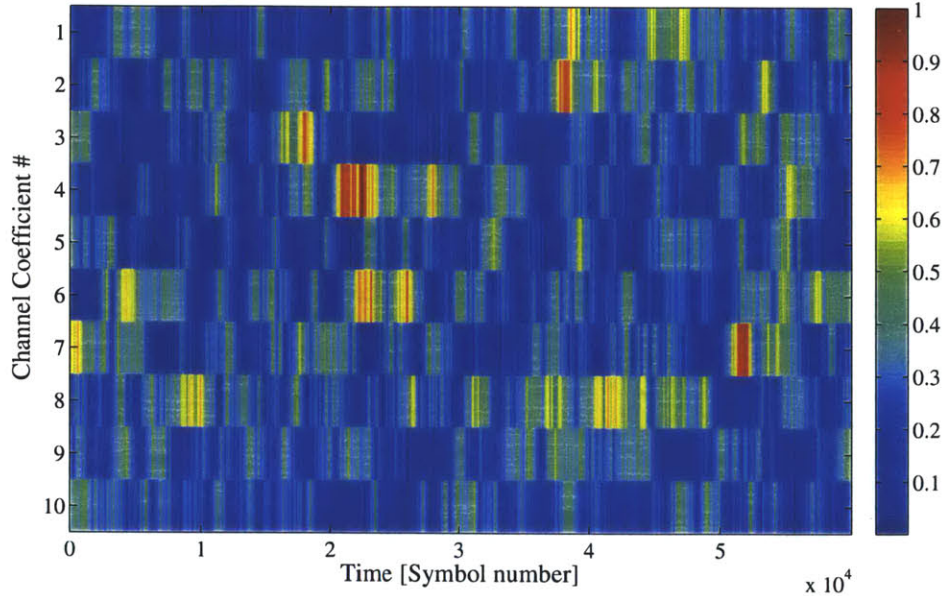
Figure 6.7.3: Realization of the 10-coefficient WSSUS, AR(1) channel where all co-efficients have equal variance. The sum of the average energy of all the channel coefficients is unity. The color indicates intensity on a linear scale.

assumed to be the first coefficient (arbitrary).

The equalizer is a DFE where perfect channel knowledge is assumed. There are 10 feed-forward coefficients and 9 feedback coefficients, so all of the precursor interference should be canceled. With perfect channel knowledge, the equalizer can use the current realization of the channel. Thus, the perfect channel knowledge equalizer is the MMSE equalizer.

Figure 6.7.3 shows the complete realization of the channel and 6.7.4 shows the equalizer coefficients calculated from the known channel impulse response realization. This figure shows that the equalizer coefficients are dominated by the first coefficient. Therefore, the use of a one-coefficient equalizer model for analysis is justified.

Using simulated data, the sample correlation coefficient, $\widehat{\rho}_{\mathrm{CORR}}(g^{-1}[n,0], h_{\mathrm{ff}}[n,0])$, between the inverse of the first channel coefficient, $g^{-1}[n,0]$, and the first equalizer
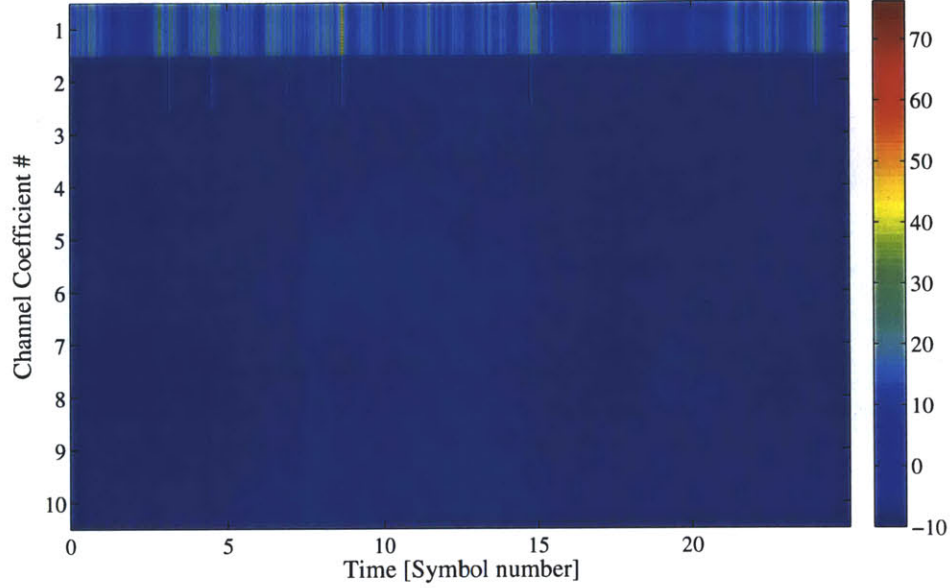
Figure 6.7.4: Realization of the MMSE feedforward DFE coefficients for the channel shown in figure 6.7.3 with no noise. Notice that the first coefficient dominates over the others for all time. The color corresponds to magnitude and the scale is $20 \log_{10}(|h|)$.

coefficient, $h_{\text{ff}},[n, 0]$, is

$$\widehat{\rho}_{\text{CORR}}(g^{-1}[n, 0], h_{\text{ff}}[n, 0]) = \frac{\frac{1}{N} \sum_{i=1}^{N}(h_{\text{ff}}[i, 0] - \widehat{\mu}_h)^*(g^{-1}[i, 0] - \widehat{\mu}_{g^{-1}})}{\sqrt{\frac{1}{N} \sum_{i=1}^{N}|h_{\text{ff}}[i, 0] - \widehat{\mu}_h|^2 \frac{1}{N} \sum_{i=1}^{N}|g^{-1}[i, 0] - \widehat{\mu}_{g^{-1}}|^2}}$$

$$(6.7.1)$$

$$= 0.9935 + j \, 0.0002$$

where

$$\widehat{\mu}_h = \frac{1}{N} \sum_{i=1}^{N} h_{\text{ff}}[i, 0] \qquad\qquad \widehat{\mu}_{g^{-1}} = \frac{1}{N} \sum_{i=1}^{N} g^{-1}[i, 0]$$

This correlation coefficient is very close to 1, confirming that there is a high correlation between the inverse of the first channel coefficient and the first feedforward equalizer coefficient. The imaginary part of the correlation is nearly 0, showing that the phases are well correlated.
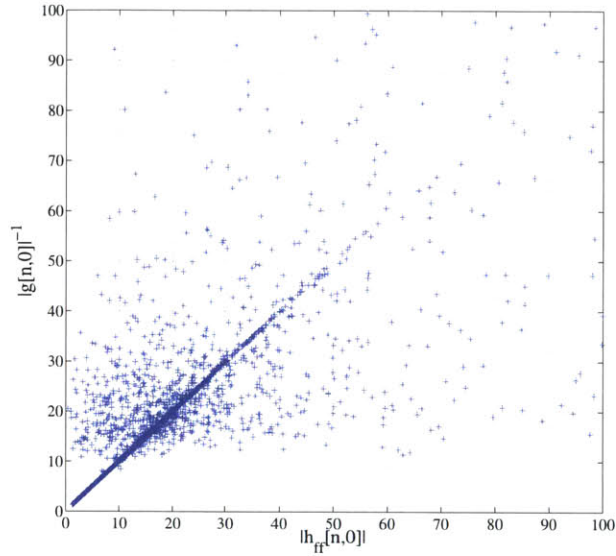
194

Figure 6.7.5: Correlation between the first coefficient of the equalizer and the inverse of the first coefficient of the channel. There is a strong linear correlation between the two. There is also many non-correlated events indicating the approximation is not perfect.

Figure 6.7.5 shows a linear relationship between the magnitude of the first equalizer coefficient and the inverse of the magnitude of the first channel coefficient. There is observable noise indicating that the equalizer coefficient is not exactly equal to the inverse of the first channel coefficient. The high correlation coefficient indicates the they are nearly equal and so an equality approximation is justified.

Figure 6.7.6 shows the normalized correlation function of the first equalizer coefficient for several different SNR values. At low SNR the equalizer coefficient correlation function is equivalent to the channel impulse-response correlation function. A similar effect was observed for the one-coefficient equalizer in the previous subsection. There is a smooth transition from the low-noise (high SNR) regime where one-coefficient is dominant and the correlation is low, to the high-noise (low SNR) regime where the correlation function of the equalizer is the same as channel impulse-response correlation function. The transition region for the multiple-coefficient equalizer extends over a wider SNR range than the single-coefficient equalizer.
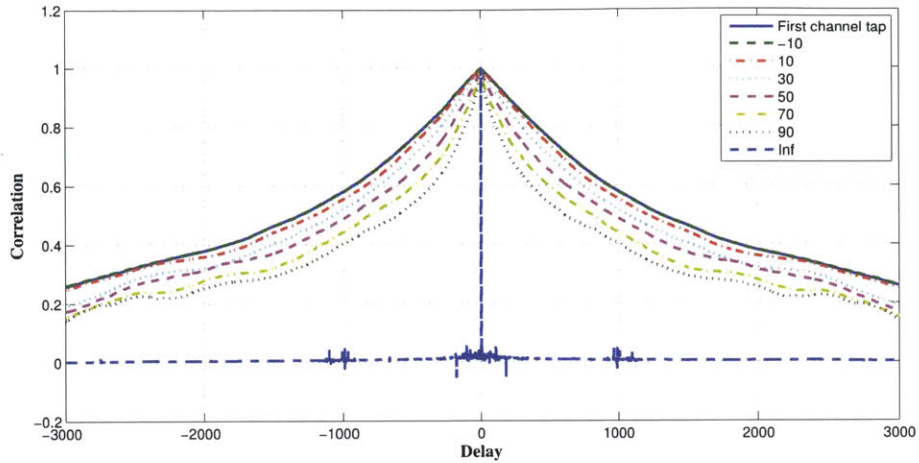
195

Figure 6.7.6: Correlation function for the first coefficient of the channel and the first coefficient of the equalizer for several SNR values. Notice that there is a smooth transition from the correlation of the channel down to the 90dB. This trend continues as the SNR continues to be increased (not shown). The transition to the no-noise correlation levels happens at much higher SNR than for the single coefficient channel (shown in the figure at 200dB).

To complete this discussion, the CEB and DA DFE are compared using the simulated 10-coefficient Rayleigh fading channel. Figure 6.7.7 is the MSE results using the CEB and DA DFE algorithms.

The results show that the performance of the DA algorithm levels degrades faster than the CEB algorithm. The reason is that the coherence time of the equalizer coefficients is reduced as the SNR is increased, which decreases the optimal averaging window. There is a lower limit to the averaging useful averaging window, below which the MSE increases rapidly. The correlation of the equalizer coefficients is reduced as the SNR increases so the equalizer coefficients are data limited at a higher SNR than the channel coefficients. A range of exponential weighting factors were used and the results show the weighting factor with the lowest MSE.

Note that the superior MSE performance of the CEB algorithm depends heavily on the accuracy of the channel model. As has been shown in other chapters, when the channel model is inaccurate, the performance of the CEB degrades markedly compared with the DA equalizer.
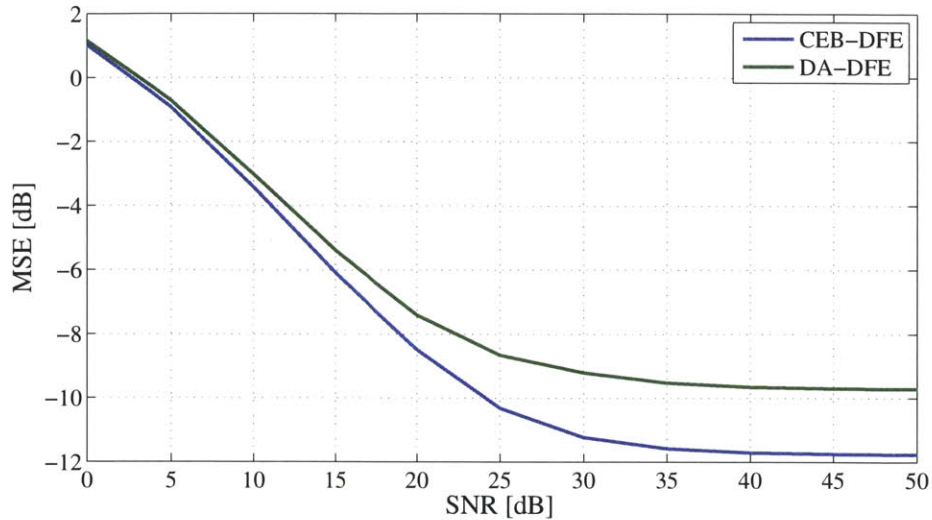
196

Figure 6.7.7: Comparison of the CEB and DA algorithms using a 10-coefficient Rayleigh fading channel.

6.8   Discussion

This chapter compared the performance difference of the CEB equalizer algorithm with the performance of the DA equalizer algorithm. At low SNR both methods have nearly equivalent MSE performance since at low SNR the observation noise is the dominant error term. Underwater communication systems generally operate with a low enough SNR that the performance of the DA and CEB methods is equivalent, so the DA methods should be considered when designing these systems since the computational complexity of the DA method is much lower than the CEB method.

When the SNR is low, the equalizer coefficients and the channel impulse response coefficients have the same correlation structure, so the DA and the CEB methods had very similar MSE performance. This transition from the high-SNR to the low-SNR regime was shown to be a transition from an operating regime where the statistics of the received data correlation matrix are time varying to an operating regime where the statistics are time-invariant. If the noise also had time-varying statistics, the CEB would always outperform the DA algorithm.

197

Chapter 7

Summary and conclusions

7.1   Summary of results

Equalization is a very useful communication component for overcoming ISI in a highly time-spread channel. The underwater environment provides a particularly challenging environment for equalization due to very long delay spreads and time variability. This thesis looked at several aspects and improvements of the EW-DFE applied to the underwater acoustic channel.

Several of the key results provided in this thesis include:

- The effective noise correlation matrix used in the computation of a CEB-DFE includes off diagonal elements due to correlated channel motion. The statistics of the channel motion are nearly time-invariant and so estimation techniques that assume the error correlation matrix is Toeplitz both reduce computational complexity and improve performance.

- In shallow water communication channels, the arrival angles of the multipath components are bounded into a narrow cone of angles. Beams can be formed which span this angular spread to capture most of the energy and do nearly as well as adaptive beamforming but without some of the instabilities that result from fully adaptive methods.

- The number of multipath arrivals can be estimated using either a geometric

199

ray-path model when environmental data is available or using χ^2 statistical matching techniques. These techniques provide a method for determining the number of beams that should be used for either an adaptive or non-adaptive beamformer to both improve performance and reduce computational complexity in a time-varying ocean environment.

- Unmodeled channel impulse response coefficients become additional noise terms when estimating equalizer coefficients using a CEB method. This may cause a estimated noise correlation matrix mismatch which leads to increased MSE at the output of the DFE. Additional processing steps can be used to mitigate this effect and improve performance.

- Channel estimate based equalization has lower MSE than direct adaptation equalization due to lower temporal correlation of equalizer coefficients at high SNR. As the SNR is reduced, these two methods perform equivalently. At most practical SNR observed in experiments, the methods are practically equal, so the DA method is preferred if computation complexity is an issue.

- A DA DFE is not sensitive to modeling errors since the parameters are all estimated directly from the data. When environmental information is available, however, the information can be included in the CEB-DFE framework easily which can increase performance dramatically.

7.2 Future directions

This work suggests several directions which need further study. The first direction is to identify a method that is more effective at estimating channel state information when little is known about the channel except the time and delay spread of the channel. This includes applying adaptive exponential weighting parameter techniques where the exponential weighting factor is another parameter of the problem. There has been some work on this in the literature, but the techniques are still crude and there is still not a good formulation of the problem.

In this work, the equalizer coefficients were treated as the system being estimated (direct adaptation techniques). Much of the literature has focused on CEB techniques due to the improved performance at high SNR. CEB techniques require a reliable channel model and accurate channel assumptions to be effective. This thesis suggests that DA techniques are valuable, especially in lower SNR ranges due to their lower computational complexity and lack of channel assumptions in the formulation. Further work is needed to improve DA equalizers, especially in data limited environments; adapting sparse or random matrix techniques for the DA equalizer useful.

Introducing channel knowledge into the DA equalizer to create a hybrid approach between the CEB and DA equalizers would allow for a trade-off between performance and complexity. When the channel state information is good, knowledge of the channel reduces error. If some channel parameter is known, such as the number of channel coefficients or the sparsity measure of the channel, error could be reduced for the DA equalizer. Further study is needed to determine if the decrease in error is enough to justify the increase in computational complexity.

A alternative to recovering the channel state information after using a set model order would be an algorithm which adaptively selects the appropriate model order. The structure of a universal prediction filter would be an appropriate start. This structure runs multiple filter lengths simultaneously and chooses the model order (or combination of model orders) that produces the lowest MSE. This usually requires a lattice filter so stability issues must be considered carefully.

To continue the work on beamforming methods, a method for including the time-variability of the channel explicitly into the optimization problem, the adaptation techniques, and the angle of arrival estimation will greatly improve all of these methods. For the underwater environment, this is an especially hard problem due to the plethora channel types and causes of time-variability that are observed in the ocean.

None of the results in this thesis make any assumptions that the channel is sparse, even though we know the UWA communications channel often is. Much work has been done in the area of exploiting this sparseness, so combining the work from this thesis with work from the literature would help generalize the results.

One other large open problem not directly addressed in this thesis is how to determine which paths and channel coefficients are useful to track. In order to make this determination, a model which includes the estimation error as a function of the correlation time of environmental parameters must be created. Thus far, models to include this information are very crude and analytical results are only available for the simplest models using base assumptions. Access to these models would allow better optimization criterion to be formed which would lead to equalizers with better performance.

The algorithms proposed in this thesis reduce computation and improve performance. The improved performance at a low SNR could be used to transmit data at or below the noise floor (especially for the array processing techniques) for covert communication. More research is needed to apply these advances to improve communication systems by reducing overall power, increasing the data rate (for a given SNR), or both.

References

[1] M. Abramowitz and I. A. Stegun, editors. *Handbook of Mathematical Functions.* Dover, 1964.

[2] H. Akaike. Information Theory and the Maximum Likelihood Principle. In *Proc. IEEE Internat. Symp. on Information Theory*, 1973.

[3] H. Akaike. A new look at the statistical model identification. *IEEE Trans. Autom. Control*, 19(6):716–723, 1974.

[4] T. W. Anderson. Asymptotic theory for principal component analysis. *Ann. Math. Statist.*, 34:122–148, 1963.

[5] A. B. Baggeroer. Acoustic telemetry–an overview. *IEEE J. Ocean. Eng.*, 9(4):229 – 235, 1984.

[6] N. A. Bagrov. On the equivalent number of independent data (in Russian). *Tr. Gidrometeor. Cent.*, 44:3–11, 1969.

[7] P.-P. J. Beaujean and L. R. LeBlanc. Adaptive array processing for high-speed acoustic communication in shallow water. *IEEE J. Ocean. Eng.*, 29(3):807 – 823, 2004.

[8] B. Bell, D. B. Percival, and A. T. Walden. Calculating Thomson's spectral multitapers by inverse iteration. *J. Comput. Graph. Statist.*, 2(1):119–130, 1993.

[9] B. A. Brandwood. A complex gradient operator and its application in adaptive array theory. *Proc. IEE, Parts F and H*, 130:11–16, 1983.

[10] L. M. Brekhovskikh and Y. P. Lysanov. *Fundamentals of Ocean Acoustics.* Springer-Verlag, 2003.

[11] C. Bretherton, M. Widmann, V. Dymnikov, J. Wallace, and I. Blade. The effective number of spatial degrees of freedom of a time-varying field. *J. Climate*, 12(7):1990–2009, Jan 1999.

[12] D. R. Brillinger. *Time Series: Data Analysis and Theory.* SIAM, 1981.

[13] J. Capon, R. Greenfield, and R. Kolker. Multidimensional maximum-likelihood processing of a large aperture seismic array. *Proc. IEEE*, pages 192–211, 1967.

[14] J. Catipovic. Performance limitations in underwater acoustic telemetry. *IEEE J. Ocean. Eng.*, 15(3):205–216, 1990.

[15] J. Catipovic and Baggeroer. Design and performance analysis of a Digital Acoustic Telemetry System for the short range underwater channel. *Oceanic Engineering, IEEE Journal of*, 9(4):242–252, 1984.

[16] M. Chitre, S. Shahabodeen, L. Freitag, and M. Stojanovic. Recent advances in underwater acoustic communications and networking. In *Proc. IEEE/MTS OCEANS*, pages 1–10, 2008.

[17] S. E. Cho, H. C. Song, and W. S. Hodgkiss. Successive interference cancellation for time-varying underwater acoustic channels. In *Proc. IEEE/MTS OCEANS*, pages 1 – 4, 2010.

[18] S. E. Cho, H. C. Song, and W. S. Hodgkiss. Successive interference cancellation for underwater acoustic communications. *IEEE J. Ocean. Eng.*, 2011 [In Press].

[19] J. W. Choi, R. J. Drost, A. C. Singer, and J. C. Preisig. Iterative multi-channel equalization and decoding for high frequency underwater acoustic communications. In *Proc. IEEE SAM*, pages 127 – 130, 2008.

[20] J. W. Choi, T. J. Riedl, K. Kim, A. Singer, and J. C. Preisig. Adaptive linear turbo equalization over doubly selective channels. *IEEE J. Ocean. Eng.*, 2011 [In Press].

[21] J. M. Cioffi and T. Kailath. Fast, recursive-least-squares transversal filters for adaptive filtering. *IEEE Trans. Acoust., Speech, Signal Process.*, 32(2):304–337, 1984.

[22] R. J. Compton. The bandwidth performance of a two-element adaptive array with tapped delay-line processing. *IEEE Trans. Antennas Propag.*, 36(1):5–14, 1988.

[23] R. J. Compton. The relationship between tapped delay-line and FFT processing in adaptive arrays. *IEEE Trans. Antennas Propag.*, 36(1):15–26, 1988.

[24] M. J. Crocker, editor. *Handbook of Acoustics*. John Wiley and Sons, Inc, 1998.

[25] E. L. Daly, A. C. Singer, J. W. Choi, and J. C. Preisig. Linear turbo equalization with precoding for underwater acoustic communications. In *Proc. Asilomar Conf. Signals, Syst., Comp.*, pages 1–5, Nov 2010.

[26] C. Douillard, A. Picart, P. Didier, M. Jezequel, C. Berrou, and A. Glavieux. Iterative correction of intersymbol interference: Turbo-equalization. *Europ. Trans. Telecomm.*, 6:507–512, Sept. 1995.

[27] D. Dzung. Error probability of MLSE equalization using imperfect channel measurements. In *Proc. IEEE Internat. Conf. Commun.*, volume 2, pages 558 – 562, 1991.

[28] G. F. Edelmann, H. C. Song, S. Kim, W. S. Hodgkiss, W. A. Kuperman, and T. Akal. Underwater acoustic communications using time reversal. *IEEE J. Ocean. Eng.*, 30(4):852–864, 2005.

[29] T. Eggen. *Underwater acoustic communication over Doppler spread channels*. PhD thesis, MIT-WHOI Joint Program, 1997.

[30] T. H. Eggen, A. B. Baggeroer, and J. C. Preisig. Communication over Doppler spread channels. Part I: Channel and receiver presentation. *IEEE J. Ocean. Eng.*, 25(1):62 – 71, 2000.

[31] E. Eleftheriou and D. Falconer. Tracking properties and steady-state performance of RLS adaptive filter algorithms. *IEEE Trans. Acoust., Speech, Signal Process.*, 34(5):1097 – 1110, 1986.

[32] S. Fechtel and H. Meyr. An investigation of channel estimation and equalization techniques for moderately rapid fading HF-channels. In *Proc. IEEE Internat. Conf. Commun.*, volume 2, pages 768 – 772, 1991.

[33] M. Fink. Time reversed acoustics. *Physics Today*, 50:34–46, Mar. 1997.

[34] F. Fisher and V. Simmons. Sound absorption in sea water. *J. Acoust. Soc. Amer.*, 62:558, 1977.

[35] G. Golub and C. Van Loan. *Matrix Computations*. Johns Hopkins University Press, 1996.

[36] S. Haykin. *Adaptive Filter Theory*. Pearson Education, 2001.

[37] S. Haykin, J. H. Justice, N. L. Owsley, J. L. Yen, and A. C. Kak. *Array Signal Processing*. Prentice Hall, 1985.

[38] R. Horn and C. Johnson. *Matrix Analysis*. Cambridge University Press, 1990.

[39] J. Huang, H. vandenDool, and K. Georgakakos. Analysis of model-calculated soil moisture over the United States (1931-1993) and applications to long-range temperature forecasts. *J. Climate*, 9(6):1350–1362, 1996.

[40] D. Jackson, J. Ritcey, W. Fox, C. Jones, D. Rouseff, and D. Dowling. Experimental testing of passive phase conjugation for underwater acoustic communication. In *Proc. Asilomar Conf. Signals, Syst., Comp.*, pages 680–683, 2000.

[41] F. B. Jensen and W. A. Kuperman. Optimum frequency of propagation in shallow water environments. *J. Acoust. Soc. Amer.*, 73:813–819, 1983.

[42] F. B. Jensen, W. A. Kuperman, M. Porter, and H. Schmidt. *Computational Ocean Acoustics*. Springer-Verlag, 2000.

[43] D. H. Johnson and D. E. Dudgeon. *Array Signal Processing: Concepts and Techniques*. Prentice Hall, 1993.

[44] T. Kailath, A. H. Sayed, and B. Hassibi. *Linear Estimation*. Prentice Hall, 2000.

[45] D. Kilfoyle and A. B. Baggeroer. The state of the art in underwater acoustic telemetry. *IEEE J. Ocean. Eng.*, 25(1):4 – 27, 2000.

[46] J. S. Kim, H. C. Song, and W. A. Kuperman. Adaptive time-reversal mirror. *J. Acoust. Soc. Amer.*, 109(5):1817–1825, May 2001.

[47] S. Kim, W. A. Kuperman, W. S. Hodgkiss, H. C. Song, G. F. Edelmann, and T. Akal. Robust time reversal focusing in the ocean. *J. Acoust. Soc. Amer.*, 114(1):145–157, July 2003.

[48] J. P. Kitchens. *Acoustic vector-sensor array processing*. PhD thesis, Massachusetts Institute of Technology, 2010.

[49] R. Koetter, A. C. Singer, and M. Tuchler. Turbo equalization. *IEEE Signal Process. Mag.*, 21(1):67 – 80, 2004.

[50] A. L. Kraay and A. B. Baggeroer. A physically constrained maximum-likelihood method for snapshot-deficient adaptive array processing. *IEEE Trans. Signal Process.*, 55(8):4048 – 4063, 2007.

[51] H. J. Kushner. *Approximation and Weak Convergence Methods for Random Processes with Applications to Stochastic System Theory*. MIT Press, Cambridge, MA, 1984.

[52] A. Laferriere and J. C. Preisig. Bayesian channel estimation for K-distributed fading models. In *J. Acoust. Soc. Amer.*, page 2599, 2011.

[53] A. B. Laferriere. *K-distribution fading models for Bayesian estimation of an underwater acoustic channel*. PhD thesis, MIT-WHOI Joint Program, 2011.

[54] P. Lancaster and M. Tismenetsky. *The Theory of Matrices*. Academic Press, Inc., 1985.

[55] L. R. LeBlanc. Angular-spectral decomposition beamforming for acoustic arrays. *IEEE J. Ocean. Eng.*, 9(1):31 – 39, 1984.

[56] L. R. LeBlanc and P.-P. J. Beaujean. Spatio-temporal processing of coherent acoustic communication data in shallow water. *IEEE J. Ocean. Eng.*, 25(1):40 – 51, 2000.

[57] Y. Lee and J.-H. Chen. The effect of channel estimator memory mismatch on the performance of MLSE in wireless data communications. In *Proc. IEEE Internat. Conf. Commun.*, volume 1, pages 134 – 138, 2002.

[58] Y. Lee and D. C. Cox. Adaptive DFE with regularization for indoor wireless data communications. In *Proc. IEEE GLOBECOM*, volume 1, pages 47 – 51, 1997.

[59] B. Li, S. Zhoul, M. Stojanovic, L. Freitag, J. Huang, and P. Wilet. MIMO-OFDM over an underwater acoustic channel. In *Proc. IEEE/MTS OCEANS*, pages 1 – 6, 2007.

[60] K. Li, X. Wang, G. Yue, and L. Ping. A low-rate code-spread and chip-interleaved time-hopping UWB system. *IEEE J. Sel. Areas Commun.*, 24(4):864 – 870, 2006.

[61] M. Lopez, A. C. Singer, S. Whitney, and G. Edelson. A DFE coefficient placement algorithm for underwater digital acoustic communications. In *Proc. IEEE/MTS OCEANS*, volume 2, pages 996 – 1001, 1999.

[62] R. W. Lucky. Automatic equalization for digital communication. *AT&T Tech. J.*, 44(4):547–588, Jan 1965.

[63] R. W. Lucky. The adaptive equalizer. *IEEE Signal Process. Mag.*, 23(3):104 – 107, 2006.

[64] P. Monsen. Theoretical and measured performance of a DFE modem on a fading multipath channel. *IEEE Trans. Commun.*, 25(10):1144 – 1153, 1977.

[65] R. Nadakuditi and J. C. Preisig. A channel subspace filtering approach to adaptive equalization of highly dynamic realistic channels. In *Proc. Asilomar Conf. Signals, Syst., Comp.*, volume 2, pages 1616 – 1623, 2001.

[66] R. Nadakuditi and J. C. Preisig. A channel subspace post-filtering approach to adaptive least-squares estimation. *IEEE Trans. Signal Process.*, 52(7):1901 – 1914, 2004.

[67] R. R. Nadakuditi and A. Edelman. Sample eigenvalue based detection of high-dimensional signals in white noise using relatively few samples. *IEEE Trans. Signal Process.*, 56(7):2625 – 2638, 2008.

[68] R. R. Nadakuditi and J. W. Silverstein. Fundamental limit of sample eigenvalue based detection of signals in colored noise using relatively few samples. In *Proc. Asilomar Conf. Signals, Syst., Comp.*, pages 686 – 690, 2007.

[69] R. R. Nadakuditi and J. W. Silverstein. Fundamental limit of sample generalized eigenvalue based detection of signals in noise using relatively few signal-bearing and noise-only samples. *IEEE J. Sel. Topics Signal Process.*, 4(3):468 – 480, 2010.

[70] A. Papoulis. *Probability, Random Variables, and Stochastic Processes.* McGraw-Hill, 3rd edition, 1991.

[71] J. C. Papp. Physically constrained maximum likelihood (PCML) mode filtering and its application as a pre-processing method for underwater acoustic communication. Master's thesis, MIT-WHOI Joint Program, 2009.

[72] J. C. Papp, J. C. Preisig, and A. K. Morozov. Physically constrained maximum likelihood mode filtering. *J. Acoust. Soc. Amer.*, 127:2385–2391, Jan 2010.

[73] D. B. Percival and A. T. Walden. *Spectral Analysis for Physical Applications.* Cambridge University Press, 1993.

[74] J. C. Preisig. The impact of underwater acoustic channel structure and dynamics on the performance of adaptive coherent equalizers. In *Proc. AIP High Freq. Ocean Acoust. Conf.*, volume 728, page 57, Nov 2004.

[75] J. C. Preisig. Performance analysis of adaptive equalization for coherent acoustic communications in the time-varying ocean environment. *J. Acoust. Soc. Amer.*, 118:263–278, Jul 2005.

[76] J. C. Preisig. Acoustic propagation considerations for underwater acoustic communications network development. In *Proc. ACM WUWNet*, Sep 2006.

[77] J. C. Preisig. Acoustic propagation considerations for underwater acoustic communications network development. *SIGMOBILE Mobile Computing and Communications Review*, 11(4), Oct 2007.

[78] J. C. Preisig and G. B. Deane. Surface wave focusing and acoustic communications in the surf zone. *J. Acoust. Soc. Amer.*, 116:2067–2080, Oct 2004.

[79] J. G. Proakis. *Digital Communications.* McGraw-Hill, 2000.

[80] J. G. Proakis, M. Stojanovic, and J. Catipovic. Adaptive equalization algorithms for high rate underwater acoustic communications. In *Proc. IEEE AUV Workshop*, pages 157 – 164, 1994.

[81] S. U. H. Qureshi. Adaptive equalization. *Proc. IEEE*, 73(9):1349 – 1387, 1985.

[82] S. U. H. Qureshi and G. D. Forney. Performance properties of a T/2 equalizer. In *Proc. IEEE Nat. Telecom. Conf.*, volume 1, pages 11:1.1 – 11:1.9, 1977.

[83] J. Rissanen. Modeling by shortest data description. *Automatica*, 14:465–471, 1978.

[84] W. Rodgers and R. Compton. Adaptive Array Bandwidth with Tapped Delay-Line Processing. *IEEE Trans. Aerosp. Electron. Syst.*, 15(1):21–28, 1979.

[85] D. Rouseff, D. Jackson, W. Fox, C. Jones, J. Ritcey, and D. Dowling. Underwater acoustic communication by passive-phase conjugation: Theory and experimental results. *IEEE J. Ocean. Eng.*, 26(4):821–831, 2001.

[86] A. H. Sayed. *Fundamentals of Adaptive Filtering.* Wiley-Interscience, 2003.

[87] A. H. Sayed and T. Kailath. A state-space approach to adaptive filtering. In *Proc. IEEE ICASSP*, volume 3, pages 559 – 562, 1993.

[88] A. H. Sayed and T. Kailath. A state-space approach to adaptive RLS filtering. *IEEE Signal Process. Mag.*, 11(3):18 – 60, 1994.

[89] H. Schmidt, A. B. Baggeroer, W. A. Kuperman, and E. K. Scheer. Environmentally tolerant beamforming for high-resolution matched field processing: Deterministic mismatch. *J. Acoust. Soc. Amer.*, 88(4):1851–1862, oct 1990.

[90] G. Schwarz. Estimating dimension of a model. *Ann. Statist.*, 6(2):461–464, Jan 1978.

[91] P. K. Shukla and L. F. Turner. Channel-estimation-based adaptive DFE for fading multipath radio channels. *Proc. IEE, Part I*, 138(6):525 – 543, 1991.

[92] J. F. Sifferlen, H. C. Song, W. S. Hodgkiss, W. A. Kuperman, and J. M. Stevenson. An iterative equalization and decoding approach for underwater acoustic communication. *IEEE J. Ocean. Eng.*, 33(2):182–197, 2008.

[93] A. C. Singer, J. K. Nelson, and R. Koetter. Linear iterative turbo-equalization (LITE) for dual channels. In *Proc. Asilomar Conf. Signals, Syst., Comp.*, volume 2, pages 1670 – 1674, 1999.

[94] D. Slepian. Prolate spheroidal wave functions, Fourier analysis, and uncertainty. V - the discrete case. *AT&T Tech. J.*, 57:1371–1430, Jun 1978.

[95] A. Song, M. Badiey, and V. McDonald. Multichannel combining and equalization for underwater acoustic MIMO channels. In *Proc. IEEE/MTS OCEANS*, pages 1–6, 2008.

[96] H.-C. Song, W. S. Hodgkiss, and W. A. Kuperman. MIMO time reversal communications. In *Proc. WuWNet*. ACM, Sept. 2007.

[97] H. C. Song, W. S. Hodgkiss, W. A. Kuperman, T. Akal, and M. Stevenson. Multiuser communications using passive time reversal. *IEEE J. Ocean. Eng.*, 32(4):915–926, 2007.

[98] H. C. Song, W. S. Hodgkiss, W. A. Kuperman, M. Stevenson, and T. Akal. Improvement of time-reversal communications using adaptive channel equalizers. *IEEE J. Ocean. Eng.*, 31(2):487–496, Apr. 2006.

[99] G. W. Stewart and J. Sun. *Matrix Perturbation Theory*. Academic Press, Inc., 1990.

[100] M. Stojanovic. Underwater acoustic communications. In *Proc. IEEE Electro/Internat.*, pages 435–440, 1995.

[101] M. Stojanovic. High speed underwater accoustic comunications. In *Underwater Acoustic Digital Signal Processing and Communication Systems*. Kluwer Academic Publishers, 2002.

[102] M. Stojanovic. On the relationship between capacity and distance in an underwater acoustic communication channel. *SIGMOBILE Mobile Computing and Communications Review*, 11(4):34–43, Oct 2007.

[103] M. Stojanovic. Design and capacity analysis of cellular-type underwater acoustic networks. *IEEE J. Ocean. Eng.*, 33(2):171 – 181, 2008.

[104] M. Stojanovic. Underwater acoustic communications: Design considerations on the physical layer. In *Proc. IEEE WONS*, pages 1 – 10, 2008.

[105] M. Stojanovic, J. Catipovic, and J. G. Proakis. Adaptive multichannel combining and equalization for underwater acoustic communications. *J. Acoust. Soc. Amer.*, 94:1621-16131, Sep 1993.

[106] M. Stojanovic, J. Catipovic, and J. G. Proakis. Reduced-complexity spatial and temporal processing of underwater acoustic communication signals. *J. Acoust. Soc. Amer.*, 98:961-972, Aug 1995.

[107] M. Stojanovic and L. Freitag. Hypothesis-feedback equalization for direct-sequence spread-spectrum underwater communications. In *Proc. IEEE/MTS OCEANS*, volume 1, pages 123 – 129 vol.1, 2000.

[108] M. Stojanovic, L. Freitag, and M. Johnson. Channel-estimation-based adaptive equalization of underwater acoustic signals. In *Proc. IEEE/MTS OCEANS*, volume 2, pages 985 – 990, 1999.

[109] M. Stojanovic, J. G. Proakis, and J. Catipovic. Analysis of the impact of channel estimation errors on the performance of a decision-feedback equalizer in fading multipath channels. *IEEE Trans. Commun.*, 43(234):877 – 886, 1995.

[110] M. Stojanovic, J. G. Proakis, and J. Catipovic. Performance of high-rate adaptive equalization on a shallow water acoustic channel. *J. Acoust. Soc. Amer.*, 100:2213-2219, Oct 1996.

[111] M. Stojanovic and Z. Zvonar. Multisensor multiuser receivers for time-dispersive multipath fading channels. In *Proc. IEEE Internat. Symp. on Information Theory*, 1995.

[112] G. Strang. *Introduction to Linear Algebra*. Wellesley-Cambridge Press, 2003.

[113] M. G. TerMegreditchian. On the determination of the number of independent stations which are equivalent to prescribed systems of correlated stations (in Russian). *Meteor. Hydrol.*, 2:24-36, 1969.

[114] D. J. Thomson. Spectrum estimation and harmonic analysis. *Proc. IEEE*, 70(9):1055 – 1096, 1982.

[115] W. H. Thorp. Deep-ocean sound attenuation in the sub- and low-kilocycle-per-second region. *J. Acoust. Soc. Amer.*, 38:648–654, Jan 1965.

[116] W. H. Thorp. Analytic description of the low-frequency attenuation coefficient. *J. Acoust. Soc. Amer.*, 42:270, Jan 1967.

[117] M. Tuchler, R. Koetter, and A. C. Singer. Turbo equalization: Principles and new results. *IEEE Trans. Commun.*, 50(5):754 – 767, 2002.

[118] M. Tuchler and A. Singer. Turbo equalization: An overview. *IEEE Trans. Informat. Theory*, 57(2):920–952, 2011.

[119] R. J. Urick. *Principles of Underwater Sound.* Peninsula Publishing, 1983.

[120] H. L. Van Trees. *Radar-Sonar Signal Processing and Gaussian Signals in Noise: Detection, Estimation, and Modulation Theory, Part III.* Wiley-Interscience, 2001.

[121] H. L. Van Trees. *Optimum Array Processing: Detection, Estimation, and Modulation Theory, Part IV.* Wiley-Interscience, 2002.

[122] F. Vook and R. J. Compton. The bandwidth performance of linear adaptive arrays with tapped delay-line processing. In *Proc. Antennas Propag. Soc. Internat. Sympos.*, pages 1692–1695, 1990.

[123] F. Vook and R. J. Compton. Bandwidth performance of linear adaptive arrays with tapped delay-line processing. *IEEE Trans. Aerosp. Electron. Syst.*, 28(3):901–908, 1992.

[124] Y. Wang, G. Leus, and A. Pandharipande. Direction estimation using compressive sampling array processing. In *Proc. IEEE/SP Statistical Signal Process. Workshop*, pages 626 – 629, 2009.

[125] M. Wax and T. Kailath. Detection of signals by information theoretic criteria. *IEEE Trans. Acoust., Speech and Signal Process.*, 33(2):387 – 392, 1985.

[126] G. M. Wenz. Review of Underwater Acoustics Research: Noise. *J. Acoust. Soc. Amer.*, 51:1010–1024, 1972.

[127] I. Woodhouse. The ratio of the arithmetic to the geometric mean: a cross-entropy interpretation. *IEEE Trans. Geosci. Remote Sens.*, 39(1):188–189, 2001.

[128] T. C. Yang. Differences between passive-phase conjugation and decision-feedback equalizer for underwater acoustic communications. *IEEE J. Ocean. Eng.*, 29(2):472–487, 2004.

[129] M. R. Zarnetske. *Long-range ocean acoustic propagation experiment (LOAPEX): Preliminary analysis of source motion and tidal signals.* PhD thesis, University of Washington, 2005.

[130] J. Zhang, J. Cross, and Y. Zheng. Statistical channel modeling of wireless shallow water acoustic communications from experiment data. In *Proc. MILCOM*, pages 2412–2416, 2010.

[131] R. A. Ziegler and J. M. Cioffi. Estimation of time-varying digital radio channels. *IEEE Trans. Veh. Technol.*, 41(2):134 – 151, 1992.